PB85-137370

Continued Research in Mesoscale Air Pollution Simulation Modeling. Volume 6 Further Studies in the Modeling of Microscale Phenomena

Systems Applications, Inc., San Rafael, CA

Prepared for

Environmental Sciences Research Lab.
Research Triangle Park, NC

Dec 84

U.S. Department of Commerce
National Technical Information Service
NTIS

TECHNICAL REPORT DATA

(Please read Instructions on the reverse before completing)

1. REPORT NO. EPA-600/3-84-095b	2.	3. RECIPIENT'S ACCESSION NO. PB85 137370
4. TITLE AND SUBTITLE CONTINUED RESEARCH IN MESOSCALE AIR POLLUTION SIMULATION MODELING: Volume VI -- Further Studies in the Modeling of Microscale Phenomena		5. REPORT DATE December 1984
		6. PERFORMING ORGANIZATION CODE
7. AUTHOR(S) R.G. Lamb, W.R. Shu, D.R. Durran, J.H. Seinfeld, and L.E. Reid		8. PERFORMING ORGANIZATION REPORT NO.
9. PERFORMING ORGANIZATION NAME AND ADDRESS Systems Applications, Inc. 101 Lucas Valley Road San Rafael, CA 94903		10. PROGRAM ELEMENT NO. CDWA1A/02-2260 (FY-84)
		11. CONTRACT/GRANT NO. Contract No. 68-02-2216
12. SPONSORING AGENCY NAME AND ADDRESS Environmental Sciences Research Laboratory-RTP, NC Office of Research and Development U.S. Environmental Protection Agency Research Triangle Park, NC 27711		13. TYPE OF REPORT AND PERIOD COVERED Final (10/79 - 7/82)
		14. SPONSORING AGENCY CODE EPA/600/09

15. SUPPLEMENTARY NOTES

16. ABSTRACT

This report describes the development of techniques for modeling the microscale phenomena associated with urban air pollution. Such phenomena include turbulent diffusion, turbulent concentration fluctuations, and sub-grid scale variations in the time averaged concentration field. Optimal eddy diffusivities were reexamined to determine whether (1) the diffusivities are unique, (2) they have a universal form when properly scaled, and (3) they are dependent on source height. A model for describing the effects of turbulent concentration fluctuations on second-order chemical reactions has also been developed and tested. It was applied to the case of NO emanating from a point source into an O_3 laden atmosphere. Results showed that the rate of conversion of NO to NO_2 is greatly inhibited by turbulent concentration fluctuations, even under stable conditions. A method of paramaterizing the effects of chemical reaction rates of both subgrid-scale concentration variations arising from ground-level sources and turbulence-induced concentration fluctuations has also been developed. In addition, theoretical frameworks for two models of pollutant levels around roadways are introduced.

17. KEY WORDS AND DOCUMENT ANALYSIS

a. DESCRIPTORS	b. IDENTIFIERS/OPEN ENDED TERMS	c. COSATI Field/Group

18. DISTRIBUTION STATEMENT RELEASE TO PUBLIC	19. SECURITY CLASS *(This Report)* UNCLASSIFIED	21. NO. OF PAGES 307
	20. SECURITY CLASS *(This page)* UNCLASSIFIED	22. PRICE

EPA Form 2220-1 (9-73)

EPA-600/3-84-095b
December 1984

PB85-137370

CONTINUED RESEARCH IN MESOSCALE AIR POLLUTION SIMULATION MODELING

VOLUME VI -- Further Studies in the Modeling of Microscale Phenomena

by

R.G. Lamb, D.R. Durran, and L.E. Reid

Systems Applications, Incorporated
101 Lucas Valley Road
San Rafael, California 94903

W.R. Shu and J.H. Seinfeld

California Institute of Technology
Pasadena, California 91125

Contract No. 68-02-2216

Project Officer

Kenneth L. Demerjian
Meteorology and Assessment Division
Environmental Sciences Research Laboratory
Research Triangle Park, North Carolina 27711

ENVIRONMENTAL SCIENCES RESEARCH LABORATORY
OFFICE OF RESEARCH AND DEVELOPMENT
U.S. ENVIRONMENTAL PROTECTION AGENCY
RESEARCH TRIANGLE PARK, NORTH CAROLINA 27711

REPRODUCED BY
NATIONAL TECHNICAL
INFORMATION SERVICE
U.S. DEPARTMENT OF COMMERCE
SPRINGFIELD, VA. 22161

NOTICE

This document has been reviewed in accordance with U.S. Environmental Protection Agency policy and approved for publication. Mention of trade names or commercial products does not constitute endorsement or recommendation for use.

ABSTRACT

This report describes the development of techniques for modeling the microscale phenomena associated with urban air pollution. Such phenomena include turbulent diffusion, turbulent concentration fluctuations, and subgrid scale variations in the time averaged concentration field. Optimal eddy diffusivities were reexamined to determine whether (1) the diffusivities are unique, (2) they have a universal form when properly scaled, and (3) they are dependent on source height. A model for describing the effects of turbulent concentration fluctuations on second-order chemical reactions has also been developed and tested. It was applied to the case of NO emanating from a point source into an O_3 laden atmosphere. Results showed that the rate of conversion of NO to NO_2 is greatly inhibited by turbulent concentration fluctuations, even under stable conditions. A method of parameterizing the effects of chemical reaction rates of both subgrid-scale concentration variations arising from ground-level sources and turbulence-induced concentration fluctuations has also been developed. In addition, theoretical frameworks for two models of pollutant levels around roadways are introduced.

ACKNOWLEDGEMENTS

The authors would like to note that portions of this work were supported by Systems Applications, Incorporated internal research funds.

CONTENTS

ABSTRACT iii

ACKNOWLEDGEMENTS iv

LIST OF ILLUSTRATIONS viii

LIST OF TABLES xi

I INTRODUCTION 1

II PARAMETERIZATION OF TURBULENT MATERIAL FLUXES USING "OPTIMAL" EDDY DIFFUSIVITIES 4

- A. The Uniqueness of the Optimal Diffusivities 6
- B. The Range of Atmospheric Stability to Which the Optimal K_z Profiles Apply. 19
- C. The Effect of Release Height on the Optimal K_z 24
- D. Recapitulation 31

III MODELING THE EFFECTS OF TURBULENT CONCENTRATION FLUCTUATIONS ON SECOND-ORDER CHEMICAL REACTIONS IN THE PLANETARY BOUNDARY LAYER 33

- A. Formulation of an Expression for the Concentration Fluctuation Term $\overline{A'B'}$. 35
- B. Approximations of the Reaction Parameter λ 43
  - 1. General Considerations 43
  - 2. Case 1: Point Source Release of A into a Uniform Field of B 45
  - 3. Case 2: One-Dimensional Reactors 46
- C. Approximations of the Mixing Parameters ζ_A and ζ_B 52
  - 1. General Considerations 52
  - 2. Case 1: Point Source Release of A into a Uniform Field of B 54
  - 3. Case 2: One-Dimensional Reactors 54
- D. Comparison of the Model Predictions with Laboratory Data 55
- E. Recapitulation 61

III MODELING THE EFFECTS OF TURBULENT CONCENTRATION FLUCTUATIONS ON SECOND-ORDER CHEMICAL REACTIONS IN THE PLANETARY BOUNDARY LAYER (Continued)

F. Application of the Model to Point Source Plumes in the Atmosphere 62
    1. Model for a Chemically Reacting Plume 64
    2. Numerical Formulation of ζ_B 67
    3. Creation of an Ensemble of Particle Trajectories 70
    4. Sampling Procedure and Statistical Error of the Estimate of p_2 71
    5. Estimate of the ζ_B 77
    6. Study of the Reaction Between Nitric Oxide and Ozone in Simulated Atmospheric Turbulence 78
    7. Discussion 84

IV PARAMETERIZATION OF SUBGRID-SCALE MEAN CONCENTRATION VARIATIONS IN MODELS OF URBAN AIR POLLUTION 85

A. Formulation of a Simplified SSV Parameterization Scheme . . . 86
    1. Mass Balance Equations in $V - \delta v$ 91
    2. Mass Balance Equations in δv 93
    3. Formulation of Expressions for Material Fluxes Across $z = \Delta z_0$ 96
    4. Formulation of Expressions for Averaged Concentrations in the Lowest Layer 99

B. Approximations for the Parameters Used in the Simplified Subgrid-Scale Variation Scheme. 102
    1. The Depth of the Lowest Layer, Δz_0 102
    2. The Parameters λ_- w_+, w_-, and ξ. 106
    3. The Vertical Turbulent Velocity, $\overline{w^2}$ 107
    4. The Fractional Area of Updrafts, λ_+. 108
    5. The Entrainment Velocity, ν 108
    6. The Plume Volume Fraction, ζ 109

C. Comments 112

V RESTORATION OF POINT SPATIAL RESOLUTION TO GRID MODELS OF URBAN AIRSHED POLLUTION 113

A. Formulation of a Stochastic Microscale Model for Second-Order Reactants 118
    1. The Scaling Constants ν_i 126
    2. Generating the Random Turbulent Velocity Component $\underline{u}'$ . . 127

V RESTORATION OF POINT SPATIAL RESOLUTION TO GRID MODELS OF URBAN AIRSHED POLLUTION (Continued)

B. An Integral Equation Model of the Far-Field 131
Microscale Point Source Concentration Distribution 138

C. A Methud of Solving the Integral Equations Governing the Steady-State A'' and B'' Distributions. 138

VI MODELING POLLUTANT CONCENTRATIONS IN THE VICINITY OF A ROADWAY 152

A. Background 152

B. ROADWAY 1 160

1. Governing Equations 160
2. Formulation of the Parameters $\bar{x}$, $\bar{z}$, σ_x, σ_z, ρ_{nn}, and ρ_{nm} for an at-Grade Roadway 165

C. ROADWAY 2 170

VII SUMMARY 172

APPENDICES

A MULTIJET REACTOR DATA 175

B A PARAMETERIZATION OF TWO-PARTICLE SUBGRID-SCALE VELOCITY FLUCTUATIONS FOR USE IN DERIVING LAGRANGIAN TURBULENCE STATISTICS FROM EULERIAN TURBULENCE MODELS 178

C LAGRANGIAN ANALYSIS OF A PASSIVE SCALAR IN TURBULENT FLUID--PART 2 193

D LAGRANGIAN ANALYSIS OF NONLINEAR CHEMICAL REACTIONS IN TURBULENT FLUID 246

REFERENCES 290

ILLUSTRATIONS

1 Comparison of the K_z Profiles and Performance Index Values Given by Algorithms D and P 8

2 K_z Profiles and Performance Index Values for Algorithms D and P for the Problem Described by Eqs. (8) Through (11) . . 12

3 Comparison of the K_z Profiles and Performance Index Values Given by Algorithms D and P for an Initial Guess of $K_z(z) = 0.2z^2$ with Algorithm D Extended to 60 Iterations 13

4 K_z Profiles and Performance Index Values Produced by Algorithms D and P When Applied to the Mean Concentration Field for the Unstable Case $z_i/L = -4.5$ 15

5 Mean Material Concentration Calculated from Eq. (2) Using an Expression for the Density Function p Derived from Numerical Turbulance Data, Where the Source Height $z_s = 30$ m, Inversion Height $z_i = 1150$ m, $w_* = 1.9$ m/sec, and $\bar{u} = 2.6$ m/sec. 20

6 Percentage Deviation (100ε) from the Mean Concentration Field of the Solution of the Diffusion Equation [Eq. (3)] Obtained Using the K_z Profiles in Figure 4 21

7 Optimal K_z for Source Height $z_s/z_i = 0.025$ for Two Different Stabilities 25

8 Mean Material Concentration Calculated from Eq. (2) Using an Expression for the Density Function p Derived from Numerical Turbulence Data, Where the Source Height $z_s = 300$ m, Inversion Height $z_i = 1150$ m, $w_* = 1.9$ m/sec, and $\bar{u} = 2.6$ m/sec 27

9 Percentage Deviation (100ε) from the Mean Concentrations Shown in Figure 8 of the Solution of the Diffusion Equation [Eq. (3)]. 28

10 Optimal Diffusivities Obtained for the Same Stability ($z_i/L = -1100$) but Different Source Heights 30

11 Schematic of Turbulent Mixing. 38

12 Temporal Behavior of λ for Various Values of κ at $\rho = \gamma = 1$ . . . 53

13 Temporal Behavior of λ for Various Values of ρ at $\kappa = 100$ and $\gamma = 1$ 50

14 Comparison of the Predictions of the Closure Model with Chemical Reactor Data for Various Values of A_0 and β with $k = 1.24 \times 10^4$ ℓ/mole·sec 58

15 Comparison of the Predictions of the Closure Model with Chemical Reactor Data, the Predictions of the Kattan and Adler (1967) Model, and the Solution of the Homogeneous Model, Eq. (76), with $k = 1.24 \times 10^4$ ℓ/mole·sec, $A_0 = 0.00658$ mole/ℓ, and $\rho = 2.52$ 58

16 Comparison of the Predictions of the Closure Model with the Predictions of the Mao and Toor (1970, 1971) Models with $k = 8.32 \times 10^3$ ℓ/mole·sec, $A_0 = 0.0333$ mole/ℓ, and $\rho = 1.0$ 59

17 Sensitivity of the Closure Model to Changes in the Damkohler Number κ When $k = 8.32 \times 10^3$ ℓ/mole·sec, $A_0 = 0.034$ mole/ℓ, and $\rho = 1.5$ 59

18 Comparison of the Predictions of the Closure Model with Chemical Reactor Data, the Predictions of the Yieh (1970) Model, and the Solution of the Homogeneous Model, Eq. (76), with $k = 0.832 \times 10^4$ ℓ/mole·sec, $A_0 = 0.3363$ mole/ℓ, and $\rho = 1.5$. . 60

19 Comparison of the Predictions of the Closure Model with the Toor (1962) Model, and with Chemical Reactor Data for Very Rapid Reactions. 60

20 Calculated Form of the Mixing Parameter ζ_B, Normalized by Its Initial Value $\zeta_B(0)$, as a Function of Travel Time t for Two Source Heights 77

21 Comparison of the Predicted NO Conversion F_A (Solid Curves) with Observations (Circles) and the Prediction of a Homogeneous Gaussian Model That Ignores Turbulent Concentration Fluctuation Effects (Dashed Line) 81

22 Schematic Illustration of a Lowest Layer Cell Containing a Single Line Source 87

23 A Nested Grid System for Use in Evaluating the Integral Equations Governing A" and B". 142

24 A Three-Dimensional View of the Grid Shown in Fgiure 23 143

25 Quadratic Representation of a Function f(x) 143

26 An Expanded Series of y-z Meshes for Solving Eqs. (312) and (313) . 150

27 Schematic Illustration of the Relationship Among the ROADWAY Models Described in This Report and EPA's HIWAY Model 154

28 Coordinate System Used in the ROADWAY Model To Compute Concentrations at an Arbitrary Receptor Site 156

29 Averaging Area (ℓ_x,ℓ_y) Used in the Definition of $\langle \bar{c}(\underline{r}_r,t)\rangle$ 162

30 Example of a Roadway Depression of Arbitrary Width and Depth 171

A-1 Extent of Reaction of a Very Rapid Stoichiometric Reaction for Two Different Jet Reynolds Numbers 177

C-1 Schematic Summary of the Model Equations for the Mean, Variance, and Correlation of the Displacement of a Pair of Particles in Stationary, Homogeneous Turbulence 238

C-2 Comparison of the Nondimensionalized Root-Mean-Square Particle Displacement σ^* Given by the Model Equation (C-109) with Empirical Data as a Function of Nondimensional Distance x^* from the Point of Release 238

C-3 Comparison of the Predicted Normalized Root-Mean-Square Concentration Fluctuation Γ_0 with Observations 241

D-1 Profiles of the Nondimensionalized Function β for Three Different Turbulence Regimes 285

TABLES

1 Summary of Expressions for the Mixing and Reaction Parameters ζ_A, ζ_B, and λ 51

C-1 Experimental Conditions of Four Data Sets 236

I INTRODUCTION

This report describes our continued efforts on a research project begun in mid-1975 under contract to the Environmental Protection Agency (EPA) to develop techniques for modeling the microscale phenomena associated with urban air pollution. In this context, the term "microscale" refers to all phenomena that have characteristic temporal or spatial scales that are too small to be resolvable in an explicit, deterministic manner in urban-scale air pollution models. Examples of microscale phenomena include turbulent diffusion, turbulent concentration fluctuations, and subgrid-scale variations in the time-averaged concentration field. The reader is referred to Chapter I of Lamb (1976) for a discussion of the various microscale phenomena we have considered, the relationships among them, and the quantities calculated in urban-scale air pollution models.

Although it is obvious that some microscale phenomena have a major impact on the quality of air pollution model predictions, the effects of others are very difficult to assess. For example, it has long been realized that the grid-cell-averaged concentrations provided by an air pollution model are not comparable with measurements made at a fixed receptor if the concentrations at that receptor have been influenced by a point or line source plume that is smaller than the grid cell dimensions. Developing a method of modifying grid model predictions to compensate for these subgrid-scale concentration variations is one of the problems we have considered in this project (see Chapters IV and V). In studying turbulent concentration fluctuations, we investigated the question of whether this phenomenon affects concentration levels of reactive pollutants only within the immediate vicinity of a source or whether it has a lasting effect reflected by the concentration distributions far from the source. This question would be rather straightforward to answer if the chemical kinetics were simple. For example, if we were considering a plume of species A emitted into a uniform field of B and the only reaction possible was A + B → C, where C is a stable product, it is obvious that far from the source all A would be converted to C regardless of whether concentration fluctuations were present. Fluctuations would affect the rate at which A is converted to C, and this in turn would affect the concentration levels near the source; but the presence of fluctuations that die out in time (as turbulence induced fluctuations do) cannot alter the final outcome of all A being converted to C.

The situation would be different if in addition to A + B → C another reaction, A + B → E, occurred, where E is a stable product and both B and D are present in the ambient field. In this case, fluctuations in the concentrations of B and D would permanently alter the ratio of the product concentrations C and E. In other words, if concentration fluctuations caused more particles of A to contact B particles than D particles during their flights, then more particles of C would be produced than E; therefore, both the near- and far-field concentrations would be affected.

In the case of photochemical air pollution, the system of chemical reactions is much too complicated to cast into one of the simple forms just discussed, and consequently, the impact of turbulent concentration fluctuations remains to a large extent unknown. A quantitative assessment of this problem would require numerical model studies that we have not yet performed. In this report, we have tentatively adopted the position that concentration fluctuations affect the near-source field only. Further discussion of the effects of concentration fluctuations on second-order chemical reactions and a method for modeling them is contained in Chapter III. The analogous problem that arises from subgrid-scale variations in the mean concentration distributions is discussed in Chapter IV.

Chapter II describes further studies of diffusion in the unstable planetary boundary layer and attempts to parameterize diffusion using "optimal" eddy diffusivities. This work is a continuation of that reported in Lamb, Chen, and Seinfield (1975) and Lamb (1976).

The diffusivity algorithms presented in Chapter II and the scheme for parameterizing subgrid-scale concentration variation effects developed in Chapter IV have been incorporated in the SAI airshed model. The model developed in Chapter III to treat turbulent concentration fluctuation effects in reactive plumes has also been implemented. However, the roadway model described in Chapter V and the point source resolution model formulated in Chapter VI have not yet been translated into computer model forms. We plan to complete this final phase of the work in the months ahead.

II PARAMETERIZATION OF TURBULENT MATERIAL FLUXES USING "OPTIMAL" EDDY DIFFUSIVITIES

R. G. Lamb
D. Durran

Under a previous contract with the EPA, we explored the possibility of using a numerical turbulence model in conjunction with Lagrangian diffusion theory and control theory techniques to determine "optimal" eddy diffusivity profiles for use in air pollution models (Lamb, Chen, and Seinfeld, 1975). Owing to limitations in the data base upon which those studies were founded, several important questions regarding the adequacy of the diffusivities derived remained unanswered:

- > The manner in which the optimal diffusivities depend on atmospheric stability.
- > The degree to which the profiles depend on source height.
- > The uniqueness of the results--are the "optimal" diffusivities merely an artifact of the procedure used to calculate them, or do they truly optimize the accuracy of the classical diffusion equation as a model of turbulent diffusion?

In this chapter, we discuss each of these questions in light of recent studies. Before proceeding with that discussion, we briefly review the method used to compute the optimal diffusivities [see Lamb, Chen, and Seinfeld (1975) for details].

The form of the diffusion equation that represents the cross-wind integrated concentrations arising from a continuous point source is:

$$\frac{\partial\bar{c}}{\partial t} + \bar{u}(z)\,\frac{\partial\bar{c}}{\partial x} = \frac{\partial}{\partial z}\,K_z\,\frac{\partial\bar{c}}{\partial z} + Q\delta(z - z_s)\,\delta(x - x_s) \quad , \qquad (1)$$

where

δ = the delta function,
(x_s,z_s) = the source location,
Q = the source emissions rate,
$\bar{c}$ = the cross-wind integrated concentration,
$\bar{u}$ = the mean wind speed,
K_z = the vertical component of the eddy diffusivity.

Equation (1) ignores diffusion in the direction of the mean flow; the adequacy of this assumption is discussed later. The Lagrangian counterpart of Eq. (1) is

$$\bar{c}(x,z,t) = \int_0^t p(x,z,t|x_s,z_s,t')\,Q(t')\,dt' \quad , \qquad (2)$$

where $p(x,z,t|x_s,y_s,t')$ is the probability density that a particle released from (x_s,y_s) at time t' will be found at (x,y) at time t. The first step in computing the optimal K_z profile is to determine the density function p that enters in Eq. (2). This task is accomplished by releasing particles in a numerically simulated turbulence field and creating an ensemble of particle trajectories from which p can be determined. Once the form of p has been established, Eq. (2) is solved for $\bar{c}(x,z,t)$. This field and the wind profile $\bar{u}(z)$, which is implicit in p and which is available from the turbulence model, are substituted into Eq. (1), and the resulting equation is "solved" for the diffusivity K_z.

A. THE UNIQUENESS OF THE OPTIMAL DIFFUSIVITIES

Once the wind speed profile $\bar{u}(z)$ and the concentration field $\bar{c}(x,z)$ obtained from Eq. (2) have been substituted into Eq. (1) the resulting functional differential equation must be solved for K_z. The available techniques for solving such equations are all approximate methods, none of which have been rigorously shown to produce unique solutions, i.e., solutions that are independent of the initial guess of the solution. We investigated the uniqueness question by applying our solution technique to problems in which the true K_z profile was known exactly. This task was accomplished with the aid of the analytic solution obtained by Rounds (1955) for the steady-state form of Eq. (1), namely,

$$\bar{u}(z) \frac{\partial \bar{c}}{\partial z} = \frac{\partial}{\partial z} K_z \frac{\partial \bar{c}}{\partial z} + Q\delta(x)\ \delta(z - z_s) \tag{3}$$

with boundary conditions

$$\left.\frac{\partial \bar{c}}{\partial z}\right|_{z=0} = \left.\frac{\partial \bar{c}}{\partial z}\right|_{z=1} = 0 \quad . \tag{4}$$

Rounds obtained a Bessel function series solution of Eqs. (3) and (4) subject to the conditions that the wind speed and diffusivity have the power law forms

$$\bar{u}(z) = az^{\alpha}, \qquad K_z = bz^{\beta} \quad . \tag{5}$$

We evaluated Rounds' solution, in nondimensional form, for the case

$$\bar{u}^* = 60z^* \quad , \tag{6}$$

$$K_z^* = 0.5z^* \quad , \tag{7}$$

where $\bar{u}^*$, K_z^*, and z^* are nondimensional variables. We substituted this solution and Eq. (6) into the nondimensionalized form of Eq. (3)

and solved the resulting functional differential equation using two methods. In the first, Algorithm D, K_z^* was evaluated at each of 20 points equally spaced between the ground ($z^* = 0$) and the top of the mixed layer ($z^* = 1$). In the second method, Algorithm P, only the coefficients of a fourth-order Chebyshev polynomial expansion of K_z^* were determined. The results of each test, grouped according to the initial guess of the diffusivity profile, are displayed in Figure 1. The "performance index" plotted for each test case is the integral over the domain of interest of the square of the difference between the true concentration--in this case, Rounds' analytic solution of Eq. (3)--and the corresponding value obtained from numerical solution of Eq. (3) using intermediate approximations of K_z^*.

It is immediately obvious from Figure 1 that after 20 interations the K_z^* profiles given by Algorithm P are considerably different from those given by Algorithm D and that the latter are particularly sensitive to the initial estimate of K_z^*. In two of the cases shown, the diffusivity profiles predicted by Algorithm D fail by a considerable margin to match the true profile well enough to make the performance index acceptably small. In contrast, Algorithm P shows little sensitivity to the initial guess of K_z, and it produces diffusivity estimates that, when used in the evaluation of the finite difference analog of Eq. (3), yield concentrations that actually agree better with the analytic solution than the corresponding values obtained when the true K_z profile is used. This apparent paradox is attributable to the truncation errors contained in the finite difference representation of Eq. (3), for which the optimal diffusivity given by Algorithm P compensates to some extent.

As a further test and comparison of Algorithms D and P, we applied them to the simple steady-state problem

$$\bar{u} \frac{\partial c}{\partial x} = K_z \frac{\partial^2 c}{\partial z^2} \qquad (8)$$

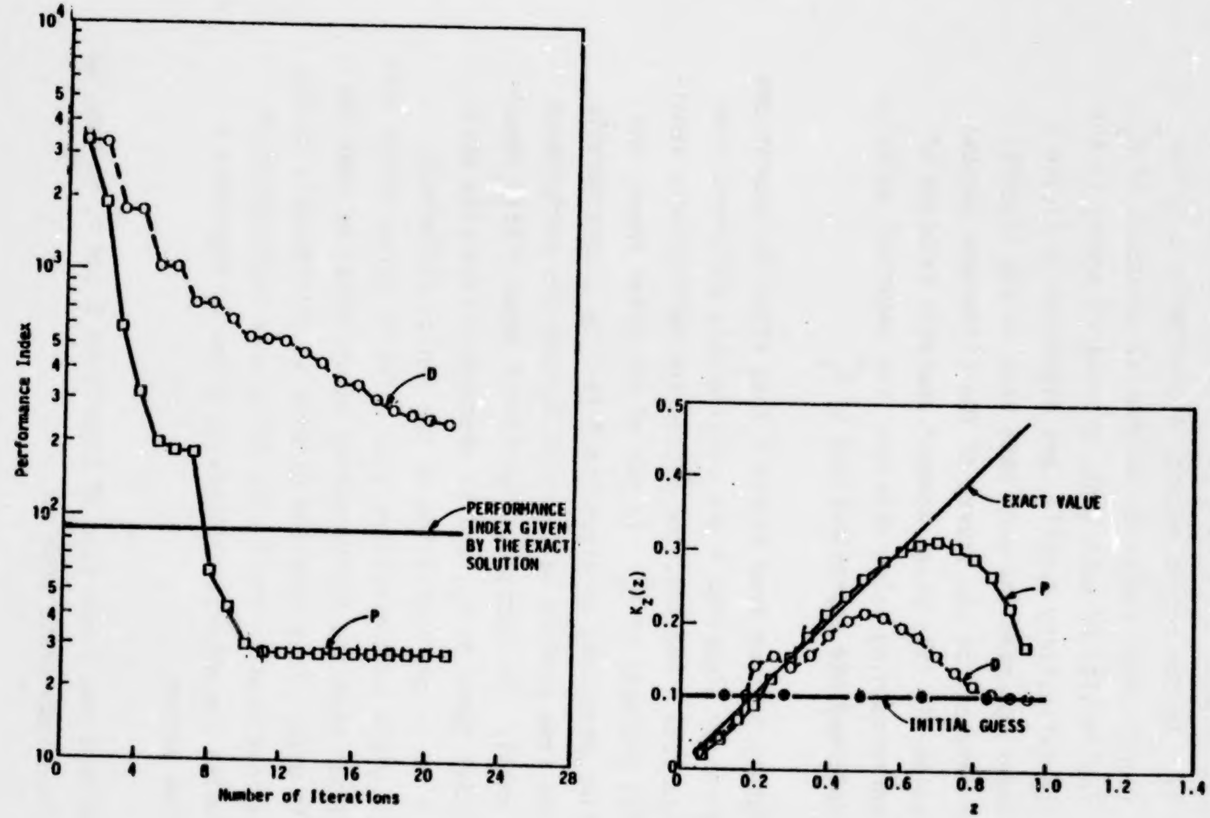

(a) Results for an Initial Guess of $K_z(z) = 0.1$

FIGURE 1. COMPARISON OF THE K_Z PROFILES AND PERFORMANCE INDEX VALUES GIVEN BY ALGORITHMS D AND P

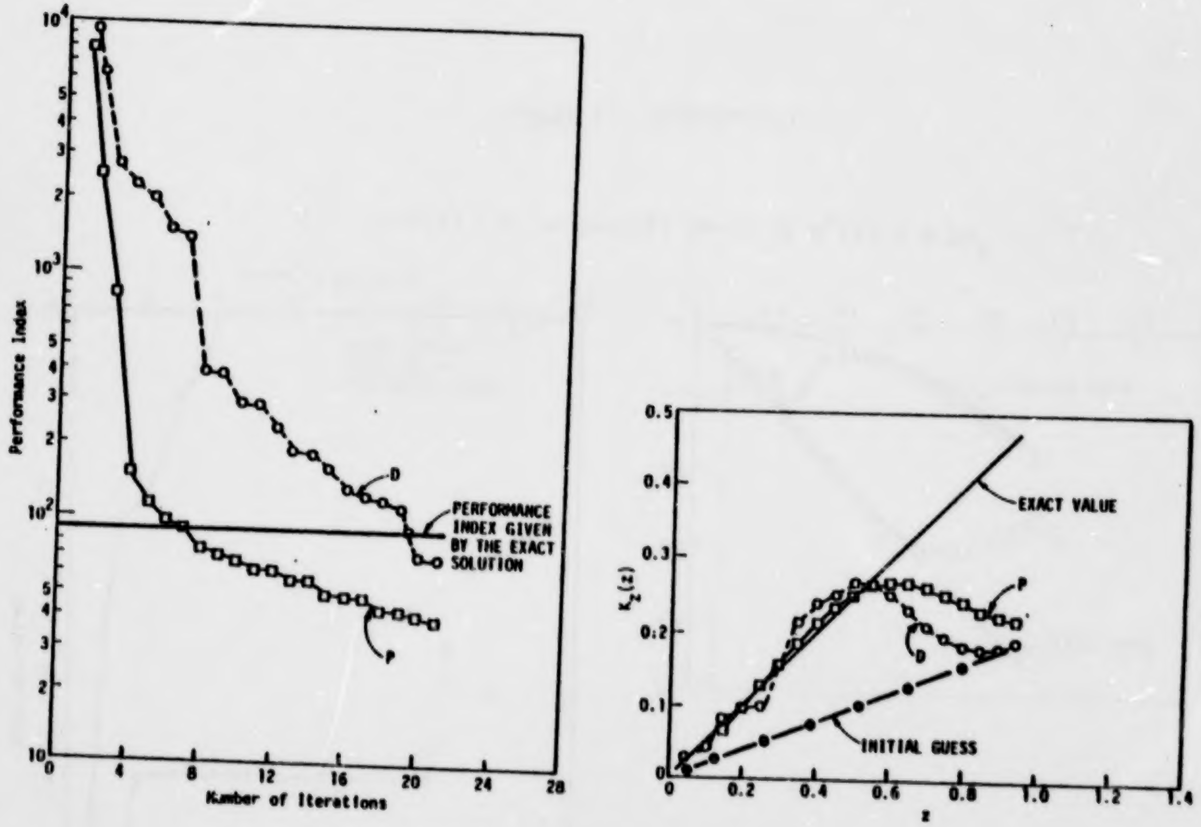

(b) Results for an Initial Guess of $K_z(z) = 0.2z$

FIGURE 1 (Continued)

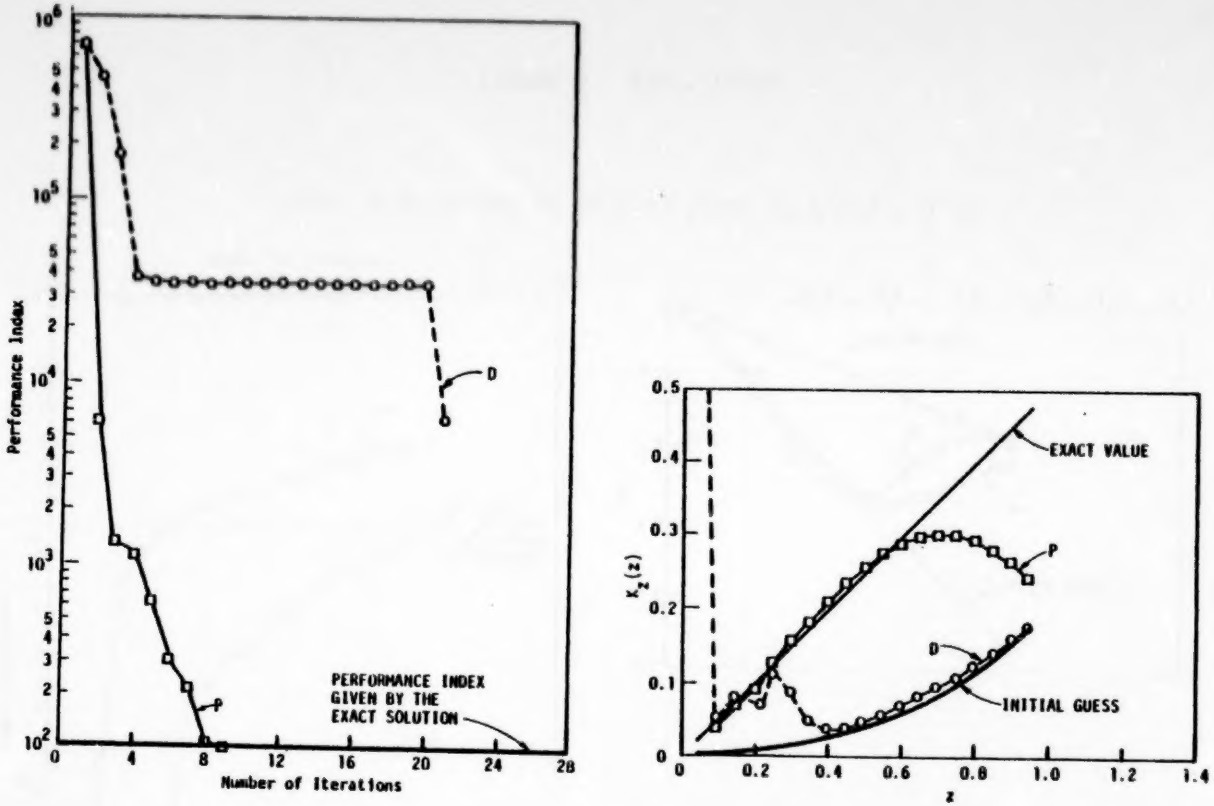

(c) Results for an Initial Guess of $K_z(z) = 0.2z^2$

FIGURE 1 (Concluded)

with the boundary conditions

$$\frac{\partial c(x,0)}{\partial z} = \frac{\partial c(x,1)}{\partial z} = 0 \quad , \tag{9a}$$

$$c(0,z) = 200(1 - \cos 2\pi z) \tag{9b}$$

and with

$$\bar{u} = 10 \quad , \tag{10}$$

$$K_z = \frac{1}{4\pi^2} \quad . \tag{11}$$

The exact solution of Eqs. (8) and (9) is

$$c(x,z) = 200(1 - e^{-x/10} \cos 2\pi z) \quad . \tag{12}$$

We applied Algorithms D and P to Eq. (8), after substituting Eqs. (10) and (12) for $\bar{u}$ and c, respectively, and obtained the K_z results shown in Figure 2. Again, Algorithm P gave results that agree quite well with the true expression, whereas D yielded a K_z profile that is strongly tied to the initial guess.

The fact that in all cases shown above the performance index of Algorithm D is still decreasing after 20 iterations suggests that after a sufficiently large number of iterations, this algorithm would produce K_z estimates as good as those of Algorithm P. To test this hypothesis, we extended the test run shown in Figure 1(c) out to 60 iterations and obtained the K_z^* results shown in Figure 3. Except for the anomalous K_z value near the ground, the diffusivity profile is a good approximation of the true one up to $z^* \sim 0.8$ and is of the same form as that predicted after 20 iterations by Algorithm P. The performance index achieved after 60 iterations is also close to that attained by Algorithm P.

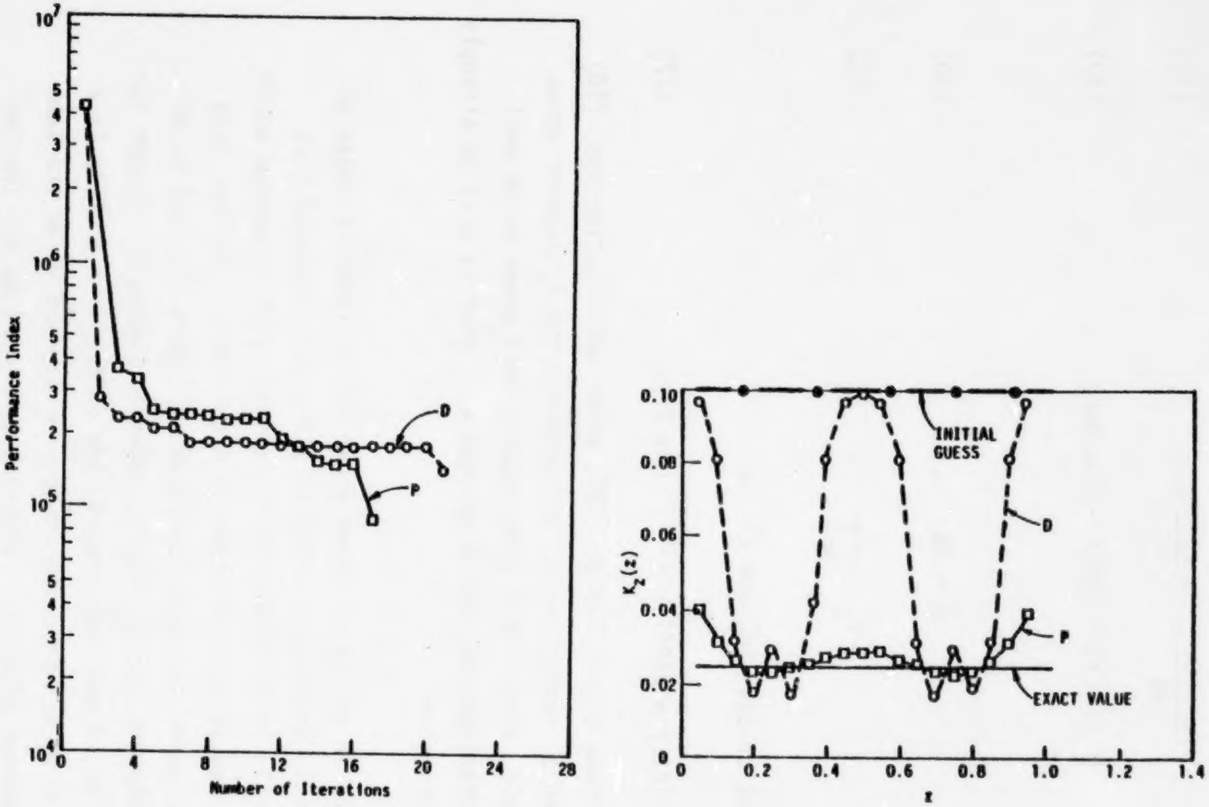

FIGURE 2. K_Z PROFILES AND PERFORMANCE INDEX VALUES FOR ALGORITHMS D AND P FOR THE PROBLEM DESCRIBED BY EQS. (8) THROUGH (11)

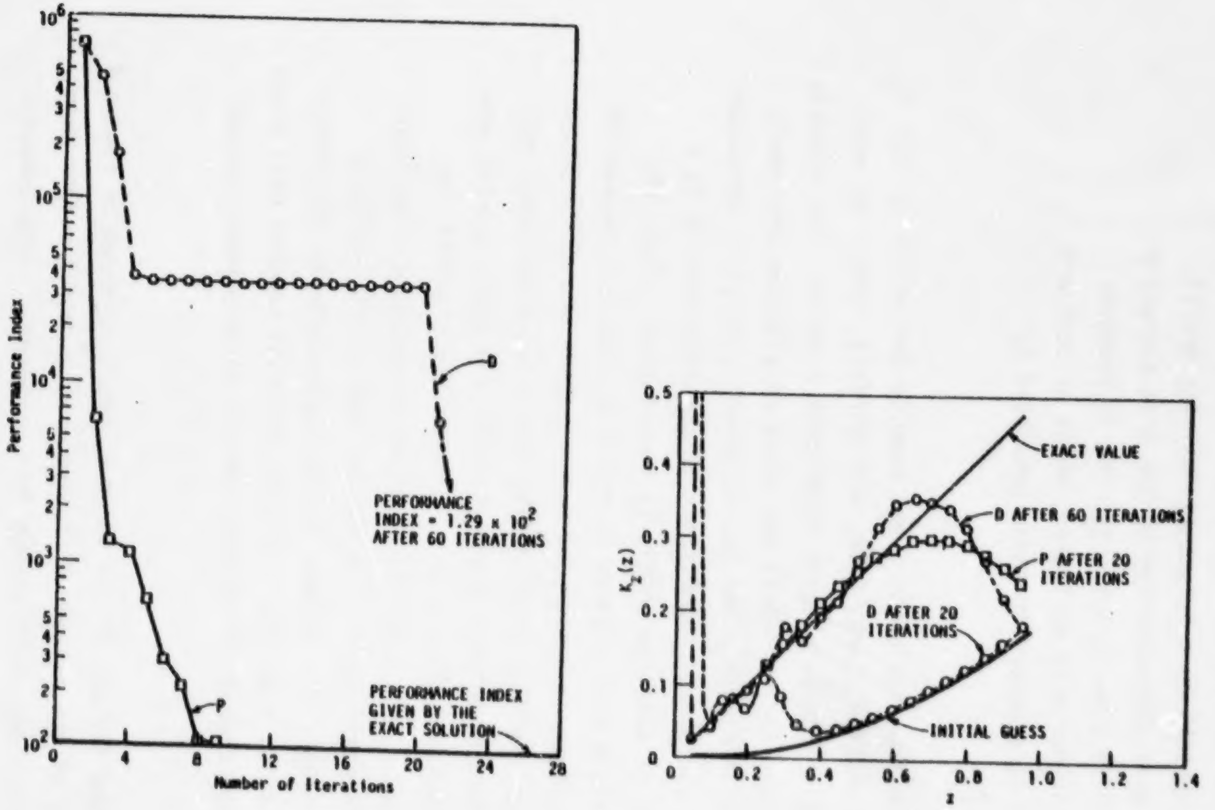

FIGURE 3. COMPARISON OF THE K_z PROFILES AND PERFORMANCE INDEX VALUES GIVEN BY ALGORITHMS D AND P FOR AN INITIAL GUESS OF $K_z(z) = 0.2z^2$ WITH ALGORITHM D EXTENDED TO 60 ITERATIONS

Based on all of the evidence presented above, we conclude that:

> Regardless of the initial K_z estimate, Algorithm P converges rapidly to a unique diffusivity profile that is a good approximation of the true expression.

> Algorithm D is slow to converge, and it produces nonunique diffusivity estimates, which at best are comparable in accuracy to those predicted by Algorithm P.

Since an algorithm similar to D was used to derive the optimal K_z profiles reported earlier (Lamb, Chen, and Seinfeld, 1975), we reperformed those calculations using both Algorithms P and D. The outcomes for the unstable case ($z_i/L = -4.5$) are compared with the previously derived K_z profile in Figure 4 for two different initial K_z estimates. The ability noted earlier of Algorithm P to converge rapidly to a unique diffusivity is displayed again in that figure. Also, the inability of Algorithm D to produce K_z profiles that are independent of the initial estimate is again apparent. Despite the differences in the forms of the profiles predicted by these two algorithms, and despite the differences between these profiles and that reported previously, the performance indices of all three diffusivities are virtually identical. This indicates that in an unstable mixed layer where diffusion is confined below a stable layer aloft, vertical concentration gradients are so weak in the region between the source and the downwind point where the diffusing material becomes well mixed vertically that the concentration distribution is only weakly dependent on K_z.

One noteworthy feature of all three K_z profiles shown in Figure 4 is the occurrence of the minimum diffusivity at $z^* \simeq 0.1$ rather than at the ground, where one would expect it. Apparently, this behavior

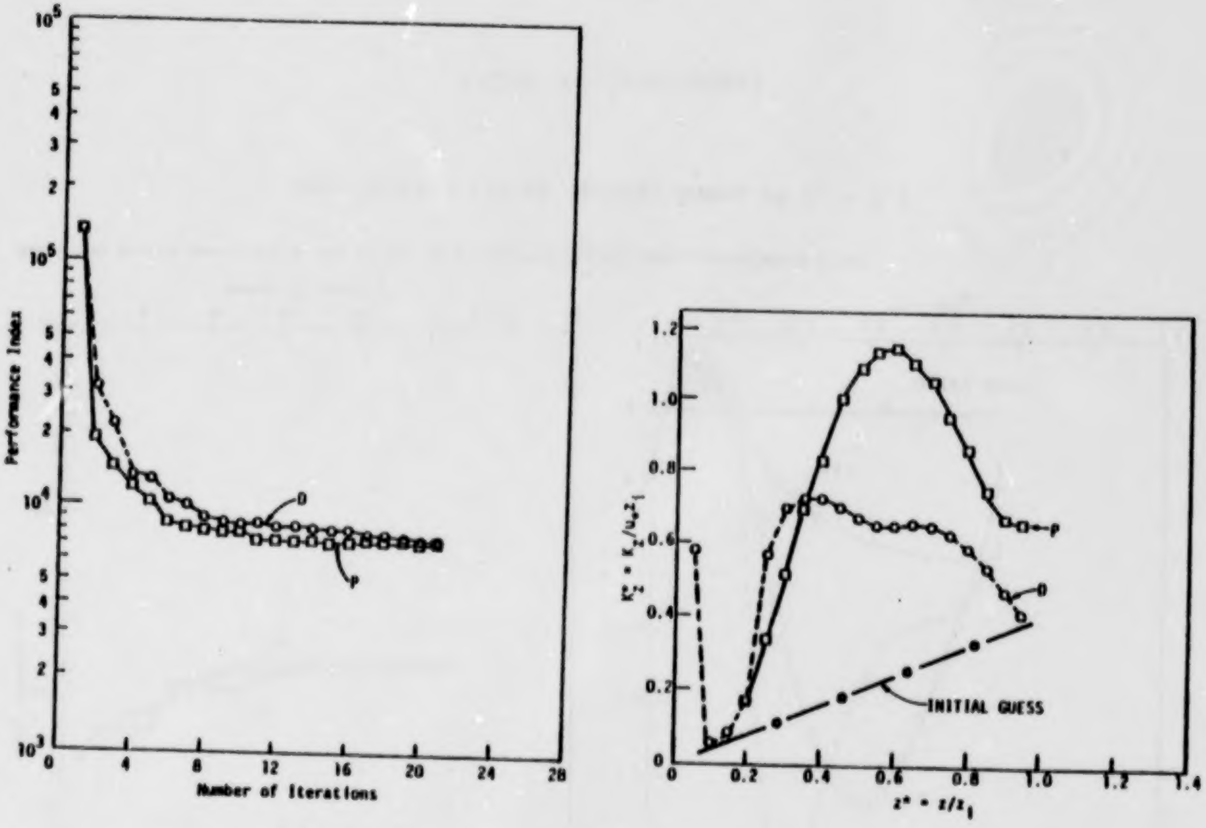

(a) Results for an Initial Guess of $K_z^* = 0.4z^*$

FIGURE 4. K_z PROFILES AND PERFORMANCE INDEX VALUES PRODUCED BY ALGORITHMS D AND P WHEN APPLIED TO THE MEAN CONCENTRATION FIELD FOR THE UNSTABLE CASE $z_i/L = -4.5$

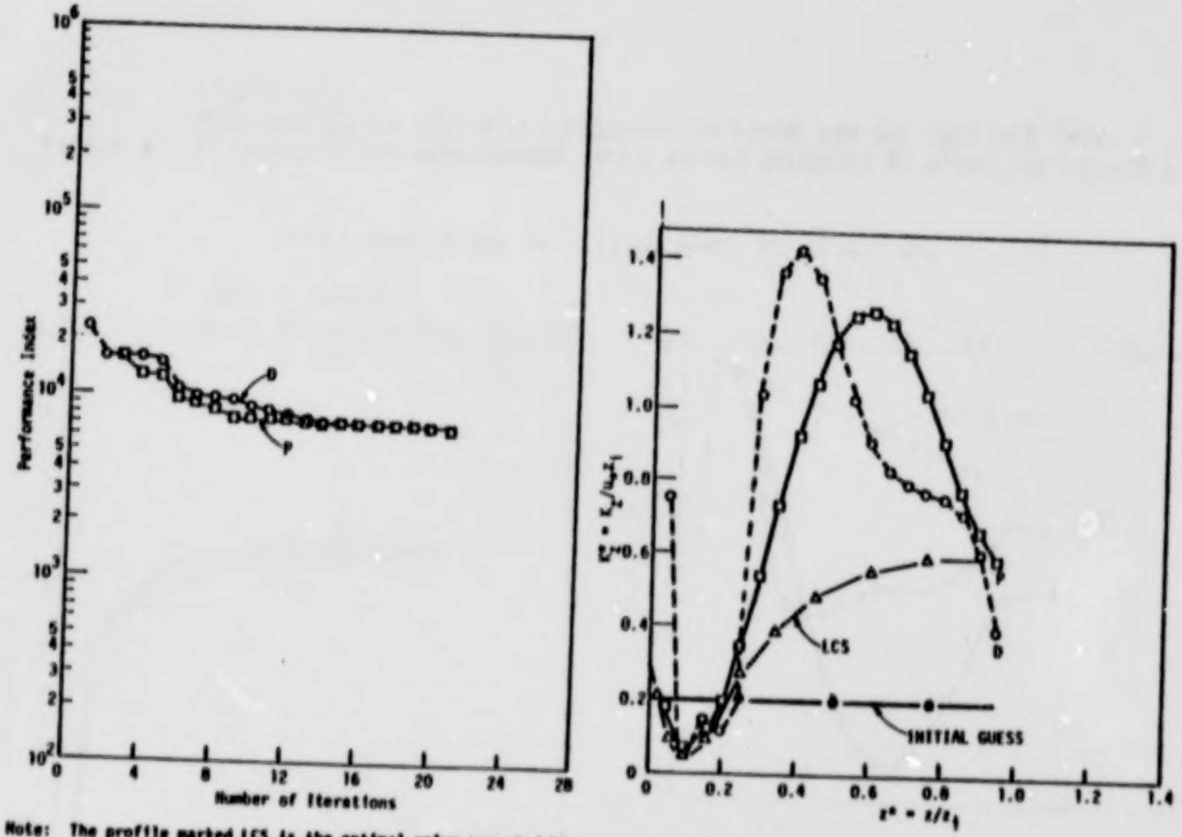

Note: The profile marked LCS is the optimal value reported by Lamb, Chen, and Seinfeld (1975).

(b) Results for an Initial Guess of K_z = 0.2

FIGURE 4 (Concluded)

is the result of an attempt by the optimal K_z algorithm to compensate for discrepancies between the mixing length model of turbulent diffusion, upon which K_z is defined, and the true character of diffusion in the unstable boundary layer, at least insofar as Deardorff's model depicts it.

Two other aspects of the previously reported diffusivity (Profile LCS in Figure 4) that raised questions are its magnitude and its increase to a maximum at the very top of the mixed layer. The magnitude of the LCS diffusivity in the upper portion of the unstable mixed layer is about three times larger than comparable diffusion coefficients proposed by other investigators [the reader is referred to Jerskey et al. (1976) for these comparisons]. Empirical data suitable for assessing the validity of these diffusivity estimates are available from the laboratory studies by Willis and Deardorff (1974, 1975) and Deardorff and Willis (1974, 1975). These papers do not give an explicit estimate of K_z; but if we use as an estimate of the order of magnitude the well-known relationship

$$\sigma_z^2 \sim K_z t \quad , \tag{13}$$

where σ_z is the rms spread of particles after a (long) time t, then we obtain from the σ_z data given in Deardorff and Willis (1974)

$$K_z \sim \frac{1}{3} w_* z_i \quad , \tag{14}$$

where w_* is the convective velocity scale given by

$$w_* = \left(-\frac{1}{k}\frac{z_i}{L}\right)^{1/3} u_* \quad , \tag{15}$$

z_i is the mixed layer depth, L the Obukhov length, k the von Karman constant, and u_* is the friction velocity. The maximum value of the

LCS diffusivity K_z is $0.26w_*z_i$. Thus, empirical data support the magnitude of the LCS diffusivity.

In contrast to the LCS diffusivity shown in Figure 4, most other proposed profiles reach a maximum near the middle of the mixed layer and decrease above that. The diffusivity expressions predicted by Algorithms D and P support the latter behavior. But since the amplitude of the diffusivity is so large, concentration gradients are quite small, and consequently, the material distribution is only weakly dependent on the exact shape of the diffusivity profile. This is evident in Figure 4 in that the three K_z profiles shown have markedly different shapes yet virtually identical performance indices.

We also applied Algorithms D and P to the concentration data from the neutrally stable planetary boundary layer simulation of Deardorff and obtained essentially the same diffusivity expression as that reported in Lamb, Chen, and Seinfeld (1975). We conclude from this and the findings cited above that the K_z profiles reported in Lamb (1976) and in Lamb, Chen, and Seinfeld (1975), are not artifacts of the mathematical process that was used to derive them because essentially the same profiles were obtained regardless of the form of the initial guess of the profile or the technique used. However, we have found that under unstable conditions, the overall accuracy of the diffusion equation is only weakly dependent on the exact shape of the K_z profile. This conclusion does not apply if one is considering the concentration distribution very close to the source, say, within a distance $x \approx 0.5z_i(\overline{u}/w_*)$. In our study, we dealt with the field over the region within $x = 1.1z_i(\overline{u}/w_*)$ of the source, but it is clear that as the size of the region of interest increases beyond the point where material becomes well mixed vertically [about $x = 1.6z_i(\overline{u}/w_*)$] dependence on K_z eventually vanishes.

B. THE RANGE OF ATMOSPHERIC STABILITY TO WHICH THE OPTIMAL K_z PROFILES APPLY

Having examined the procedure used to derive the optimal diffusivity, we turn now to the question of whether the K_z profile presented earlier for the unstable case is applicable to all unstable conditions. This question is prompted by the finding of Deardorff (1972) that under unstable conditions the vertical velocity variance $\overline{w'^2}(z)$ scales with z_i and the convective velocity scale w_* [see Eq. (15)]. This suggests that the vertical diffusivity K_z should have a universal form when expressed in units of $w_* z_i$.

To test this hypothesis, we obtained velocity data from a simulation by Deardorff's latest model [see Deardorff (1973)] of Day 33 of the Wangara study, in which $z_i/L \approx -1100$. (Recall that in the unstable case discussed earlier, $z_i/L = -4.5$.) From these data, we calculated the Lagrangian turbulence statistics needed to predict the mean concentration field for a point source. The resulting concentrations are shown in Figure 5.

Next, using the optimal K_z profile derived for the case $z_i/L = -4.5$ (the profile labeled P in Figure 4), we solved the diffusion equation [Eq. (3)] to determine how closely the solution would compare with the "observed" values given in Figure 5. The results are presented in Figure 6(a) in the form 100ε, where

$$\varepsilon = \frac{c_0(x,z) - c_D(x,z)}{c_0(x,z)} \quad , \tag{16}$$

where c_0 is the field shown in Figure 5 and c_D is the solution of the diffusion equation. The isopleths shown in Figure 6(a) can be interpreted in lines of constant percentage error. For comparison, we have plotted in Figure 6(b) the corresponding error field, i.e., 100ε, that we obtained in the earlier study. Comparison of Figures 6(a) and 6(b) shows that, whereas the former optimal diffusivity yields solutions that are in close agreement

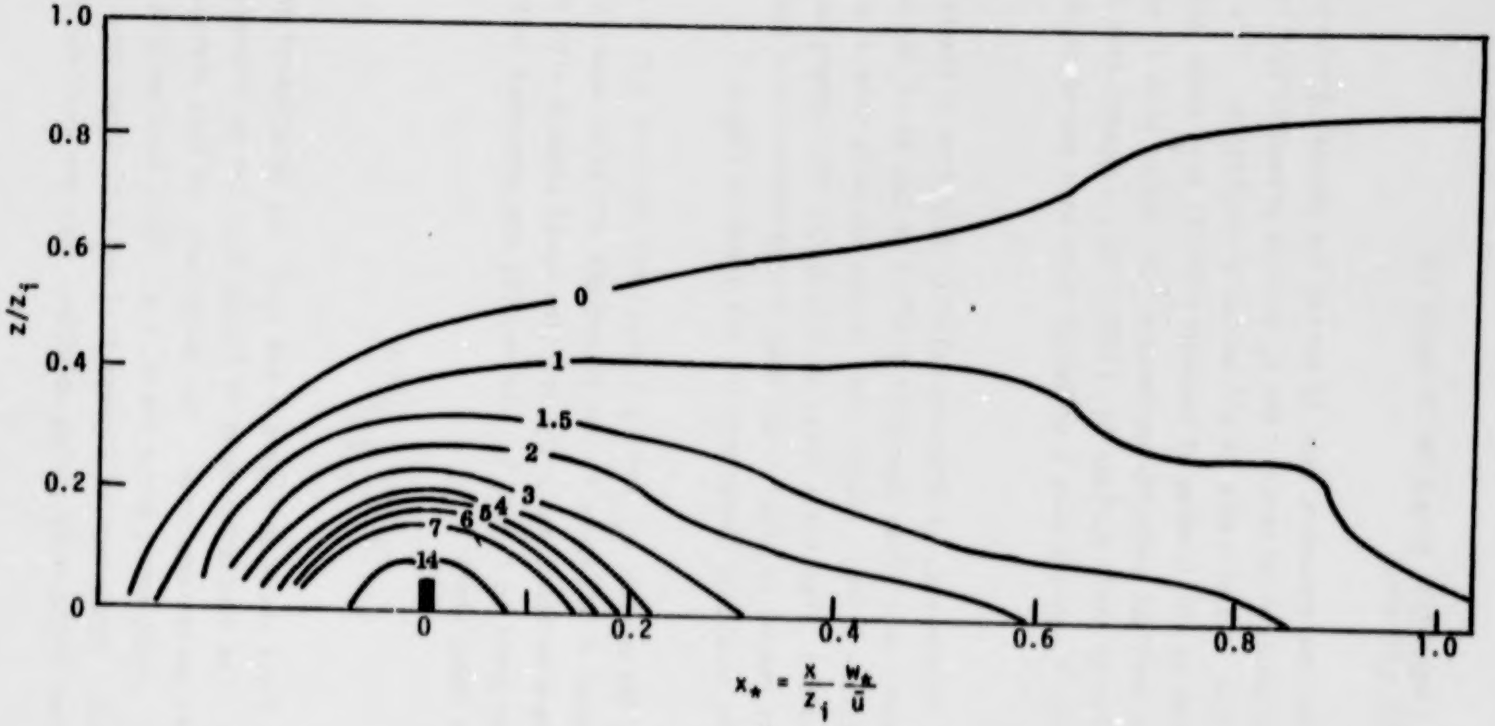

FIGURE 5. MEAN MATERIAL CONCENTRATION CALCULATED FROM EQ. (2) USING AN EXPRESSION FOR THE DENSITY FUNCTION p DERIVED FROM NUMERICAL TURBULENCE DATA, WHERE THE SOURCE HEIGHT z_s = 30 m, INVERSION HEIGHT z_i = 1150 m, w_* = 1.9 m/sec, and $\bar{u}$ = 2.6 m/sec. Concentration values shown have been nondimensionalized by $\bar{C}z_i/Q$, where Q is the source emissions rate (mass/time).

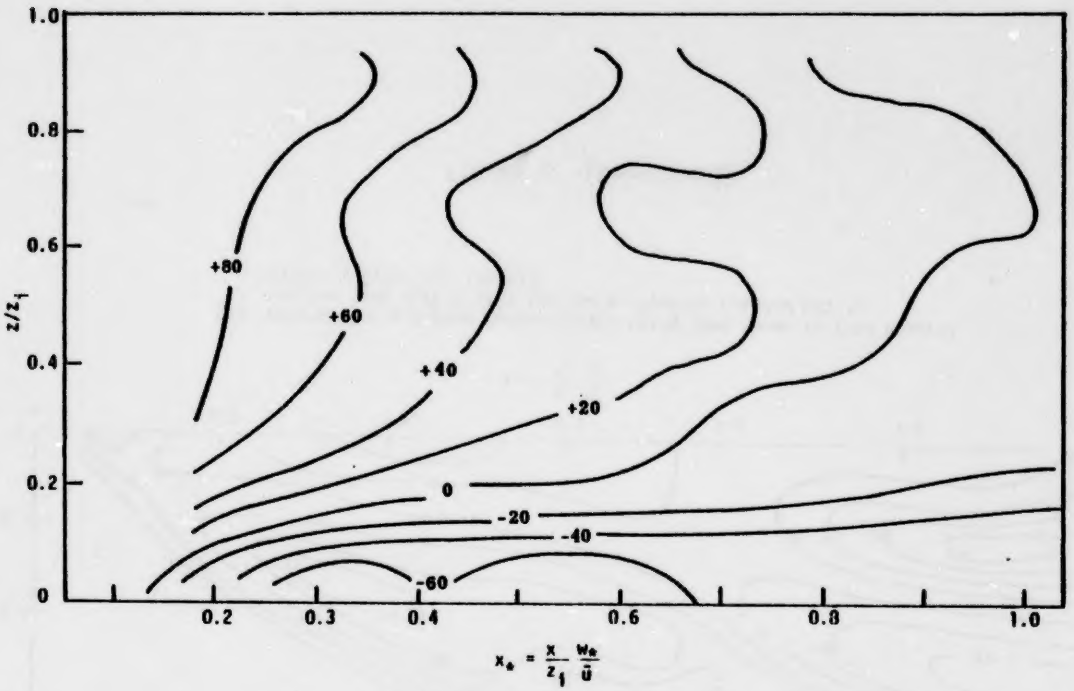

(a) Results Using the Mean Concentration Field in Figure 5 and the K_z Profile Labeled P in Figure 4

FIGURE 6. PERCENTAGE DEVIATION (100 ε) FROM THE MEAN CONCENTRATION FIELD OF THE SOLUTION OF THE DIFFUSION EQUATION [EQ. (3)] OBTAINED USING THE K_z PROFILES IN FIGURE 4

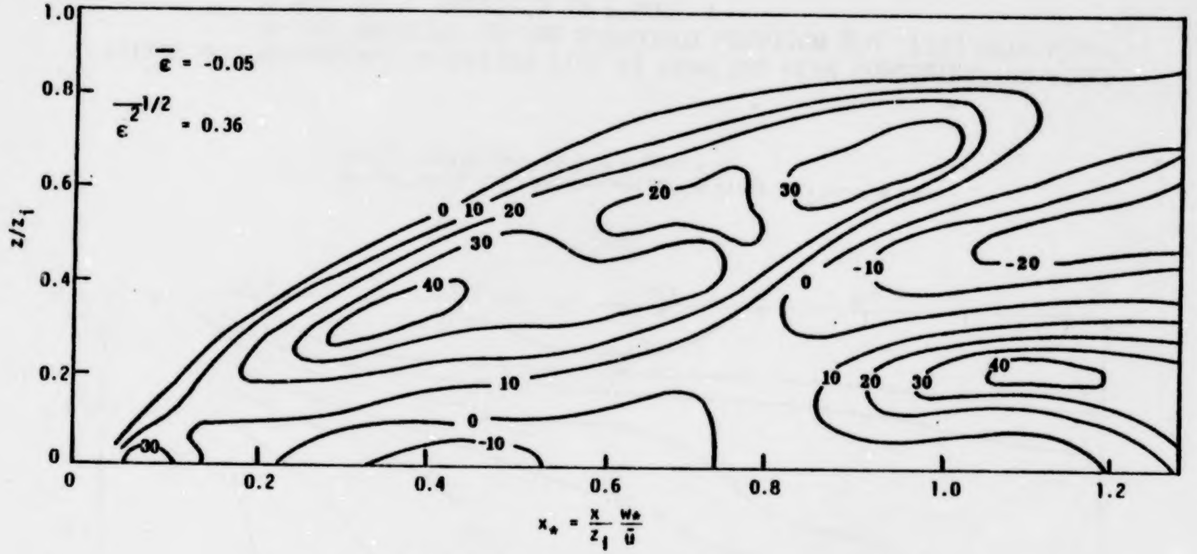

(b) Results Using a Mean Concentration Field (Not Shown in This Report) for the Case $z_i/L = -4.5$ and the K_z Profile Labeled LCS in Figure 4 [see Lamb (1976)]

FIGURE 6 (Continued)

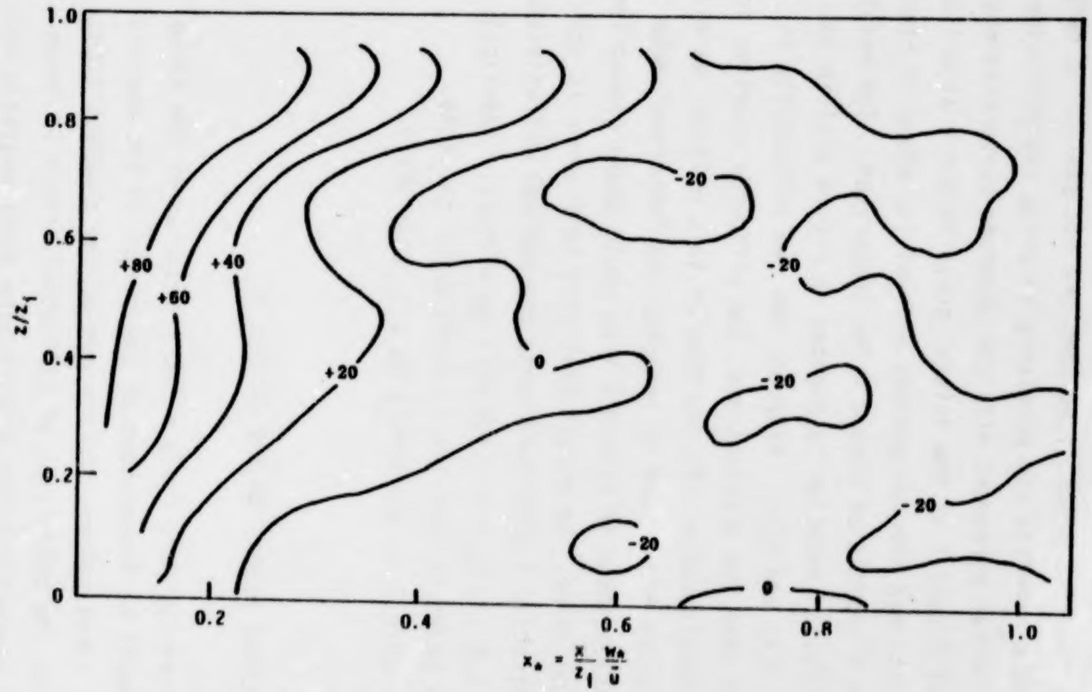

(c) Results Using the Mean Concentration Field in Figure 5 and the Optimal K_z Profile Derived for This Stability ($z_i/L = -1100$)

FIGURE 6 (Concluded)

with the observed mean concentrations at ground level when $z_i/L = -4.5$, the same profile produces concentrations that are larger than those observed at ground level when $z_i/L = -1100$. (Negative values of 100ε in Figure 6 represent areas where the diffusion equation predictions are too large, and positive values of 100ε indicate predictions that are too small.) To determine what changes in the K_z profile are necessary to bring the diffusion equation solution into better agreement with the observed concentrations, we used the P profile of Figure 4 as the initial guess in the P algorithm described earlier and obtained the new optimal diffusivity shown in Figure 7, which also gives the P profile of Figure 4 for comparison. The resulting solution of the diffusion equation is plotted in Figure 6(c) in the same format as Figures 6(a) and 6(b). Although the new diffusivity is only slightly different from the previous one, the diffusion equation predictions are improved considerably. At the time of this writing, we discovered a data error in the model used to generate the "observed" mean concentration distribution shown in Figure 5 that would cause ground-level concentrations to be too large. We expect that once this error is corrected the mean concentration fields (and hence the optimal diffusivities) for the cases $z_i/L = -4.5$ and $z_i/L = -1100$ will be virtually identical. Our conclusion at this point is that the K_z profile for the case $z_i/L = -4.5$ shown in Figure 7 is applicable to all cases where $z_i/L \leq -4.5$.

C. THE EFFECT OF RELEASE HEIGHT ON THE OPTIMAL K_z

If the eddy diffusivity were truly a local property of the turbulent fluid, then K_z would be independent of the height of the sources. But, as noted several times before, the concept of the gradient transfer hypothesis on which the definition of diffusivity rests is inconsistent with observed characteristics of diffusion under unstable conditions. For this reason, we cannot expect the same K_z profile to hold for all release heights. To investigate just how much variability source height induces in the optimal K_z profile, we repeated the experiments discussed in the previous section using a release height of

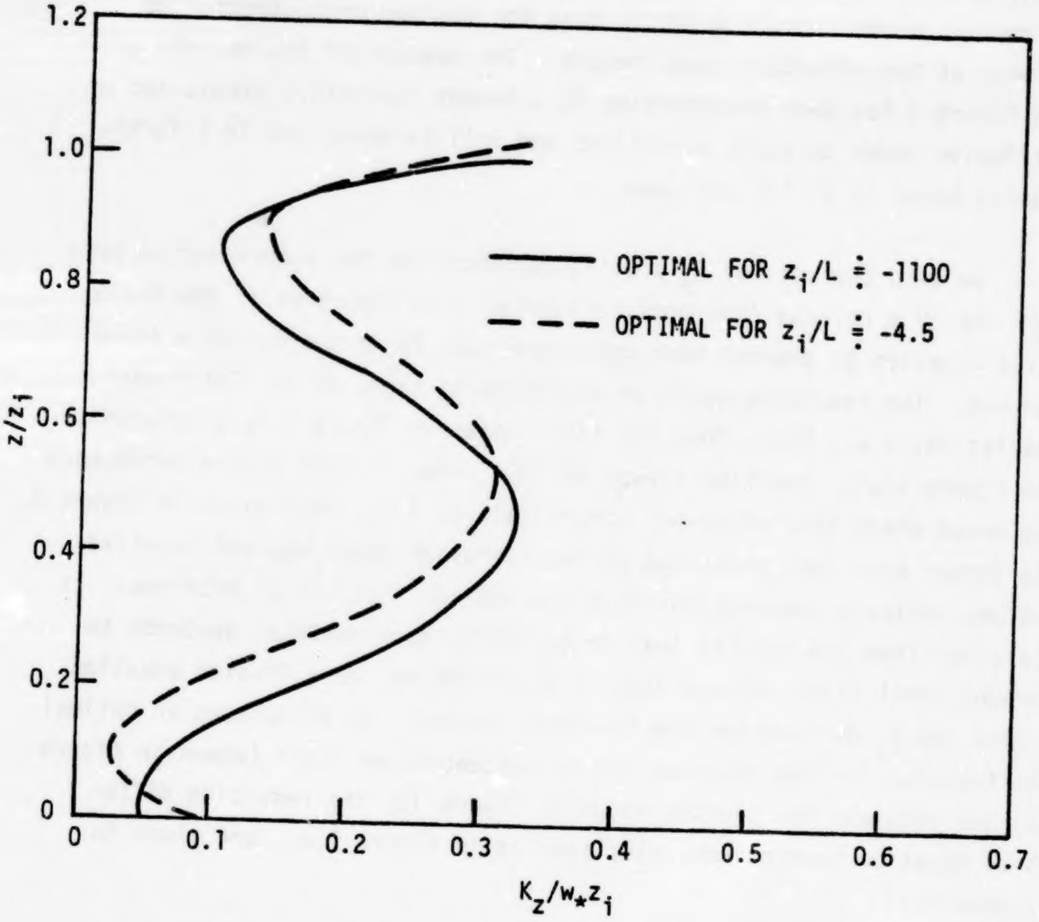

FIGURE 7. OPTIMAL K_z FOR SOURCE HEIGHT $z_s/z_i = 0.025$ FOR TWO DIFFERENT STABILITIES

300 meters. The mean concentration profile calculated for this case is displayed in Figure 8. An interesting aspect of the concentration distribution shown in this figure is the rapid descent of the locus of maximum concentration from the point of release to the ground. The classical plume formula predicts that the maximum concentration is always at the effective stack height. The descent of the maximum shown in Figure 8 has been corroborated in a recent laboratory simulation of diffusion under unstable conditions and will be described in a forthcoming paper by Willis and Lamb.

We used the optimal K_z profile derived from the concentration data for the 30 m release (the profile labeled P in Figure 4) in the diffusion equation to predict mean concentrations for a source 300 m above ground. The resulting solution expressed in terms of its fractional deviation, i.e., 100ε, from the field shown in Figure 8 is displayed in Figure 9(a). Positive values of 100ε shown in this figure correspond to areas where the "observed" concentration, i.e., that given in Figure 8, is larger than that predicted by the diffusion equation, and negative values indicate observations that are smaller than the predictions. It is clear from the results that in actuality more material descends to ground level after release than is predicted by the diffusion equation using the K_z derived for the low-level source. We calculated an optimal diffusivity for the elevated source concentration field (shown in Figure 8) and obtained the profile shown in Figure 10; the resulting diffusion equation predictions, displayed as in Figure 9(a), are given in Figure 9(b).

The marked difference between this new profile and that derived for the low-level source (also shown in Figure 10) indicates that the optimal diffusivities are indeed strongly dependent on the height of the source. As mentioned earlier, this dependence occurs because under unstable conditions turbulent dispersion does not behave in a way that is consistent with the notion that K_z is a local property of the fluid. The gradient

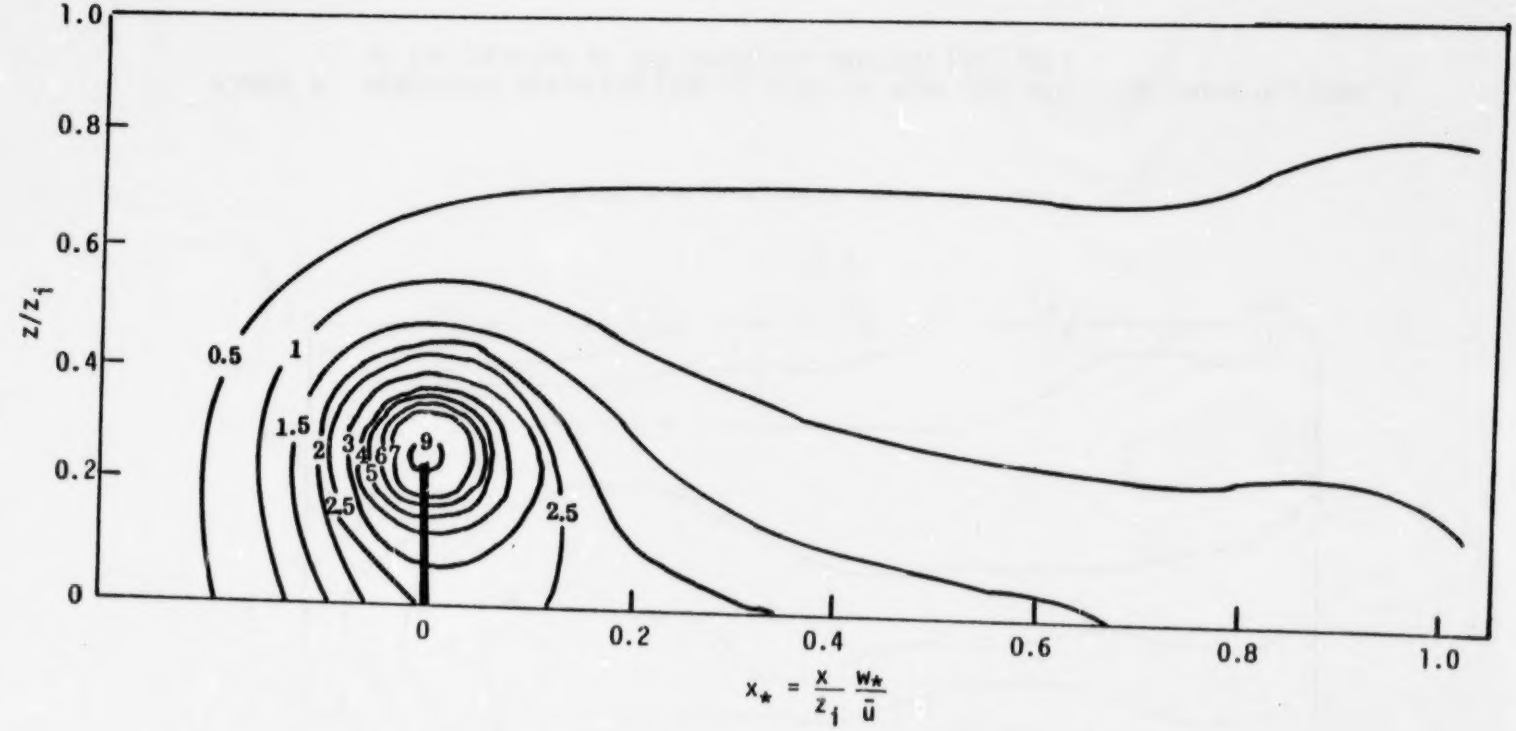

FIGURE 8. MEAN MATERIAL CONCENTRATION CALCULATED FROM EQ. (2) USING AN EXPRESSION FOR THE DENSITY FUNCTION p DERIVED FROM NUMERICAL TURBULENCE DATA, WHERE THE SOURCE HEIGHT z_s = 300 m, INVERSION HEIGHT z_i = 1150 m, w_* = 1.9 m/sec, AND $\bar{u}$ = 2.6 m/sec. Concentration values shown have been nondimensionalized by $\bar{u}z_i/Q$, where Q is the source emissions rate (mass/time).

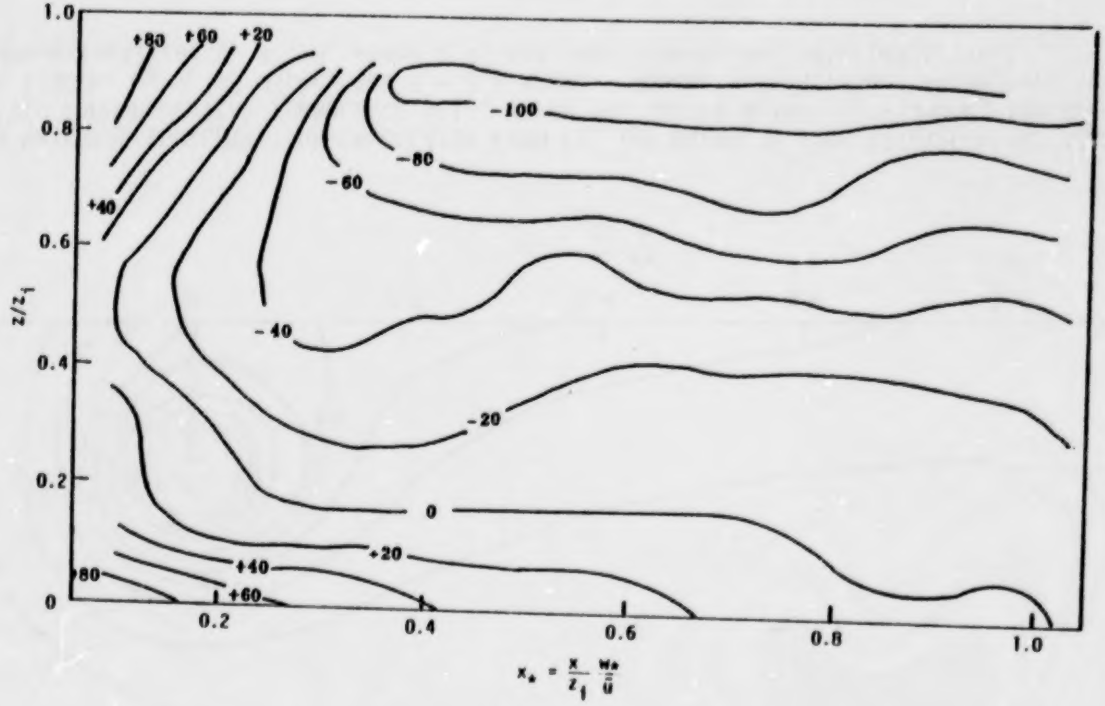

(a) Results Using the K_z Profile Labeled P in Figure 4

FIGURE 9. PERCENTAGE DEVIATION (100 ε) FROM THE MEAN CONCENTRATIONS SHOWN IN FIGURE 8 OF THE SOLUTION OF THE DIFFUSION EQUATION [EQ. (3)]

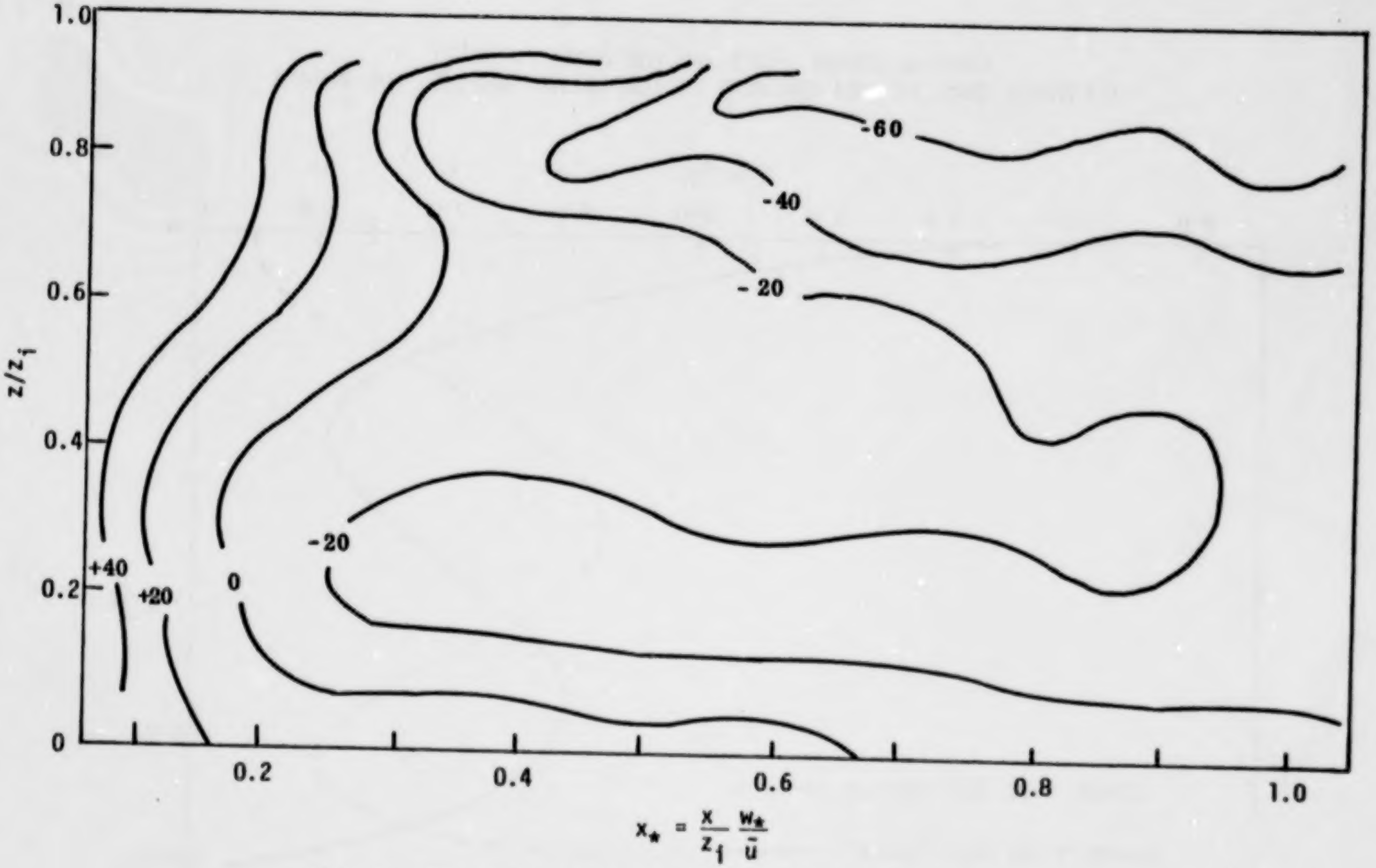

(b) Results Using the Optimal Diffusivity (see Figure 10) for this Stability Case (z_i/L = -1100)

FIGURE 9 (Concluded)

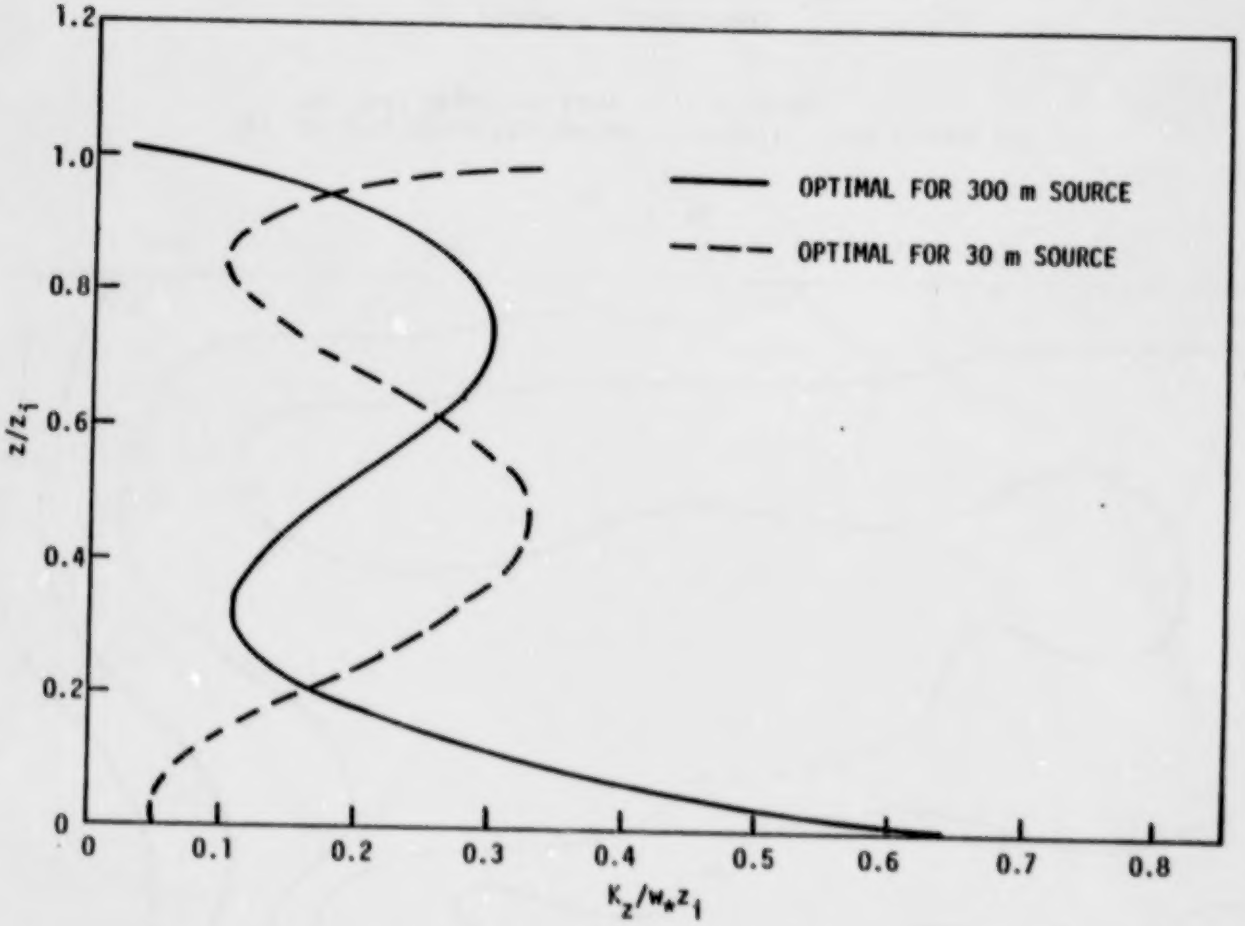

FIGURE 10. OPTIMAL DIFFUSIVITIES OBTAINED FOR THE SAME STABILITY (z_i/L = -1100) BUT DIFFERENT SOURCE HEIGHTS

transfer assumption inherent in the diffusion equation itself is not correct under unstable conditions; but judging from its performance shown in Figures 6(b) and 9(b), this equation provides a viable description of diffusion under unstable conditions as long as the diffusivity K_z is allowed to vary with source height.

This situation immediately raises the question of how to handle multiple sources of various heights in an urban-scale model of photochemical pollution. Either elevated sources can be separated and modeled separately in the manner described in Chapter V (a very time-consuming process involving large numbers of elevated sources) or a single K_z profile obtained by weighting the diffusivity expressions for each source height with the number of sources of that height can be used. Since vertical diffusion is so rapid under unstable conditions, we expect that the exact form used for K_z will be of minor importance in urban-scale pollution models, where grid cells have horizontal dimensions of several kilometers. In fact, under certain conditions a two-dimensional model should suffice. For example, Deardorff and Willis (1974) have found that under unstable conditions material becomes well mixed vertically in a time $t \approx 2z_i/w_*$ after release. In the Los Angeles basin, where we frequently find $z_i \sim 500$ m, $w_* \sim 1$ m/sec, and $\overline{u} \sim 4$ m/sec [see Jerskey et al. (1976)], pollutants become well mixed vertically within a distance of about 4 km from the source. This distance is roughly equal to the horizontal dimensions of grid cells used in air pollution models.

D. RECAPITULATION

We have shown in this chapter that the classical diffusion equation can be made to yield solutions that agree reasonably well with diffusion calculations based on sophisticated turbulence models if the diffusivity K_z is properly chosen. We have introduced a technique for determining the optimal form of K_z and have shown that the technique produces unique expressions. Under unstable conditions, the optimal diffusivity acquires a universal form when scaled with w_* and z_i, but it varies in form with the height of the source. The expressions that we derived for K_z for source heights of z_s/z_i = 0.025 and 0.25 are given below. Each is applicable to all unstable conditions in the range $z_i/L \le -4.5$.

Release Height z_s/z_i	β_0	β_1	β_2	β_3	β_4
0.025	0.178	0.066	-0.067	0.067	0.074
0.25	0.259	-0.134	0.084	-0.156	0.009

In Chebychev polynomial form, the optimal diffusivity is

$$\frac{K_z}{w_* z_i} = \beta_0 + \beta_1 \zeta + \beta_2(2\zeta^2 - 1) + \beta_3(4\zeta^3 - 3\zeta) + \beta_4(8\zeta^4 - 8\zeta^2 + 1) \quad ,$$

where

$$\zeta = 2\frac{z}{z_i} - 1 \quad .$$

III MODELING THE EFFECTS OF TURBULENT CONCENTRATION FLUCTUATIONS ON SECOND-ORDER CHEMICAL REACTIONS IN THE PLANETARY BOUNDARY LAYER

R. G. Lamb
W. R. Shu
J. H. Seinfeld
L. E. Reid

Snapshots of smoke plumes in the atmosphere always reveal an erratic distribution of smoke concentration within the local vicinity of the smoke source. In contrast, time exposures usually show a smooth distribution that closely resembles the classical Gaussian profile. If two such photographs of the same plume were superimposed, the difference in apparent smoke concentration at any point would represent the instantaneous magnitude at that point of the so-called turbulent concentration fluctuation. That is, if A denotes the instantaneous concentration, portrayed by the snapshot, and $\bar{A}$ denotes the mean, revealed by the time exposure, then $A' = A - \overline{A}$ gives the concentration fluctuation.

In situations where nonlinear chemical reactions occur among constituents of the plume or between the plume's constituents and chemical species entrained from the ambient atmosphere, the presence of concentration fluctuations can have a profound impact on the behavior of the mean concentrations of all the reacting species. This can be seen from the form of the equations governing the mean concentrations of two reactant species, A and B, that undergo the bimolecular (nonlinear) reaction

$$A + B \rightarrow \text{Products} \quad . \qquad (16)$$

The instantaneous concentration of A is given by

$$\mathcal{L}A = -kAB \quad , \qquad (17a)$$

where

$$\mathcal{L} \equiv \frac{\partial}{\partial t} + \frac{\partial}{\partial x_i} u_i - \mathcal{D}_A \frac{\partial^2}{\partial x_i \partial x_i} \quad . \qquad (17b)$$

Here u_i denotes the i-th component of the instantaneous fluid velocity, $\mathcal{D}_A$ is the molecular diffusivity of the species A, and k is the rate coefficient of Reaction (16). In a turbulent, incompressible fluid, we find after decomposing A, B, and u_i into the conventional mean and fluctuating components that the mean concentration of A is governed by

$$\frac{\partial \bar{A}}{\partial t} + \bar{u}_i \frac{\partial \bar{A}}{\partial u_i} + \frac{\partial}{\partial x_i} \overline{u_i' A'} = \mathcal{D}_A \frac{\partial^2 \bar{A}}{\partial x_i \partial x_i} - k\bar{A}\bar{B} - k\overline{A'B'} \quad . \qquad (18)$$

Equations analogous to (17) and (18) describe B and $\bar{B}$, respectively.

The effect of concentration fluctuations on the mean concentration of species A is represented by the term $\overline{A'B'}$ in Eq. (18). There have been numerous attempts to develop closure approximations for terms like this [see Brodkey (1975) and Hill (1976) for a review of these works]. Unfortunately, most of the currently available expressions require the solution of rather large systems of differential equations and, therefore, are not readily accessible to air pollution engineers who have limited computer facilities. This chapter presents a model of nonlinear chemical reactions in turbulent fluid that can provide simple expressions for the mean concentrations of reactive pollutants in point source plumes in the planetary boundary layer.

The essential difference between our approach to modeling the fluctuation term $\overline{A'B'}$ and the approaches taken by most other investigators is that we attempt to separate the effects of turbulence and molecular diffusion from those of the chemical kinetics. In particular, we decompose $\overline{A'B'}$ into several terms, some of which are independent of the chemistry. Then, in applications to problems where the turbulence is quasi-stationary and homogeneous, the terms that are free of chemistry effects can be expressed as universal functions of the surface heat flux, mixed layer depth, mean flow speed, surface roughness, travel time, and source height, and they can be expressed in polynomial form, say, in the approximation of $\overline{A'B'}$. The terms that are affected by the chemistry turn out to have very simple forms in most air pollution applications; consequently, the overall expression for $\overline{A'B'}$ acquires a simple algebraic form.

Lin and O'Brien (1972) suggested a model for nonlinear chemical reactions in turbulence that involves dividing the problem into three components, each involving only two of the three governing processes: turbulent transport, molecular diffusion, and chemical reaction. Apparently, this model has not yet been tested. Toor (1975) developed a model of chemical reactions in turbulence that in essence divides the problem into reactive and nonreactive phenomena. Although the assumptions Toor employs are valid in certain chemical reactors, they are not necessarily applicable to point source emissions in the atmosphere. We used some of Toor's results in the formulation of our model. The efforts described in this chapter are a modification of the method developed in Lamb (1976).

A. FORMULATION OF AN EXPRESSION FOR THE CONCENTRATION FLUCTUATION TERM $\overline{A'B'}$

The decomposition of $\overline{A'B'}$ into the desired form, namely, one in which at least one term is independent of the chemical kinetics, was achieved using the following functions:

$$a(\underset{\sim}{r},t) = \begin{cases} A(\underset{\sim}{r},t) & \text{if } B(\underset{\sim}{r},t) = 0 \quad , \\ 0 & \text{otherwise} \quad . \end{cases} \tag{19}$$

$$\alpha(\underset{\sim}{r},t) = \begin{cases} 0 & \text{if } B(\underset{\sim}{r},t) = 0 \quad , \\ A(\underset{\sim}{r},t) & \text{otherwise} \quad . \end{cases} \tag{20}$$

$$b(\underset{\sim}{r},t) = \begin{cases} B(\underset{\sim}{r},t) & \text{if } A(\underset{\sim}{r},t) = 0 \quad , \\ 0 & \text{otherwise} \quad . \end{cases} \tag{21}$$

$$\beta(\underset{\sim}{r},t) = \begin{cases} 0 & \text{if } A(\underset{\sim}{r},t) = 0 \quad , \\ B(\underset{\sim}{r},t) & \text{otherwise} \quad , \end{cases} \tag{22}$$

where A and B denote the instantaneous concentrations of species A and B, respectively. It should be clear from these definitions that the function a marks those regions of the fluid where the species A is found in isolation, and b marks zones where B is present alone. Similarly, α and β are markers of the fluid domain where A and B are mixed. It follows from Eqs. (19) through (22) that

$$A(\underset{\sim}{r},t) = a(\underset{\sim}{r},t) + \alpha(\underset{\sim}{r},t) \quad , \tag{23}$$

$$B(\underset{\sim}{r},t) = b(\underset{\sim}{r},t) + \beta(\underset{\sim}{r},t) \quad , \tag{24}$$

and that

$$ab = \alpha a = \alpha b = \beta a = \beta b = 0 \quad , \tag{25a}$$

$$\alpha,\ a,\ \beta,\ b \geq 0 \quad . \tag{25b}$$

Substituting Eq. (23) into Eq. (17a) and making use of Eq. (25), we obtain

$$\mathcal{L}(a + \alpha) = -k\alpha\beta \quad . \tag{26}$$

Suppose that inert surrogates A_I and B_I of the reactive species A and B are released from the same sources at the same rates into the same flow system. Using the instantaneous concentrations A_I and B_I, we can define four functions--a_I, α_I, b_I, and β_I--in exactly the same manner as Eqs. (19) through (22). Being inert and having (by design) the same molecular diffusivities $\mathcal{D}_A$ and $\mathcal{D}_B$ of their reactive counterparts, A_I and B_I satisfy

$$\mathcal{L}A_I = \mathcal{L}(a_I + \alpha_I) = 0 = \mathcal{L}(b_I + \beta_I) = \mathcal{L}B_I \quad . \tag{27}$$

A physical picture of the relationships among the eight functions a, a_I, and so forth is provided in Figure 11. This figure emphasizes that if A and B (hence A_I and B_I) are not mixed initially, then α, β, α_I, and β_I will remain zero for all time unless $\mathcal{D}_A$ or $\mathcal{D}_B$ or both are nonzero. In other words, turbulence acting alone cannot bring about mixing on the molecular scale that is required for chemical reaction and that is implicit in the definitions of α, α_I, β, and β_I.

Intuitively, one would expect the functions a and a_I to be equivalent since both describe concentrations in regions of the fluid where chemical reactions cannot occur. That a_I and a are equivalent can be demonstrated as follows. Multiplying Eq. (26) by a^n and making use of Eq. (25), we obtain

$$a^n\mathcal{L}a = -a^n\mathcal{L}\alpha \quad . \tag{28}$$

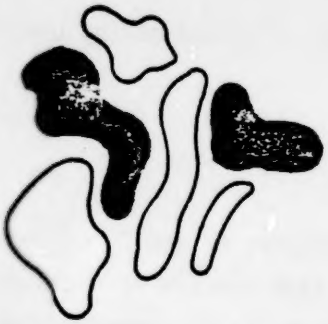

(a) Without Molecular Diffusion

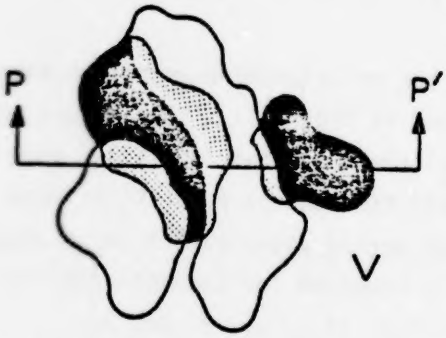

(b) With Molecular Diffusion

LEGEND: ☐ V_A ■ V_B ▨ V_{AB}

FIGURE 11. SCHEMATIC OF TURBULENT MIXING

In a similar fashion, Eq. (27) gives

$$a_I^n \mathcal{L} a_I = -a_I^n \mathcal{L} \alpha_I \quad . \tag{29}$$

Similar equations can be derived for the components of B and B_I. It follows from their definitions that at points in the fluid where $\alpha(\alpha_I)$ is nonzero, $a(a_I)$ is identically zero. Thus, at all such sites the right-hand sides of Eqs. (28) and (29) are zero. However, on the surfaces of the mixed zone (see Figure 11), both a and $\mathcal{L}\alpha$ (and a_I and $\mathcal{L}\alpha_I$) can have nonzero values. To express these results, we write Eqs. (28) and (29) in the forms

$$a^n \mathcal{L} a = -a^n \mathcal{L} \alpha \Big|_S \quad , \tag{30}$$

$$a_I^n \mathcal{L} a_I = -a_I^n \mathcal{L} \alpha_I \Big|_S \quad . \tag{31}$$

We wish to show now that the terms on the right-hand side of these two equations are equal.

First, recall that by the definitions of A_I and B_I,

$$a_I(\underline{r},0) = a(\underline{r},0) \quad , \tag{32a}$$

$$\alpha_I(\underline{r},0) = \alpha(\underline{r},0) \quad . \tag{32b}$$

Similar relationships exist between B and B_I. Next, we point out that except for infinitely fast reactions, two reactant species can coexist in the mixed zone for an arbitrarily long time. Concentrations of one or both species may be exceedingly small, but they will be nonzero, and this is all that is required to make $a = 0$, $\alpha \neq 0$. This fact and

Eq. (32) indicate that if A and B are released simultaneously with A_I and B_I, then at each instant the regions of fluid where a and a_I are nonzero coincide, those where α and α_I are nonzero coincide, and consequently, the surfaces of the mixed zones of the reactive and inert species also coincide. Finally, we note that when A and B are not premixed (premixing results in a and a_I being identically zero everywhere), the mixed zone surfaces represent the leading edges of the advance of one species into the region occupied by the other. Along this edge, the concentration of the advancing species must be vanishingly small, with the consequence that no reaction occurs there (except in the case of infinitely fast reactions). In short, on the mixed zone boundaries, the inert and reactive species are indistinguishable: $a = a_I$, $\alpha = \alpha_I$. From this and the coincidence of the reactive and inert species mixed zone boundaries, we conclude that the right-hand sides of Eqs. (30) and (31) are equal and, consequently, that

$$a^n L a = a_I^n L a_I \quad . \tag{33}$$

Under the initial conditions given by Eq. (32), Eq. (33) yields the anticipated result $a = a_I$, and in particular,

$$\overline{a^n} = \overline{a_I^n} \quad , \quad n = 1, 2, \ldots \quad . \tag{34}$$

This is one of the main results upon which our expression for $\overline{A'B'}$ is based.

It is more convenient to work with $\overline{AB} = \bar{A}\bar{B} + \overline{A'B'}$ than with $\overline{A'B'}$. The former is found from Eqs. (23), (24), and (25) to be

$$\overline{AB} = \overline{\alpha\beta} \quad , \tag{35}$$

which we now write in the alternate form

$$\overline{AB} = \lambda(\bar{A} - \bar{a})(\bar{B} - \bar{b}) \frac{\overline{\alpha_I\beta_I}}{\bar{\alpha}_I\bar{\beta}_I} \quad . \tag{36}$$

Here λ is defined as

$$\lambda \equiv \frac{\overline{\alpha\beta}}{\bar{\alpha}\bar{\beta}} \cdot \frac{\bar{\alpha}_I\bar{\beta}_I}{\overline{\alpha_I\beta_I}} \quad . \tag{37}$$

We refer to λ as the reaction parameter because it is a measure of the effect of the reaction on the distribution of A and B within the mixed zone. After making use of Eq. (34) and rearranging terms, we finally obtain

$$\overline{AB} = \frac{\lambda\Gamma_{AB}}{\zeta_A\zeta_B}[\bar{A} - (1 - \zeta_A)\bar{A}_I][\bar{B} - (1 - \zeta_B)\bar{B}_I] \quad , \tag{38}$$

where

$$\Gamma_{AB} \equiv \frac{\overline{A_IB_I}}{\bar{A}_I\bar{B}_I} \quad , \tag{39}$$

$$\zeta_A \equiv \frac{\bar{\alpha}_I}{\bar{A}_I} \quad , \quad \zeta_B \equiv \frac{\bar{\beta}_I}{\bar{B}_I} \quad . \tag{40}$$

We call ζ_A and ζ_B the mixing parameters because they are simply the fractions of the total quantities of A_I and B_I that are within the mixed zone. Thus, $0 \le \zeta_A, \zeta_B \le 1$.

Inspection of each of the terms in Eq. (38) reveals that in essence we have transferred much of the closure problem associated with $\overline{A'B'}$ into the reaction parameter λ, but in the process we have brought a great deal of additional information into play in the form of the ζ's, Γ_{AB}, A_I, and B_I. Being independent of the chemistry, these last parameters can be either expressed as functions of the flow conditions and source configuration or calculated from models, in which chemistry-caused closure problems do not occur. These observations suggest that the utility of Eq. (38) is restricted mainly to problems where λ plays a subordinate role in determining $\overline{AB}$ or to cases where accurate estimates of λ are available. Many problems of air pollution and chemical reactor design fall within these categories. For example, if the reactants are premixed, then $\zeta_A = \zeta_B = 1$; and if the reaction is slow or if A and B are released in stoichometric ratio, $\lambda = 1$ (as we show later), and hence, Eq. (38) gives

$$\overline{AB} = \Gamma_{AB}\,\bar{A}\bar{B} \quad . \tag{41}$$

If this expression is substituted into Eq. (18) and if the resulting equation is applied to a batch reactor, where mean values denote averages over the reactor volume, we obtain

$$\frac{\partial\bar{A}}{\partial t} = -k\Gamma_{AB}\,\bar{A}\bar{B} \quad . \tag{42}$$

This equation provides a means of estimating reaction rates in reactors in which the chemical species are not uniformly distributed (in which case $\Gamma_{AB} \neq 1$). The equation commonly used to study chemical reactors is identical to Eq. (42) except that Γ_{AB} is always set to unity in accordance with the assumption that the reactants are uniformly distributed within the reactor.

In the next section, we develop approximations for the reaction and mixing parameters required to implement Eq. (38).

B. APPROXIMATIONS OF THE REACTION PARAMETER λ

1. General Considerations

The general behavior of λ can best be assessed from the form of its governing equation. To derive this equation, we first need the equation for $\overline{\alpha\beta}$, obtained by first substituting Eq. (23) into Eq. (17a), and then multiplying the result by β and making use of Eq. (25). This yields:

$$\left[\beta\left(\frac{\partial a}{\partial t} + \frac{\partial}{\partial x_i} u_i a - \mathcal{D}_A \frac{\partial^2 a}{\partial x_i \partial x_i}\right)\right] + \beta\frac{\partial \alpha}{\partial t} + \beta\frac{\partial}{\partial x_i} u_i \alpha = \beta\mathcal{D}_A \frac{\partial^2 \alpha}{\partial x_i \partial x_i} - k\alpha\beta^2 \quad . \tag{43}$$

From the definitions of β and a and the point made earlier that β is vanishingly small on the surfaces of the mixed zone, we conclude that the term in brackets in Eq. (43) is zero everywhere. Multiplying the counterpart of Eq. (17a) that governs B by α, combining the result with Eq. (43), and restricting attention, for simplicity, to spatially homogeneous mean concentrations and species with equal diffusivities (i.e., $\mathcal{D}_A = \mathcal{D}_B = \mathcal{D}$), we obtain

$$\frac{\partial}{\partial t}\overline{\alpha\beta} = -2\mathcal{D}\,\overline{\frac{\partial \alpha}{\partial x_i}\frac{\partial \beta}{\partial x_i}} - k\overline{\alpha\beta(\alpha + \beta)} \quad . \tag{44}$$

Through a similar set of operations, we obtain

$$\frac{\partial}{\partial t}\overline{\alpha_I\beta_I} = -2\mathcal{D}\,\overline{\frac{\partial \alpha_I}{\partial x_i}\frac{\partial \beta_I}{\partial x_i}} \quad . \tag{45}$$

Under the same set of conditions, the corresponding equations for $\overline{\alpha}$ and $\overline{\beta}$ are

$$\frac{\partial \bar{\alpha}}{\partial t} = \frac{\partial \bar{\alpha}_I}{\partial t} - k\bar{\alpha}\bar{\beta}\lambda \, \frac{\overline{\alpha_I \beta_I}}{\bar{\alpha}_I \bar{\beta}_I} \quad , \tag{46}$$

$$\frac{\partial \bar{\beta}}{\partial t} = \frac{\partial \bar{\beta}_I}{\partial t} - k\bar{\alpha}\bar{\beta}\lambda \, \frac{\overline{\alpha_I \beta_I}}{\bar{\alpha}_I \bar{\beta}_I} \quad . \tag{47}$$

Combining Eqs. (44) through (47) with the definition in Eq. (37) of λ, we obtain finally

$$\frac{1}{\lambda}\frac{\partial \lambda}{\partial t} = -2\mathcal{D}(\xi - \xi_I) - k\,\frac{\overline{\alpha\beta(\alpha + \beta)}}{\overline{\alpha\beta}} + k\lambda\,\frac{\overline{\alpha_I \beta_I}}{\bar{\alpha}_I \bar{\beta}_I}\,(\bar{\alpha} + \bar{\beta})$$

$$+ \left(\frac{1}{\bar{\alpha}_I} - \frac{1}{\bar{\alpha}}\right)\frac{\partial \bar{\alpha}_I}{\partial t} + \left(\frac{1}{\bar{\beta}_I} - \frac{1}{\bar{\beta}}\right)\frac{\partial \bar{\beta}_I}{\partial t} \tag{48a}$$

with the initial condition

$$\lambda(0) = 0 \quad . \tag{48b}$$

In Eq. (48),

$$\xi = \frac{\overline{\dfrac{\partial \alpha}{\partial x_i}\dfrac{\partial \beta}{\partial x_i}}}{\overline{\alpha\beta}} \quad , \tag{49}$$

and

$$\xi_I = \frac{\overline{\dfrac{\partial \alpha_I}{\partial x_i}\dfrac{\partial \beta_I}{\partial x_i}}}{\overline{\alpha_I \beta_I}} \quad . \tag{50}$$

Since all parameters with the subscript I in Eqs. (46) through (48) are controlled solely by the fluid motions, we can regard them as given, independent variables, in which case Eqs. (46) through (48) can be solved simultaneously for λ. Solving this system in general would require that ξ and $\overline{\alpha\beta(\alpha + \beta)}$ be expressed in terms of $\overline{\alpha}$, $\overline{\beta}$, λ, and other known quantities. Fortunately, in the problems of interest to us in this study, λ can be evaluated without recourse to any closure models. The first case is described below.

2. Case 1: Point Source Release of A into a Uniform Field of B

Implicit in Eqs. (46) through (48) is the assumption that the mean concentrations of the reactants and surrogates are spatially homogeneous. Therefore, these equations are applicable to point source emissions only if the mean concentrations represent averages over the cross section of the plume. Later in this chapter we discuss such a problem in the process of modeling the total mass of pollutants in cross sections of a plume as a function of downstream distance. It is the purpose of the present section to develop an approximation for λ that is suitable for that model.

The problem we treat is the oxidation of nitric oxide (NO) in a power plant plume by ozone (O_3) in the ambient air. Generally, NO concentrations in a plume initially are of the order of several thousand parts per million, and background O_3 levels are no more than a few tenths of a part per million. As a result, ozone is consumed as rapidly as it is entrained into the plume. Or, stated in terms of the present model, if A = NO and B = O_3, then $\beta = 0$, and consequently, $\overline{\alpha\beta}$ and $\overline{\beta}$ are in a pseudo-steady state with values near zero. Under these conditions, Eqs. (44), (45), and (47) yield

$$\frac{1}{\lambda}\frac{\partial\lambda}{\partial t} = 2\mathcal{D}\xi_I + \frac{\partial\overline{\beta}_I}{\partial t}\left(\frac{1}{\overline{\alpha}} + \frac{1}{\overline{\beta}_I}\right) + \left(\frac{1}{\overline{\alpha}_I} - \frac{1}{\overline{\alpha}}\right)\frac{\partial\overline{\alpha}_I}{\partial t} \quad . \qquad (51)$$

Initially, the reactants A and B are totally segregated with A uniformly distributed in the source emissions and B uniformly distributed in the ambient air (by assumption). However, if we were to assume that B is present everywhere initially, including the interior of the plume, then we would have $\overline{A}_I = \overline{\alpha}_I$ = Constant and $\overline{\alpha_I\beta_I} = \overline{\alpha}_I\overline{\beta}_I$, whereupon Eq. (51) would reduce to (during the time that $\overline{\alpha}_I >> \overline{\beta}_I$)

$$\frac{\partial}{\partial t} \ell n\, \lambda = \frac{\partial}{\partial t} \ell n\, \frac{\overline{\beta}_I}{\overline{\alpha_I\beta_I}} = 0 \quad , \tag{52}$$

or $\lambda(t) = 1$. In view of the great disparity in the initial levels of NO and O_3, the evaluation of NO concentrations in the plume will be virtually unaffected by the presence or absence of ozone in the plume initially. We conclude, therefore, that $\lambda(t) = 1$ in all problems of the type described above where $\alpha_I >> \beta_I$ initially and the reaction is fast, i.e., $k\overline{\alpha}_I\overline{\beta}_I >> \partial\overline{\beta}_I/\partial t$. Since the same result applies when the reaction is slow [as can be seen by taking the limit $k \rightarrow 0$ in Eqs. (46) through (48)], we assume in general that $\lambda = 1$ in point source problems.

3. Case 2: One-Dimensional Reactors

Later in this report we describe the use of laboratory data gathered from a tubular chemical reactor in which the reactants were injected into one end of the tube through alternate jets clustered over the entire cross-sectional area. Since many reactors are of this design, it is worthwhile to develop a general expression for λ that is applicable to them.

Rather than approach this task through Eqs. (46) through (48), which would require the adoption of approximations of unknown accuracies for ξ and $\overline{\alpha\beta(\alpha + \beta)}$, we use a heuristic model that does not require mathematical closure. The proposed model exploits the fact that, because of the reactor design, the regions of mixed and unmixed reactants compose a mosaic of small, intermingling patches of fluid that, statistically speaking, have identical concentration frequency distributions (at any fixed axial distance from the reactor head) and that give rise to time mean reactant concentrations that are uniform over any plane normal to the reactor axis.

Suppose that $\mathcal{D}_A = \mathcal{D}_B = \mathcal{D}$, that the turbulent fluid has kinematic viscosity ν, and that turbulent energy is being dissipated at a rate ε. Velocity fluctuations of spatial scales that are large compared with the Kolmogoroff microscale $(\nu^3/\varepsilon)^{1/4}$ serve to distort the initial patches of reactants by pulling and squeezing them into convoluted sheets and ribbons of ever-decreasing thickness. At scales small compared with $(\nu^3/\varepsilon)^{1/4}$, the velocity field appears as a pure straining motion, and consequently, sheets and ribbons of reactants produced by larger scale velocity perturbations are squeezed still further. If the Schmidt number defined as $\nu/\mathcal{D}$ is infinite, the stretching and squeezing of reactant sheets continues indefinitely, and mixing at the molecular level occurs only in the limit of infinitely large times. However, for a Schmidt number comparable to or larger than one, Batchelor (1959) showed that once the sheet widths approach a thickness comparable to $\delta = (\nu\mathcal{D}^2/\varepsilon)^{1/4}$, the concentration gradients normal to the sheet are sufficiently large that molecular fluxes of marked fluid just balance the compression of the sheet by the straining motion. At points in the fluid where this occurs, thorough mixing of the marked and convecting fluids results, and hence, by our definition, portions of the mixed ozone are created. At scales large compared with δ, concentration gradients are too weak to cause significant mixing. Thus, the generation of the mixed ozone is confined primarily to those portions of the fluid where the reactant sheet thickness is comparable to δ. Considering these observations, we propose to develop expressions for λ based on a one-dimensional model of reactant fluids of initial widths and separations of the order of δ.

Since the expansion of reactant fluid sheets of widths smaller than or comparable to δ is dominated by molecular diffusion, the governing equations are assumed to be

$$\frac{\partial A}{\partial t} = \mathcal{D}_A \frac{\partial^2 A}{\partial x^2} - kAB \quad , \tag{53}$$

$$\frac{\partial B}{\partial t} = \mathcal{D}_B \frac{\partial^2 B}{\partial x^2} - kAB \quad , \tag{54}$$

$$\frac{\partial A_I}{\partial t} = \mathcal{D}_A \frac{\partial^2 A_I}{\partial x^2} \quad , \tag{55}$$

$$\frac{\partial B_I}{\partial t} = \mathcal{D}_B \frac{\partial^2 B_I}{\partial x^2} \quad , \tag{56}$$

with the following initial and boundary conditions:

$$A(x,0) = A_I(x,0) = \begin{cases} A_0 & \text{if } -3/2\ \delta \le x \le -1/2\ \delta \quad ; \\ 0 & \text{otherwise} \quad . \end{cases} \tag{57}$$

$$B(x,0) = B_I(x,0) = \begin{cases} B_0 & \text{if } 1/2\ \delta \le x \le 3/2\ \delta \quad ; \\ 0 & \text{otherwise} \quad . \end{cases} \tag{58}$$

$$A(x,t) = B(x,t) = 0 \quad , \quad x \to \pm\infty \quad . \tag{59}$$

The initial conditions expressed in Eqs. (57) and (58) have been selected to account at least approximately for turbulence strain rate effects. treating these effects explicitly in Eqs. (53) through (56) is not generally possible because of the random character of the strain rate field.

Shu (1976) solved Eqs. (53) through (56) for a variety of values of feed ratio $\rho = B_0/A_0$, diffusivity ratio $\gamma = \mathcal{D}_B/\mathcal{D}_A$, and Damkohler number

$$\kappa = \frac{k\delta^2 A_0}{\mathcal{D}_A} \quad , \tag{60}$$

From the results, he estimated λ using its definition in Eq. (37). Although these estimates were based on reactant and surrogate concentrations averaged over only the two patches of material considered, rather than over the entire reactor cross section as is implicit in the mean values entering in Eq. (37), the uniformity mentioned earlier of the concentration distributions within the patches renders the patch and cross-sectional averages equal. Some of the results of the λ calculations are shown in Figures 12 and 13.

An important point to keep in mind in interpreting these figures is that by virtue of the time scaling, significant chemical reaction cannot occur before $t^* \approx 1$. The calculations showed that for the case of stoichiometric feed ($\beta = 1$) and given κ, λ maintains its minimum value (shown in Figure 12) until $t^* \approx 10^4$. However, when $\beta \neq 1$, the value of λ returns to unity more quickly (see Figure 13), but not until the reactant in the smaller quantity has been almost completely consumed. Thus, during the period within which most of the chemical reaction occurs, λ has its minimum value λ_{min}. Thus, we assume in general that

$$\lambda = \lambda_{min} \quad . \tag{61a}$$

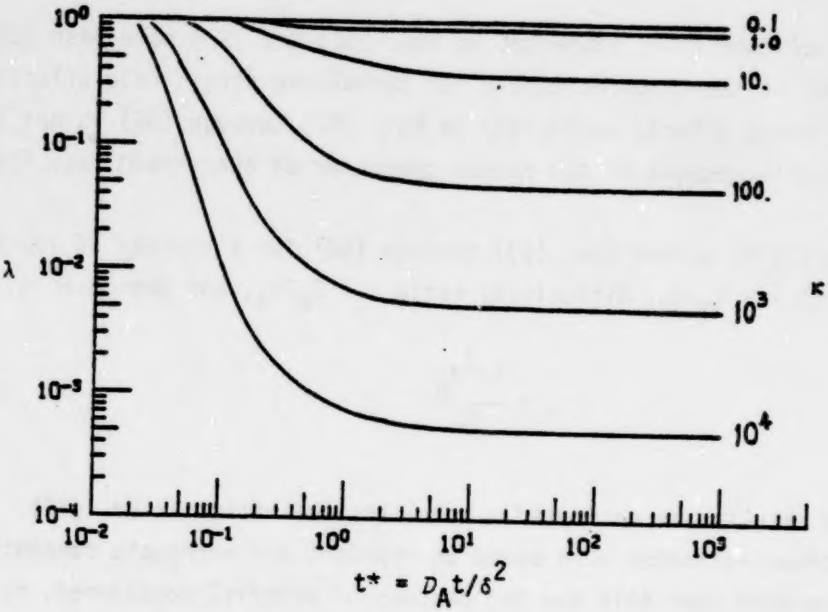

FIGURE 12. TEMPORAL BEHAVIOR OF λ FOR VARIOUS VALUES OF κ AT $\rho = \gamma = 1$

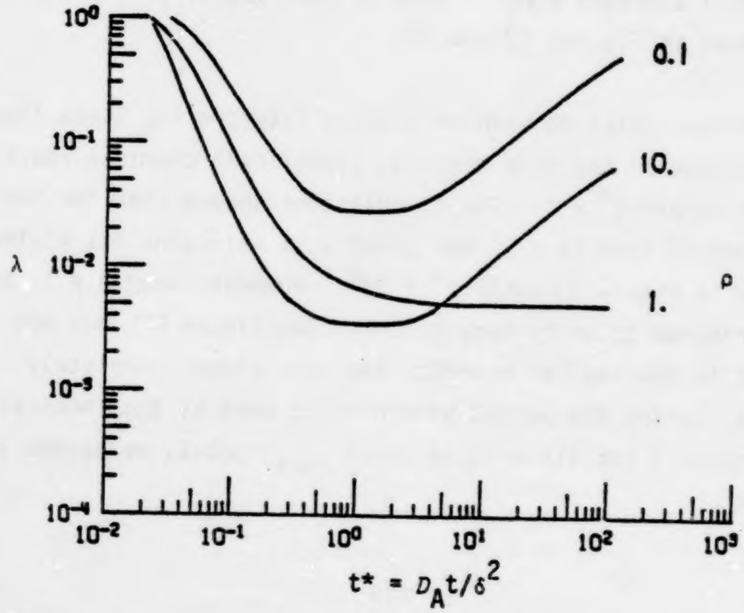

FIGURE 13. TEMPORAL BEHAVIOR OF λ FOR VARIOUS VALUES OF ρ AT $\kappa = 1000$ AND $\gamma = 1$

We have found from an analysis of the results presented in Figures 12 and 13 that the dependence of λ_{min} on the variables, κ, ρ, and γ is described by the simple expression

$$\lambda_{min} = \frac{1}{1 + 0.16\kappa} \quad , \qquad (61b)$$

where

$$\kappa = \frac{k\delta^2 \min(A_0, B_0}{\max(\mathcal{D}_A, \mathcal{D}_B)} \quad . \qquad (61c)$$

For the case of premixed reactants, λ is calculated by solving Eqs. (53) through (59) for the case of a single initial fluid pulse containing uniform concentrations of both A and B. The temporal behavior of λ in this case shows two distinct patterns. For the case of $\rho = 1$, λ stays at unity for all times; but for the cases where $\rho \neq 1$, λ decays to the same minimum value as its nonpremixed counterpart. The results presented above are summarized in Table 1.

TABLE 1. SUMMARY OF EXPRESSIONS FOR THE MIXING AND REACTION PARAMETERS ζ_A, ζ_B, AND λ

System	Initial Condition on Mixing and Stoichiometric Ratio $\rho = B_0/A_0$	Parameter*		
		λ	ζ_A	ζ_B
One-dimensional reactor	Premixed			
	$\rho = 1$	1	1	1
	$\rho \neq 1$	$(1 + 0.16\kappa)^{-1}$	1	1
	Nonpremixed--all ρ	$(1 + 0.16\kappa)^{-1}$	Γ_{AB}/Γ_B	Γ_{AB}/Γ_A
Point source of A in a uniform field of B	$\rho << 1$	1	1	$1/\Gamma_A$

---

*κ is defined by Eq. (50).

C. APPROXIMATIONS OF THE MIXING PARAMETERS ζ_A AND ζ_B

1. General Considerations

Because the functions α_I and β_I, which enter into the definitions of the mixing parameters, are only piecewise continuous, the equations that govern ζ_A and ζ_B are awkward to handle. We can avoid these equations by formulating the mixing parameters in the following manner.

Let $v_{\alpha\beta}$ denote the subspace of the averaging region represented by the overbars in Eq. (30) that is occupied by the mixed zone, i.e., the domain in which α_I and β_I are nonzero. (The averaging may be either time, space, or ensemble averaging.) Similarly, let v_a and v_b denote the subspaces where a_I and b_I, respectively, are nonzero. Then by straightforward analyses, we obtain

$$\frac{\Gamma_{AB}}{\Gamma_A} = \zeta_B \frac{\dfrac{\mu_{\alpha\beta}}{\mu_{\alpha\alpha}}}{\dfrac{\mu_{aa}\hat{a}}{\mu_{\alpha\alpha}\hat{\alpha}}(1 - \zeta_A) + \zeta_A} \tag{62}$$

and a similar expression for Γ_{AB}/Γ_B. Here

$$\Gamma_A = \frac{\overline{A_I^2}}{\bar{A}_I^2} \quad ; \tag{63}$$

$$\hat{a} = \frac{1}{v_a}\int_{v_A} a_I \, dv \quad ; \tag{64}$$

$$\hat{\alpha} = \frac{1}{v_{\alpha\beta}}\int_{v_{\alpha\beta}} \alpha_I \, dv \quad ; \tag{65}$$

with similar expressions for Γ_B, $\hat{b}$, and $\hat{\beta}$;

$$\mu_{\alpha\beta} = \frac{1}{\hat{\alpha}\hat{\beta}v_{\alpha\beta}} \int_{v_{\alpha\beta}} \alpha_I \beta_I \, dv \quad ; \tag{66}$$

$$\mu_{aa} = \frac{1}{\hat{a}^2 v_a} \int_{v_a} a_I \, dv \quad ; \tag{67}$$

with similar expressions for μ_{bb}, $\mu_{\alpha\alpha}$, and $\mu_{\beta\beta}$.

The μ's in Eq. (62) are a measure of the spatial variations of A_I and B_I within the various subspaces v_a, v_b, and $v_{\alpha\beta}$. If concentrations are uniform within these spaces, then the μ's acquire values of unity. We expect concentrations to be uniform within v_a and v_b initially and in all subspaces in the limit of long times as diffusion succeeds in wiping out all concentration gradients. [It is important to keep in mind that all parameters in Eq. (62) pertain to the inert surrogate species A_I and B_I and not to the reactants.] For simplicity, we assume that spatial variations in concentrations are negligible in v_a, v_b, and $v_{\alpha\beta}$ and, moreover, that $\hat{a} = \hat{\alpha}$ and $\hat{b} = \hat{\beta}$. These assumptions, which are tantamount to a closure approximation, yield the simple results

$$\zeta_B = \frac{\Gamma_{AB}}{\Gamma_A} \quad , \quad \zeta_A = \frac{\Gamma_{AB}}{\Gamma_B} \quad . \tag{68}$$

These expressions are consistent with the limiting values $\zeta_A, \zeta_B \to 1$ as $t \to \infty$ and $\zeta_A = \zeta_B = 0$ at $t = 0$ for unpremixed reactants. We use Eq. (68) generally subject to checks of its performance against empirical data.

2. Case 1: Point Source Release of A into a Uniform Field of B

In developing an approximation of λ for this case in Section III.C.2, we found that a considerable simplification of the mathematics could be achieved with a negligible loss of accuracy by assuming that the species B is present everywhere, even within the source emissions. If the same assumption is made here, we have $\Gamma_B = \Gamma_{AB} = \mu_{\alpha\beta} = \mu_{bb} = \mu_{\beta\beta} = 1$, in which case Eq. (62) and its counterpart reduce to

$$\Gamma_A = 1 \quad , \quad \Gamma_B = \frac{\mu_{\alpha\alpha}}{\Gamma_A} \quad . \tag{69}$$

Using a model similar to that employed in Section III.C to evaluate λ, Shu (1976) computed the form of μ and found it to increase from a value of 1 at $t = 0$ to a maximum value of 2 at $t = 0.1\delta^2/\mathcal{D}$ and then to decay to a final value of 1 within a period of about $10^4\delta^2/\mathcal{D}$. The proper value of μ_a for use in the model is a weighted mean of the temporal variations just described; but because of a lack of information to use to estimate this weighting function, we assume that $\mu_{\alpha\alpha} = 1$ [in conformity with Eq. (68)].

3. Case 2: One-Dimensional Reactors

In one-dimensional reactors of the type described in Section III.C.2, Toor (1969) predicted, and later confirmed through measurements, that reactants that are fed into the reactor in stoichiometric ratios and that subsequently undergo extremely fast reactions satisfy

$$\overline{A'B'} = \overline{A'_I B'_I} \quad . \tag{70}$$

This result provides a means of estimating ζ (= $\zeta_A = \zeta_B$ for this reactor). If we substitute our closure formula Eq. (38) into Eq. (18) and make the pseudo-steady-state assumption $\partial\bar{A}/\partial t \approx 0$, which is valid for fast reactions, we find that

$$\bar{A} = (1 - \zeta)\bar{A}_I \quad ,$$

$$\bar{B} = (1 - \zeta)\bar{B}_I \quad .$$

Using Eqs. (23), (24), and (34) and keeping in mind that for very fast reactions $\overline{\alpha\beta} = 0$, we obtain

$$\zeta = 1 - (1 - \Gamma_{AB})^{1/2} \quad . \tag{71}$$

This formula reduces to Eq. (68) when the conditions implicit in the latter are invoked and when it is assumed that the reactants are the only fluids in the reactor (this is not shown here). This finding provides reassurance that our proposed general formulas [Eq. (68)] are basically sound.

D. COMPARISON OF THE MODEL PREDICTIONS WITH LABORATORY DATA

The best test of the adequacy of the model developed in the previous sections is to compare its predictions with observations. Data suitable for this purpose have been reported by Vassilatos and Toor (1965), Mao (1969), McKelvey (1968), and Zakanycz (1971). All of these experimenters used a multijet reactor of the one-dimensional type described earlier [see Vassilatos and Toor (1965)] in which alternate jets of acid and base were injected into a tube from a circular plate containing numerous small holes. Conditions were such that the mean concentrations of $\bar{A}$ and $\bar{B}$ varied only with distance from the entrance. (In the inert case, $\bar{A}_I$ and $\bar{B}_I$ are constant throughout the reactor, where the overbar refers to averaging across the cross section of the reactor.) The reactor affords the opportunity to measure the rate of reaction between two species in the presence of rather well-characterized turbulent mixing. In this section, we apply the model developed in the previous sections to several of the experiments conducted with the multijet reactors.

Since $\bar{A}_I$ and $\bar{B}_I$ are constant in the reactor, it is convenient to let $F_A = \bar{A}/\bar{A}_I$ and $F_B = \bar{B}/\bar{B}_I$, in which case Eqs. (18) and (38) give

$$\frac{dF_A}{dt} = - \frac{k\lambda\Gamma_{AB}\bar{B}_I}{\zeta_A\zeta_B} (F_A - 1 + \zeta_A)(F_B - 1 + \zeta_B) \quad . \tag{72}$$

Since the reactions studied in the multijet reactor were of the general form A + nB → Products, we can write

$$\bar{B} = \bar{B}_I + n(\bar{A} - \bar{A}_I) \tag{73}$$

or

$$F_B = 1 + \frac{n\bar{A}_I}{\bar{B}_I} (F_A - 1) \quad . \tag{74}$$

Substituting Eq. (74) into Eq. (72), we obtain

$$\frac{dF_A}{dx} = - \frac{k\lambda\Gamma_{AB}n\bar{A}_I}{U(x)\zeta_A\zeta_B} (F_A - 1 + \zeta_A)(F_B - 1 + \rho\zeta_B) \quad , \tag{75}$$

where $\rho = \bar{B}_I/n\bar{A}_I$ and the relationship $dx/dt = U(x)$ has been used to convert time to distance x down the reactor. Following Yieh (1970), we have used the velocity data measured between the jets as the mean axial velocity $U(x)$. Values of Γ_{AB}, Γ_A, and Γ_B required to evaluate ζ_A and ζ_B were obtained from conversion data for very rapid reactions in the case of $\rho = 1$ (see Appendix A). Equations (61a) through (61c) were used to calculate λ.

We have used four separate sets of experimental data to test the model (see Shu, 1976) but only a few of these are discussed here. Basically, two types of reactions were considered: those of intermediate rate, $0.1 < \kappa < 1$; and very fast reactions $\kappa >> 1$. Very slow reactions ($\kappa <<<< 1$) were not considered because they can often be represented by the homogeneous law

$$u(x) \frac{d\bar{A}}{dx} = -k\bar{A}\bar{B} \quad . \tag{76}$$

Equation (75) was solved numerically for F_A as a function of distance from the reactor inlet. The results are presented in Figures 14 through 19. In each case, the inert concentration correlations required in Eq. (75) were obtained using Toor's model, as described in Appendix A; hence, errors inherent in his model and in the laboratory data are reflected in our calculations. In general, the predictions agree more closely with the data of Vassilatos and Toor (1965), Figures 14 and 15, than with those of Mao (1969), Figures 16 through 19.

To show the extent to which concentration fluctuations can affect the rate of second-order reactions, we plotted the solution of the homogeneous equation [Eq. (76)], which ignores fluctuation effects, in Figures 15 and 18 (dash-dot curves). In the two situations shown, it is clear that the fluctuations actually control the rate of the chemical conversion process. Further evidence of the effects of inhomogeneous mixing is given by the

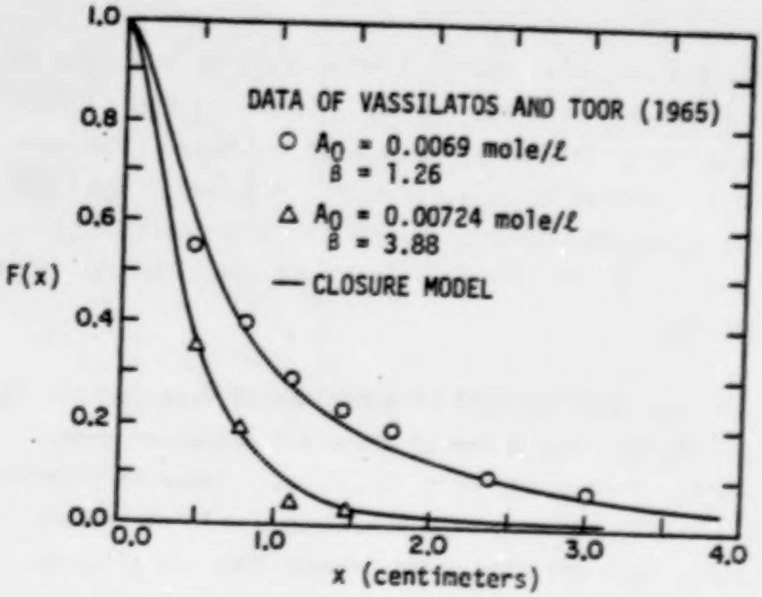

FIGURE 14. COMPARISON OF THE PREDICTIONS OF THE CLOSURE MODEL WITH CHEMICAL REACTOR DATA FOR VARIOUS VALUES OF A_0 AND β WITH $k = 1.24 \times 10^4$ ℓ/mole·sec

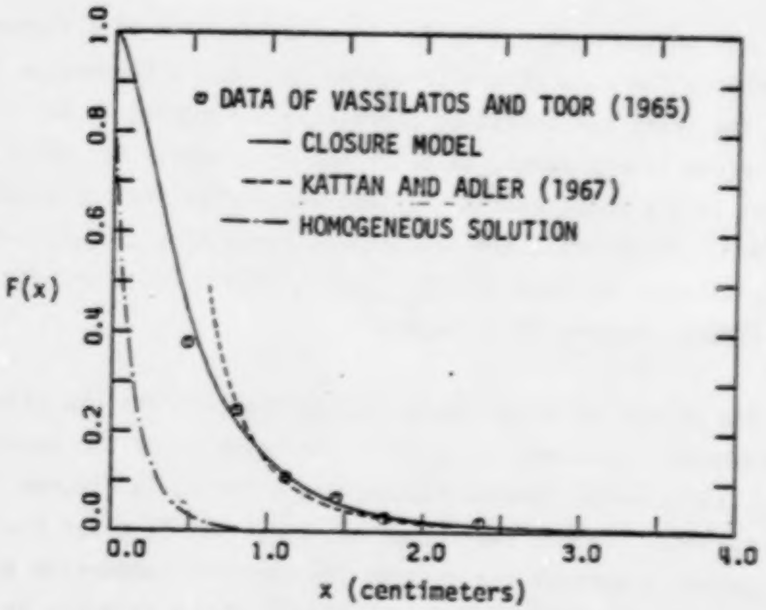

FIGURE 15. COMPARISON OF THE PREDICTIONS OF THE CLOSURE MODEL WITH CHEMICAL REACTOR DATA, THE PREDICTIONS OF THE KATTAN AND ADLER (1967) MODEL, AND THE SOLUTION OF THE HOMOGENEOUS MODEL, EQ. (76), WITH $k = 1.24 \times 10^4$ ℓ/mole·sec, A_0 = 0.00658 mole/ℓ, AND ρ = 2.52

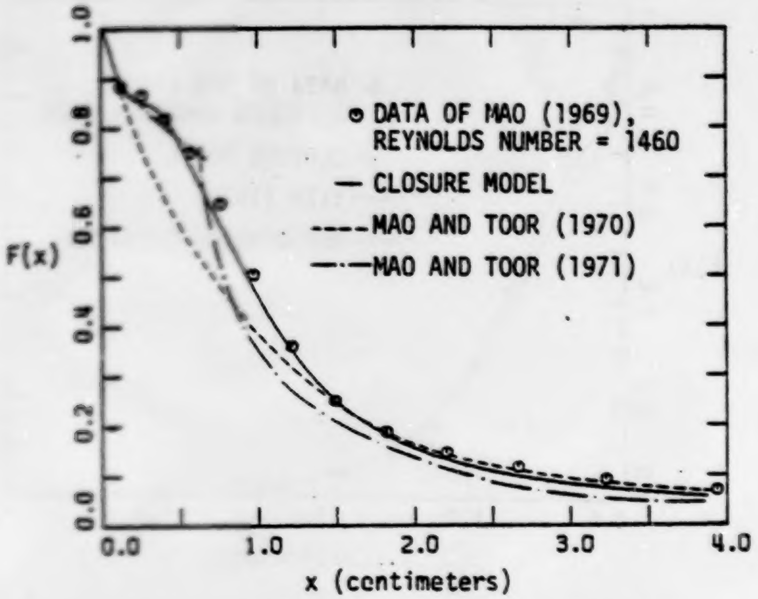

FIGURE 16. COMPARISON OF THE PREDICTIONS OF THE CLOSURE MODEL WITH CHEMICAL REACTOR DATA AND WITH THE PREDICTIONS OF THE MAO AND TOOR (1970, 1971) MODELS WITH k = 8.32 x 10^3 ℓ/mole·sec, A_0 = 0.0333 mole/ℓ, AND ρ = 1.0

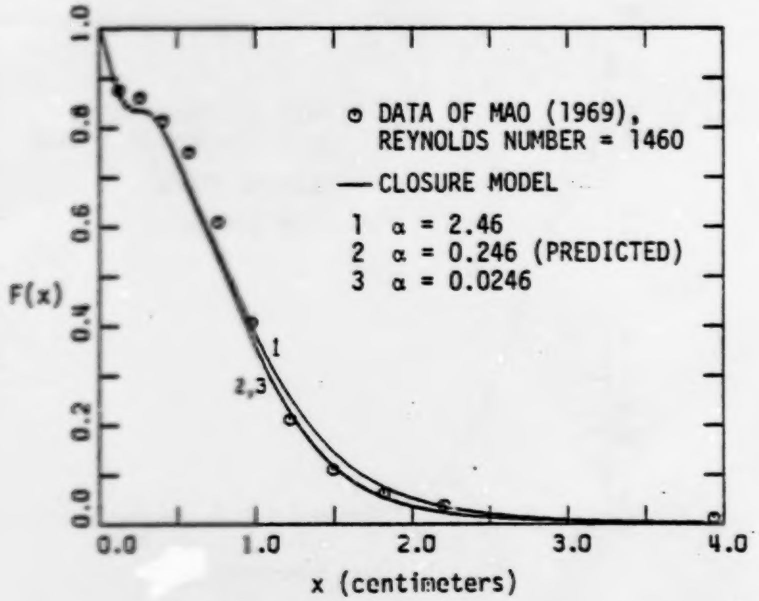

FIGURE 17. SENSITIVITY OF THE CLOSURE MODEL TO CHANGES IN THE DAMKOHLER NUMBER α WHEN k = 8.32 x 10^3 ℓ/mole·sec, A_0 = 0.034 mole/ℓ, AND ρ = 1.5

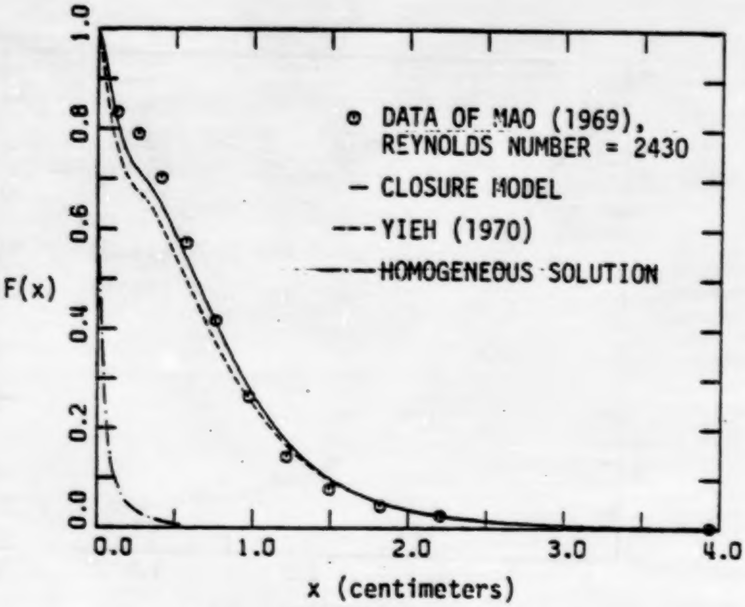

FIGURE 18. COMPARISON OF THE PREDICTIONS OF THE CLOSURE MODEL WITH CHEMICAL REACTOR DATA, THE PREDICTIONS OF THE YIEH (1970) MODEL, AND THE SOLUTION OF THE HOMOGENEOUS MODEL, EQ. (76), WITH $k = 0.832 \times 10^4$ ℓ/mole·sec, $A_0 = 0.3363$ mole/ℓ, AND $\rho = 1.5$

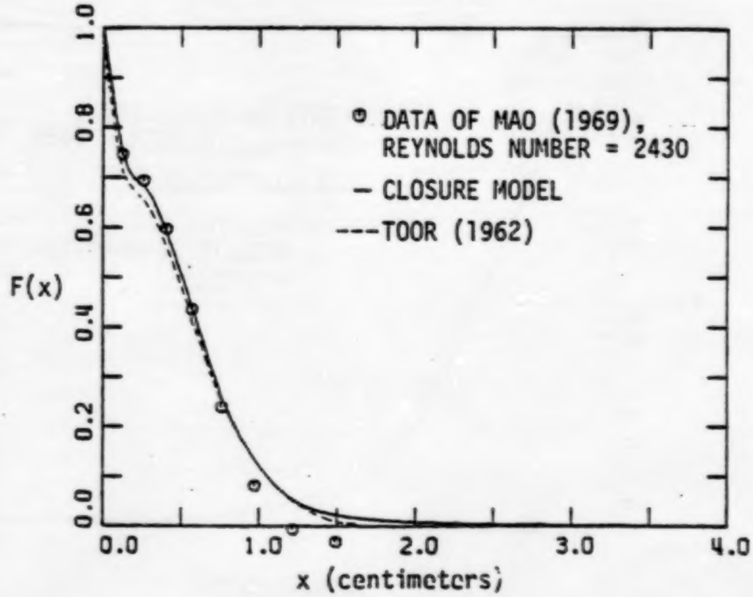

FIGURE 19. COMPARISON OF THE PREDICTIONS OF THE CLOSURE MODEL WITH THE TOOR (1962) MODEL, AS EVALUATED BY MAO (1969), AND WITH CHEMICAL REACTOR DATA FOR VERY RAPID REACTIONS

hump in the F(x) profiles between $x = 0$ and $x = 0.5$ cm shown in Figures 16 through 19. This same feature occurs in the profiles of Γ_{AB} and Γ_A shown in Appendix A. It is caused by a zone of backflow created in the reactor at the point where the jets from the reactor head meet. Comparison of Figures 16 and 17 with Figures 18 and 19 shows that, as expected, the nature of this phenomenon is affected by the Reynolds number.

To show the sensitivity of the closure model to the Damkohler number κ, we plotted in Figure 17 the solutions of Eq. (75) for three different values of this parameter. The results shown, and others not presented, indicate that for reactions of intermediate speed, the changes induced in F by an order-of-magnitude deviation in κ are within the range of experimental error. This indicates that in applications of the present model to air pollution studies, where the Damkohler number of the fastest reaction (namely, that between ozone and nitric oxide) is of the order of 10, the accuracy of the simulation will be much more sensitive to errors in the mixing parameters ζ_A and ζ_B than to deficiencies in the estimate of λ.

In Figures 15, 16, 18, and 19, we compare the predictions of the closure model both with measured data and with predictions made by other closure models reported in the literature. A qualitative description of these and other models and how they compare with the present model is given in Shu (1976).

E. RECAPITULATION

We have presented a closure method for approximating the covariance of concentration fluctuations of two reactive species undergoing a bimolecular reaction in turbulent fluid. The method does not require the solution of additional differential equations. The approximation involves a reaction parameter λ, which is expressed in terms of the reaction rate coefficient k and several properties of the fluid [see Eq. (61)], and two mixing parameters ζ_A and ζ_B, which are expressible in terms of the inert species concentration mean values $\bar{A}_I$, $\bar{B}_I$, $\overline{A_I^2}$, $\overline{B_I^2}$, and $\overline{A_I B_I}$, where the subscript I denotes the inert surrogate of the reactant species. Being independent of the chemistry, these mean values are functions only of the reactant source distribution and the characteristics of the turbulence and mean flow; and consequently, for any given source configuration, it is possible that they can be expressed as universal functions of the flow system. An attempt to develop a universal form for ζ_A, applicable to a point source in the unstable planetary boundary layer, is described later in this chapter. The main uses foreseen for this model are studies of chemical reaction in point source plumes in the atmosphere and design studies of chemical reactors in which homogeneity of the reactant concentration field is maintained in planes normal to the flow (as in the reactor discussed later).

Judging from the comparisons of the predicted and measured values presented in Figures 14 through 19, we conclude that the model developed here provides a good description of second-order chemical reactions in turbulent fluid over a considerable range of experimental conditions, at least for the reactor considered in this study.

F. APPLICATION OF THE MODEL TO POINT SOURCE PLUMES IN THE ATMOSPHERE

In this section, we adapt the model developed earlier in this chapter to simulate chemical reactions among pollutants in atmospheric plumes.

In principle, the steady-state ensemble mean concentrations of two species, A and B, in a turbulent flow, when A and B react according to $A + B \rightarrow P$, can be determined by solution of the continuity equations:*

$$\langle u_k \rangle \frac{\partial \langle A \rangle}{\partial x_k} = - \frac{\partial}{\partial x_k} \langle u_k' A' \rangle - k \langle AB \rangle \quad , \qquad (77)$$

$$\langle u_k \rangle \frac{\partial \langle B \rangle}{\partial x_k} = - \frac{\partial}{\partial x_k} \langle u_k' B' \rangle - k \langle AB \rangle \quad , \qquad (78)$$

where $A' = A - \langle A \rangle$, $B' = B - \langle B \rangle$, and $u_k' = u_k - \langle u_k \rangle$. If appropriate expressions are available for the turbulent flux terms $\langle u_k' A' \rangle$ and the kinetic term $\langle AB \rangle$, Eqs. (77) and (78) can be solved to predict $\langle A \rangle$ and $\langle B \rangle$.

The model developed in Section III.B provides a general expression for the kinetic term $\langle AB \rangle$. To implement this model, one needs the quantities Γ_A, Γ_B, and Γ_{AB} to evaluate the mixing parameters ζ_A and ζ_B that enter in this model (see Table 1). These quantities could be estimated by solving their governing equations numerically; but for the purposes of air pollution modeling, where the number of differential equations to be solved is already large, it is desirable to express the required concentration statistics in parametric form. In this section, we attempt to derive such formulations using the numerical planetary boundary layer model of Deardorff (1974a, 1974b). We use Lagrangian techniques very similar to those employed by Lamb, Chen, and Seinfeld (1975) to study diffusion in the planetary boundary layer. Deardorff and Peskin (1970) and Riley and Patterson (1974) have also used Lagrangian methods to study turbulent flows.

---

*In this section, ensemble averages are denoted by angled parentheses $\langle \ \rangle$ to simplify necessary notation.

In Section G.1, we adapt the model (developed in Section III.B) to a chemically reacting plume. Since our primary concern in this study is the reaction term $\langle AB \rangle$, we circumvent the need for expressions for the flux terms $\langle u_k'A' \rangle$ and $\langle u_k'B' \rangle$ by computing the total chemical conversion, integrated across the plume, as a function of distance from the point of release. The inert concentration statistics required in this model are derived in Section G.2, and the full model is applied in Section G.3 to the problem of predicting the rate of conversion of nitric oxide in the plume from the Potomac Electric Company power plant in Morgantown, Maryland.

1. Model for a Chemically Reacting Plume

Let us consider a continuous, elevated point source in the atmospheric boundary layer with the x-axis aligned in the direction of the mean wind. If the slender plume approximation can be made, i.e., that turbulent diffusion in the x-direction is negligible relative to advection by the mean flow, Eq. (77) becomes

$$\langle u \rangle \frac{\partial \langle A \rangle}{\partial x} = \frac{\partial}{\partial y} (-\langle v'A' \rangle) + \frac{\partial}{\partial z} (-\langle w'A' \rangle) - k\langle AB \rangle \quad , \qquad (79)$$

where (x_1, x_2, x_3) is replaced by (x, y, z) and (u_1, u_2, u_3) by (u, v, w). Since the equation for $\langle B \rangle$ is similar, we consider Eq. (79) only.

Let z_i be the height of the inversion layer below which convection and mixing are confined, and let L_y be a distance large enough that the spread of the plume in the y-direction does not exceed L_y for all values of x of interest. We now define the spatial averages:

$$\bar{A}(x) = \frac{1}{A_c} \int_{-L_y}^{L_y} \int_0^{z_i} \langle A(x,y,z) \rangle \, dz \, dy \quad , \qquad (80)$$

$$\widetilde{A^2}(x) = \frac{1}{A_c} \int_{-L_y}^{L_y} \int_0^{z_i} \langle A^2(x,y,z) \rangle \, dz \, dy \quad , \qquad (81)$$

where $A_c = 2L_y z_i$. The main quantity of interest to us is $\bar{A}(x)A_c$, which is the mean value of the total mass of A at location x. As we show later, neither this quantity nor its rate of change is dependent on A_c when A_c is sufficiently large.

If there is little wind shear in the plume and no surface flux of A or B, Eq. (79) can be integrated with respect to y and z over A_c to yield

$$\langle u \rangle \frac{d\bar{A}}{dx} = -k\widetilde{AB} \quad , \qquad (82)$$

where

$$\widetilde{AB} = \frac{1}{A_c} \int_{-L_y}^{L_y} \int_0^{z_i} \langle AB \rangle \, dz \, dy \quad . \qquad (83)$$

Equation (82), together with its counterpart,

$$\langle u \rangle \frac{d\bar{B}}{dx} = -k\widetilde{AB} \quad , \qquad (84)$$

describes the overall rate of conversion as a function of downwind distance in the plume.

The closure model presented earlier can be used to represent $\widetilde{AB}$ in Eq. (79) if the tilde average, defined in Eqs. (80) and (81), is regarded as an integration of the instantaneous species concentrations over the "volume" S, which consists of an ensemble of plume cross sections (bounded by $-L_y \leq y \leq L_y$, $0 \leq z \leq z_i$) at a distance x from the source. Thus, from Eq. (84), we obtain Eq. (38) of Section III.B:

$$\langle u \rangle \frac{d\tilde{A}}{dx} = - \frac{k\lambda\tilde{\Gamma}_{AB}}{\zeta_A \zeta_B} \left[\tilde{A} - (1 - \zeta_A)\tilde{A}_I\right]\left[\tilde{B} - (1 - \zeta_B)\tilde{B}_I\right] \quad , \qquad (85)$$

$$\langle u \rangle \frac{d\tilde{B}}{dx} = - \frac{k\lambda\tilde{\Gamma}_{AB}}{\zeta_A \zeta_B} \left[\tilde{A} - (1 - \zeta_A)\tilde{A}_I\right]\left[\tilde{B} - (1 - \zeta_B)\tilde{B}_I\right] \quad , \qquad (86)$$

where

$$\tilde{\Gamma}_{AB} = \frac{\widetilde{A_I B_I}}{\tilde{A}_I \tilde{B}_I} \qquad (87)$$

and where λ, ζ_A, and so forth have the same meanings as before. Equations (85) and (86) constitute the basic model for $\tilde{A}$ and $\tilde{B}$ as a function of x in a plume in which A and B are undergoing a second-order reaction.

For simplicity, we consider only situations in which A is released into a fluid containing a uniform concentration of B. Earlier, we showed that in problems of this type $\zeta_A = \tilde{\Gamma}_{AB} = 1$ and that ζ_B can be represented to good approximation by

$$\zeta_B = \frac{\tilde{A}_I^2}{\widetilde{A_I^2}} \quad , \qquad (88)$$

where A_I denotes the concentration that would be observed if the species A were chemically inert. Since all mean and product mean values of A_I are independent of the chemistry, ζ_B is expressible in terms of certain Lagrangian properties of the turbulence. These are derived in the next section.

2. Numerical Formulation of ζ_B

To evaluate the quantities $\widetilde{A_I^2}$ and $\bar{A}_I$, which enter in the definition of ζ_B, we need expressions for $\langle A_I^2 \rangle$ and $\langle A_I \rangle$ [see Eqs. (81) and (82)]. The former is given by (Lamb, 1975):

$$\langle A_I^2(\underline{x},t) \rangle = \frac{1}{\Delta V^2} \int_{\Delta V} \int_{\Delta V} \int_0^t \int \int_0^t \int p(\underline{x}',\underline{x}'',t \,|\, \underline{x}_0',t_0',\underline{x}_0'',t_0'') \cdot S(\underline{x}_0',t_0')S(\underline{x}_0'',t_0'')\, d\underline{x}_0'\, dt_0'\, d\underline{x}_0''\, dt_0''\, d\underline{x}'\, d\underline{x}'' \quad , \qquad (89)$$

where p is the probability density function that two particles, one released at $\underline{x}_0'$ at time t_0' and the other at $\underline{x}_0''$ at time t_0'', are found at $\underline{x}'$ and $\underline{x}''$, respectively, at time t; $S(\underline{x}_0,t_0)$ is the source distribution; and ΔV is the sample volume centered at x. If ΔV is sufficiently small that $p(\underline{x}',\underline{x}'',\ldots)$ is approximately constant for all $\underline{x}'$ and $\underline{x}''$ within ΔV, Eq. (89) reduces to the form

$$A_I^2(x,t) = \int_0^t \int \int_0^t \int p(\underline{x},\underline{x},t \,|\, \underline{x}_0,t_0;\underline{x}_0',t_0') \cdot S(\underline{x}_0,t_0)S(\underline{x}_0',t_0')\, d\underline{x}_0\, dt_0\, d\underline{x}_0'\, dt_0' \quad , \qquad (90)$$

where $\underset{\sim}{x}_0 = (x_0,y_0,z_0)$ and ΔV is the sample volume centered at $\underset{\sim}{x}$. Assume that the source is a circular area perpendicular to the x-axis, with area a_S and uniform strength Q_a; that the turbulence is stationary so that p is a function only of the time differences $t - t'_0$ and $t - t''_0$; and that x-dispersion in the plume can be neglected. Then Eq. (90) becomes (Shu, 1976)

$$\left\langle A_I^2(\underset{\sim}{x})\right\rangle = Q_A^2 \int_{a_s}\int_{a_s} p(\underset{\sim}{y},\underset{\sim}{y},t|\underset{\sim}{y}_0,\underset{\sim}{y}'_0)\, d\underset{\sim}{y}_0\, d\underset{\sim}{y}'_0 \quad , \qquad (91)$$

where $t = x/\langle u\rangle$ and $\underset{\sim}{y} = (y,z)$. Thus, we find that

$$\tilde{A}_I^2(t) = \frac{Q_A^2}{\langle u\rangle^2 A_c}\int_{a_s}\int_{a_s} P(t,\underset{\sim}{y}_0,\underset{\sim}{y}'_0)\, d\underset{\sim}{y}'_0\, d\underset{\sim}{y}_0 \quad , \qquad (92)$$

where

$$P(t,\underset{\sim}{y}_0,\underset{\sim}{y}'_0) = \int_{A_c} p(\underset{\sim}{y},\underset{\sim}{y},t|\underset{\sim}{y}_0,\underset{\sim}{y}'_0)\, d\underset{\sim}{y} \quad . \qquad (93)$$

In the limit of large t, P becomes independent of the particle release points $\underset{\sim}{y}_0$ and $\underset{\sim}{y}'_0$, and Eq. (92) reduces to

$$\tilde{A}_I^2(t) = \frac{Q_A^2 a_s^2}{\langle u\rangle^2 A_c}\, \underset{\sim}{P}(t,\underset{\sim}{\xi},\underset{\sim}{\xi}') \quad , \qquad (94)$$

where $\underset{\sim}{\xi}$ and $\underset{\sim}{\xi}'$ are any two points in the source area a_s. When t is small, P is not independent of $\underset{\sim}{y}_0$ and $\underset{\sim}{y}'_0$, and the general expression Eq. (92) must be evaluated numerically. This poses quite a computational burden, however, because the evaluation of P for a single set of initial release points $(\underline{y}_0, \underline{y}'_0)$ requires a large amount of computer time. Therefore, we seek a way of reducing Eq. (92) to a form like that of Eq. (94). This can be achieved if we can find the set of vectors $(\bar{\underline{y}}_0, \bar{\underline{y}}'_0)$ for which

$$P(t, \bar{\underline{y}}_0, \bar{\underline{y}}'_0) = \frac{1}{a_s^2} \int_{a_s} \int_{a_s} P(t, \underline{y}_0, \underline{y}'_0)\, d\underline{y}'_0\, d\underline{y}_0 \qquad (95)$$

because with this expression we can write Eq. (92) in the desired form:

$$\tilde{A}_I^2(t) = \frac{Q_A^2 a_s^2}{\langle u \rangle^2 A_c} P(t, \bar{\underline{y}}_0, \bar{\underline{y}}'_0) \quad . \qquad (96)$$

Shu (1976) showed that for a circular source of radius r_s, $(\bar{\underline{y}}_0, \bar{\underline{y}}'_0)$ is any vector pair lying in the source such that $\bar{\ell}_0 = |\bar{\underline{y}}_0 - \bar{\underline{y}}'_0| = 0.66 r_s$. Thus,

$$\tilde{A}_I^2(t) = \frac{Q_A^2 a_s^2}{\langle u \rangle^2 A_c} \int_{A_c} p_2(\underline{y}, t)\, d\underline{y} \quad , \qquad (97)$$

where $p_2(\underline{y}, t) = p(\underline{y}, \underline{y}, t | \bar{\ell}_0)$ is the probability density function that two particles separated initially by a distance $\bar{\ell}_0$ will be found together in the sample volume centered at $\underline{y}$ at time t. Since

$$\bar{A}_I = \frac{Q_A a_s}{\langle u \rangle A_c} \qquad (98)$$

[this follows from Eq. (86) and the assumptions made just before Eq. (91)], ζ_B can be evaluated immediately once the form of the two-particle probability density p_2 that enters in Eq. (97) is known. In the remainder of this section, we describe how we evaluated this function for the planetary boundary layer using the velocity field simulated numerically by Deardorff (1974a, 1974b), for Day 33 of the Wangara study (Clarke et al., 1971).

The simulation covers an area of 5 x 5 km^2 with a vertical depth of 2 km. This volume is divided into a 40 x 40 x 40 grid, each cell of which measures $\Delta x = \Delta y = 125$ m and $\Delta z = 50$ m. Owing to the vast amount of data generated, only data for the period from 1229 to 1321 local time were stored. During this period, convection is confined below a stable layer whose base height z_i is given by

$$z_i = 1134.4 + 0.039t \quad , \tag{99}$$

where t is in seconds and z_i in meters. The convective velocity scale w_* during this interval varies slightly about a mean value of about 1.96 m/sec. (The convective velocity scale is defined by

$$w_* = \left(\frac{g}{\theta_m} \overline{w'\theta_s'} \, z_i \right)^{1/3} \quad , \tag{100}$$

where g is the gravitational acceleration, θ_m is the mean potential temperature in the mixed layer, and $\overline{w'\theta_s'}$ is the kinematic heat flux close to the ground.) Owing to the slowness of the variations in z_i, w_*, and the horizontal pressure gradient that drives the flow, we assume that the turbulence is in a quasi-stationary state.

3. Creation of an Ensemble of Particle Trajectories

We can construct an ensemble of particle trajectories suitable for calculating p_2 by releasing pairs of particles into the simulated flow and tracing their motions. A particle located at x has the instantaneous velocity

$$\underline{u}_P(\underline{x}) = \underline{u}_D(\underline{x}) + u_{SG}(\underline{x}) \quad , \tag{101}$$

where $\underline{u}_D(x)$ is the supergrid-scale velocity calculated at $\underline{x}$, through a linear interpolation of the velocities at neighboring grid points in Deardorff's data set, and $\underline{u}_{SG}$ is the subgrid-scale velocity component at $\underline{x}$. In an application of his model to a study of single particle statistics, Deardorff (1972) found that subgrid-scale effects were unimportant; but this is not the case in the present study where we are concerned with the relative motion of particle pairs whose initial separations are much smaller than the grid size. The method we used to parameterize the subgrid-scale motions incorporates the similarity theory developed by Batchelor (1950) and is described in detail in Appendix B.

Starting at 1231 local time, 1225 pairs of particles, each separated initially by a distance of 4 m, were released from the center of each grid cell on the horizontal plane at z = 125 m, a level well above the shear layer. The particles were tracked for a period of 1432 seconds. The trajectory of each particle was determined from the expression

$$\underline{x}_p(t + \Delta t) = \underline{x}_p(t) + \underline{u}_D[\underline{x}_p(t)]\Delta t + \int_t^{t+\Delta t} \underline{u}_{SG}[\underline{x}_p(t')]\, dt' \quad .$$

From the ensemble of particle trajectories created by the process just described, particle displacement statistics and mean square particle separations have been computed and compared with data gathered from atmospheric field studies, laboratory simulations of the planetary boundary layer, and other numerical turbulence models [see Lamb (1977)]. These comparisons indicate that the present model provides a reliable description of one- and two-particle displacement statistics in the unstable boundary layer. These statistics alone will determine the form of the mixing parameter ζ_B that we subsequently consider.

4. Sampling Procedure and Statistical Error of the Estimate of p_2

We mentioned in Section G.2 that implicit in p_2 is a sample volume ΔV whose dimensions must be small compared with the length scale of spatial variations in p_2. Based on a joint-normal approximation of p_2, we estimate that a suitable sample size $V = \Delta y \Delta z$ is

$$\Delta y = 0.2\ \ell_y(t) \quad , \tag{102a}$$

$$\Delta z = 0.2\ \ell_z(t) \quad , \tag{102b}$$

where $\ell_y(t)$, $\ell_z(t)$ are the y- and z-components of the root-mean-square particle separation $\langle \ell^2 \rangle^{1/2}$ at time t. (The adequacy of this sample volume size was confirmed through a series of test runs.) Using this sample volume, we computed p_2 in the following manner. First, the coordinate system of the recorded particle trajectories was rotated to align the x-axis with the mean wind direction. The mean wind speed is 2.74 m/sec at an angle of 157° with respect to the east-west axis.

Next, the coordinates of each pair of particles were translated to a new system (η,ζ):

$$\eta_1 = y_1(t) - y_1(t_0) \quad , \quad \zeta_1 = z_1 \quad ,$$

$$\eta_2 = y_2(t) - y_2(t_0) \quad , \quad \zeta_2 = z_2 \quad .$$

Each pair of particles was then considered to constitute one realization of the ensemble of particle pair trajectories. After the above operations were performed, the sample volume ΔV was determined from Eq. (102), and the averaging area A_c was divided into cells of size ΔV. Within this framework, we have

$$p_2(\underset{\sim}{y},t) = \langle c(\underset{\sim}{y},t) \rangle \quad , \tag{103}$$

where $\langle\ \rangle$ denotes ensemble averaging and

$$c(\underset{\sim}{y},t) = \begin{cases} 1/\Delta V^2 & \text{if both particles are located in } \Delta V \text{ centered at } \underset{\sim}{y} \text{ at time t on any given realization;} \\ 0 & \text{otherwise.} \end{cases} \tag{104}$$

We can approximate Eq. (103) by

$$p_2(\underset{\sim}{y},t) = \frac{1}{N_R} \sum_{i=1}^{N_R} c_i(\underset{\sim}{y},t) \quad , \tag{105}$$

where c_i is the value of c on the i-th realization. Upon substituting this expression into Eq. (97), we obtain

$$\tilde{A}_I^2(t) = \frac{Q_A^2 a_s^2}{\langle u\rangle^2 A_c} \int_{A_c} \frac{1}{N_R} \sum_{i=1}^{N_R} c_i(\underset{\sim}{y},t)\, d\underset{\sim}{y} \quad . \tag{106}$$

That Eq. (106) provides an unbiased estimate of $\tilde{A}_I^2(t)$ can be seen by taking the ensemble average of this expression and using Eq. (103). We find that

$$\langle \tilde{A}_I^2 \rangle \frac{Q_A^2 a_s^2}{\langle u\rangle^2 A_c} \int_{A_c} \frac{1}{N_R} \sum_{i=1}^{N_R} \langle c_i \rangle \, d\underset{\sim}{y}$$

$$= \frac{Q_A^2 a_s^2}{\langle u\rangle^2 A_c} \int_{A_c} p_2 \, d\underset{\sim}{y} = \tilde{A}_I^2 \quad . \tag{107}$$

This result assures us that we can make the error in the estimate of $\tilde{A}_I^2$ arbitrarily small by making N_R sufficiently large. However, for all practical values of N_R, there is an error associated with Eq. (106). Keeping in mind that $\tilde{A}_I^2$ is an approximation, namely, the solution of Eq. (106) for finite N_R, and $\langle \tilde{A}_I^2 \rangle$ is the exact value, i.e., the limit of Eq. (106) as $N_R \rightarrow \infty$, we define the mean square error in Eq. (106) to be $\chi = \langle (\tilde{A}_I^2 - \langle \tilde{A}_I^2 \rangle)^2 \rangle$.

We obtain

$$\chi = \left(\frac{Q_A^2 a_s^2}{\langle u\rangle^2 A_c} \right)^2 \int_{A_c} \int_{A_c} \frac{1}{N_R^2} \sum_{i=1}^{N_R} \sum_{j=1}^{N_R} \langle c_i(\underset{\sim}{y}) c_j(\underset{\sim}{y}') \rangle \, d\underset{\sim}{y} \, d\underset{\sim}{y}' - \langle \tilde{A}_I^2 \rangle^2 \quad . \tag{108}$$

In our experiment, each particle pair released from every grid is considered to be one realization, but these realizations are not statistically independent because of the proximity of the particle pairs to one another at their time of release. Suppose that for each i, c_i is perfectly correlated with m other realizations but is statistically independent of all the rest, i.e.,

$$\left\langle c_i(\underline{y})c_j(\underline{y}')\right\rangle = \begin{cases} \left\langle c(\underline{y})c(\underline{y}')\right\rangle & \text{if the i-th and the j-th realizations are correlated;} \\ \left\langle c(\underline{y})\right\rangle\left\langle c(\underline{y}')\right\rangle & \text{otherwise.} \end{cases} \tag{109}$$

Substituting Eq. (109) into Eq. (108), we find that

$$x = \frac{m+1}{N_R}\left[\left(\frac{Q_A^2 a_s^2}{\langle u\rangle^2 A_c}\right)^2 \int_{A_c}\int_{A_c} \left\langle c(\underline{y})c(\underline{y}')\right\rangle \, d\underline{y}\, d\underline{y}' - \widetilde{A_I^2}^{\,2}\right] . \tag{110}$$

By virtue of its definition, $c_i(\underline{y})$ can have a nonzero value at only one location. Therefore,

$$\left\langle c(\underline{y})c(\underline{y}')\right\rangle = \begin{cases} \left\langle c^2(\underline{y})\right\rangle & \text{if } \underline{y}' = \underline{y}; \\ 0 & \text{if } \underline{y}' \neq \underline{y}. \end{cases}$$

Applying this relationship to Eq. (110), we have

$$x = \frac{m+1}{N_R}\left[\left(\frac{Q_A^2 a_s^2}{\langle u\rangle^2 A_c}\right)^2 \Delta V \int_{A_c} \left\langle c^2(\underline{y})\right\rangle d\underline{y} - \left\langle \widetilde{A_I^2}\right\rangle^2\right] .$$

The mean fractional error ε is then

$$\varepsilon \equiv \left(\frac{\chi}{\langle A_I^2 \rangle}\right)^{1/2} = \left(\frac{m+1}{N_R}\right)^{1/2} (\gamma - 1)^{1/2} \quad , \tag{111}$$

where

$$\gamma = \frac{\Delta V \int_{A_c} \langle c^2(\underline{y}) \rangle \, d\underline{y}}{\left[\int_{A_c} \langle c(\underline{y}) \rangle \, d\underline{y}\right]^2} \tag{112}$$

To estimate ε, we must first approximate γ. Toward this end, we assume that in each realization the particles are equally likely to be found anywhere within a box of size $n\Delta V$. Two extreme cases are considered:

(1) If the two particles are totally correlated, they are always observed together. Consequently,

$$\langle c(\underline{y}) \rangle = \begin{cases} \frac{1}{n}\left(\frac{1}{\Delta V}\right)^2 & \text{if } \underline{y} \in n\Delta V, \\ 0 & \text{otherwise.} \end{cases}$$

$$\langle c^2(\underline{y}) \rangle = \begin{cases} \frac{1}{n}\left(\frac{1}{\Delta V}\right)^4 & \text{if } y \in n\Delta V, \\ 0 & \text{otherwise.} \end{cases}$$

It follows that in this case $\gamma = 1$ and $\varepsilon = 0$. The error vanishes in this case because we integrated the concentration over the entire y-z plane instead of attempting to determine the concentration at a particular point.

(2) If positions of the two particles are statistically independent, then

$$\left\langle c(\underline{y})\right\rangle = \begin{cases} \dfrac{1}{n^2}\left(\dfrac{1}{\Delta V}\right)^2 & \text{if } y \in n\Delta v, \\ 0 & \text{otherwise.} \end{cases}$$

$$\left\langle c^2(\underline{y})\right\rangle = \begin{cases} \dfrac{1}{n^2}\left(\dfrac{1}{\Delta V}\right)^4 & \text{if } y \in n\Delta V, \\ 0 & \text{otherwise.} \end{cases}$$

It follows that $\gamma = n$, and

$$\varepsilon = \left(\frac{m+1}{N_R}\right)^{1/2} (n-1)^{1/2} \quad .$$

We note that the error is larger in the statistically independent case. This situation occurs because when the particle motions are correlated, the particles are more likely to be found together and fewer realizations are needed to detect all of their possible positions. In reality, particle pairs are correlated initially and then become independent gradually. Hence, the true error is expected to lie somewhere between the two error bounds given above. Let us assume that

$$\varepsilon = (1-\rho)\left(\frac{m+1}{N_R}\right)^{1/2} (n-1)^{1/2} \quad , \qquad (113)$$

where ρ is the position correlation coefficient.

Based on the computed spatial velocity correlations, we estimate that initially m has a value of 10 and decays to 0 in about 500 sec. Using $N_R = 1225$, $n\Delta V = 4\sigma_y\sigma_z$, and the time-dependent values of ρ calculated from the ensemble of particle trajectories, we estimate that by the maximum travel time of interest, namely, about 1400 seconds, ε has grown to only 14 percent.

5. Estimate of the ζ_B

Combining Eqs. (88), (98), and (106), we obtain the desired expression

$$\zeta_B(t) = \frac{N_R \Delta V}{N A_c} \quad ,$$

where N is the total number of realizations in which $c(\underset{\sim}{y},t)$ is nonzero somewhere in A_c. Figure 20 shows the computed value of $\zeta_B(t)/\zeta_B(0)$ for two release heights: $z_{p0} = 0.25\ z_i$ and $z_{p0} = 0.025\ z_i$. (Note that by definition $\zeta_B(0) = a_s/A_c$.) As expected, ζ_B, which is proportional to the quantity of ambient fluid that has mixed with the plume fluid, increases with time but not nearly as fast (as shown later) as the rate of expansion of the mean plume width would suggest. It is also evident from Figure 20 that mixing occurs more rapidly for an elevated source than for a low-level source.

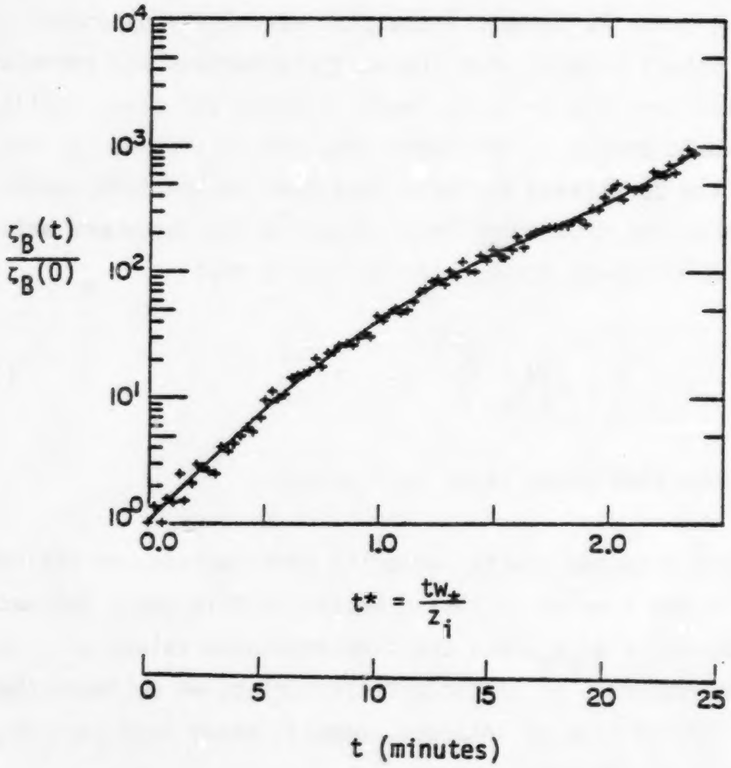

FIGURE 20. CALCULATED FORM OF THE MIXING PARAMETER ζ_B, NORMALIZED BY ITS INITIAL VALUE $\zeta_B(0)$, AS A FUNCTION OF TRAVEL TIME t FOR TWO SOURCE HEIGHTS

Deardorff (1972) found that mean properties of the unstable boundary layer can be made universal if all lengths are scaled by z_i, the height of the inversion below which convection is confined, and times are scaled by z_i/w_*, where w_* is the convective velocity scale defined in Eq. (100). Assuming that ζ_B possesses a similar universal form, we have fit the following least-squares polynomial to the data shown in Figure 20 for use in other studies:

$$\log_{10} \frac{\zeta_B(t^*)}{\zeta_B(0)} = a_1 t^* + a_2 t^{*2} + a_3 t^{*3} + a_4 t^{*4} \quad , \tag{114}$$

where $a_1 = 1.736$, $a_2 = 0.111$, $a_3 = -0.359$, $a_4 = 0.095$. These coefficients are not necessarily independent of the source area a_s. In the next section, we utilize these results in the model to simulate a reactive plume in the planetary boundary layer.

6. Study of the Reaction Between Nitric Oxide and Ozone in Simulated Atmospheric Turbulence

Two major air pollutant sources for which the influence of turbulence on chemical reactions may be important are highways and power plants. Nitric oxide (NO) is emitted in significant quantities from each type of source. Since NO then participates in a complex series of reactions leading to photochemical smog, understanding the fate of NO from these two types of sources is important in understanding photochemical smog chemistry.

Measurements have been reported by Davis, Smith, and Klauber (1974) of NO, O_3, and SO_2 concentrations in plumes produced by the Potomac Electric Company power plant in Morgantown, Maryland. The conditions under which these data were measured are sufficiently similar to those of the turbulence simulation reported here that these data provide a partial check of the closure model and our implementation of it.

It is assumed that the chemical reactions dominant in the plume after its release to the atmosphere are (Davis, Smith, and Klauber, 1974):

$$NO + O_3 \xrightarrow{k_1} NO_2 + O_2 \quad , \quad k_1 = 29 \text{ ppm}^{-1}\text{min}^{-1} \quad , \tag{115a}$$

$$NO_2 + h\nu \xrightarrow[O_2]{k_2} NO + O_3 \quad , \quad k_2 \cong 0.3 \text{ min}^{-1} \quad , \tag{115b}$$

where the NO is emitted into a background atmosphere containing O_3.

Let A, B, and C be the concentrations of NO, O_3, and NO_2, respectively. The equation governing the plume cross-section averaged concentration $\tilde{A}$ is identical to Eq. (85) except for the term $+k_2C$ on the right-hand side that accounts for the generation of NO by Reaction (115b). Since A is emitted into an environment with uniform B, $\zeta_A = 1$, $\Gamma_{AB} = 1$, and ζ_B is given by Eq. (114). Also, since the background O_3 concentration in the present instance is 80 ± 3 ppb (Davis, Smith, and Klauber, 1974), we have $A_0 >> B_0$ and therefore from Table 1, $\lambda = 1$. Under these conditions, we find that the conversion rate of NO in the plume is given by

$$\langle u \rangle \frac{dF_A}{dx} = -k_1 \left[\frac{Q_A}{\langle u \rangle} \frac{\zeta_B(0)}{\zeta_B(x)} \right] \left[F_A - 1 + B_0 \frac{\langle u \rangle}{Q_A} \frac{\zeta_A(x)}{\zeta_A(0)} \right] F_A + k_2(1 - F_A) \quad , \tag{116}$$

where

$$F_A = \frac{\tilde{A}}{\tilde{A}_I} \tag{117}$$

and $\tilde{A}_I$ is the initial value of $\tilde{A}$.

To compare the results of the simulation with the data of Davis, Smith, and Klauber, one must know the emissions flux Q_A of NO at the stack; but unfortunately, this value was not available. Using values of the fuel consumption rate supplied by an engineer at the Morgantown plant, we estimated the NO emissions rate to be between 2900 and 4900 kg/hr at the stacks.

Because of the tremendous amount of thermal energy exhausted by the power plant, the plume near the stacks behaves like a thermal jet rather than a passive plume carried by a turbulent fluid. Thus, only the portion of the plume dominated by ambient turbulence can be compared with our simulation. For this reason, we treat the data as representing a plume emanating from a fictitious source perpendicular to the plume axis and located at the point downwind where the plume first becomes horizontal. Suppose that at this point the plume radius is four times the radius of the stack. Assuming the twin stacks each have a radius of 5 m, the average emissions flux Q_A at the fictitious source is estimated to be 1.1 to 2.0 kg/hr m^2. Using a mean wind speed of 24 km/hr as observed by Davis, Smith, and Klauber (1974), we find the fictitious source concentration $Q_A/\langle u\rangle$ to be 39 to 67 ppm. Estimation of the location of this fictitious source so defined requires more information, such as plume temperature, than we have. However, Davis and Klauber (1975) reported that at 0.8 km downwind, NO concentration was approximately 2 ppm. This suggests that the fictitious source must be rather near to the stack, and so we assume that no appreciable chemical conversion has taken place before NO reaches the fictitious source location. Admittedly, these estimates are rather crude, but without them there is no basis for judging the accuracy of the simulation.

The extent of conversion F_A is plotted in Figure 21 as a function of $t^* = tw_*/z_i$. The data of Davis, Smith, and Klauber are shown on the same graph for comparison. The error bar on each of the data points indicates the range of observed values. To connect these data with the t* coordinate, we first transformed distance into travel time by using a uniform wind speed of 24 km/hr. Then we normalized t using z_i = 1000 m, supplied by Davis (private communication, 1976), and w_* = 1.8 m/sec estimated from the observed cloud cover, wind speed, and approximate surface roughness of the Morgantown area.

Because of the uncertainty in the estimate of NO emissions rate, we computed F_A for both the maximum and the minimum of the estimated $Q_A/\langle u\rangle$ values. Although there are too few data points to make a definite judgment, the computed and observed conversion rates agree quite well. The

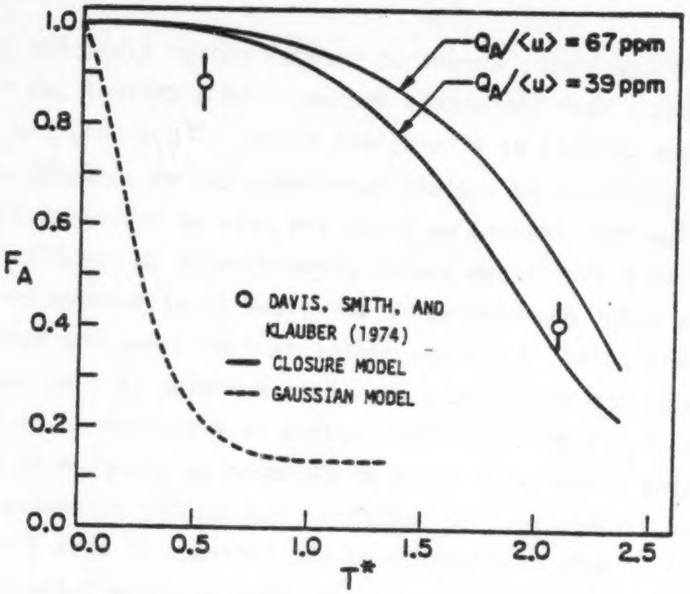

FIGURE 21. COMPARISON OF THE PREDICTED NO CONVERSION F_A (SOLID CURVES) WITH OBSERVATIONS (CIRCLES) AND THE PREDICTION OF A HOMOGENEOUS GAUSSIAN MODEL THAT IGNORES TURBULENT CONCENTRATION FLUCTUATION EFFECTS (DASHED LINE)

observed conversion is greater at small travel times than that predicted by the model, suggesting that the buoyancy-generated turbulence in the initial portion of the plume might be more effective in mixing the NO and ambient ozone than we had assumed. Recall that since buoyancy effects are not included in our simulation, we treated the observational data as though the observed plume were neutrally buoyant and issuing from a fictitious source some distance from the stack. Also, differences in the release heights of the simulated and observed plumes may have some effect.

An important aspect in which the computed and observed data are in close agreement is the magnitude of the time scale of conversion of NO. As is evident in Figure 21, in both the simulation and the observations, 50 percent of the NO released was converted to NO_2 during about the first 20 minutes of travel. Davis, Smith, and Klauber (1974) reported that the conversion times they observed ranged from about 12 to 60 minutes, depending on the meteorology and background ozone concentration.

In view of the rather large initial computational effort that is necessary to derive the parameters (such as ζ_B) required to implement the closure model, it is appropriate to inquire whether a plume simulation of comparable accuracy could be achieved using a simple, conventional approach. To investigate this matter, we constructed a Gaussian-type model of the NO plume treated above and exercised it under the same conditions as those implicit in the data shown in Figure 21. For an axisymmetric plume, we set up the conventional model in the form

$$\frac{\partial\langle A\rangle}{\partial t} = \frac{\partial\langle B\rangle}{\partial t} = K(t)\left(\frac{\partial^2\langle A\rangle}{\partial r^2} + \frac{1}{r}\frac{\partial\langle A\rangle}{\partial r}\right) - k_1\langle A\rangle\langle B\rangle + k_2(B_0 - \langle B\rangle) \quad , \tag{118}$$

where $t = x/\langle u\rangle$ and $r = \sqrt{y^2 + z^2}$. We assume that K(t) is related to the mean square displacement of a single particle by

$$K(t) = \frac{d\sigma^2}{dt} \quad , \tag{119}$$

and we use $\sigma^2(t)$ from the simulation. These assumptions are not critical; since the conversion F_A is defined by

$$F_A(t) = \frac{\int_0^\infty 2\pi r\langle A(r,t)\rangle\, dr}{a_s \dfrac{Q_A}{\langle u\rangle}} \quad , \tag{120}$$

the effect of cross-sectional diffusion is reduced. Test runs indicate a weak dependence of F_A on the eddy diffusivity K(t). The initial conditions on Eq. (118) are:

$$\langle A(r,0)\rangle = \begin{cases} Q_A/\langle u\rangle & \text{if } 0 \le r \le r_0, \\ 0 & \text{otherwise.} \end{cases}$$

$$\langle B(r,0)\rangle = B_0 \quad \text{for all } r.$$

The boundary conditions are:

$$\frac{\partial\langle A\rangle}{\partial r} = \frac{\partial\langle B\rangle}{\partial r} = 0 \qquad \text{at } r = 0,$$

$$\langle A\rangle = 0 \quad , \quad \langle B\rangle = B_0 \qquad \text{at } r \to \infty ,$$

where r_0 is the source radius (= 5.66 m). We chose a value of $Q_A/\langle u\rangle$ = 47 ppm and solved Eq. (118) numerically. The results, represented by the dashed curve in Figure 21, indicate a 50 percent conversion time of NO of three minutes and a much more rapid initial rate of reaction than is observed. If the value of $Q_A/\langle u\rangle$ is increased, the prediction of F_A agrees more closely with the observations; but to obtain good agreement, the NO emission at the Morgantown plant would have to be 112,000 kg/hr. We should add that as indicated in Figure 21, F_A does not fall to zero but rather to the point where Reactions (115a) and (115b) are in equilibrium.

Since the dependence of F_A on K is weak, the difference between the prediction of the closure model and that of the Gaussian model can be attributed only to the neglect of the fluctuation term $\langle A'B'\rangle$. When NO is first emitted, the O_3 in the plume itself is quickly depleted by the reaction, and the excess NO must wait for turbulent mixing to supply fresh ozone from outside the plume for the reaction to proceed. In this initial period, reactants are highly segregated, and $\langle A'B'\rangle$ has a negative value virtually equal to that of the product $\langle A\rangle\langle B\rangle$.

7. Discussion

We have developed a special version of the closure model introduced earlier for simulating second-order chemical reactions in a point source plume in the planetary boundary layer. The parameters required to implement the model were derived from data generated by Deardorff's numerical turbulence model. Because the turbulent structure of the unstable boundary layer possesses certain universal characteristics (Deardorff, 1972), the parameter values we derived can be used in a wide range of simulation studies, provided that the variables are expressed in terms of the length and time scales z_i and z_i/w_*, respectively. Further analyses are necessary to develop parameter values applicable to source heights and meteorological conditions other than those treated in this study.

The difficulty in determining eddy diffusivities was circumvented in our simulation by computing the total material in the plume cross section as a function of downwind distance. This approach involves fewer sources of uncertainty than that of calculating the detailed concentration distribution within the plume. For this reason, our approach can be of particular value if a method can be found to relate concentration extrema at each distance x to the cross-sectional average $\tilde{A}(x)$. Within the limitations of the available data, we have shown that our model yields reasonably accurate estimates of total chemical conversion in plumes in the planetary boundary layer. Our calculations indicate that turbulent concentration fluctuations play a major role in chemical conversion processes in the near-source plume. When fluctuation effects were eliminated from the model, the 50 percent NO conversion time in a point source plume dropped from 20 minutes to about 3 minutes.

IV PARAMETERIZATION OF SUBGRID-SCALE MEAN CONCENTRATION VARIATIONS IN MODELS OF URBAN AIR POLLUTION

R. G. Lamb

In Lamb (1976), we investigated a phenomenon that had not been considered in air pollution modeling: the effect of subgrid-scale mean concentration variations on the predicted rates of reaction of photochemical air pollutants. It has long been realized that, owing to the highly localized character of air pollutant sources, the grid-cell-averaged concentrations predicted by an airshed model are not necessarily representative of the time-averaged values one would observe at a particular point. However, it has not been fully appreciated that the same concentration variations that are responsible for this discrepancy between volume-averaged and point concentration values can also adversely affect the ability of a model to simulate pollutant species that undergo second-order chemical reactions. We call this the subgrid-scale variation (SSV) effect.

The nature of the SSV effect is virtually identical to that of the turbulent concentration fluctuations analyzed in Chapter III. In Lamb (1976), we exploited this similarity by using the closure model for turbulent concentration fluctuation effects (described in Chapter III of this report) as the basis of a scheme for parameterizing the SSV effects. Despite the conciseness and simplicity that we built into that scheme, it appears now that its use in its general form in the current version of the SAI model will be infeasible because the machine time and storage requirements of this model are already at the limits of practicality. For this reason, we have had to simplify the SSV parameterization still further. All time-dependent equations have now been eliminated from it, and all variables are expressed in terms of quantities either predicted or used as inputs by the SAI model. In its new form, the scheme places no additional core storage requirements on the airshed model, and it operates with a minimum of additional machine time. This chapter outlines the development of this modified SSV parameterization.

A. FORMULATION OF A SIMPLIFIED SSV PARAMETERIZATION SCHEME

Development of a scheme simple enough to be accommodated in the latest SAI model requires invocation of several simplifying assumptions. The first, and probably most restrictive, is that all SSV is generated by ground-based sources. This condition can be satisfied generally by removing all elevated sources from the airshed model and simulating them separately using the special microscale model described in Chapter V. (One of the main features of the microscale model is that, by design, its output and that of the airshed model are additive.) With elevated sources removed, SSV is found only in a relatively shallow layer next to the ground; consequently, it can be treated in a single level of the airshed model. This is illustrated in Figure 22.

In this figure are two grid cells overlying a single line source. The depth Δz_0 of the lowest cell was selected to be large enough to contain the majority of the SSV produced by this source. In this case, the cell atop the lower one and all higher cells can be treated as being free of SSV, i.e., concentrations of all species within those cells are uniformly distributed. This is illustrated in Figure 22 by the abrupt cutoff of the line source plume at the top of the lowest cell. Our objectives now are twofold: to treat explicitly the SSV effects in the lowest layer using the ideas developed in Lamb (1976) and to represent the resulting pollutant fluxes across the plane $z = \Delta z_0$ in terms of source strengths and configurations, mean concentrations in the cells above the lowest layer, meteorology, and the like. This will reduce the SSV parameterization to a boundary condition that can be incorporated easily into any airshed model simply by making the bottom surface of the model coincide with the plane $z = \Delta z_0$ rather than with the ground. Information concerning mean concentrations in the layer below Δz_0 is not lost in this process because in the mathematical development of expressions for the pollutant fluxes

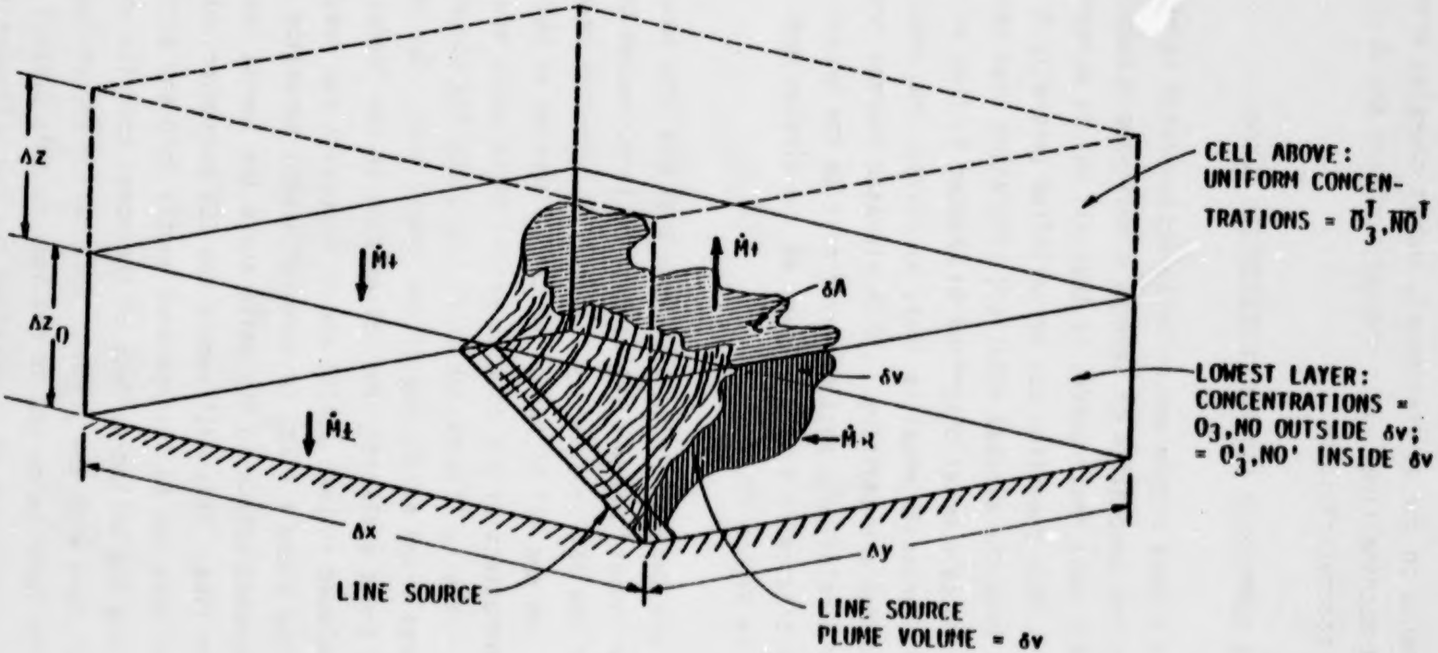
Δz
Δz$_0$
$\dot{M}_\downarrow$
$\dot{M}_\uparrow$
δA
δv
$\dot{M}_\perp$
$\dot{M}_\parallel$
CELL ABOVE:
UNIFORM CONCENTRATIONS = $\bar{O}_3^T, \bar{NO}^T$
LOWEST LAYER:
CONCENTRATIONS = O_3,NO OUTSIDE δv;
= O_3',NO' INSIDE δv
Δx
Δy
LINE SOURCE
LINE SOURCE
PLUME VOLUME = δv

FIGURE 22. SCHEMATIC ILLUSTRATION OF A LOWEST LAYER CELL CONTAINING A SINGLE LINE SOURCE

through the plane $z = z_0$, formulas relating the mean species concentrations and their fluctuations in the lowest layer to the concentrations in the cell just above Δz_0, source emissions rates, and so forth arise as intermediate results. Thus, in this new model structure, concentrations at ground-level sites are not calculated at every time step and every grid cell as is normally done, but rather, only at those times and places designated.

To formulate the scheme outlined above, one must introduce several special parameters. Referring to Figure 22, let λ_- represent the fraction $(0 \leq \lambda_- \leq 1)$ of the top of the lowest cell occupied on the average by descending air, and let λ_+ denote the corresponding fraction covered by ascending fluid. Assuming that the area occupied by fluid whose vertical velocity is identically zero is negligibly small, we have

$$\lambda_- + \lambda_+ = 1 \quad . \tag{121}$$

For neutrally stable, nondivergent flow, we expect $\lambda_- = \lambda_+ = 1/2$; but for stable and unstable stratifications, this is not necessarily the case.

Let w_- be the mean vertical fluid speed averaged over the zones of descending air on the plane $z = \Delta z_0$, and let w_+ be the corresponding value for the upward directed air. Since these two quantities are not normally measured, we propose to approximate them from, among other data, the expression

$$\lambda_- w_-^2 + \lambda_+ w_+^2 = \overline{w^2} \quad , \tag{122}$$

where $\overline{w^2}$ is the mean square vertical component of turbulent velocity measured at a height Δz_0 above ground.

The area marked δA in Figure 22 is formed by the intersection of the line source plume with the plane $z = \Delta z_0$. Since the source is at ground level, fluid within δA must on the average be ascending. We assume then that

$$\frac{\delta A}{\lambda_+ A} = \xi \quad , \quad 0 \leq \xi \leq 1 \quad , \tag{123}$$

where

$$A = \Delta x \Delta y \quad . \tag{124}$$

In other words, it is assumed that at the level $z = \Delta z_0$ the plumes of all sources in the lowest layer and their associated SSV are confined to zones of ascending fluid; once these emissions reach the cells above the lowest layer, thorough mixing of all pollutants is assumed to result, so that in all fluid descending through $z = \Delta z_0$ concentrations are uniformly distributed. Material fluxes through the side walls of the lowest cells are neglected in this study because (as shown later) under typical daytime conditions vertical fluxes through a ground-based cell with dimensions $\Delta x, \Delta y \sim 2$ km, $\Delta z_0 \sim 20$ m are one to two orders of magnitude larger than horizontal fluxes.

Within each of the lowest cells, we distinguish between two domains: δv, the volume occupied by all emissions of sources in that cell; and $V - \delta v$, the region outside δv (see Figure 22). Here V is the volume of the lowest cell,

$$V = A\Delta z_0 = \Delta x \Delta y \Delta z_0 \quad . \tag{125}$$

Within the restrictions of assumptions introduced above, the only source of fluid in $V - \delta v$ is subsidence through the top of the lowest layer. However, there are three avenues by which fluid leaves this domain. One is by direct transport back through the cell top, i.e., through an area $(1 - \xi)\lambda_+ A$. A second path of escape is turbulent entrainment into the plume volume δv. Finally, pollutant species can leave $V - \delta v$ by deposition on the ground surface. Chemical reactions within $V - \delta v$ are neglected because in view of the origin of fluid in this domain, pollutants there are somewhat aged, and consequently, the ratios of their concentrations are probably close enough to their chemical equilibrium values that little reaction occurs during the brief time that species are in residence.

Fluids enter the domain δv by entrainment from $V - \delta v$ and from pollutant sources, and they leave by chemical removal and by ascent through an area $\xi\lambda_+ A$ of the top of the cell. (Note that by definition of δv, all source emissions are injected directly into this volume.) For species such as O_3 and NO, chemical processes within δv are expected to be rapid because the concentrations of these pollutants are greatly disturbed from their chemical equilibrium values by the fresh injections of NO_x. In Lamb (1976), we showed that these three particular pollutants are the only ones explicitly computed by the airshed model that are sufficiently reactive to be affected by SSV as it exists within δv. Accordingly, we assumed in this study that only ozone and nitric oxide undergo significant conversion within δv and that, moreover, the rate of reaction between these species is infinite. All other pollutants were treated as pseudo-inert substances inasmuch as the time scales of their reactions are much larger than the characteristic residence time of material within the lowest layer.

Our plan now is to write the mass balance equations for each of the pollutant species in δv and $V - \delta v$ and, from these, to formulate the desired expressions for the net material fluxes through $z = \Delta z_0$ and the mean pollutant concentrations in the lowest layer. For these purposes, it is convenient to introduce the following special notation:

$\dot{M}_{\chi\downarrow}$ = net downward mass flow rate (mass/time) of given species χ across $z = \Delta z_0$ into $V - \delta v$,

$\dot{M}_{\chi\underline{\downarrow}}$ = mass flow rate of species χ into the ground surface in $V - \delta v$ by deposition,

$\dot{M}_{\chi\rightarrow\wr}$ = mass flow rate of χ from $V - \delta v$ into δv by entrainment,

$\dot{M}_{\chi\rightarrow|}$ = mass rate of removal of species χ in δv by chemical reaction,

$\dot{M}_{\chi\uparrow}$ = net upward mass flow rate of χ across $z = \Delta z_0$ from δv,

$\bar{\chi}^T$ = average concentrations of species χ in the cell atop the lowest layer,

χ = average concentration of species χ in $V - \delta v$,

χ' = average concentration of species χ in δv.

Many of the terms listed above are illustrated in Figure 22.

1. Mass Balance Equations in $V - \delta v$

Consider first the mass balance of ozone. We have

$$\dot{M}_{O_3\downarrow} = \dot{M}_{O_3\rightarrow\ell} + \dot{M}_{O_3\underline{\downarrow}} \quad . \tag{126}$$

Straightforward analysis gives

$$\dot{M}_{O_3\downarrow} = \bar{O}_3^T w_- \lambda_- A - O_3 w_+ (1 - \xi) \lambda_+ A \tag{127}$$

and

$$\dot{M}_{O_3\rightarrow\ell} = \nu \delta a O_3 \quad . \tag{128}$$

In the last equation, ν is the entrainment velocity of fluid into δv and δa is the effective surface area of δv. We use the approximation

$$\delta a = \frac{\delta v}{\Delta z_0} \quad , \tag{129}$$

where δv denotes the total volume of the domain δv. It is convenient at this point to introduce a final parameter,

$$\zeta = \frac{\delta v}{V} = \frac{\delta v}{\Delta x \Delta y \Delta z_0} \quad . \tag{130}$$

This is the fraction ($0 \leq \zeta \leq 1$) of the lowest cell occupied by source emissions.

For the deposition mass flow rate of ozone in $V - \delta v$, we assume

$$\dot{M}_{O_{3\pm}} = \beta_{O_3} A O_3 (1 - \zeta) \quad , \tag{131}$$

where β_{O_3} is the deposition velocity of ozone. The factor (1 -) in Eq. (131) is intended to account for the fact that the demain $V - \delta v$ does not necessarily cover the entire ground surface. We assume that a fraction ζ of it is covered by δv.

Substituting Eqs. (127), (128), and (131) into Eq. (126) and making use of the relationship

$$\nu\zeta = w_+ \lambda_+ \xi \tag{132}$$

imposed by conservation of mass, we obtain

$$O_3 = \frac{\bar{O}_3^T w_- \lambda_-}{w_+ \lambda_+ + (1 - \zeta)\beta_{O_3}} \quad . \tag{133}$$

By analogy with this relationship, we obtain

$$NO = \frac{\overline{NO}^T w_- \lambda_-}{w_+ \lambda_+ + (1 - \zeta)\beta_{NO}} \quad , \tag{134}$$

$$NO_2 = \frac{\overline{NO}_2^T w_- \lambda_-}{w_+ \lambda_+ + (1 - \zeta)\beta_{NO_2}} \quad , \tag{135}$$

and in general

$$\chi = \frac{\bar{\chi}^T w_- \lambda_-}{w_+ \lambda_+ + (1 - \zeta)\beta_\chi} \quad . \tag{136}$$

2. Mass Balance Equations in δv

For ozone, we have

$$\dot{M}_{O_3\to l} = \dot{M}_{O_3'\to|} + \dot{M}_{O_3'\underline{\downarrow}} + \dot{M}_{O_3\uparrow} \quad . \tag{137}$$

The first term of this equation was given earlier:

$$\dot{M}_{O_3\to l} = \nu\delta a O_3 \quad . \tag{138}$$

The deposition term is given by [Eq. (131)]

$$\dot{M}_{O_3'\underline{\downarrow}} = \beta_{O_3}\zeta A O_3' \quad , \tag{139}$$

and the upward mass flow by

$$\dot{M}_{O_3'\uparrow} = w_+\lambda_+\xi O_3' A \quad . \tag{140}$$

The chemical removal term $\dot{M}_{O_3'\to|}$ is somewhat more complicated. Under the assumption adopted previously that NO and O_3 react infinitely rapidly in δv, it is clear that ozone will be destroyed in $\delta\nu$ at the same rate at which NO is produced by sources. But the rate of destruction of ozone cannot exceed the rate $\dot{M}_{O_3\to l}$ at which it is entrained into δv no matter how large the No emissions rate might be. Let $\bar{\bar{S}}_{NO}$ represent the NO emissions rate averaged over the lowest cell in units of moles/area/time. Then from the considerations cited above, we conclude

$$\dot{M}_{O_3'\to l} = \begin{cases} O_3\nu\delta a & \text{if } \bar{\bar{S}}_{NO} > \nu\zeta O_3 \quad , \\ \bar{\bar{S}}_{NO}A & \text{otherwise} \quad . \end{cases} \tag{141}$$

Substituting Eqs. (138) through (141) into Eq. (137) and simplifying, we obtain

$$O_3' = \begin{cases} 0 \quad \text{if} \quad \tilde{S}_{NO} > \nu\zeta O_3 \quad , \\ \\ \dfrac{O_3\nu - \dfrac{\tilde{S}_{NO}}{\zeta}}{\beta_{O_3} + \nu} \quad \text{otherwise} \quad . \end{cases} \tag{142}$$

The mass balance equation for NO in ζv is

$$\dot{M}_{NO\rightarrow\wr} + \tilde{S}_{NO}A = \dot{M}_{NO'\rightarrow|} + \dot{M}_{NO'\underline{\pm}} + \dot{M}_{NO'\uparrow} \quad . \tag{143}$$

All of the terms here can be written down immediately based on information supplied above:

$$\dot{M}_{NO\rightarrow\wr} = NO\nu\delta a \quad , \tag{144}$$

$$\dot{M}_{NO'\uparrow} = NO'w_+\lambda_+\xi A \quad , \tag{145}$$

$$\dot{M}_{NO'\underline{\pm}} = \beta_{NO}NO'\zeta A \quad , \tag{146}$$

$$\dot{M}_{NO'\rightarrow|} = \begin{cases} \nu\zeta O_3 \quad \text{if } \tilde{S}_{NO} > \nu\zeta O_3 \quad , \\ S_{NO}A \quad \text{otherwise} \quad . \end{cases} \tag{147}$$

Combining these expressions with Eq. (143), we obtain

$$NO' = \begin{cases} \dfrac{\dfrac{\tilde{S}_{NO}}{\zeta} + \nu(NO - O_3)}{\beta_{NO} + \nu} & \text{if } \tilde{S}_{NO} > \nu\zeta O_3 \quad , \\ \\ \dfrac{\nu NO}{\beta_{NO} + \nu} & \text{otherwise} \quad . \end{cases} \tag{148}$$

The mass balance equation for NO_2 is

$$\dot{M}_{NO_2 \to \ell} + \tilde{S}_{NO_2} A + \dot{M}_{O_3' \to |} = \dot{M}_{NO_2' \uparrow} + \dot{M}_{NO_2' \underline{\downarrow}} \quad . \tag{149}$$

Following procedures like those used above, we obtain

$$\dot{M}_{NO_2 \to \ell} = NO_2 \nu \delta a \quad , \tag{150}$$

$$\dot{M}_{NO_2' \uparrow} = NO_2' w_+ \lambda_+ \xi A \quad , \tag{151}$$

$$\dot{M}_{NO_2' \underline{\downarrow}} = \beta_{NO_2} NO_2' \zeta A \quad , \tag{152}$$

$$\dot{M}_{O_3' \to |} = \begin{cases} O_3 \nu \delta a & \text{if } \tilde{S}_{NO} > \nu\zeta O_3 \quad , \\ \tilde{S}_{NO} A & \text{otherwise} \quad . \end{cases} \tag{153}$$

Upon combining these equations with Eq. (149), we obtain

$$NO_2' = \begin{cases} \dfrac{NO_2 \nu + O_3 \nu + \dfrac{\tilde{S}_{NO_2}}{\zeta}}{\beta_{NO_2} + \nu} & \text{if } S_{NO} > \nu\zeta O_3 \quad , \\ \\ \dfrac{NO_2 \nu + \dfrac{\tilde{S}_{NO_2} + \tilde{S}_{NO}}{\zeta}}{\beta_{NO_2} + \nu} & \text{otherwise} \quad . \end{cases} \tag{154}$$

One of the assumptions we made earlier is that all pollutant species calculated in the airshed model, except ozone and nitric oxide, react too slowly to undergo significant chemical transformation during the brief time they are in the lowest layer. Let χ_I' represent the mean concentration of one of these species in δv. Its mass balance equation then has the form

$$\dot{M}_{\chi_I \to \ell} + \bar{S}_\chi A = \dot{M}_{\chi' \underline{\downarrow}} + \dot{M}_{\chi' \uparrow} \quad , \tag{155}$$

which reduces after analyses like those performed earlier to

$$\chi_I' = \frac{\chi_I \nu + \dfrac{\bar{S}_{\chi_I}}{\xi}}{\beta_{\chi_I} + \nu} \quad . \tag{156}$$

Recall that χ_I can be obtained from Eq. (136).

3. Formulation of Expressions for Material Fluxes Across $z = \Delta z_0$

We are now in a position to derive the desired expressions for the pollutant fluxes across the top of the lowest layer. Let $F_{O_3\downarrow}$ be the net downward flux of ozone through the top surface $z = \Delta z_0$ of a given lowest layer cell. It follows that

$$F_{O_3\downarrow} = \frac{1}{A}\left(\dot{M}_{O_3\downarrow} - \dot{M}_{O_3\uparrow}\right) \quad , \tag{157}$$

which reduces with the aid of Eqs. (127) and (140) to

$$F_{O_3\downarrow} = \bar{O}_3^T w_- \lambda_- - O_3 w_+ \lambda_+ (1 - \xi) - w_+ \lambda_+ \xi O_3' \quad . \tag{158}$$

Making use of Eqs. (133) and (142), we obtain finally

$$F_{O_3\downarrow} = \bar{O}_3^T w_- \lambda_- - O_3 w_+ \lambda_+ (1 - \xi)$$

$$- \begin{cases} 0 & \text{if } \tilde{S}_{NO} > \nu\zeta O_3 \quad , \\ \dfrac{O_3 \nu^2 \zeta - \tilde{S}_{NO} \nu}{\beta_{O_3} + \nu} & \text{otherwise} \quad , \end{cases} \tag{159a}$$

where

$$O_3 = \frac{\bar{O}_3^T w_- \lambda_-}{w_+ \lambda_+ + (1 - \xi)\beta_{O_3}} \quad . \tag{159b}$$

Note that Eqs. (159a) and (159b) give the flux in terms of the predicted mean concentration $\bar{O}_3^T$ in the cell above the lowest layer, the NO emissions rate in the lowest cell, and other quantities, all of which are specified.

With the NO flux $F_{NO\downarrow}$ defined in the same manner as Eq. (157), we obtain through a process similar to that leading to Eq. (159):

$$F_{NO\downarrow} = \overline{NO}^T w_- \lambda_- \left[\frac{(1 - \zeta)\beta_{NO} + w_+ \lambda_+ \xi}{(1 - \zeta)\beta_{NO} + w_+ \lambda_+} \right]$$

$$- \begin{cases} \dfrac{\tilde{S}_{NO} + \nu\zeta(NO - O_3)}{1 + \dfrac{\beta_{NO}}{\nu}} & \text{if } \tilde{S}_{NO} > \nu\zeta O_3 \quad , \\ \dfrac{\nu\zeta NO}{1 + \dfrac{\beta_{NO}}{\nu}} & \text{otherwise} \quad , \end{cases} \tag{160a}$$

where

$$NO = \frac{\overline{NO}^T w_- \lambda_-}{\omega_+ \lambda_+ + (1 - \zeta)\beta_{NO}} \qquad (160b)$$

and O_3 is given by Eq. (159b).

The NO_2 flux is found to be

$$F_{NO_2+} = \overline{NO}_2^T w_- \lambda_- \left[\frac{(1 - \zeta)\beta_{NO_2} + w_+ \lambda_+ \xi}{(1 - \zeta)\beta_{NO_2} + w_+ \lambda_+} \right]$$

$$- \begin{cases} \dfrac{\nu\zeta(NO_2 + O_3) + \bar{S}_{NO_2}}{1 + \dfrac{\beta_{NO_2}}{\nu}} & \text{if } \bar{S}_{NO} > \nu\zeta O_3 \quad , \\[2ex] \dfrac{\nu\zeta NO_2 + \bar{S}_{NO_2} + \bar{S}_{NO}}{1 + \dfrac{\beta_{NO_2}}{\nu}} & \text{otherwise} \quad , \end{cases} \qquad (161a)$$

where

$$NO_2 = \frac{\overline{NO}_2^T w_- \lambda_-}{w_+ \lambda_+ + (1 - \zeta)\beta_{NO_2}} \qquad (161b)$$

and O_3 is given by Eq. (159b).

Finally, for all pollutants other than NO, O_3, and NO_2, we have

$$F_{\chi_I+} = \overline{\chi}_I^T w_- \lambda_- \left[\frac{(1 - \zeta)\beta_{\chi_I} + w_+ \lambda_+ \xi}{(1 - \zeta)\beta_{\chi_I} + w_+ \lambda_+}\right] - \frac{\nu\zeta\chi_I + \tilde{S}_{\chi_I}}{1 + \frac{\beta_{\chi_I}}{\nu}} \quad , \qquad (162a)$$

where

$$\chi_I = \frac{\overline{\chi}_I^T w_- \lambda_-}{w_+ \lambda_+ + (1 - \zeta)\beta_{\chi_I}} \quad . \qquad (162b)$$

Equations (159) through (162) constitute part of our condensed subgrid-scale variation parameterization scheme. They can be implemented in any airshed model by substituting them for the lower boundary conditions presently used. Implicit in this scheme is the assumption that the bottom surface of the model--i.e., the plane on which the flux conditions Eqs. (159) through (162) apply--has a constant elevation Δz_0, to be specified later, above ground. Next, we need to formulate expressions for the mean concentrations in the layer below Δz_0.

4. Formulation of Expressions for Averaged Concentrations in the Lowest Layer

We need to supplement the flux equations given above with formulas relating concentrations in the lowest layer to the predicted concentrations in the cells atop the lowest layer, source emissions rates, and so on. Without such formulas, the airshed model would be rendered incapable of calculating ground-level concentrations. In the earlier discussions of the species mass balance equations, we gave formulas for concentrations in the two domains $V - \delta v$ and δv of each lowest cell. If desired, those expressions could be incorporated in the model. Here we use them to express the cell-averaged species concentrations.

The average over the volume V of a lowest cell of the concentration of any pollutant is defined as

$$\tilde{\chi} = \frac{1}{V}\int_V \chi \, dv \quad . \tag{163}$$

The assumed constancy of concentrations within each of the two domains V - δv and δv of each cell leads to

$$\tilde{\chi} = (1 - \zeta)\chi + \zeta\chi' \quad . \tag{164}$$

Using this equation and those given earlier for O_3, O_3', NO, and so on, we obtain the following:

$$\tilde{O}_3 = \begin{cases} (1 - \zeta)O_3 & \text{if } \tilde{S}_{NO} > \nu\zeta O_3 \quad , \\ O_3\left[\dfrac{1 + (1 - \zeta)\dfrac{\beta_{O_3}}{\nu}}{1 + \dfrac{\beta_{O_3}}{\nu}}\right] - \dfrac{\tilde{S}_{NO}}{\beta_{O_3} + \nu} & \text{otherwise} \quad , \end{cases} \tag{155}$$

where O_3 is given by Eq. (159b);

$$\widetilde{NO} = NO\left[\frac{\nu + (1 - \zeta)\beta_{NO}}{\nu + \beta_{NO}}\right] + \begin{cases} \dfrac{\tilde{S}_{NO} - \zeta\nu O_3}{\beta_{NO} + \nu} & \text{if } \tilde{S}_{NO} > \nu\zeta O_3 \quad , \\ 0 \quad \text{otherwise} \quad , \end{cases} \tag{166}$$

where NO is given by Eq. (160b);

$$\widetilde{NO}_2 = NO_2\left[\frac{\nu + (1 - \zeta)\beta_{NO_2}}{\nu + \beta_{NO_2}}\right] + \frac{\tilde{S}_{NO_2}}{\beta_{NO_2} + \nu} + \begin{cases} \dfrac{O_3\nu\zeta}{\beta_{NO_2} + \nu} & \text{if } \tilde{S}_{NO} > \nu\zeta O_3 \ , \\[2ex] \dfrac{\tilde{S}_{NO}}{\beta_{NO_2} + \nu} & \text{otherwise} \ , \end{cases} \tag{167}$$

and NO_2 is given by Eq. (161b);

$$\tilde{x}_I = \frac{\bar{x}_I^T w_- \lambda_- \left[\nu + (1 - \zeta)\beta_{x_I}\right]}{\nu + \beta_{x_I}\left[\omega_+\lambda_+ + (1 - \zeta)\beta_{x_I}\right]} + \frac{\tilde{S}_{x_I}}{\beta_{x_I} + \nu} \quad . \tag{168}$$

As we noted earlier, it is not necessary to evaluate the concentration formulas Eqs. (165) through (168) at every time step and in every grid cell. In the computer program, these equations can be coded as a subroutine and called only at those times and sites where ground-level concentration estimates are needed.

In the same manner in which we defined $\tilde{x}$ [see Eq. (163)], we could define $\widetilde{x''^2}$, the mean square deviation of concentration from its well-averaged value $\tilde{x}$, and then write formulas for this quantity as we did for

$\tilde{O}_3$, $\widetilde{NO}$, and so on. No air pollution models currently predict quantities like $\widetilde{\chi''^2}$, but information about mean concentration variations that is provided by such quantities would be of value in estimating concentration extrema, in assessing the magnitude of modeling errors from comparisons of predicted volume-averaged concentrations with values measured at a fixed point, and in other studies where the magnitudes of subgrid-scale concentration variations play a role. The development of formulas for $\widetilde{\chi''^2}$ for each pollutant from the information given above is straightforward; thus, for brevity we do not derive them here.

In the remainder of this chapter, we develop approximations for the various parameters that enter into the SSV model equations [Eqs. (159) through (161) and (165) through (168)].

B. APPROXIMATIONS FOR THE PARAMETERS USED IN THE SIMPLIFIED SUBGRID-SCALE VARIATION SCHEME

1. The Depth of the Lowest Layer, Δz_0

Three main constraints were placed upon the depth Δz_0 of the lowest layer:

- Δz_0 is large enough to include the majority of SSV produced by ground-level sources.
- Vertical fluxes through a cell of dimensions Δx, Δy, Δz_0 are much larger than those through the side walls of the cell.
- Δz_0 is sufficiently small that the residence time of pollutants in the lowest layer is short compared with the reaction time scales of all explicitly calculated pollutant species except O_3 and NO.

Our task now is to determine what value of Δz_0 best satisfies these criteria under typical daytime conditions in an urban area.

In Lamb (1976), Section V.B, it was shown that SSV from a single source vanishes as the plume from that source approaches the dimensions of the grid cells or as the plumes from multiple sources acquire widths comparable to the mean distance between sources. These observations suggest that in instances where a grid cell is traversed by a single major line source, it may be infeasible to make the depth of the lowest layer great enough to confine the majority of the SSV. Indeed, we expect that the parameterization scheme presented above, confined to a single shallow layer as it is, will be least effective in describing SSV around isolated sources. Optimum performance will probably be obtained for cells containing networks of streets. For these cases, we assume that the bulk of the SSV is confined to a depth Δz_0 such that within a period comparable to the mean residence time of material in this layer, an instantaneous line source puff will have grown to a size comparable to the mean street separation; or, for simplicity, that the size $\overline{\ell^2}^{\,1/2}$ of the cloud is much larger than its initial dimension ℓ_0.

The rate of expansion of a cloud in homogeneous turbulence was found by Batchelor (1950) using similarity theory to be

$$\overline{\ell^2} = c_1 \varepsilon^{2/3} \ell_0^{2/3} \tau^2 \quad , \qquad (169)$$

where

c_1 = a constant of order unity,
ε = the energy dissipation rate of the turbulence,
τ = the travel time of the cloud,
ℓ_0 = the initial cloud size,
$\overline{\ell^2}$ = the mean square diameter after a time τ.

Similarity theory also claims that the mean rate of rise of the centroid of a cloud in the surface layer is

$$\langle z \rangle \sim u_* \tau \quad , \tag{170}$$

where u_* is the friction velocity. Thus, using our criterion, SSV will be small at the level Δz_0 if

$$\varepsilon^{2/3} \ell_0^{2/3} \frac{(\Delta z_0)^2}{u_*^2} \gg \ell_0^2 \quad . \tag{171}$$

According to Wyngaard and Cote (1971), in the surface layer,

$$\varepsilon = \frac{u_*^3}{kz} \left(1 + 0.5 \left|\frac{z}{L}\right|^{2/3}\right)^{3/2} \quad , \tag{172}$$

where k is the von Karman constant and L is the Obukhov length. Combining Eqs. (171) and (172), we obtain the approximate condition

$$(\Delta z_0)^2 \gg \ell_0^{4/3} |L|^{2/3} \quad . \tag{173}$$

For motor vehicle emissions, $\ell_0 \sim 1$ m is a reasonable approximation; and in an urban area during clear daylight conditions, $|L|$ is usually less than 50 m. Thus, values of Δz_0 as small as 15 m should satisfy the requirement that SSV be negligible above the lowest layer.

To examine the limits placed on Δz_0 by the flux assumption, let Δc be a characteristic difference between concentration in a given lowest cell and values outside it. Normally, concentration gradients are steeper in the vertical than in the horizontal direction, but we ignore this distinction here. Then the total mass flux through the cell top is

$$F_{\uparrow} = w\Delta c\Delta x\Delta y \quad , \tag{174}$$

where w is the rms vertical turbulence velocity at $z = \Delta z_0$ and Δx and Δy are the grid cell dimensions. The horizontal side wall flux is

$$F_{\rightarrow} = \bar{u}\Delta c\Delta x\Delta z_0 \quad , \tag{175}$$

where $\bar{u}$ is the mean horizontal wind speed below Δz_0 and $\Delta x = \Delta y$ is assumed. We now require that

$$\frac{F_{\uparrow}}{F_{\rightarrow}} = \frac{w\Delta x}{\bar{u}\Delta z_0} >> 1 \quad . \tag{176}$$

Later in this section [see Eq. (190)] we present evidence that in the surface layer

$$w \sim 2u_* \quad ; \tag{177}$$

and from Wooding, Bradley, and Marshall (1973), we obtain for the case $1 \leq \Delta z_0/z_h \leq 10$, where z_h is the height of roughness elements in the urban area,

$$\frac{\bar{u}}{u_*} \approx 2.5 \, \ell n\left(\frac{\Delta z_0}{z_h}\right) + 10.8 \quad . \tag{178}$$

Combining Eqs. (177) and (178), we can convert Eq. (176) into the form, applicable where $\Delta z_0 \approx 10 \, z_h$,

$$\frac{\Delta x}{\Delta z_0} >> 10 \quad . \tag{179}$$

In urban airshed models, Δx usually has a value of at least 2 km; so any value of Δz_0 in the range of 25 m or smaller would satisfy Eq. (179).

Up to this point, we have shown that a value of Δz_0 of about 25 m will satisfy the SSV and flux conditions placed on the lowest layer. It remains to be shown only that this depth is compatible with the constraint placed on the mean residence time of material in the lowest layer. This time scale is given roughly by

$$T \sim \frac{\Delta z_0}{u_*} \quad . \tag{180}$$

As shown in Eq. (178), typically $\overline{u} \approx 15u_*$. Using this information and a value of about 2 m/sec for $\overline{u}$; we find that $T \sim 3$ minutes when $\Delta z_0 \sim 25$ m. This time scale is indeed smaller than that of most reactions in the urban atmosphere after mixing has occurred. We conclude from this finding and the preceding analyses that an acceptable lowest layer depth is

$$\Delta z_0 \sim 25 \text{ m} \quad . \tag{181}$$

2. The Parameters λ_-, w_+, w_-, and ξ

There are seven parameters in our scheme (λ_-, λ_+, w_-, w_+, ν, ζ, and ξ), but only three of these can be specified independently because the following four conditions (discussed earlier) must be satisfied:

$$\lambda_- + \lambda_+ = 1 \quad , \tag{182}$$

$$\lambda_- w_- = \lambda_+ w_+ \quad , \tag{183}$$

$$\lambda_- w_-^2 + \lambda_+ w_+^2 = \overline{w^2}\Big|_{z=z_0} \quad , \tag{184}$$

$$\nu\zeta = \omega_+ \lambda_+ \xi \quad . \tag{185}$$

The first condition arises from the assumption that all fluid on $z = \Delta z_0$ has nonzero vertical velocity; the second and last conditions express conservation of mass; and Eq. (184) is roughly a definition of w_- and w_+ in terms of the mean square vertical turbulent velocity component $\overline{w^2}$. Thus, $\overline{w^2}$ and the three remaining parameters (λ_+, ν, and ξ) must be specified. When this is done, we have

$$\lambda_- = 1 - \lambda_+ \quad , \tag{186}$$

$$w_+ = \left(\frac{1 - \lambda_+}{\lambda_+}\right)^{1/2} \overline{w^2}^{\,1/2} \quad , \tag{187}$$

$$w_- = \left(\frac{\lambda_+}{1 - \lambda_+}\right)^{1/2} \overline{w^2}^{\,1/2} \quad , \tag{188}$$

$$\xi = \frac{\nu\zeta}{w_+\lambda_+} \quad . \tag{189}$$

3. The Vertical Turbulent Velocity, $\overline{w^2}$

Using the empirical work of Wyngaard, Cote, and Izumi (1971), we approximate $\overline{w^2}$ as follows:

$$\overline{w^2}^{\,1/2} = \begin{cases} 1.9\, u_*\left(-\dfrac{\Delta z_0}{L}\right)^{1/6} \quad , & 0 \le \Delta z_0 \le -L \quad , \\ 1.9\, u_*\left(-\dfrac{\Delta z_0}{L}\right)^{1/3} \quad , & -L \le \Delta z_0 \le -3L \quad . \end{cases} \tag{190}$$

The friction velocity u_* is calculated by a subprogram in the SAI model [see Lamb (1976), pp. 53-57], and the Obukhov length L is based on estimated stability data.

4. The Fractional Area of Updrafts, λ_+

This parameter is difficult to specify precisely, but judging from measurements reported by Warner and Telford (1963) and Lenchow (1970), we estimate that at $z = \Delta z_0$,

$$\lambda_+ \begin{cases} \simeq 1/3 \text{ under unstable conditions,} \\ \\ = 1/2 \text{ under neutral conditions.} \end{cases} \tag{191}$$

5. The Entrainment Velocity, ν

We use as a measure of ν the mean rate of expansion of an instantaneous point source cloud. Earlier we presented an expression, Eq. (169), derived by Batchelor (1950) for the mean square diameter $\overline{\ell^2}$ of a cloud after a travel time τ in homogeneous turbulence. Deardorff and Peskin (1970) have shown that Eq. (169) is also valid for shear flows, such as that characteristic of the lowest layer in our study. Defining

$$\nu = \frac{d}{dt}\,\overline{\ell^2}^{\,1/2} \tag{192}$$

and making use of Eq. (169), we obtain

$$\nu = c_1^{1/2}\,(\varepsilon\ell_0)^{1/3} \quad . \tag{193}$$

Combining this expression with Eq. (172) gives

$$\nu = \frac{c_1^{1/2}}{k^{1/3}}\,u_*\left(1 + 0.5\left|\frac{z}{L}\right|^{2/3}\right)^{3/2} \quad , \tag{194}$$

where c_1 is a constant of order unity and k is the von Karman constant (≈ 0.4). If we take the release height z of the cloud to be $z = \ell_0$ (which is not unreasonable for motor vehicle emissions) and ℓ_0 to be approximately 1 m, then the term in brackets in Eq. (194) has a value near unity for values of L typical of urban regions; consequently,

$$\nu = \alpha u_* \quad , \tag{195}$$

where α is a constant that we assume for the time being to be 1.

6. The Plume Volume Fraction, ζ

This term is a carry-over from the turbulent concentration fluctuation closure model (see Chapter III) on which the present SSV scheme is based. In the context of the present problem, the approximate formula proposed for ζ in Chapter III (see Table 1) is

$$\zeta = \frac{\bar{c}^2}{\widetilde{c^2}} \quad , \tag{196}$$

where the tilde denotes an average over a lowest layer cell. Although ζ is restricted to the interval $0 \leq \zeta \leq 1$, this parameter has considerable influence on the overall accuracy of the SSV parameterization. For example, in the limit as ζ approaches zero, the parameterization assumes a totally passive role, and the airshed model of which it is a part yields concentration predictions that are identical to those that would be produced if the scheme were not present.

In Lamb (1976), Section IV.E, expressions for ζ were derived that take into account detailed aspects of the source distributions within grid cells. Being somewhat generalized, those expressions have rather complicated mathematical forms that might be impractical to apply in some instances. Thus, we develop below much simpler, but only approximate, formulas for ζ for application to motor vehicle emissions.

Consider the effluent plume of a single vehicle. Assuming as before that the mean residence time of particles in the lowest layer is $\Delta z_0/u_*$, we estimate that the length of the plume from a vehicle of speed v contained within a lowest cell is

$$\ell = \frac{v\Delta z_0}{u_*} \quad . \tag{197}$$

Treating the plume as axially symmetric, we have

$$\tilde{c}_i = \frac{1}{v}\int_0^\ell c_0 \int \psi \, da \, d\xi \quad , \tag{198}$$

where $v = \Delta x \Delta y \Delta z_0$; c_0 is the mean concentration on the plume axis, a function of distance ξ from the vehicle; and ψ is a function, which we assume is independent of ξ, that describes the mean concentration over a plane normal to the plume axis. In short, we are assuming that the mean concentration profile in the wake is self-preserving. Similarly, we have

$$\widetilde{c_i^2} = \frac{1}{v}\int_0^\ell \Gamma_0 c_0^2 \int \psi \, da \, d\xi \quad , \tag{199}$$

where we have assumed that the distribution of c^2, normalized by the plume centerline value, over planes normal to the plane axis is described by the same function ψ as c. This is not quite correct, but the errors introduced by this assumption are minor (see Appendix C). In Eq. (199), Γ_0 is the ratio of $\overline{c^2}$ at the plume centerline to $\bar{c}^2$ at the same location (Γ_0 is roughly 2.5 or less; see Appendix C.) In decaying turbulence, there is a rather long interval of distance from the plume source in which Γ_0 is constant (the self-preserving region). Making use of the constancy of Γ_0 and the lack of dependence of ψ on ξ, we obtain from Eqs. (196), (198), and (199) the approximate formula

$$\zeta_i = \frac{\eta_i}{v\Gamma_0} \quad , \tag{200}$$

where η_i is the volume encompassed by the mean plume of the i-th source. Section VI.B.2 gives theoretical expressions for the rate of growth of a plume in the surface layer. Using that information together with Eq. (197), we estimate that

$$\eta_i = \alpha\left(\frac{v}{u_*}\right)\left(\frac{\Delta z_0^4}{|L|}\right) \quad , \tag{201}$$

where L is the Obukhov length. Combining Eqs. (200) and (201) and restricting our focus to cases with vehicle densities small enough that plumes from neighboring vehicles do not overlap, we obtain

$$\zeta = \left(\frac{Nv\alpha}{u_*|L|\Gamma_0}\right)\left(\frac{\Delta z_0^3}{\Delta x \Delta y}\right) \text{ for small } N \quad , \tag{202}$$

where N is the total number of vehicles operating in the cell in question. We caution that Eq. (202) is an approximate formula valid only when N is small enough that vehicle plumes do not overlap.

In situations where Eq. (202) is not applicable, approximations of ζ can be formulated by treating freeways and major streets rather than individual vehicles as the sources of plumes. In this case, the resulting expression for ζ involves the total length of line sources in each cell with appropriate modifications to compensate also for wind direction variations on the shapes and sizes of the plumes. The reader can develop his own expressions for this case, perhaps using the steps outlined above [and in Lamb (1976)] as a guide.

C. COMMENTS

Because of the large number of constraints placed upon its operational form, the SSV scheme developed here possesses only first-order accuracy. This scheme is probably best suited to treating SSV effects arising from networks of streets and small, near-ground point sources and least capable of describing isolated freeway segments. Also, the scheme is designed to handle ground-level sources only--elevated sources must be simulated separately using the microscale techniques presented in Chapter V. The lowest layer method developed above is now being implemented in the SAI model and will undergo a series of tests in the near future.

V RESTORATION OF POINT SPATIAL RESOLUTION TO GRID MODELS OF URBAN AIRSHED POLLUTION

R. G. Lamb
D. Durran

The most unwieldy of the microscale problems we have treated has been restoring to grid models the spatial resolution required to describe in detail the concentration fields within the vicinity of point sources. Point spatial resolution is essential for predicting concentration extrema in urban areas where major point sources exist and in simulating the concentrations at monitoring sites influenced by point and line source emissions.

Restoring point resolution is not difficult in situations where only first-order reactants such as SO_2 or CO are of interest because in these cases the superposition principle can be invoked to reduce the mathematics to easily tractable forms. This case was considered in detail in Lamb (1976), Chapter IV, where a model was developed and implemented that can be used as a subprogram in any urban-scale model to resolve concentrations around point or line sources or groups of sources. However, in cases where second-order reactants such as O_3 or NO are of concern, the chemical interaction of the species with one another precludes the use of the superposition principle, and the governing equations must be dealt with in their differential form. Solving differential equations numerically requires the use of some form of finite differencing technique, which gives rise to the basic spatial resolution problem: it is infeasible, given computer speed and storage limitations, to select finite differencing intervals that are as small as those desired. For example, obtaining 50 m horizontal resolution and 20 m vertical resolution of a plume 4 km long and 1 km wide and 200 m deep at its terminus would require 16,000 grid points, a number comparable to that used to model an entire urban region. Operation of such a model would require as much machine time for each source as that required to run an entire urban-scale model.

The problem of restoring point resolution to models of second-order reactants is particularly complicated when estimates of the background pollutant concentrations in the vicinity of each point source are derived from an urban-scale model in which those same sources were lumped into the source inventory. To illustrate both this problem and that of restoring point spatial resolution in general, we consider the simple case of two species, A and B, that undergo the bimolecular reaction

$$A + B \rightarrow \text{Products} \quad .$$

The (time) mean concentration of A is governed by

$$\frac{\partial A}{\partial t} + LA = -kAB - k\langle A'B'\rangle + S_A \quad , \tag{203}$$

where L is the transport and diffusion operator,

$$L \equiv \frac{\partial}{\partial x_i} u_i - \frac{\partial}{\partial x_i} K_{ij} \frac{\partial}{\partial x_j} \quad , \tag{204}$$

k is the reaction rate constant, $\langle A'B'\rangle$ is the turbulent concentration fluctuation product mean value, and S_A is the source strength function. An expression similar to Eq. (203) governs B. It is important to note that Eq. (203) is a general equation in which point and line sources are described in detail (using delta functions in S_A). The solution A of Eq. (203) corresponds in principle to the time-averaged concentration one would observe at a specified point; consequently, it is this function that we would like to predict. Unfortunately, Eq. (203) cannot be solved analytically: only an analog of it can be evaluated, say,

$$\frac{\partial \tilde{A}}{\partial t} + L\tilde{A} = -k\tilde{A}\tilde{B} + \tilde{S}_A \quad . \tag{205}$$

Here the tilde denotes an average over a grid cell, i.e.,

$$\tilde{(\ )} = \frac{1}{\Delta x \Delta y \Delta z} \int_{V} (\ )\, d\underline{r} \quad , \tag{206}$$

where $v = \Delta x \Delta y \Delta z$ is the volume of a grid cell. The source function $\tilde{S}$ in the model equation [Eq. (205)] represents a network of volume sources formed by lumping all area, point, and line sources within each grid cell. In the context of Eq. (205), to restore point spatial resolution is to provide the capability of computing the quantity

$$A''(\underline{r},t) = A(\underline{r},t) - \tilde{A}(\underline{r},t) \quad . \tag{207}$$

By adding A'' to the model prediction $\tilde{A}$, we obtain the desired point mean value A.

The equation governing A'' can be obtained by subtracting Eq. (205) from Eq. (203) and using Eq. (207):

$$\frac{\partial A''}{\partial t} + L A'' = -k(\tilde{A}B'' + A''\tilde{B} + A''B'' + \langle A'B'\rangle) + S''_{A} \quad . \tag{208}$$

Consider the situation where N point sources are present. In this case, we have

$$S_{A}(\underline{r},t) = \sum_{n=1}^{N} Q_{an}(t)\, \delta(\underline{r} - \underline{r}_{n}) \quad , \tag{209}$$

where Q_{an} is the emissions rate of the n-th source and $\underline{r}_n$ is its location;

$$\tilde{S}_{A}(\underline{r},t) = \frac{1}{V} \sum_{n=1}^{N} Q_{an}(t)\, U(\underline{r}:\underline{r}_{n}) \quad , \tag{210}$$

where

$$U(\underset{\sim}{r}:\underset{\sim}{r}_n) = \begin{cases} 1 & \text{if r lies in the same grid cell as } \underset{\sim}{r}_n \quad , \\ 0 & \text{otherwise} \quad ; \end{cases} \tag{211}$$

and

$$S_A''(\underset{\sim}{r},t) = S_A(\underset{\sim}{r},t) - \bar{S}_A(\underset{\sim}{r},t) \quad . \tag{212}$$

The function $\bar{S}_A$ is the volume source representation of the network of point sources that enters into the $\bar{A}$ model, Eq. (205). This same function appears as a negative source in the A" equation [see Eqs. (208) and (212)] because unless the volume source effects are subtracted from A", when $\bar{A}$ and A" are added to obtain A [see Eq. (207)], volume source effects would be treated twice: once in $\bar{A}$ and once in A". Now, the method that we develop later in this chapter for solving Eq. (208) is designed to handle point source terms such as Eq. (209) and not volume sources such as Eq. (210). Thus, the presence of $\bar{S}_A$ in Eq. (208) presents a problem. This is the difficulty we referred to earlier when we mentioned that restoring point spatial resolution is particularly difficult when the background concentrations, in this case $\bar{A}$, are obtained from a model in which the source function, in this case $\bar{S}_A$, contains the point sources in question, as is the case here. In Lamb (1976), a discrete time-continuous space model was developed that we hoped would solve all of the problems associated with modeling A". Subsequent studies showed, however, that the model could not handle the near-source field as well as we had wanted. Incidentally, the A" model that was developed in Lamb (1976) to treat first-order reactants is applicable regardless of the form of S_A''. This generality results from the use of the superposition principle which, as we stated earlier, is not applicable where second-order reactants are involved.

The method we now propose to use to model A" is to reformulate the A" equation so that volume source terms like $\tilde{S}_A$ do not arise. Then, we develop a method for treating point sources that can be used to solve the resulting A" equation.

To reformulate the A" equation, we first write

$$S_A(\underset{\sim}{r},t) = \tilde{S}_A(\underset{\sim}{r},t) + \sum_{i=1}^{M} Q_{Ai}(t)\ \delta(\underset{\sim}{r} - \underset{\sim}{r}_i) \quad , \tag{213}$$

where $\tilde{S}_A$ is a volume source network constructed in the usual manner by lumping point, line, and area sources within each cell but excluding the M point sources indicated in Eq. (213). These M sources are those around which the microscale concentration field A" is to be computed. We now define $\tilde{A}$ to be the solution of the equation

$$\frac{\partial\tilde{A}}{\partial t} + L\tilde{A} = -k\tilde{A}\tilde{B} - k\langle A'B'\rangle + \tilde{S}_A \quad . \tag{214}$$

We can think of $\tilde{A}$ as the prediction of an urban-scale model that has ignored the M point sources indicated in Eq. (213). Using Eqs. (203), (213), and (214), we can show that the desired point source fields A and B are given by

$$A = \tilde{A} + \sum_{i=1}^{M} A_i'' \quad , \tag{215a}$$

$$B = \tilde{B} + \sum_{i=1}^{M} B_i'' \quad , \tag{215b}$$

where A_i'' satisfies the equation

$$\frac{\partial A_i''}{\partial t} + LA_i'' = -k\left(\tilde{A}B_i'' + \tilde{B}A_i'' + A_i'' \sum_{j=1}^{M} B_j''\right) + Q_{Ai}(t)\,\delta(\underset{\sim}{r} - \underset{\sim}{r}_i) \quad . \quad (216)$$

The function B_i satisfies an equation similar to Eq. (216). Note that the subgrid-scale fields A_i'' and B_i'' interact linearly with $\tilde{A}$ and $\tilde{B}$ (the latter are independent of A_i'' and B_i'') but nonlinearly with one another. Note also that Eq. (216) is free of volume source terms. Our objective now is to develop a method for solving Eq. (216) and thereby of restoring, through Eq. (215), point spatial resolution to the urban-scale model.

A. FORMULATION OF A STOCHASTIC MICROSCALE MODEL FOR SECOND-ORDER REACTANTS

The generalized Lagrangian equation

$$C(\underset{\sim}{r},t) = \int_0^t \int p(\underset{\sim}{r},t|\underset{\sim}{r}',t')\, S_c(\underset{\sim}{r}',t')\, d\underset{\sim}{r}'\, dt' \quad , \quad (217)$$

which we have used extensively in the past to model point sources, has heretofore never been utilized to simulate second-order reactants. The reason for this is not that Eq. (217) is not applicable to such pollutants. Indeed, the few assumptions implicit in this equation make no reference at all to the chemical nature of the contaminant. Rather, the problem in applying Eq. (217) to nonlinear problems is that the kernel p acquires an extremely complex form. To see this, recall that $p(\underset{\sim}{r},t|\underset{\sim}{r}',t')\, d\underset{\sim}{r}'$ is the probability that a particle released at $\underset{\sim}{r}'$ at time t' will be found at $\underset{\sim}{r}$ at the later time t. If the particle is inert, then $p(\underset{\sim}{r},t|\underset{\sim}{r}',t')\, d\underset{\sim}{r}'$ is just the fraction of all possible paths that particles released from $(\underset{\sim}{r}',t')$ can take that terminate at $(\underset{\sim}{r},t)$. But if the particle is a second-order reactant like NO, then only those paths between $(\underset{\sim}{r}',t')$ and $(\underset{\sim}{r},t)$ that do not result in a collision of the given particle with one with which it reacts will contribute nonzero values to the kernel p. Thus, for second-order reactants, p is a function not only of the fluid motion, but also of the source emissions rates and configurations, the ambient pollutant concentrations, and the chemical kinetics. In short, p is not simply a two-parameter function like the Gaussian density, but rather a function of many variables involving species concentrations, rate constants, source characteristics, and so on.

Despite these difficulties, we propose to use Eq. (217) as the basis of a model of the subgrid-scale field A_i'' of second-order reactants produced by point sources. This decision is based on the lack of any alternative method of accurately simulating point sources and on the fact that the complexities mentioned above are greatly mitigated when, instead of attempting to determine the full functional form of p, one elects to evaluate p at selected sites around each source in each situation of interest.

Our approach is to construct a scaled-down prototype of the actual problem in which the numbers of reacting particles are made finite and tractable. Specially devised methods of simulating chemical reactions in this prototype system and Monte Carlo techniques for simulating turbulence are applied to produce an ensemble of particle trajectories from which p can be determined.

We illustrate the scale-down procedure first using the general reaction rate equation

$$\frac{dC_i}{dt} = - \sum_{j=1}^{M} k_{ij} C_i C_j + \sum_{j=1}^{M} \sum_{l=j+1}^{M} k_{ijl} \, C_j C_l \quad , \qquad (218)$$

where C_i denotes the concentration of the i-th species, of which a total of M are present; k_{ij} is the rate coefficient for the reaction between the i-th and j-th constituents; and k_{ijl} is the rate constant for the production of species i through reaction between species j and l. The concentration C_i can be expressed as

$$C_i = \frac{N_i}{V} \quad , \tag{219}$$

where N_i is the number of particles of the i-th species in the volume V. In actual systems, the N_i may be exceedingly large numbers. We desire to construct a scaled-down system in which these numbers are of manageable size. Thus, let

$$n_i = \frac{N_i}{\nu_i} \quad , \tag{220}$$

where ν_i is some scaling constant. Using Eqs. (218) through (220), we obtain

$$\frac{dn_i}{dt} = - \sum_{j=1}^{M} \hat{k}_{ij}\nu_j n_i n_j + \frac{1}{\nu_i}\sum_{j=1}^{M} \sum_{l=j+1}^{M} \hat{k}_{ijl}\nu_j\nu_l n_j n_l \tag{221}$$

where $\hat{k}_{ij} = k_{ij}/V$ is the rate constant per particle; i.e., $\hat{k}_{ij}$ has units of inverse time. A similar definition applies to $\hat{k}_{ijl}$. The particle concentration n_i/V in the scaled-down system is related to C_i in the full system by

$$C_i = \frac{n_i\nu_i}{V} \quad . \tag{222}$$

Thus, the prototype system, Eq. (221), provides a convenient model of the full system, Eq. (218) through the scaling relationship given in Eq. (222).

Having formulated a model of the actual system, we need some method of simulating chemical reactions in this model. First-order reactions are simple to handle because they are dependent on parameters that are unaffected by the concentrations of the reacting species. For example, to simulate the first-order reaction represented by the term $-k\tilde{B}A_i''$ in Eq. (216), we generate for each "particle" of A_i'' a random sequence of zeros and ones with each successive number in the sequence corresponding to each successive time step (of length δt). The probability of a one occurring during any single time step is made proportional to $k\tilde{B}\delta t$; and in the first time step--counting from $t = 0$--that a one occurs, the identity marker of the given A_i'' particle is changed to that of the product species of the reaction $A + B \rightarrow$ Product. The process is identical to that of radioactive decay (which is also a first-order reaction) in that the probability that a given particle will decay during any given time interval is independent of the presence of other radioactive material and of the particle's past history.

Simulating second-order reactions such as that represented by the terms $k_{ij}A_i''B_j''$ in Eq. (216) is not quite as simple in our model because in this case the reactions are affected by the configurations of particles at each time step. To treat reactions of this type, we propose the following scheme. In the course of its translation by the fluid motion, each particle sweeps out, in a period δt, a "reaction volume" of size $\delta v_{ij} \propto \delta a_{ij}\delta t$, where δa_{ij} is proportional to the rate constant k_{ij}. If, during any time step, a particle of species j is found within the reaction volume δv_{ij} of a particle of species i, the identity marker of the latter is changed from i to that of the product of the i-j reaction.

The techniques we have presented above for simulating first- and second-order chemical reactions in our scaled-down model are developed in detail in Appendix D and are validated analytically for the case of reactions in a homogeneous reactor. These techniques are the means by which our model treats the reaction terms on the right-hand side of Eq. (216). The transport and diffusion processes, which are represented in Eq. (216) by the operator L, are handled by giving to each particle at each time step a velocity equal to the sum of the mean wind vector $\overline{\underline{u}}$ at the particle's location and a random computer-generated vector $\underline{u}'$ that represents the turbulence. The process used to generate $\underline{u}'$ is discussed later. The way in which the particle trajectories produced by the velocity $\underline{u} = \overline{\underline{u}} + \underline{u}'$ combines with the chemistry simulation described above to yield ultimately the solution of Eq. (216) is perhaps best shown using the case of an inert species ($k = 0$). For this situation, Eq. (216) reduces to

$$\frac{\partial C}{\partial t} + LC = Q(t)\ \delta(\underline{r} - \underline{r}_s) \quad , \tag{223}$$

where for convenience we have substituted C for A_i''. The solution of Eq. (223) is

$$C(\underline{r},t) = \int_0^t Q(t')\ p_I(\underline{r},t|\underline{r}_s,t')\ dt' \tag{224}$$

[cf Eq. (217)]. We have added the subscript I to p to indicate that this kernel pertains to an inert chemical species.

By definition,

$$p_I(\underline{r},t|\underline{r}',t') = \overline{\psi}(\underline{r},t;\underline{r}',t') \text{ for } t \geq t' \quad , \tag{225}$$

where ψ is the solution of

$$\frac{\partial \psi}{\partial t} + \frac{\partial}{\partial x_i}(\overline{u}_i + u_i') = 0 \tag{226}$$

$$\psi(\underline{r},t') = \delta(\underline{r} - \underline{r}') \quad , \tag{227a}$$

$$\lim_{|\underline{r}-\underline{r}'|\to\infty} \psi = 0 \quad , \tag{227b}$$

$$\left.\frac{\partial \psi}{\partial z}\right|_{z=0} = 0 \quad . \tag{227c}$$

In Eq. (226), $\bar{u}$ represents the mean wind given by meteorological data and $\underline{u}'$ represents the instantaneous turbulent wind component. The analytic solution of Eqs. (226) and (227) is

$$\psi(\underline{r},t) = \delta[\underline{r} - \underline{r}''(t)] \quad , \tag{228}$$

where

$$\underline{r}''(t) = \int_0^t \left\{ \bar{\underline{u}}[\underline{r}''(t')] + \underline{u}'[\underline{r}''(t')] \right\} dt' + \underline{r}' \quad . \tag{229}$$

The overbar on ψ in Eq. (226) denotes an ensemble average, i.e., the average over an infinite number of realizations of ψ. (Keep in mind that ψ is stochastic because $\underline{u}'$ is stochastic.) We must approximate $\bar{\psi}$ by an average over a finite ensemble, i.e.,

$$p_I(\underline{r},t|\underline{r}',t') \simeq \frac{1}{N} \sum_{n=1}^{N} \psi_n(\underline{r},t;\underline{r}',t') \quad , \tag{230}$$

$$\simeq \frac{1}{N} \sum_{n=1}^{N} \delta[\underline{r} - \underline{r}_n''(t;\underline{r}',t')] \quad , \tag{231}$$

where

$$\underline{r}_n''(t;\underline{r}',t') = \int_{t'}^{t} \left\{ \bar{\underline{u}}[\underline{r}_n''(t'')] + \underline{u}_n'[\underline{r}_n''(t'')] \right\} dt'' + \underline{r}' \tag{232}$$

and $\underline{u}_n'$ is the n-th realization of the turbulent velocity field. Note that $\bar{\underline{u}}$ is deterministic, i.e., it is constant for all realizations. Substituting Eq. (231) into Eq. (224), we obtain

$$C(\underline{r},t) = \frac{1}{N} \sum_{n=1}^{N} \int_0^t Q(t')\, \delta[\underline{r} - \underline{r}_n''(t;\underline{r}_s,t')]\, dt' \quad . \tag{233}$$

The evaluation of Eq. (233) can be expedited if we consider only receptors that are close enough to the source or sources (approximately 1 to 2 km) that meteorological conditions are almost constant during the time pollutants are in transit to the receptor. For our purposes here, one hour is the longest time over which meteorological conditions can be considered constant. Thus, for all wind speeds greater than 0.5 m/sec, meteorological conditions can be regarded as fixed for receptors as far as about 2 km from the source. In this case, r_n'' is dependent on the travel time, $\tau = t - t'$, rather than on t and t' separately. If the source emissions rate is also constant over at least one-hour periods, then Eq. (233) becomes

$$C(\underset{\sim}{r}) = QP_I(\underset{\sim}{r};\underset{\sim}{r}_s,\phi) \quad , \tag{234}$$

where

$$P_I(\underset{\sim}{r};\underset{\sim}{r}_s,\phi) = \frac{1}{N}\sum_{n=1}^{N}\int_0^{\infty}\delta[\underset{\sim}{r} - \underset{\sim}{r}_n''(\tau;\underset{\sim}{r}_s,\phi)]\,d\tau \quad , \tag{235}$$

and ϕ denotes the set of meteorological conditions existing at time t'. The term ϕ is merely a reminder that P_I is conditioned on a particular set of meteorological conditions, i.e., the three-dimensional $\bar{u}$ field, turbulence, stabilities, and so on. [Note that P_I is analogous to the term X/Q in Turner's workbook of atmospheric dispersion estimates (Turner, 1969).] Let Δv denote a small sample volume centered at the receptor point $\underset{\sim}{r}$. Then by virtue of the definition of the delta function, Eq. (235) is equivalent to

$$P_I(\underset{\sim}{r};\underset{\sim}{r}_s,\phi) = \frac{1}{N\Delta v}\sum_{n=1}^{N}T_n(\underset{\sim}{r};\underset{\sim}{r}_s,\phi,\Delta v) \quad , \tag{236}$$

where T_n is the total time that the particle released at $\underset{\sim}{r}_s$ on the n-th realization is in the sample volume Δv centered at $\underset{\sim}{r}$. For example, if on the n-th realization the particle passes through Δv at $\underline{r}$ only once and has a velocity

$$\underline{v} = \bar{\underline{u}} + \underline{u}' \tag{237}$$

during the time it is in Δv, then

$$T_n = \min\left(\frac{\Delta x}{|v_x|}, \frac{\Delta y}{|v_y|}, \frac{\Delta z}{|v_z|}\right) \quad . \tag{238}$$

Note that as Δv is made smaller, the computer time needed to evaluate Eq. (236) increases because N must be increased to achieve an acceptable convergence. Thus, we can determine T_n, and hence P_I and C, once we have a simulator of the particle path $\underline{r}_n''(\tau;r_s,\phi)$. Such a simulator is immediately available from Eq. (229), namely,

$$\underline{r}_n''(t + \Delta t) = \underline{r}_n''(t) + \left\{\bar{\underline{u}}[\underline{r}_n''(t)] + \underline{u}_n'[\underline{r}_n''(t)] + \underline{w}_{PR}(t)\right\} \Delta t \quad , \tag{239}$$

where $\underline{w}_{PR}$ is a plume rise velocity prescribed by the stack parameters and meteorological conditions [namely, $\underline{w}_{PR}(t)$ is constructed so that the particle rises to the predicted plume height]; $\bar{\underline{u}}[\underline{r}_n''(t)]$ is the mean wind vector evaluated at the particle's position at time t ($\bar{\underline{u}}$ is taken from meteorological data, pibals, flow simulation models, or the like); and $\underline{u}_n'$ is generated by a Monte Carlo process described below. The $\underline{u}_n'$ simulator requires only an estimate of the total mean square turbulent velocity fluctuation, $\overline{\underline{u}'^2}$, at the particle's position. This information is taken from meteorological data, for example, lapse rate, wind speed and shear, proximity to terrain features, and so on. The calculation of P_I proceeds as follows:

- A particle is released at source point $\underline{r}_s$ and its trajectory is determined from Eq. (239).
- The values of T_n are determined at previously selected (arbitrary) receptor sites for this realization.

> The above two steps are repeated until P_I, as given by the right-hand side of Eq. (236), becomes approximately independent of N.
> The resulting value of P_I is used in Eq. (234) to obtain the desired solution C of Eq. (223).

If in the process described above we had started with a group of particles representing the reactive species A and B and had superposed the proper chemical kinetics simulation, as described earlier, we would have derived in Eq. (236) the functions P_A and P_B. Substituted into Eq. (234), these would yield the solutions of Eq. (216) and its counterpart governing B. In essence, this is the method we propose for modeling the microscale concentration fields around point sources. Two aspects of the model that require further discussion are the method of selecting the scaling constants ν_i and the Monte Carlo technique used to generate the random vectors $\underline{u}'$.

1. The Scaling Constants ν_i

The constants ν_i that are used to scale down the given reaction system [see Eq. (220)] can be selected to achieve one of two objectives: a model in which the initial numbers of each reactant are the same regardless of their ratios in the actual system or a model in which the initial ratios are preserved. The latter case is straightforward. We use the same value ν for all species, i.e.,

$$\nu_i = \nu, \quad i = 1, \ldots, M \quad , \tag{240}$$

where ν is chosen so that the total number of particles in the model, namely, $\Sigma_{i=1}^{M} n_i$, is a tractable number.

To construct a model in which the numbers of reactant particles initially are equal, say, $n_i(0) = n_0$, $i = 1, \ldots, M$, we find that from Eq. (220)

$$\nu_i = \frac{N_{i0}}{n_0} \quad , \tag{241}$$

where $N_{10} = N_1(0)$. This case presents some problems in the chemistry simulation because the effective rate constant is not necessarily invariant from one rate equation to another. For example, consider the case where only two species, n_1 and n_2, are present. Equation (221) gives

$$\frac{dn_1}{dt} = -\hat{k}_{12}\nu_2 n_1 n_2 \quad , \tag{242}$$

$$\frac{dn_2}{dt} = -\hat{k}_{12}\nu_1 n_1 n_2 \quad . \tag{243}$$

These equations are not equal if $\nu_1 \neq \nu_2$ (or $N_{10} \neq N_{20}$) even though in the actual system the rates of loss of species 1 and 2 are the same regardless of the initial concentrations. One must be careful in the model to take these discrepancies into account.

2. Generating the Random Turbulent Velocity Component $\underline{u}'$

If turbulent dispersion had the same character as molecular diffusion, we could simulate its effects by assigning to each particle statistically independent random velocities $\underline{u}'$ whose mean square values conformed with the known energy of the turbulence. But this is not the case. Turbulence causes the velocities of particles that are close to one another to be correlated, and this correlation leads in turn to the phenomenon of concentration fluctuations, which as shown in Chapter III can have a large effect on the rates of second-order chemical reactions. To account for this phenomenon in our model, we need some method of generating turbulent velocities $\underline{u}'$ that will produce the proper correlations among neighboring particles. The basic problem of designing a scheme that produces given correlations between pairs of particles is discussed in detail in Appendix B. Here we consider briefly the related task of simulating the joint velocities of particle triplets and higher order groups.

Consider the particles emerging from a point source during the interval t_1 to $t_2 = t_1 + \delta t$. The mean displacement $\overline{\underset{\sim}{X}}_n$ of the n-th particle due to the turbulence alone is zero because the mean motion is treated in $\bar{\underset{\sim}{u}}$. Since the source is a point, the mean square displacements of all particles will be the same, and the mean square separation of all pairs of particles will be equal. These conditions can be summarized as follows:

$$\overline{X}_n = X_{n0} \quad , \qquad (244)$$

$$\overline{(X_n - X_{n0})^2} = \sigma_1^2 \quad , \qquad (245)$$

$$\overline{(X_n - X_m)^2} - (X_{n0} - X_{m0})^2 = \overline{\ell_1^2} \quad , \qquad (246)$$

where X_{n0} is the point of release of the n-th particle, and σ_1 and $\overline{\ell_1^2}$ are the mean square displacements and separations, respectively, of particles determined by the characteristics of the turbulence (see Appendix B).

Let X_n be the displacement of the n-th particle produced by our simulation of the turbulence velocity $\underset{\sim}{u}'$. The constraints expressed in Eqs. (244) through (246) on the statistics of X_n can be satisfied if X_n is of the form

$$X_n - X_{n0} = a\xi + bx_n \quad , \qquad (247)$$

where a and b are constants and ξ and x_n are computer-generated random numbers. To satisfy Eq. (244), we must have

$$\overline{\xi} = \overline{x}_n = 0 \quad . \qquad (248)$$

It is also convenient to have ξ and x_n statistically independent, i.e.,

$$\overline{\xi x_n} = \bar{\xi}\,\bar{x}_n = 0 \quad . \tag{249}$$

To satisfy Eq. (245), we need

$$\overline{(X_n - X_{n0})^2} = a^2\overline{\xi^2} + b^2\overline{x_n^2} = \sigma_1^2 \quad , \tag{250}$$

and to satisfy Eq. (246), we must have

$$\overline{(X_n - X_m)^2} - (X_{n0} - X_{m0})^2 = b^2\overline{x_n^2} + b^2\overline{x_m^2} = \overline{\ell_1^2} \quad . \tag{251}$$

If we make

$$\overline{\xi^2} = 1 \quad , \tag{252}$$

$$\overline{x_n^2} = \overline{x_m^2} = \sigma_1^2 \quad , \tag{253}$$

then it follows that Eqs. (244) through (246) will be satisfied by Eq. (247) if, in addition to Eqs. (248), (249), (252), and (253),

$$a^2 = \sigma_1^2 - \frac{\overline{\ell_1^2}}{2} \quad , \tag{254}$$

$$b^2 = \frac{\overline{\ell_1^2}}{2\sigma_1^2} \quad . \tag{255}$$

The algorithm for generating u' is now obtained by differentiating Eq. (247):

$$u_n' = a\dot{\xi} + \xi\dot{a} + b\dot{x}_n + x_n\dot{b} \quad . \tag{256}$$

(See Appendix B for further details.)

Consider now the particles leaving the source in the interval t_2 to $t_3 = t_2 + \Delta t$. The velocities of these particles will be correlated with one another and with those of the particles that left the source during t_1 to t_2. Designating the displacements of these particles with Greek subscripts, we have in analogy with Eqs. (244) through (246):

$$\overline{X}_\nu = X_{\nu 0} \quad , \tag{257}$$

$$\overline{(X_\nu - X_{\nu 0})^2} = \sigma_2^2 \quad , \tag{258}$$

$$\overline{(X_\nu - X_\mu)^2 - (X_{\nu 0} - X_{\mu 0})^2} = \overline{\ell_2^2} \quad , \tag{259}$$

$$\overline{(X_\nu - X_\eta)^2 - (X_{\nu 0} - X_{\eta 0})^2} = \overline{\ell_{12}^2} \quad . \tag{260}$$

The last condition expresses the correlation of the motions of the first and second groups of particles. Conditions (257) through (260) will be satisfied if

$$X_\nu - X_{\nu 0} = \alpha\eta + \beta(X_\eta - X_{\eta 0}) + \gamma\chi_\nu \quad , \tag{261}$$

where η and χ_ν are random variables with properties

$$\left.\begin{aligned} \overline{\eta} = \overline{\chi}_\nu &= 0 \quad , \\ \overline{\eta\chi_\nu} = \overline{\eta}\,\overline{\chi}_\nu &= 0 \quad , \\ \overline{\eta^2} &= 1 \end{aligned}\right\} \tag{262}$$

and

$$\beta = \frac{\sigma_1^2 + \sigma_2^2 - \overline{\ell_{12}^2}}{2\sigma_1^2} \quad , \tag{263}$$

$$\gamma^2 = \frac{\overline{\ell_2^2} - \beta^2\overline{\ell_1^2}}{2\sigma_2^2} \quad , \tag{264}$$

$$\alpha^2 = \sigma_2^2 - \frac{1}{2}\overline{\ell_2^2} - \beta^2\left(\sigma_1^2 - \frac{1}{2}\overline{\ell_1^2}\right) \quad . \tag{265}$$

As in the case of Eq. (256), we obtain the velocity algorithm for the particles released between t_2 and t_3 by differentiating Eq. (261) with respect to time.

The technique just described for formulating the turbulence velocity algorithm for the reactant particles can be extended to treat any number of successive groups of correlated particles. In applications of our model to specific problems, we do not anticipate the need for algorithms higher than third order [Eq. (256) and the velocity form of Eq. (261) being first and second order, respectively].

As of this writing, our stochastic microscale model of Eq. (216) has not been implemented or tested, but we hope in the very near future to test this technique and to install it in the SAI urban-scale air pollution model. One possible problem that we foresee is that this model is best suited to treating the near-source field. To apply it to the portions of a plume far from the source might necessitate the use of large amounts of machine time because in those areas where the concentrations are low, a larger ensemble of trajectories is needed to obtain a reasonably convergent approximation of the kernel p. To handle the far field, the discrete time-continuous space model described in Lamb (1976) can be used. In the next section, we outline this approach.

B. AN INTEGRAL EQUATION MODEL OF THE FAR-FIELD MICROSCALE POINT SOURCE CONCENTRATION DISTRIBUTION

For simplicity, we consider again the bimolecular reaction A + B → Products, where the concentrations A and B are governed by

$$\frac{\partial A}{\partial t} + \mathcal{L}A = -kAB - k\left\langle A'B' \right\rangle + S_A \quad , \qquad (266)$$

$$\frac{\partial B}{\partial t} + \mathcal{L}B = -kAB - k\left\langle A'B' \right\rangle + S_B \quad . \qquad (267)$$

As before, we define the subgrid-scale fields

$$A'' = A - \tilde{A} \quad , \quad B'' = B - \tilde{B} \quad , \qquad (268)$$

where $\tilde{A}$ and $\tilde{B}$ are the solutions of the urban-scale model versions of Eqs. (266) and (267):

$$\frac{\partial \tilde{A}}{\partial t} + L\tilde{A} = -k\tilde{A}\tilde{B} + \tilde{S}_A \quad , \qquad (269)$$

$$\frac{\partial \tilde{B}}{\partial t} + L\tilde{B} = -k\tilde{A}\tilde{B} + \tilde{S}_B \quad , \qquad (270)$$

where

$$\tilde{S}_A = \frac{1}{V}\int_V S \, dV \quad ,$$

and V is the grid cell volume. Using Eq. (268) in Eqs. (266) and (267) and then subtracting Eqs. (269) through (270), we obtain

$$\frac{\partial A''}{\partial t} + LA'' = -k(\tilde{A}B'' + A''\tilde{B} + A''B'' + \langle A'B' \rangle) + S''_A \quad , \qquad (271)$$

$$\frac{\partial B''}{\partial t} + LB'' = -k(\tilde{A}B'' + A''\tilde{B} + A''B'' + \langle A'B' \rangle) + S''_B \quad . \qquad (272)$$

To develop a discrete time-continuous space model of these equations, we proceed as discussed in Lamb (1976). First, we look at the case where A'' is spatially homogeneous so that $LA'' = 0$ and where $S''_A = 0$. In this case, Eq. (271) reduces to

$$\frac{dA''}{dt} = -k(\tilde{A}B'' + A''\tilde{B} + A''B'' + \langle A'B' \rangle) \qquad (273)$$

and Eq. (272) gives

$$\frac{dB''}{dt} = -k(\tilde{A}B'' + A''\tilde{B} + A''B'' + \langle A'B'\rangle) \quad . \tag{274}$$

Since dA"/dt = dB"/dt, we have

$$A'' - A''_0 = B'' - B''_0 \quad , \tag{275}$$

where the 0 subscripts denote initial values. From Eq. (275),

$$B'' = A'' - A''_0 + B''_0 \quad ;$$

combining this with Eq. (273), we obtain

$$\frac{dA''}{dt} = -k\left[\tilde{A}A'' - \tilde{A}A''_0 + \tilde{A}B''_0 + A''\tilde{B} + A''^2 - A''A''_0 + A''B''_0 + \langle A'B'\rangle\right] \quad . \tag{276}$$

For brevity, let

$$\zeta = A'' \quad , \quad \zeta_0 = A''_0 \quad .$$

Then Eq. (276) becomes

$$\frac{d\zeta}{dt} = -k(\zeta^2 + \alpha\zeta + \beta) \quad , \tag{277}$$

where

$$\alpha = \tilde{A} + \tilde{B} - A''_0 + B''_0 \quad , \tag{278}$$

$$\beta = \langle A'B'\rangle + \tilde{A}B''_0 - \tilde{A}A''_0 \quad . \tag{279}$$

The solution of Eq. (277) is

$$\zeta = A'' = \frac{d(\alpha + q) - \alpha + q}{2(1 - d)} = -\frac{1}{2}\left(\alpha + q\,\frac{d + 1}{d - 1}\right) \quad , \tag{280}$$

where

$$d = \frac{2A''_0 + \alpha - q}{2A''_0 + \alpha + q}\, e^{-kqt} \quad , \tag{281}$$

$$q = (\alpha^2 - 4\beta)^{1/2} \quad . \tag{282}$$

Thus,

$$\begin{aligned} A''(\underline{r},t_n) = &\int p'(\underline{r},t_n|\underline{r}',t_{n-1}) \left(-\frac{1}{2}\right)\left(\gamma + q\,\frac{d + 1}{d - 1}\right) d\underline{r}' \\ &+ \iint_{t_{n-1}}^{t_n} p'(\underline{r},t_n|\underline{r}',t') \; S''_A(\underline{r}',t') \left[-\frac{1}{2A''(\underline{r}',t_{n-1})}\right] \\ &\cdot \left(\gamma + q\,\frac{d' + 1}{d' - 1}\right) dt'\, dr' \quad , \end{aligned} \tag{283}$$

where α, q, and d are given by Eqs. (278), (282), and (281), respectively. In each case, the variables entering in the definitions of α, q, and d are evaluated at $(\underline{r}',t_{n-1})$. The parameter d' is given by Eq. (281) but with t replaced by $t_n - t'$. In the definition of d, t in Eq. (281) is replaced by Δt. From Eq. (275), the model equation for B" is found to be

$$\begin{aligned} B''(\underline{r},t_n) = &\int p'(\underline{r},t_n\big|\underline{r}',t_{n-1}) \left(-\frac{1}{2}\right)\left(\gamma + q\,\frac{d + 1}{d - 1}\right) d\underline{r}' \\ &+ \iint_{t_{n-1}}^{t_n} p'(\underline{r},t_n\big|\underline{r}',t') \; S''_B(\underline{r}',t') \left[-\frac{1}{2B''(\underline{r}',t_{n-1})}\right] \\ &\cdot \left(\gamma + q\,\frac{d' + 1}{d' - 1}\right) dt'\, dr' \quad . \end{aligned} \tag{284}$$

where

$$\gamma = \tilde{A} + \tilde{B} + A''_0 - B''_0 \quad . \tag{285}$$

Let us consider the problem of evaluating Eq. (283) [the treatment of Eq. (284) is identical and is thus not discussed separately]. If Δt is small, the product of the two terms in brackets in the last integral in Eq. (283) is approximately unity, and Eq. (283) reduces in the case of a single point source to

$$A''(\underline{r},t_n) = \int p'(\underline{r},t_n|\underline{r}',t_{n-1}) \left(-\frac{1}{2}\right)\left(\alpha + q\,\frac{d+1}{d-1}\right) d\underline{r}'$$

$$+ Q_A(t_{n-1})\,\overline{p'}(\underline{r}|\underline{r}_0,t_{n-1}) - \tilde{S}_A(\underline{r},t_{n-1})\Delta t \quad , \tag{286}$$

where

$$\overline{p'}(\underline{r}|\underline{r}_0,t_{n-1}) = \int_{t_{n-1}}^{t_n} p'(\underline{r},t_n|\underline{r}_0,t')\,dt' \quad . \tag{287}$$

The factors in brackets in the integral in Eq. (286) can also be simplified under the assumed smallness of Δt. Going back to Eq. (273), from which these terms came, we have [using Eq. (275)]

$$\frac{\partial A''}{\partial t} = -k(\tilde{A} + \tilde{B} + A'' - A''_0 + B''_0)A'' - k\left(\langle A'B'\rangle - \tilde{A}A''_0 + \tilde{A}B''_0\right) \quad , \tag{288}$$

where

$$A''_0 = A''(t_{n-1}) \quad , \quad B''_0 = B''(t_{n-1}) \quad .$$

Since we are interested in small time intervals Δt, it is not unreasonable to assume that the difference $A'' - A''_0$ that appears in the brackets in the first term on the right-hand side of Eq. (288) is negligible compared with the other three terms with which $A'' - A''_0$ is grouped. Therefore, we approximate Eq. (288) by

$$\frac{dA''}{dt} = -k'A'' - \kappa \quad , \tag{289}$$

where

$$k' = (\tilde{A} + \tilde{B} + B''_0)k \quad . \tag{290}$$

$$\kappa = \left(\langle A'B' \rangle - \tilde{A}A''_0 + \tilde{A}B''_0\right)k \quad . \tag{291}$$

The solution of Eq. (289) is

$$A''(t) = A''_0 - \kappa t - k'A''_0 t \quad , \tag{292}$$

where $A''_0 = A''(0)$. In Eq. (292), we have used the approximation (valid for small t)

$$e^{-k't} \doteq (1 - k't) \quad .$$

With the aid of Eq. (292), we can reduce Eq. (286) to the form

$$A''(\underset{\sim}{r},t_n) = \int p'(\underset{\sim}{r},t_n|\underset{\sim}{r}',t_{n-1})[A''(\underset{\sim}{r},t_{n-1}) - \kappa\Delta t - k'\Delta t A''(\underset{\sim}{r}',t_{n-1})]\, d\underset{\sim}{r}'$$

$$+ Q_A(t_{n-1})\overline{p^T}(\underset{\sim}{r}|\underset{\sim}{r}_0,t_{n-1}) - \tilde{S}_A(\underset{\sim}{r},t_{n-1})\Delta t \quad , \tag{293}$$

where κ and k' are given by Eqs. (290) and (291). The variables entering in the expressions for κ and k' are evaluated at $(\underset{\sim}{r}',t_{n-1})$.

We have in Eq. (293) the basis of a microscale model that could be used to restore point spatial resolution to any urban-scale pollution model, even one in which the sources in question have already been incorporated in the model's source inventory [note the presence of $\tilde{S}_A$ in Eq. (293)]. However, solving this equation requires the use of some finite array of grid points,and as we have stated earlier, achieving the desired resolution in such a system is often not possible. It is conceivable that we could get around this difficulty by using the stochastic model developed earlier to treat the near-source field where fine detail exists in the concentration distributions and to use Eq. (293) to model the plume farther from the source where spatial variations are no larger than that compatible with a grid network of practicable size. Of course, combining two techniques in this way would complicate the microscale model considerably. And this raises the question of just how many of the chemical intricacies that these techniques describe in detail and that are responsible for the mathematical complexities are important over the space and time scales within which we desire to resolve the microscale concentration fields. If, on the one hand, many of the nonlinear processes behave like linear ones over the scales of interest, then the linear microscale model described in Lamb (1976) should suffice. Even if this were not the case, a great deal of information could be derived from a plume model such as that presented in Chapter III but only for unstable conditions. But if, on the other hand, the detailed chemical interactions among the pollutant species prove to have a significant effect on concentrations within the regions of interest, then there appear to be no other ways than those proposed above for modeling the microscale concentration distributions.

To carry our development of Eq. (293) through to a workable model equation, we consider in the remainder of this chapter the possibility of solving Eq. (293) numerically for its steady-state solution. Considering the steady state is not unreasonable since over the limited spatial regions of interest the plume responds quickly to changes in meteorology. Furthermore, by solving for the steady-state values, we may be able to reduce the computer time requirements.

C. A METHOD OF SOLVING THE INTEGRAL EQUATIONS GOVERNING THE STEADY-STATE A" AND B" DISTRIBUTIONS

By definition in the steady state, we have

$$A''(\underset{\sim}{r},t_n) = A''(\underset{\sim}{r},t_{n-1}) \quad , \qquad (294)$$

$$B''(\underset{\sim}{r},t_n) = B''(\underset{\sim}{r},t_{n-1}) \quad . \qquad (295)$$

In this case, Eq. (293) and its counterpart governing B" reduce to a pair of simultaneous integral equations of the form

$$F_1(\underset{\sim}{x}) = \phi(\underset{\sim}{x}) + \int_{-\infty}^{\infty} p(\underset{\sim}{x},\underset{\sim}{s})[\alpha_1\phi(\underset{\sim}{s}) + \beta_1\phi(\underset{\sim}{s})\psi(\underset{\sim}{s}) + \gamma_1\psi(\underset{\sim}{s})]\, d\underset{\sim}{s} \quad , \qquad (296)$$

$$F_2(\underset{\sim}{x}) = \psi(\underset{\sim}{x}) + \int_{-\infty}^{\infty} p(\underset{\sim}{x},\underset{\sim}{s})[\alpha_2\phi(\underset{\sim}{s}) + \beta_2\phi(\underset{\sim}{s})\psi(\underset{\sim}{s}) + \gamma_2\psi(\underset{\sim}{s})]\, d\underset{\sim}{s} \quad , \qquad (297)$$

where

$\underset{\sim}{x} = (x,y,z)$,

$\alpha_1 = -1 + \tilde{B}k\Delta t$,

$\beta_1 = k\Delta t$,

$\gamma_1 = \tilde{A}k\Delta t$,

$\underset{\sim}{s} = (x_s,y_s,z_s)$,

$\alpha_2 = \tilde{B}k\Delta t$,

$$\beta_2 = k\Delta t,$$

$$\gamma_2 = -1 + \tilde{A}k\Delta t,$$

$$F_1(\underline{x}) = -k\Delta t\int_{-\infty}^{\infty} \langle A'B'\rangle\, p(\underline{x},\underline{s})\, d\underline{s} + Q_A p(\underline{x},\underline{x}_0) - \tilde{S}_A\Delta t \quad ,$$

$$F_2(\underline{x}) = -k\Delta t\int_{-\infty}^{\infty} \langle A'B'\rangle\, p(\underline{x},\underline{s})\, d\underline{s} + Q_B p(\underline{x},\underline{x}_0) - \tilde{S}_B\Delta t \quad ,$$

$$p(\underline{x},\underline{x}_0) = \int_{t}^{t_0+\Delta t} p(\underline{x},t_0+\Delta t\,|\,\underline{x}_0,t')\, dt' \quad ,$$

and

$$p(\underline{x},\underline{s}) = (2\pi^{3/2}\,\sigma_x\sigma_y\sigma_z)^{-1}\exp\left[-\frac{(x - x_s - u\Delta t)^2}{2\sigma_x^2} - \frac{(y - y_s - v\Delta t)^2}{2\sigma_y^2}\right]$$
$$\cdot\left\{\exp\left[-\frac{(z - z_s)^2}{2\sigma_z^2}\right] + \exp\left[-\frac{(z + z_s)^2}{2\sigma_z^2}\right]\right\} \quad .$$

A common approach to solving a system such as that given in Eqs. (296) through (297) is to create a three-dimensional grid on which the integrand can be approximated by piecewise quadratics and then to integrate the quadratics analytically. This is equivalent to evaluating the integrals by Simpson's rule. In any case, at the i-th grid point, $\underline{x}_i$, we obtain the equations

$$F_1(\underline{x}_i) = \phi(\underline{x}_i) + \sum_{j=1}^{M} w_j p(\underline{x}_i,\underline{x}_j)[\alpha_1\phi(\underline{x}_j) + \beta_1\phi(\underline{x}_j)\psi(\underline{x}_j) + \gamma_1\psi(\underline{x}_j)] \quad , \tag{298}$$

$$F_2(\underline{x}_i) = \psi(\underline{x}_i) + \sum_{j=1}^{M} w_j p(\underline{x}_i,\underline{x}_j)[\alpha_2\phi(\underline{x}_j) + \beta_2\phi(\underline{x}_j)\psi(\underline{x}_j) + \gamma_2\psi(\underline{x}_j)] \quad . \tag{299}$$

where w_j is the weighting factor for the j-th node in the three-dimensional form of Simpson's rule, and M is the total number of nodes. We can write a similar pair of equations for every node, obtaining 2M nonlinear equations in 2M unknowns. To simplify the notation, we write this system

$$G(\underline{Y}) = 0 \quad , \tag{300}$$

where

$$\underline{Y} = [\phi(\underline{x}_1),\phi(\underline{x}_2),\ldots,\phi(\underline{x}_M),\psi(\underline{x}_1),\psi(\underline{x}_2),\ldots,\psi(\underline{x}_M)]^T \quad .$$

Since G is differentiable,

$$G(\underline{Y}) = G(\underline{Y}_0) + G'(\underline{Y}_0)(\underline{Y} - \underline{Y}_0) + \eta(\underline{Y},\underline{Y}_0) \quad , \tag{301}$$

where

$$\lim_{\underline{Y}\to\underline{Y}_0} \frac{||\eta(\underline{Y},\underline{Y}_0)||}{||\underline{Y} - \underline{Y}_0\,||} = 0 \quad .$$

If $\underline{Y}^*$ is a solution to Eq. (300), then

$$0 = G(\underline{Y}_0) + G'(\underline{Y}_0)(\underline{Y}^* - \underline{Y}_0) + \eta(\underline{Y}^*,\underline{Y}_0) \quad ,$$

which suggests that $\underline{Y}^*$ might be approximated by $\underline{Y}_1$ where

$$0 = G(\underline{Y}_0) + G'(\underline{Y}_0)(\underline{Y}_1 - \underline{Y}_0) \quad .$$

If $\underline{Y}_0$ is sufficiently close to $\underline{Y}^*$, we can obtain a sequence $\{\underline{Y}_n\}$ that converges to $\underline{Y}^*$ if we iterate according to the prescription

$$G'(\underline{Y}_n)\underline{Y}_{n+1} = G'(\underline{Y}_n)\underline{Y}_n - P(\underline{Y}_n) \quad . \tag{302}$$

Eq. (302) is a linear algebraic equation of the form $A\underline{x} = \underline{b}$. The solution of the system of nonlinear integral equations [(296) through (297)] can therefore be approximated by the repeated solution of linear algebraic equations.

Unfortunately, if we try to create a three-dimensional grid on which the integrands in Eqs. (296) and (297) can be approximated by piecewise quadratics, we find that for small Δt, $p(\underline{x},\underline{s})$ is a very sharply peaked function. Also, ϕ and ψ are sharply peaked near the source. It is this property that makes these functions impossible to resolve on a grid system of practical size. We plan to use the stochastic model to resolve the concentrations in this region and to solve Eqs. (296) and (297) to determine ϕ and ψ farther downstream where they can be approximated on grids of practical size. Figures 23 and 24 show a nested grid that could be used to model ϕ and ψ downwind from a point source. In this region, ϕ and ψ are approximated by piecewise quadratics, and $p(\underline{x},s)$ is treated analytically to describe precisely its sharp variations. This technique is essentially a modification of Simpson's rule.

Simpson's rule is designed to approximate integrals of the form

$$\int_{-h}^{h} f(x)\, dx$$

by approximating $f(x)$ with a quadratic over the interval $(-h,h)$ (see Figure 25).

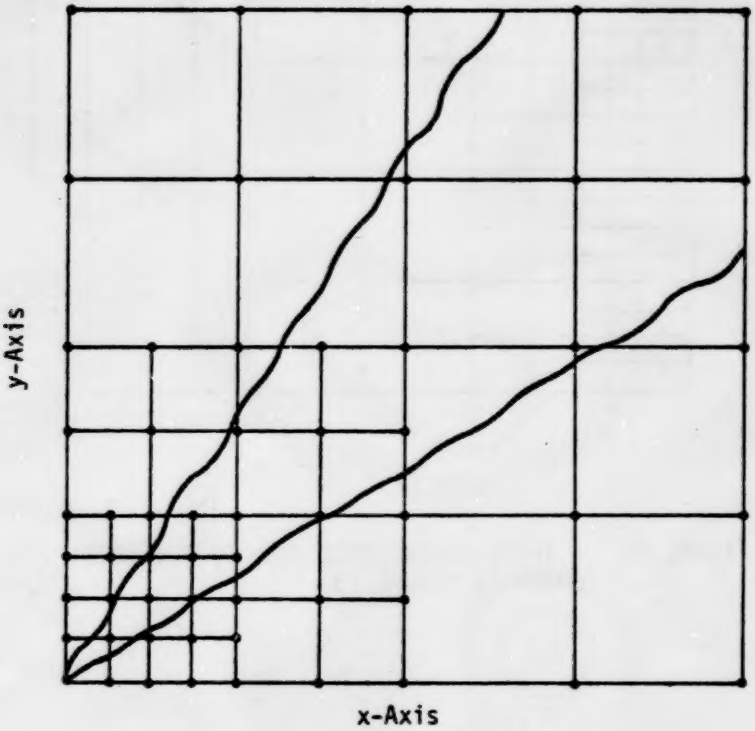
y-Axis
x-Axis

FIGURE 23. A NESTED GRID SYSTEM FOR USE IN EVALUATING THE INTEGRAL EQUATIONS GOVERNING A" AND B"

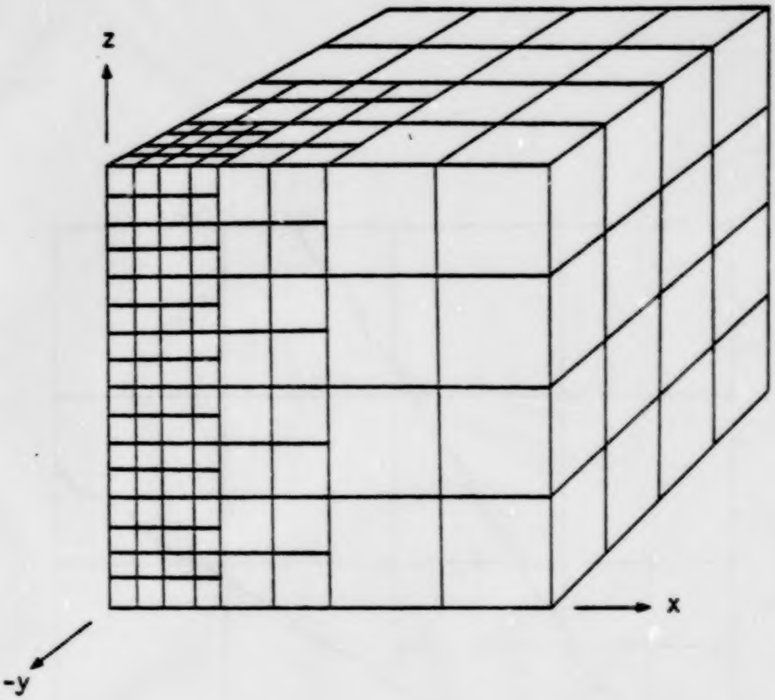

FIGURE 24. A THREE-DIMENSIONAL VIEW OF THE GRID SHOWN IN FIGURE 23

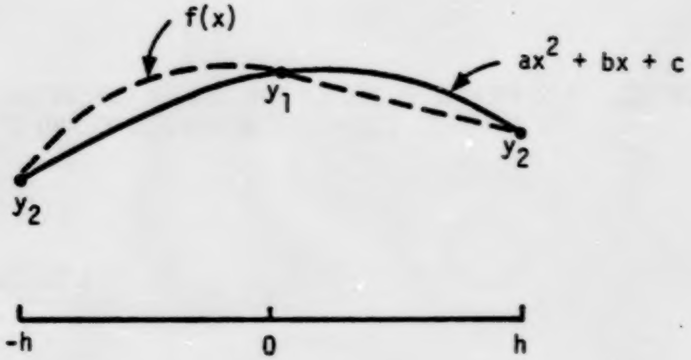
f(x)
$ax^2 + bx + c$
y_1
y_2
y_2
-h
0
h

FIGURE 25. QUADRATIC REPRESENTATION OF A FUNCTION f(x)

Then

$$\int_{-h}^{h} f(x)\,dx \approx \int_{-h}^{h} (ax^2 + bx + c)\,dx = \frac{2ah^3}{3} + 2ch \quad . \tag{303}$$

If we express a, b, and c in terms of the ordinates y_0, y_1, and y_2, we have the familiar formulation of Simpson's rule (see Figure 25):

$$\int_{-h}^{h} f(x)\,dx \approx \frac{h}{3}\,(y_0 + 4y_1 + y_2) \quad . \tag{304}$$

We develop an integration formula for integrals of the special form

$$\int_{-h}^{h} e^{-[(x-\beta)/\alpha]^2}\, f(x)\,dx$$

by approximating f(x) with a quadratic. Then it is possible to handle the integrals in Eqs. (296) and (297) without resolving $p(\underline{x},\underline{s})$ on some grid because the formula handles p analytically. Approximating f(x) by $ax^2 + bx + c$, we have

$$\int_{-h}^{h} e^{-[(x-\beta)/\alpha]^2}\, f(x)\,dx \approx a\int_{-h}^{h} x^2 e^{-[(x-\beta)/\alpha]^2}$$

$$+\, b\int_{-h}^{h} x e^{-[(x-\beta)/\alpha]^2} + c\int_{-h}^{h} e^{-[(x-\beta)/\alpha]^2} \quad .$$

Letting $u = x - \beta$, this becomes

$$a\int_{-h-\beta}^{h-\beta} (u^2 + 2u\beta + \beta^2)\, e^{-(u/\alpha)^2}\, du + b\int_{-h-\beta}^{h-\beta} (u + \beta)\, e^{-(u/\alpha)^2}\, du$$

$$+ c\int_{-h-\beta}^{h-\beta} e^{-(u/\alpha)^2}\, du \quad . \tag{305}$$

Collecting the u^2 terms in Eq. (305) and integrating by parts gives

$$a\alpha^3\int_{-h-\beta}^{h-\beta} \left(\frac{u}{\alpha}\right)^2 e^{-(u/\alpha)^2}\, d\left(\frac{u}{\alpha}\right) = -\left.\frac{a\alpha^2 u}{e}\, e^{-(u/\alpha)^2}\right|_{-h-\beta}^{h-\beta}$$

$$+\int_{-h-\beta}^{h-\beta} \frac{a\alpha^3}{2}\, e^{-(u/\alpha)^2}\, d\left(\frac{u}{\alpha}\right) \quad . \tag{306}$$

Collecting the u^1 terms in Eq. (305) and integrating gives

$$\int_{-h-\beta}^{h-\beta} \left(a\beta\alpha^2 + \frac{b\alpha^2}{2}\right)\left(\frac{-2u}{\alpha}\right) e^{-(u/\alpha)^2}\, d\left(\frac{u}{\alpha}\right) = -\left(a\beta\alpha^2 + \frac{b\alpha^2}{2}\right) e^{-(u/\alpha)^2}\Bigg|_{-h-\beta}^{h-\beta} \quad . \tag{307}$$

Collecting the u^0 terms in Eqs. (306) and (307) and integrating gives

$$\int_{-h-\beta}^{h-\beta} \left(a\beta^2 + \frac{a\alpha^3}{2} + b\beta\alpha + c\alpha\right) e^{-(u/\alpha)^2}\, d\left(\frac{u}{\alpha}\right)$$

$$= \left(a\beta^2 + \frac{a\alpha^3}{2} + b\beta\alpha + c\alpha\right)\left[\operatorname{erf}\left(\frac{h - \beta}{\alpha}\right) - \operatorname{erf}\left(\frac{-h - \beta}{\alpha}\right)\right] \quad . \tag{308}$$

Combining Eqs. (306) through (308) and using the fact that the nodes are equally spaced, i.e.,

$$a = \frac{y_0 - 2y_1 + y_2}{h^2} \quad , \quad b = \frac{y_2 - y_0}{2h} \quad , \quad c = y_1 \quad ,$$

we obtain

$$\begin{aligned}
\int_{-h}^{h} e^{-[(x-\beta)/\alpha]^2} f(x)\, dx \approx \frac{\alpha^2}{2h^2} & \left[y_0\left(\beta + \frac{h}{2}\right) - 2\beta y_1 + y_2 \left(\beta - \frac{h}{2}\right)\right] \\
& \cdot \left\{ e^{-[(h+\beta)/\alpha]^2} - e^{-[(h-\beta)/\alpha]^2} \right\} \\
& - \frac{\alpha^2}{2h}\left(y_0 + y_2 - 2y_1\right) \\
& \cdot \left\{ e^{-[(h+\beta)/\alpha]^2} + e^{-[(h-\beta)/\alpha]^2} \right\} \\
& + \frac{\alpha}{h^2}\left[y_0 \left(\beta^2 + \frac{\alpha^2}{2} - \frac{h\beta}{2}\right) + \left(h^2 - 2\right) y_1 \right. \\
& \left. + y_2 \left(\beta^2 + \frac{\alpha^2}{2} - \frac{h\beta}{2}\right)\right] \left[\operatorname{erf}\left(\frac{h-\beta}{\alpha}\right) + \operatorname{erf}\left(\frac{h+\beta}{\alpha}\right)\right] .
\end{aligned} \tag{309}$$

When Eqs. (296) and (297) are integrated using this new technique, we obtain the following equations at $\underline{x}_i$:

$$F_1(\underline{x}_i) = \phi(\underline{x}_i) + \sum_{j=1}^{M} \tilde{w}_j \left[\alpha_1 \phi(\underline{x}_j) + \beta_1 \phi(\underline{x}_j)\psi(\underline{x}_j) + \gamma_1 \psi(\underline{x}_j)\right] \quad , (310)$$

$$F_2(\underline{x}_i) = \psi(\underline{x}_i) + \sum_{j=1}^{M} \tilde{w}_j \left[\alpha_2 \phi(\underline{x}_j) + \beta_2 \phi(\underline{x}_j)\psi(\underline{x}_j) + \gamma_1 \psi(\underline{x}_j)\right] \quad . (311)$$

Here, $\tilde{w}_j$ are the weight functions given by our new formula; notice that unlike the w_j in Eqs. (298) and (299), $\tilde{w}_j$ incorporates the effects of $p(\underline{x},\underline{s})$ so that no $p(\underline{x}_i,\underline{x}_j)$ terms appear in Eqs. (310) and (311). Consequently, $p(\underline{x},\underline{s})$ need not be resolvable on the solution grid (though ϕ and ψ must be well represented). We can now solve the nonlinear equations [(310) and (311)] using Newton's method. If we use the grid in Figure 24 to represent ϕ and ψ, we can expect to obtain an accurate solution to Eqs. (296) and (297).

The computation time required to produce a solution to Eqs. (296) and (297) using Newton's method and the grid in Figure 24 is considerable but not unreasonable. Each iteration of Eq. (302) necessitates the solution of a linear system of 506 equations in 506 unknowns. The coefficient matrix may be fairly sparse; if so, successive over-relaxation may be a good solution technique. If not, direct solution can be used; the 250,000 element coefficient matrix can easily fit into the large core memory of the Lawrence Berkeley Laboratory's CDC 7600. The arithmetic operations required for each direct soltuion of Eq. (302) take approximately 4 seconds. If direct solution is used, the coefficient matrix should not be updated every time. Virtually all the time needed to solve Eq. (302) is spent computing the LU decomposition of $G'(\underline{x}_n)$. If we use the already decomposed $G'(\underline{x}_n)$ instead of $G'(\underline{x}_{n+1})$, in the next iteration of Eq. (302) two iterations can be performed for the price of one without seriously affecting the algorithm's convergence. In fact, we should update G' every n-th time, where n is some number beyond which the gain in speed per iteration is offset by a slowdown in the convergence rate of the algorithm.

Whether over-relaxation or direct methods should be used depends largely on $p(\underline{x},\underline{s})$. If p is zero at a sufficiently large number of points (almost all of them), the coefficient matrix will be sparse and iterative methods would be in order. In any case, the algorithm as a whole will converge much more rapidly when a good first approximation is available.

Consider now the problem of obtaining a good first estimate of the solution of Eqs. (296) and (297). Consider the equations

$$F_1(\underline{x}) = \phi(\underline{x}) + \int_{-\infty}^{\infty}\int_{-\infty}^{\infty}\int_{-\infty}^{x} 2p(\underline{x},\underline{s})\left[\alpha_1\phi(\underline{s}) + \beta_1\phi(\underline{s})\psi(\underline{s}) + \gamma_1\psi(\underline{s})\right] dx_s\, dy_s\, dz_s \quad , \tag{312}$$

$$F_2(\underline{x}) = \psi(\underline{x}) + \int_{-\infty}^{\infty}\int_{-\infty}^{\infty}\int_{-\infty}^{x} 2p(\underline{x},\underline{s})\left[\alpha_2\phi(\underline{s}) + \beta_2\phi(\underline{s})\psi(\underline{s}) + \gamma_2\psi(\underline{s})\right] dx_s\, dy_s\, dz_s \tag{313}$$

These equations are identical to Eqs. (296) and (297), except that instead of specifying the upwind x-direction diffusion exactly, at any point x_0 it is approximated using a reflection of the downwind diffusion. This will be reasonable whenever the concentration gradients in the x direction are not too steep. The enormous advantage of this formulation is that it has changed the x-direction part of the equations from a boundary value problem [as it was in Eqs. (296) and (297)] to an initial value problem [as it is in Eqs. (312) and (313)]. Thus, ϕ and ψ can be obtained by solving a series of y-z problems, whereas in Eqs. (296) and (297) the entire x-y-z problem must be solved together.

When solving Eqs. (312) and (313), we would specify initial values of ϕ and ψ in the two upwind y-z planes (say, the planes are at 0 and Δx), and would then write Eqs. (310) and (311) for every node $\underline{x}_i$ in the y-z plane at Δx. This would produce a nonlinear system of 2N equations in 2N unknowns, where the unknowns are the values of ϕ and ψ at the N nodes in the y-z plane at 2Δx. This nonlinear system can be solved using Newton's method according to the procedure outlined earlier.

Suppose we were to solve both Eqs. (296) and (297) and Eqs. (312) and (313) on a cubical mesh with n nodes on a side. The system represented by Eqs. (296) and (297) requires repeated solution of a $2n^3$ linear system; Eqs. (312) and (313) require n solutions of $2n^2$ linear systems. When direct methods are used to solve an s-dimensional linear system, the solution time is roughly proportional to s^3. The ratio

$$\frac{\text{Solution Time for Eqs. (296) and (297)}}{\text{Solution Time for Eqs. (312) and (313)}} = \frac{(2n^3)^3}{n \cdot (2n^2)^3} = \frac{8n^9}{8n^7} = n^2$$

clearly indicates how much quicker it is to solve Eqs. (312) and (313) than it is to solve the original problem [Eqs. (296) and (297)]. In actual practice, ϕ and ψ might represent the microscale corrections downwind from a point source; in such a case, a cubical mesh would not be suitable for either Eqs. (296) and (297) or Eqs. (312) and (313). A good mesh for Eqs. (296) and (297) was given in Figures 23 and 24. Figure 26 shows an expanding series of y-z meshes that could be used for Eqs. (312) and (313). Even when both problems are done on different meshes, we can expect Eqs. (312) and (313) to be much faster to solve.

In conclusion, we summarize below the solution procedure:

(1) Obtain an initial estimate for the solution to Eqs. (296) and (297) by solving Eqs. (312) and (313) for ϕ and ψ.
    (a) Specify the initial conditions in two upwind y-z planes and boundary conditions for y and z at the edge of the entire region.
    (b) For $n = 1$ to $n = N - 1$:
        - Use the special integral formula [Eq. (309)] to obtain Eqs. (310) and (311) at every node in the y-z plane located at $x = n\Delta x$.

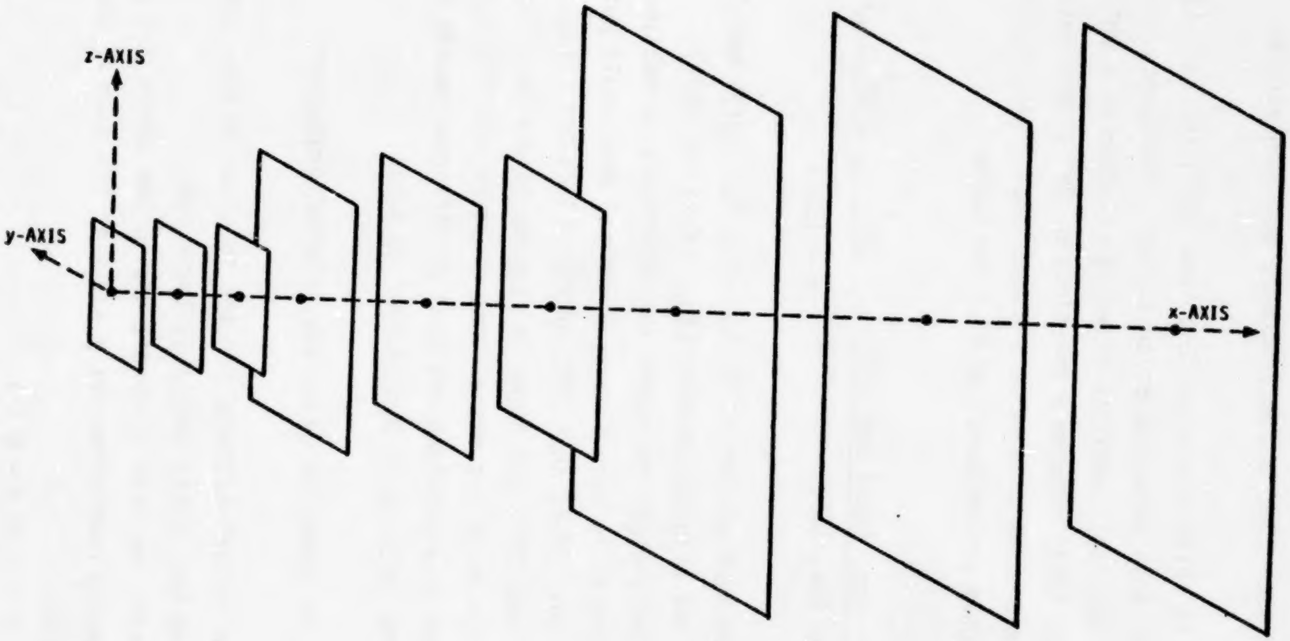
z-AXIS
y-AXIS
x-AXIS

FIGURE 26. AN EXPANDED SERIES OF y-z MESHES FOR SOLVING EQS. (312) AND (313)

(c) Solve this nonlinear equation using Newton's method to obtain ϕ and ψ values at every node in the y-z plane at $(n + 1)\Delta x$.

(d) Go back to Step (b).

(2) Solve Eqs. (296) and (297) for ϕ and ψ:

(a) Specify boundary values for x, y, and z over the entire region.

(b) Use the special integral formula [Eq. (309)] to obtain Eqs. Eqs. (310) and (311) at every node in the entire region.

(c) Solve these nonlinear equations for ϕ and ψ using Newton's method and the solution obtained in Step 1 as an initial estimate.

VI MODELING POLLUTANT CONCENTRATIONS IN THE VICINITY OF A ROADWAY

R. G. Lamb

In the preceding chapter, we analyzed the problem of resolving details in the concentration distribution in the vicinity of a point source, such as a power plant. In this chapter, we analyze the analogous problems associated with the modeling of concentrations around a roadway. In both cases, the severity of the problems encountered depends partly on the origin of the estimates of background pollutant concentrations. If, on the one hand, these estimates are derived from an urban-scale model in which the emissions of the point source or roadway in question were included as part of a volume source, then the effects of these emissions must be filtered from the model predictions to obtain the true background values. [The necessary operations are described in the preceding chapter and in Lamb (1976).] If, on the other hand, the ambient pollutant concentrations are prescribed, filtering operations are not required, and the point or roadway can be modeled independently. The latter situation is assumed to apply in this chapter. In a later study, we will adapt the roadway model developed here to work in conjunction with an urban-scale model.

A. BACKGROUND

Modeling concentrations near a roadway presents problems that are not encountered in simulating pollutants arising from a stationary point source. The motion of motor vehicles generates wakes that affect the dispersal of the vehicle emissions and that produce concentration fluctuations altering the rates of chemical transformation of these emissions. Also, the random passage of vehicles past a fixed point gives the emissions rate of the highway, as viewed locally, a random nature. And in situations where the roadway is elevated or located in a cavity, the mean flow and turbulence can be altered significantly from the classical states that pertain to flows over a flat surface. These phenomena preclude the development of a viable roadway model from the Gaussian plume formula or any similar expression that intrinsically is descriptive of point sources under the simplest of conditions--i.e., steady emissions, nonstagnant flow, flat surface, no wake effects, and no upstream diffusion. Chock (1976) revealed some of the inadequacies of the plume formula as a model of roadway emissions by comparing predictions of EPA's HIWAY model, which is based on the Gaussian plume formula, with data gathered in the General Motors sulfate dispersion experiment. He found that the neglect of wake and buoyancy effects and the breakdown of the plume formula under calm wind conditions caused the HIWAY model to overpredict concentrations in most instances, particularly those conducive to high pollutant levels. In view of these observations, we base our two roadway models on a more generalized Lagrangian diffusion equation.

In this chapter, we outline two roadway models. The relationships among them and the plume equation are shown schematically in Figure 27. As the figure shows, the model called ROADWAY 1 is based on the assumption that the p kernel is Gaussian. This model is one step closer to the generalized diffusion equation than is the plume formula; consequently, it can treat all the phenomena mentioned above that the plume formula ignores. Errors incurred through the assumption that p is Gaussian vanish when the model is used to calculate concentrations averaged over a sufficiently large cross-sectional area of a highway. The model called ROADWAY 2 attempts to calculate the p kernel through a Monte Carlo simulation of the mean flow and turbulence fields themselves. This model is intended for use in calculating concentrations in situations where the Gaussian form of p is not wholly adequate, such as around elevated or depressed roadways.

At present, only the theoretical aspects of these models have been formulated. Implementation and testing will be carried out under a future contract to EPA. When completed, these models will

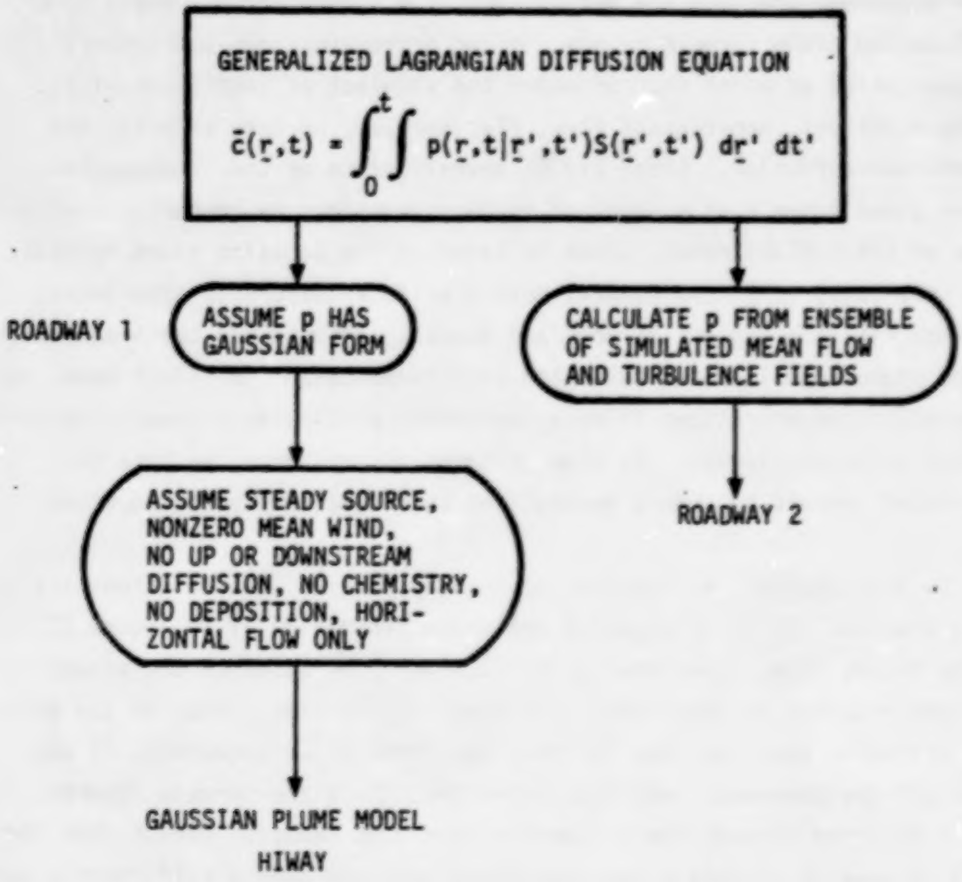
GENERALIZED LAGRANGIAN DIFFUSION EQUATION
$\bar{c}(\underset{\sim}{r},t) = \int_0^t \int p(\underset{\sim}{r},t|\underset{\sim}{r}',t')S(\underset{\sim}{r}',t')\, d\underset{\sim}{r}'\, dt'$
ROADWAY 1
ASSUME p HAS GAUSSIAN FORM
ASSUME STEADY SOURCE, NONZERO MEAN WIND, NO UP OR DOWNSTREAM DIFFUSION, NO CHEMISTRY, NO DEPOSITION, HORIZONTAL FLOW ONLY
GAUSSIAN PLUME MODEL
HIWAY
CALCULATE p FROM ENSEMBLE OF SIMULATED MEAN FLOW AND TURBULENCE FIELDS
ROADWAY 2

FIGURE 27. SCHEMATIC ILLUSTRATION OF THE RELATIONSHIP AMONG THE ROADWAY MODELS DESCRIBED IN THIS REPORT AND AND EPA'S HIWAY MODEL

provide a capability for calculating concentrations in the vicinity of a roadway, taking into account all of the following:

- Photochemistry.
- Concentration fluctuations produced by wake and ambient turbulence.
- Wake-induced dispersion.
- Buoyancy of vehicle emissions.
- Calm winds.
- Wind shear.
- Winds parallel to the roadway.
- Atmospheric stability effects on turbulence.
- Pollutant deposition.
- Multilane highways.
- Elevated, at-grade, and depressed roads.

One might argue that the development of such generalized models is not warranted given the paucity of data necessary to describe the phenomena listed above. To some extent this is a valid argument; nevertheless, a considerable quantity of information exists (some of which is presented later) about wake effects, complex flows, concentration fluctuations, and the like that cannot be incorporated in a model such as HIWAY that is based on the Gaussian plume formula. For the purposes of creating a model framework capable of handling these additional data and of treating photochemical pollutants, we propose these generalized structures.

For simplicity, both roadway models will be cast in a two-dimensional form. The process by which this is achieved is illustrated below with the aid of Figure 28. For a roadway link of sufficient length (to be established later) and oriented as shown in Figure 28, the mean concentration at the receptor shown in the figure is given by

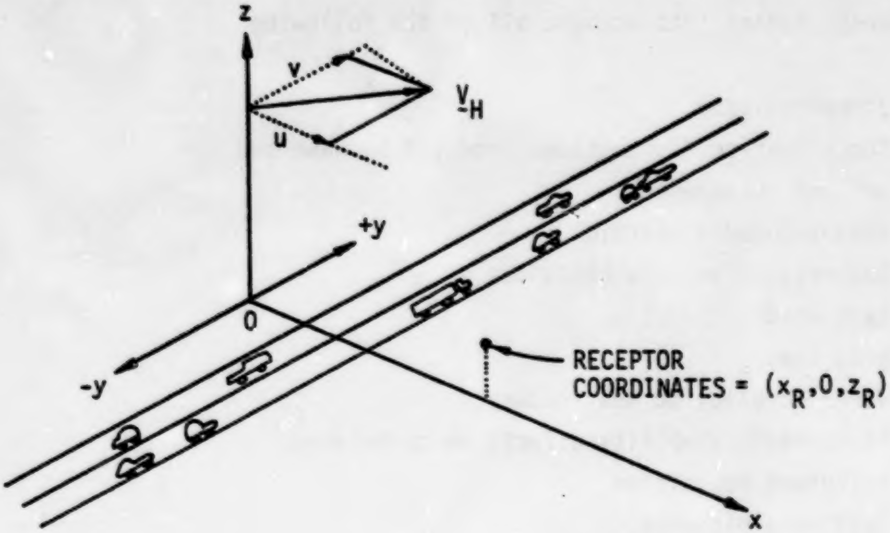
z
v
$\underset{\sim}{V}_H$
u
+y
0
-y
RECEPTOR
COORDINATES = $(x_R,0,z_R)$
x

$\underset{\sim}{V}_H$ = mean wind vector

u = component of $\underset{\sim}{V}_H$ normal to roadway

v = component of $\underset{\sim}{V}_H$ parallel to roadway

0 = coordinate origin; y-axis parallel to road with receptor lying in x-z plane

FIGURE 28. COORDINATE SYSTEM USED IN THE ROADWAY MODEL TO COMPUTE CONCENTRATIONS AT AN ARBITRARY RECEPTOR SITE

$$\bar{c}(x_r,0,z_r,t) = \int_0^t \int_{-\infty}^{\infty} p(x_r,0,z_r,t|x_s,y',z_s,t')S(y',t')\,dy'\,dt' \quad , \quad (314)$$

where z_s is the effective height of the vehicle emission; x_s denotes the location of the road in the chosen frame (only a single lane of traffic is considered here); and S is the function describing the distribution of vehicle emissions. For traffic of uniform speed v_s, we have

$$S(y',t') = \sum_{n=1}^{N} Q\delta(y' - y_{0n} - v_{sn}t') \quad , \quad (315)$$

where Q is the emissions rate (mass/time) of each vehicle; N is the total number of vehicles operating on the link; y_{0n} is the position at $t = 0$ of the n-th vehicle; $v_{sn} = v_s$ if the n-th vehicle is moving toward +y, $v_{sn} = -v_s$ otherwise; and δ is the delta function.

Owing to the symmetry of the roadway about the x-z plane, we can assume that the component of diffusion parallel to the roadway is negligible, in which case,

$$p(x_r,0,z_r,t\Big|x_s,u',z_s,t') = p(x_r,z_r,t\Big|x_s,z_s,t')\cdot\delta[y' + (t - t')v] \quad , \quad (316)$$

where v is the component of the mean wind parallel to the road (see Figure 28). Substituting Eqs. (315) and (316) into Eq. (314) and evaluating the y' integral, we obtain

$$\bar{c}(x_r,0,z_r,t) = Q\sum_{n=1}^{N} \int_0^t p(x_r,z_r,t|x_s,z_s,t')\delta[t'(v - v_{sn}) - tv - y_{0n}]\,dt' \quad . \quad (317)$$

This is the desired two-dimensional form of the roadway model equation governing $\bar{c}$.

It is perhaps instructive to comment briefly on the physical meaning of Eq. (317). The delta function in this equation is the effective source strength function. Keeping in mind that $\delta(\xi)$ is nonzero only when $\xi = 0$ and that y_{0n} is a random sequence, describing vehicle locations at $t = 0$, we see that the source function in our roadway model is a random sequence of instantaneous point sources whose temporal phasing is determined by the combination of vehicle and wind speed components v_{sn} and v. For example, if $v = 0$, i.e., the winds are either calm or blowing perpendicular to the road, then the delta function in Eq. (317) is nonzero only when $t'v_{sn} + y_{0n} = 0$. By definition of y_{0n}, this occurs only at the instant t' when the n-th vehicle passes through the x-z plane of the receptor. This is an obvious result because when $v = 0$ and the roadway is symmetric about the receptor plane, only those pollutants released in that plane can in effect influence that receptor. As a second example, suppose that all vehicles are stopped, $v_{sn} = 0$, but $v \neq 0$. In this case, the delta function in Eq. (317) is nonzero, for a given t, when $(t - t')v = -y_{0n}$. In other words, emissions released at time t' from the n-th vehicle affect the receptor at the time $t = t' - (y_{0n}/v)$ when those emissions pass through the receptor plane. Modifications of Eq. (317) to treat multilane roads, variable emissions heights z_s, emissions rates Q, and vehicle speeds v_s are straightforward and are not discussed here.

Looking back over the steps that led up to Eq. (317), we find that this equation becomes invalid if a significant fraction of the emissions that affect the receptor arise from portions of the roadway that are not parallel to the y-axis. A condition on the length of roadway that must be straight in the vicinity of the receptor to render Eq. (317) accurate can be derived as follows. Let

$$T \equiv \min\left(\frac{|x_R - x_s|}{u_c}, \frac{|z_R - z_s|}{w_c}\right) \quad , \qquad (318)$$

where

$$u_c = \frac{d}{dt}(\bar{x} + \sigma_x) \quad , \tag{319a}$$

$$w_c = \frac{d}{dt}(\bar{z} + \sigma_z) \quad , \tag{319b}$$

and $(\bar{x},\bar{z})$ is the centroid of a instantaneous cloud of emissions and σ_x and σ_z are (roughly) the cloud dimensions. The time scale T is a measure of the time required for emissions to have become so dilute or to have moved so far that they have negligible impact on the receptor. Simple reasoning then leads to the conclusion that for Eq. (317) to apply, the roadway in the vicinity of the receptor must be straight for at least a distance L_s, given by

$$L_s = vT \quad .$$

Here v is the component of the mean wind parallel to the roadway.

Applicability of the roadway model to photochemical pollutants will be achieved using the closure technique developed in Chapter III. To facilitate this operation, we assume that pollutants are either pseudo-inert or infinitely fast reacting. This division is prompted by the fact that in most cases of interest, T is of the order of several minutes, which is a long time compared with the reaction time of species such as NO and O_3 but short compared with other species such as hydrocarbons. Which category a given species falls into must be decided on a case-by-case basis, but in general we anticipate that NO and O_3 will always be treated as fast reactants. Proceeding under this assumption, we find the governing equations for $\bar{c}_{NO}$ and $\bar{c}_{O_3}$ to be [cf. Eq. (72) in the limit as $k \to \infty$]:

$$\bar{c}_{NO}(\underline{r},t) = \max\left\{0,\left[\bar{c}_{INO}(\underline{r},t) - \zeta_{NO}(\underline{r},t)x_{O_3}(\underline{r},t)\right]\right\} \quad , \tag{320}$$

$$\bar{c}_{O_3}(\underline{r},t) = \chi_{O_3}(\underline{r},t) - \bar{c}_{INO}(\underline{r},t) + \bar{c}_{NO}(\underline{r},t) \quad . \qquad (321)$$

Here χ_{O_3} is the ambient ozone concentration, assumed to be given; $\bar{c}_{INO}$ is the mean concentration of NO in the absence of any chemical reactions [$\bar{c}_{INO}$ can be calculated directly from Eq. (317)]; and ζ_{NO} is a mixing parameter, which we approximate by (see Chapter III, Table 1):

$$\zeta_{NO}(\underline{r},t) \doteq \frac{\bar{c}^2_{INO}(\underline{r},t)}{\overline{c^2_{INO}}(\underline{r},t)} \quad . \qquad (322)$$

in Eqs. (320) through (322), $\underline{r} = (x_r, z_r)$ denotes the receptor location.

In summary, Eq. (317) is the roadway model equation for the mean concentrations of all pseudo-inert pollutants. This same equation is also used to compute $\bar{c}_{INO}$, which enters in Eqs. (320) through (322). The model equations for NO and O_3, which we consider to be rapid reactants, are Eqs. (320) and (321). Similar equations can be written for other rapid reactants. The evaluation of Eq. (320) and (321) requires that the mixing parameter ζ be determined, which in turn requires an expression for $\overline{c^2_{INO}}$. These aspects of the model implementation are discussed in detail in the sections that follow.

B. ROADWAY 1

1. Governing Equations

As we stated in the introduction to this chapter, the model we call ROADWAY 1 is based on an evaluation of Eq. (317) using the approximation that the dispersion kernel p has the Gaussian form. Specifically, we assume that

$$p(\underline{r}_r,t|\underline{r}_s,t') = (2\pi\sigma_x\sigma_z)^{-1} \exp\left[-\frac{(z_r - z_s - \bar{z})^2}{2\sigma_z^2} - \frac{(x_r - x_s - \bar{x})^2}{2\sigma_x^2}\right] \quad , \qquad (323)$$

where $\underline{r}_r = (x_r, z_r)$, $\underline{r}_s = (x_s, z_s)$, and $\bar{x}$, $\bar{z}$, σ_x, and σ_z are functions of the travel time t - t', which is discussed in more detail later. Note that Eq. (323) is the Gaussian form of p that pertains to an unbounded fluid. We use this form here rather than that descriptive of conditions near the earth partly because we want to keep the mathematics simple and partly because the analyses we present here are intended only as a demonstration of the way in which Eq. (317) can be implemented, not as a formulation of the final roadway model equations.

It is known [see, for example, Willis and Deardorff (1976)] that in neutral and unstable boundary layers, p is Gaussian, to good approximation, for sufficiently small travel times $\tau = t - t'$. However, under stable conditions or when τ is large, the Gaussian form ceases to hold. Errors in the assumed form of p that propagate through Eq. (317) into the $\bar{c}$ estimates can be attenuated to any desired degree by calculating the value of $\bar{c}$ averaged over some sufficiently large area. Thus, let

$$\left\langle \bar{c}(r_r,t) \right\rangle = \frac{1}{\ell_x \ell_z} \int_{x_r-(\ell_x/2)}^{x_r+(\ell_x/2)} \int_{-\ell_z}^{\ell_z} \bar{c}(x',z',t)\, dz'\, dx' \quad , \quad (324)$$

where ℓ_x and ℓ_z are the dimensions of the averaging, or sample, area (see Figure 29) and $\ell_z > z_r$. [The integration limits $-\ell_z$, $+\ell_z$ in Eq. (324) replace 0, $+\ell_z$ because of our use of the unbounded fluid form of p.] Substituting Eq. (323) into Eq. (317) and the resulting equation into Eq. (324), we obtain after evaluation

$$\left\langle \bar{c}(\underline{r}_r,t) \right\rangle = \frac{1}{4\ell_x \ell_z} \sum_{n=1}^{N} Q \left[\mathrm{erf}\left(\frac{-\bar{x}_n}{\sqrt{2}\,\sigma_{xn}} \right) - \mathrm{erf}\left(\frac{\ell_x - \bar{x}_n}{\sqrt{2}\,\sigma_{xn}} \right) \right]$$

$$\bullet \left[\mathrm{erf}\left(\frac{-\ell_z - \bar{z}_n}{\sqrt{2}\,\sigma_{zn}} \right) - \mathrm{erf}\left(\frac{\ell_z - \bar{z}_n}{\sqrt{2}\,\sigma_{zn}} \right) \right] \quad , \quad (325)$$

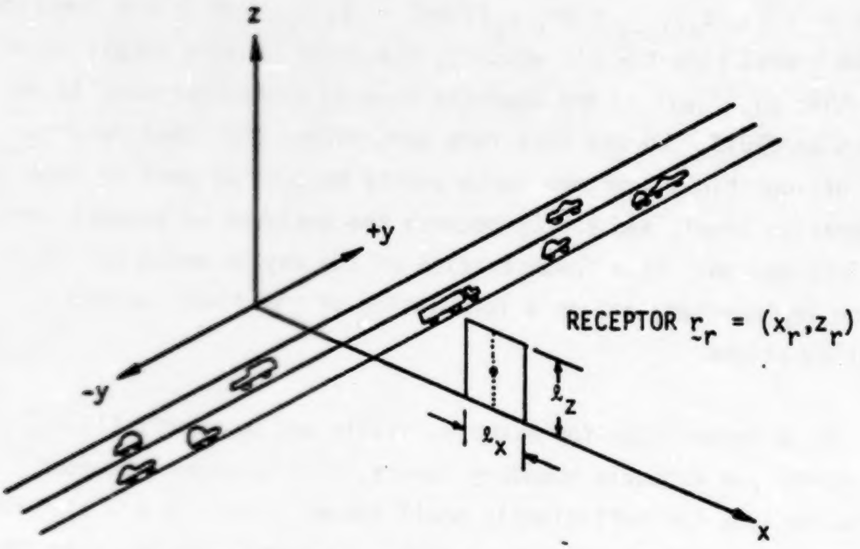

FIGURE 29. AVERAGING AREA (ℓ_x, ℓ_z) USED IN THE DEFINITION OF $\langle \bar{c}(\underset{\sim}{r}_r, t) \rangle$

where $\bar{x}_n$, $\bar{z}_n$, and so forth denote the parameters $\bar{x}$, $\bar{z}$, and so forth evaluated at travel time τ_n, given by

$$\tau_n = \frac{tv_{sn} + y_{0n}}{v_{sn} - v} \quad . \tag{326}$$

Equation (325) is applicable to averaging areas ℓ_x, ℓ_z of any size, provided that the bottom boundary of the area coincides with the ground, as shown in Figure 29, and the origin of the coordinate system is positioned at a lower corner of this area. This and other limitations of Eq. (325) can easily be relaxed, but as we stated earlier, our primary aim here is to demonstrate in as simple a manner as possible the basic approach we propose to use in developing a generalized roadway chemistry and dispersion model around Gaussian concepts. Within this context, Eq. (325) is the working equation of ROADWAY 1 that is used to calculate not only the mean concentrations of pseudo-inert pollutants, but also mean values like $\bar{c}_{INO}$ that enter into the concentration formulas of the reactive pollutant species [see Eqs. (320) and (321)].

The Lagrangian theory from which Eq. (317) was derived also provides an expression for $\overline{c^2}$ that can be used to evaluate ζ, as given by Eq. (322). We have

$$\overline{c^2}(\underset{\sim}{r}_r,t) = Q^2 \sum_{n=1}^{N}\sum_{m=1}^{N} \int_0^t\int_0^t p_2(x_r,z_r,t;x_r,z_r,t|x_s,z_s,t';x_s,z_s,t'') \cdot\delta[t'(v - v_{sn}) - tv - y_{0n}]\cdot\delta[t''(v - v_{sm}) - tv - y_{om}]\, dt'\, dt'' \quad , \tag{327}$$

where p_2 is the joint probability density for the displacements of a pair of particles. Note that p is a marginal density of p_2 in that the former can be obtained by integrating p_2 with respect to the position coordinates of one particle over all space. This relationship and our assumption that p is normal (i.e., a Gaussian density) suggest that we approximate p_2 by a joint normal density. Strictly speaking, p may be Gaussian when p_2 is not. Nevertheless, the use of the joint normal approximation for p simplifies the mathematics considerably; moreover, since we have found this model to be reasonably accurate in describing mean square concentrations in laboratory flows, we use the joint normal form for p_2 here. The study just alluded to is described in detail in Appendix C. Many of the steps in the implementation of Eq. (327) will be guided by that study.

Defining $\left\langle c_I^2 \right\rangle$ in the manner of Eq. (324) and making use of Eq. (327) and the assumed joint normal form of p_2 (see Appendix C), we obtain after some algebra

$$\left\langle \overline{c_I^2}(\underset{\sim}{r}_r,t) \right\rangle = \frac{Q^2}{\ell_x \ell_z}\left(\sum_{n=1}^{N}\bar{\phi}_{nn} + 2\sum_{n=1}^{N}\sum_{m=n+1}^{N}\bar{\phi}_{nm}\right) \tag{328}$$

where

$$\bar{\phi}_{nn} = [16\,\pi\sigma_{xn}\sigma_{zn}(1 - \rho_{nn})]^{-1}\left[\mathrm{erf}\left(\frac{-\bar{x}_n}{\sigma_{xn}(1 + \rho_{nn})^{\frac{1}{2}}}\right) - \mathrm{erf}\left(\frac{\ell_x - \bar{x}_n}{\sigma_{xn}(1 + \rho_{nn})^{\frac{1}{2}}}\right)\right]$$

$$\cdot\left[\mathrm{erf}\left(\frac{-\ell_z - \bar{z}_n}{\sigma_{zn}(1 + \rho_{nn})^{\frac{1}{2}}}\right) - \mathrm{erf}\left(\frac{\ell_z - \bar{z}_n}{\sigma_{zn}(1 + \rho_{nn})^{\frac{1}{2}}}\right)\right] \quad , \qquad (329)$$

$$\bar{\phi}_{nm} = \left(8\pi\sqrt{a_x a_z}\right)^{-1}\left\{\mathrm{erf}\left[\frac{\sqrt{a_x}\left(-\frac{b_x}{a_x}\right)}{\sqrt{2}\,\sigma_{xn}\sigma_{xm}\left(1 - \rho_{nm}^2\right)^{\frac{1}{2}}}\right]\right.$$

$$\left. - \mathrm{erf}\left[\frac{\sqrt{a_x}\left(\ell_x - \frac{b_x}{a_x}\right)}{\sqrt{2}\,\sigma_{xn}\sigma_{xm}\left(1 - \rho_{nm}^2\right)^{\frac{1}{2}}}\right]\right\} \cdot \left\{\mathrm{erf}\left[\frac{\sqrt{a_z}\left(-\ell_z - \frac{b_z}{a_z}\right)}{\sqrt{2}\,\sigma_{zn}\sigma_{zm}\left(1 - \rho_{nm}^2\right)^{\frac{1}{2}}}\right]\right.$$

$$\left. - \mathrm{erf}\left[\frac{\sqrt{a_x}\left(\ell_z - \frac{b_z}{a_z}\right)}{\sqrt{2}\,\sigma_{zn}\sigma_{zm}\left(1 - \rho_{nm}^2\right)^{\frac{1}{2}}}\right]\right\}\exp\left(d_x + d_z\right) \quad , \qquad (330)$$

and

$$a_x = \sigma_{xn}^2 + \sigma_{xm}^2 - 2\rho_{nm}\sigma_{xn}\sigma_{xm} \quad , \qquad (331)$$

$$b_x = \sigma_{xn}^2\bar{x}_m + \sigma_{xm}^2\bar{x}_n - \rho_{nm}\sigma_{xn}\sigma_{xm}(\bar{x}_n + \bar{x}_m) \quad , \qquad (332)$$

$$a_z = \sigma_{zn}^2 + \sigma_{zm}^2 - 2\rho_{nm}\sigma_{zn}\sigma_{zm} \quad , \qquad (333)$$

$$b_z = \sigma_{zn}^2\bar{z}_m + \sigma_{zm}^2\bar{z}_n - \rho_{nm}\sigma_{zn}\sigma_{zm}(\bar{z}_n + \bar{z}_m) \quad , \qquad (334)$$

$$d_x = \frac{b_x^2 - a_x c_x}{2a_x\sigma_{xn}^2\sigma_{xm}^2\left(1 - \rho_{nm}^2\right)} \quad , \qquad (335)$$

$$d_z = \frac{b_z^2 - a_z c_z}{2a_z \sigma_{zn}^2 \sigma_{zm}^2 \left(1 - \rho_{nm}^2\right)} \quad , \tag{336}$$

$$c_x = \bar{x}_n^2 \sigma_{xm}^2 + \bar{x}_m^2 \sigma_{xn}^2 - 2\rho_{nm} \sigma_{xn} \sigma_{xm} \bar{x}_n \bar{x}_m \quad , \tag{337}$$

$$c_z = \bar{z}_n^2 \sigma_{zm}^2 + \bar{z}_m^2 \sigma_{zn}^2 - 2\rho_{nm} \sigma_{zn} \sigma_{zm} \bar{z}_n \bar{z}_m \quad . \tag{338}$$

In the equations above, ρ_{nn} and ρ_{nm} are correlation coefficients of the joint displacements of prescribed particle pairs. Before Eqs. (328) or (325) can be evaluated, the parameters $\bar{x}$, $\bar{z}$, σ_x, σ_z, ρ_{nn}, and ρ_{nm} must be determined. Similarity theory provides expressions for these parameters within certain time and space bounds but only for the case of flow over a flat earth, or equivalently an "at-grade" roadway. Some of these expressions are presented below.

2. Formulation of the Parmeters $\bar{x}$, $\bar{z}$, σ_x, σ_z, ρ_{nn}, and ρ_{nm} for an at-Grade Roadway

a. The Height at τ_n of the Centroid of an Instantaneous Point Source Cloud

The parameter $\bar{z}_n$ is the height at travel time τ_n of the centroid of an instantaneous point source cloud. For all release heights z_s within the constant stress region of the boundary layer, similarity theory yields

$$\bar{z}_n = \begin{cases} \beta u_* \tau_n + z_s + f(\tau_n) \ , \quad L = \infty \ , \quad \tau_n >> \dfrac{z_0}{u_*} \quad , \\[2ex] \alpha \left(\dfrac{u_*^3}{\kappa |L|} \right)^{1/2} \tau_n^{3/2} + z_s + f(\tau_n) \ , \quad L < 0, \quad \tau_n > 0.1 \dfrac{|L|}{u_*} \quad . \end{cases} \tag{339}$$

Here, τ_n is the travel time given by Eq. (326); α and β are constants; u_* is the friction velocity; z_0 is the surface roughness; κ is the von Karman constant (≈ 0.4); $f(\tau_n)$ is a function, to be determined in a future study, describing the buoyant rise of vehicle emissions; and L is the Monin-Obukhov length (defined in Chapter III).

b. The x Component of the Puff Centroid

The parameter $\bar{x}_n$ is the x component of the puff centroid. Under the convention that the coordinate system of the roadway model is selected so that the component of the mean wind normal to the roadway is directed toward increasing x, we have

$$\bar{x}_n = \begin{cases} \dfrac{\hat{u}_*\tau_n}{\kappa}\left(\ell n \dfrac{cu_*\tau_n}{z_0} - 1\right) + x_s \ , & L = \infty \ , \ \tau_n \gg \dfrac{z_0}{u_*} \ , \\[2ex] \dfrac{(u_*|L|)^{1/2}}{\alpha^{1/3}\kappa^{5/6}} c_2 \tau_n^{1/2} + \dfrac{u_*}{\kappa} c_1 \tau_n + x_s \ , & L < 0 \ , \end{cases} \tag{340}$$

where $\hat{u}_*$ is the projection of u_* onto the x-z plane (treating u_* as a vector parellel to the mean wind); c, c_1, and c_2 are constants of order unity; and α and κ have the same values as in Eq. (339).

c. The Root-Mean-Square Verticle Displacement of a Pollutant Particle from Its Mean Displacement

The parameter σ_{zn} is the rms vertical displacement of a pollutant particle from its mean position $z_s + \bar{z}$. In approximating this term, we must take into account not only ambient turbulence effects, which similarity theory describes, but also the influence of vehicle wake turbulence. Let us assume that all vehicles produce axially symmetric wakes. The mean width ℓ of the wake is a function of the distance y from the vehicle and is given by similarity theory as

$$\ell(y) = d_\ell y^{1/3} \theta^{2/3} \tag{341}$$

$$\theta = 1/2 \ \delta C_d \quad ,$$

where δ is a characteristic vehicle width, C_d is the vehicle drag coefficient, and d_ℓ is a constant. The rms kinetic energy of the wake is also given:

$$w(y) = d_w y^{-2/3} u_\infty \theta \quad , \tag{342}$$

where

$$u_\infty = \left| v_{sn} - v \right|$$

v_{sn} is the vehicle speed [see the discussion following Eq. (315)], and d_w is another constant. The elapsed time τ_n after the passage of the nth vehicle through the receptor plane and the distance y_n of the vehicle from this plane are related by

$$\tau_n = \frac{y_n}{\left| v_{sn} - v \right|} \quad , \tag{343}$$

and Eqs. (341) and (342) become

$$\ell(y) = d_\ell \left| v_{sn} - v \right|^{1/3} \tau_n^{1/3} \; \theta^{2/3} \tag{344}$$

$$w(y) = d_w \; (\delta C_d)^{2/3} \; u_\infty{}^{1/3} \tau_n{}^{-2/3} \quad . \tag{345}$$

The turbulence intensity in the wake will have decayed to a level comparable to that (viz., $\sim u_*$) of the ambient turbulence in a time

$$\tau_a = d_w^{3/2} \; u_*^{-3/2} \; \delta C_d \; u_\infty^{-1/2} \tag{346}$$

By this time, the wake width is

$$\ell_a = d_\ell d_w^{1/2} \; (1/2)^{2/3} \; \delta C_d \left(\frac{u_\infty}{u_*} \right)^{1/2} \tag{347}$$

Using this as an effective initial cloud size and superposing the effects of ambient turbulence, we obtain approximately

$$\sigma_{zn}^2 = (\ell_a + \lambda \bar{z}_n)^2 - \bar{z}_n^2 \quad , \quad \text{all } L \quad . \tag{348}$$

The constant λ has a value of about 1.25 according to Deardorff and Willis (1975).

d. The Root-Mean-Square Horizontal Displacement of a Pollutant Particle from Its Mean Displacement

For flat earth conditions, similarity theory predicts

$$\sigma_{xn} = \ell_a + \lambda \bar{z}_n \quad . \tag{349}$$

e. The Correlation Coefficient for a Pair of Particles Separated Initially by a Distance ℓ_0

It is shown in Appendix C that the correlation coefficient ρ that enters in the joint normal form of p_2 can be expressed as

$$\rho = 1 - \frac{\overline{\ell^2} - \ell_0^2}{6\sigma^2} \quad , \tag{350}$$

where $\overline{\ell^2}$ is the mean square separation of two particles released a distance ℓ_0 apart and σ is the mean square displacement of the particle from its mean displacement. In the present problem, ρ_{nn} represents ρ evaluated for a pair of particles separated initially by a distance ℓ_0 comparable to the dimensions of a vehicle's exhaust pipe. Similarity theory gives expressions for $\overline{\ell^2}$, but these are complicated functions of travel time (see Appendix C). Rather than deal with those functions explicitly, we infer a value for ρ_{nn} from the concentration fluctuation data presented in Appendix C. In particular, measurements reveal that in stationary, homogeneous turbulence at high Reynolds number,

$$\Gamma_0^2 = \frac{\overline{c^2}(0)}{\bar{c}^2(0)} \sim 2 \quad , \tag{351}$$

where $\overline{c^2}(0)$ denotes the mean square concentration of an inert substance on the plume centerline and $\bar{c}(0)$ is the corresponding mean concentration. Moreover, Γ_0 is self-preserving sufficiently far downstream from the source. Now from Eqs. (325) and (328), we find that as $\ell_x \to \ell_z \to 0$,

$$\overline{c^2}(0) \sim \left[4\pi^2\sigma_x^2\sigma_z^2\left(1 - \rho_{nn}^2\right)\right]^{-1} \quad , \qquad (352)$$

$$\bar{c}^2(0) \sim \left(4\pi^2\sigma_x^2\sigma_z^2\right)^{-1} \quad . \qquad (353)$$

Combining these expressions with Eq. (351), we obtain

$$\rho_{nn} \simeq 0.7 \quad .$$

This value can be used in Eq. (329).

f. The Correlation Coefficient for a Pair of Particles Separated Initially by the Distance Between Two Vehicles

Like ρ_{nn}, ρ_{nm} can be determined from Eq. (350), but in this case $\overline{\ell^2}$ and ℓ_0 refer to the separation of two particles, one of which is emitted by one vehicle and the other by a different vehicle. Thus, ρ_{nm} ranges from a value of zero for vehicles that are very far apart to a maximum for vehicles with the minimum possible separation. In all cases, $\rho_{nn} > \rho_{nm}$. It will probably be impossible to formulate a theoretical expression for ρ_{nm} that takes into account rigorously the effects on this correlation of the mutual interaction of vehicle wakes and ambient turbulence. An approximation that accounts qualitatively for some of these effects is

$$\rho_{nm} = \rho_{nn} \exp\left[-\frac{(\tau_n - \tau_m)^2}{\dfrac{2\ell_a^2}{u_*^2}} - \frac{\xi_{nm}^2}{2\ell_a^2}\right] \quad , \qquad (354)$$

where

$$\xi_{nm} = y_{0n} - y_{0m} + (t - \tau_n)v_{sn} - (t - \tau_m)v_{sn} \qquad (355)$$

and ℓ_a is given by Eq. (347). Whether Eq. (354) can explain all significant correlation effects remains to be determined.

C. ROADWAY 2

Simulating pollutant transport and diffusion around an elevated or depressed roadway presents problems not encountered in modeling conditions over a flat surface. One of the added difficulties is description of the perturbations induced in the mean flow by the highway itself. Another is the inadequacy of the Gaussian density to approximate the true dispersion kernel p that enters in the basic Eq. (317). To handle both of these problems, we propose in ROADWAY 2 to estimate p (and p_2) from an ensemble of particle trajectories generated through a Monte Carlo simulation of the turbulence and mean flow fields. The approach would be nearly identical to that proposed in the previous chapter to handle point sources.

To illustrate how this process would operate, suppose we were attempting to model concentrations in a depressed roadway like that shown in Figure 30. To determine p, we need an ensemble of the possible trajectories pollutant particles released from a given source point would follow under the combined action of the turbulence and mean flow. Hotchkiss and Harlow (1973) have proposed the following functional forms for the mean two-dimensional flow patterns in a cavity like that shown in Figure 30.

$$V_x = \frac{-u_0}{\sinh(kD)}[\sinh(kz) + k(z - D)\cosh(kz)]\cos(kx) \quad , \qquad (356)$$

$$V_z = -ku_0(D - z)\frac{\sinh(kz)}{\sinh(kD)}\sin(kx) \quad , \qquad (357)$$

$$k = \frac{\pi}{w}; \; -\frac{w}{2} \le x \le \frac{w}{2}; \; 0 \le z \le D \quad .$$

Let v_x and v_z denote the local instantaneous turbulent velocity components. Then the trajectory of a particle starting from (x_0, z_0) at time t = 0 is calculated by

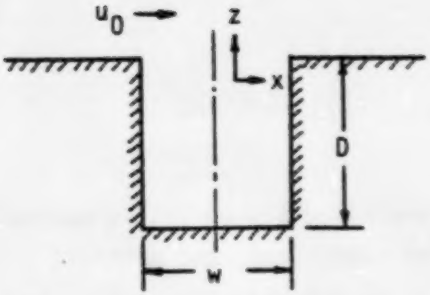

FIGURE 30. EXAMPLE OF A ROADWAY DEPRESSION OF ARBITRARY WIDTH AND DEPTH. The mean flow speed at the surface is u_0.

$$x(t) = x_0 + \int_0^t \left\{ V_x[x(t'),z(t')] + v_x[x(t'),z(t')] \right\} dt' \quad . \qquad (358)$$

The z component z(t) is obtained from a similar equation.

Equation (358) gives the path of a particle for one particular realization of the turbulence velocity $v_x(t)$. To generate the desired ensemble of trajectories, we must evaluate Eq. (358) many times, each time replacing $v_x(t)$ by a different member of the ensemble of possible turbulent velocity fields. This process is accomplished computationally by using a random number generator to produce the v_x (and v_z) values. The generator is designed so that the statistics of the v_x and v_z functions it generates conform to known statistical properties of the flow field. For example, the mean kinetic energy of the turbulence at a particular point $1/2[\overline{v_x^2}(x,z) + \overline{v_z^2}(x,z)]$ is some specified function of local gradients in V_x and V_z and heating. The Lagrangian integral time scales produced by the v_x and v_z fields can also be prescribed. Appendix B discusses these details further and describes the process needed to calculate the ensemble of particle pair trajectories that are required to estimate p_z. We plan to implement the ROADWAY 2 modeling approach in a future study.

VII SUMMARY

In Chapter II, we reexamined the so-called optimal eddy diffusivities derived in Lamb (1976) and Lamb, Chen, and Seinfeld (1975) to determine whether (1) the diffusivities are unique, (2) they have a universal form when properly scaled, and (3) they are dependent on source height. Recall that the "optimal diffusivities" are designed to make the predictions of the diffusion equation agree as closely as possible with the mean concentration distributions derived from a sophisticated numerical model of turbulence in the planetary boundary layer. Using a test case for which the analytic solution of the diffusion equation is available, we showed that the method used to derive the optimal diffusivity produces unique results that agree very closely with the true value. Using concentration data for two different unstable cases, namely, $z_i/L = -4.5$ and $z_i/L = -1100$, we showed that for all stabilities in the range $z_i/L \leq -4.5$, the optimal vertical diffusivity $K_z(z)$ appears to have a universal form when z is normalized by z_i, the depth of the mixed layer, and when K_z is scaled with $w_* z_i$, where w_* is the convective velocity scale. The universal form of K_z for a source near ground level is given at the end of Chapter II. Finally, using concentration data for sources of different heights in the same flow, we found that the optimal diffusivity depends quite strongly on the source elevation (see Figure 10). An expression for K_z applicable to a source of elevation $z_s = 0.25z_i$ is given at the end of Chapter II.

In Chapter III, we developed, implemented, and tested a model for describing the effects of turbulent concentration fluctuations on second-order chemical reactions. The model equation contains a reaction parameter, whose value can be approximated by unity in most problems of air pollution, and two mixing parameters, whose functional forms are determined solely by the nature of the turbulence and the configuration of reactant sources. For given source characteristics, the mixing parameters can be expressed as universal functions of the flow conditions. We derived approximate expressions for the mixing parameters applicable to the case where one reactant is emitted from a point source into an atmosphere containing a uniform concentration of a coreactant. Using this expression, we applied the model to the case of NO emanating from a point source into an ozone-laden atmosphere and found that the rate of conversion of NO to NO_2 is greatly inhibited by turbulent concentration fluctuations, even under stable conditions. The predictions of the model compare well with empirical data from both atmospheric and laboratory studies.

In Chapter IV, we developed a method of parameterizing the effect of chemical reaction rate of both subgrid-scale concentration variations arising from ground-level sources and turbulence-induced concentration fluctuations. In essence, the parameterization scheme is simply a modified lower boundary condition on the concentration field that takes into account the effect of subgrid-scale concentration variations. This scheme has been implemented in the SAI model and is currently undergoing tests.

In Chapter V, we treated the problem of resolving point source plumes in grid models of urban air pollution. A submodel capable of restoring point spatial resolution to any grid model was developed in Lamb (1976), but it is applicable only to inert and first-order reactants. Treating second-order reactants, such as NO and O_3, is a very complicated problem because the finite difference methods normally used to solve the equations governing the species concentrations are incompatible with the goal of achieving point spatial resolution. To circumvent this obstacle, we proposed in Chapter V a Lagrangian model of second-order reactants that is capable in principle of yielding point resolution. Using an elementary problem, we showed that the model is theoretically sound, but we have yet to demonstrate that this approach will produce a computer model that is compatible with the limitations normally imposed on computer time and storage requirements. We hope to test this model within the next several months and ultimately to include it in the SAI model.

Finally, in Chapter VI, we developed theoretical frameworks for two models of pollutant levels around roadways. The more general of the two models can treat photochemical pollutants; the effects of turbulent concentration fluctuations produced by vehicle wake and ambient turbulence; calm winds or winds parallel to the roadway; exhaust buoyancy effects; elevated, depressed, or at-grade highways; pollutant deposition; and other phenomena normally included in air pollution models. Those roadways models will be developed and tested under a future contract to the EPA.

APPENDIX A
MULTIJET REACTOR DATA

W. R. SHU

APPENDIX A
MULTIJET REACTOR DATA

The closure model for slow and very rapid reactions developed by Toor (1962) has received extensive experimental support--from Vassilatos and Toor (1965), Keeler, Peterson, and Prausnitz (1965), Mao (1969), and Torrest and Ranz (1970). According to this model, for very rapid reactions with stoichiometric feed,

$$F_\infty(x) \equiv \frac{\overline{A}(x)}{\overline{A}(x_0)} = \frac{\overline{A_I'B_I'}(x)^{1/2}}{\overline{A_I'B_I'}(x_0)^{1/2}} \quad , \tag{A-1}$$

where $x = U(x)t$ is the axial position along the reactor length and $x_0 = 0$ is the inlet point where the reactor has reached the state of cross-sectional homogeneity. Toor (1969) showed that the relationship among the concentration fluctuations of two nonpremixed inert species in this reactor is

$$-\frac{\overline{A_I'B_I'}(x)}{\overline{A}_I\overline{B}_I} = \frac{\overline{A_I'^2}(x)}{\overline{A}_I^2} = \frac{\overline{B_I'^2}(x)}{\overline{B}_I^2} \quad , \tag{A-2}$$

where A_I and B_I are independent of x because of homogeneity. Hence, by definition we obtain

$$\Gamma_{AB}(x) = 1 - F_\infty^2(x) \quad , \tag{A-3}$$

$$\Gamma_A(x) = \Gamma_B(x) = 1 + F_\infty^2(x) \quad . \tag{A-4}$$

Conversion data for reactions with rate constants greater than about 10^7 ℓ/mole/sec, which were reported by Mao (1969) to be within the diffusion limited regime, were used to determine $F_\infty(x)$, and this function was subsequently used in Eqs. (A-3) and (A-4) to determine the parameters Γ_{AB}, Γ_A, and Γ_B required in our closure model. Figure A-1 shows $F_\infty(x)$ for two different flow conditions. A cubic spline function was used to interpolate data between measurements.

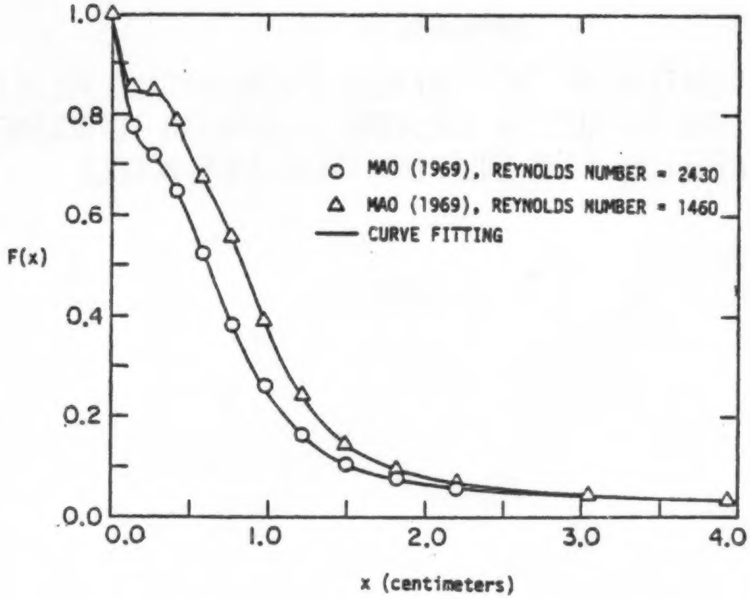

Source: Mao (1969).

FIGURE A-1. EXTENT OF REACTION OF A VERY RAPID STOICHIOMETRIC REACTION FOR TWO DIFFERENT JET REYNOLDS NUMBERS

APPENDIX B

A PARAMETERIZATION OF TWO-PARTICLE SUBGRID-SCALE VELOCITY FLUCTUATIONS FOR USE IN DERIVING LAGRANGIAN TURBULENCE STATISTICS FROM EULERIAN TURBULENCE MODELS

R. G. LAMB

APPENDIX B

A PARAMETERIZATION OF TWO-PARTICLE SUBGRID-SCALE VELOCITY FLUCTUATIONS FOR USE IN DERIVING LAGRANGIAN TURBULENCE STATISTICS FROM EULERIAN TURBULENCE MODELS

Estimating the concentration fields arising from point sources of material in the planetary boundary layer is a problem that is most conveniently formulated in terms of Lagrangian turbulence statistics, as is evident in the popularity of the classic Gaussian plume formula. Although this formula is empirical, the basic premise on which it rests and the parameters that enter into it are Lagrangian in nature. Since the plume formula is limited considerably in its scope and applicability, it is desirable to have Lagrangian expressions that can treat other problem areas of interest. Unfortunately, the Lagrangian turbulence statistics required to implement such expressions have heretofore been unavailable, primarily because of the prohibitive cost and effort required to obtain them in the field.

Within the last few years, numerical turbulence models have been developed that make it possible to derive Lagrangian turbulence properties computationally. In these models, which resolve large portions of the spectrum of turbulence motions explicitly, particles can be released and tracked at will to obtain the ensembles of particle trajectories necessary to derive Lagrangian information.

The most notable of the models of atmospheric turbulence is that developed by Deardorff (1974b). In a simulation of Day 33 of the Wangara experiments, 64,000 grid points were used to describe the velocity, pressure, temperature, moisture, and subgrid-scale energy fields in a region 5 x 5 km in horizontal area and 2 km deep. The simulated values of each field at each grid point have been recorded on tape for a period of about one hour centered at approximately 1300 local Wangara time, when the boundary layer was in a state near free convection ($-z_i/L \sim 1000$) and was capped by an inversion layer at a height $z_i = 1200$ m. When these data are used to calculate Lagrangian turbulence statistics, the effects of subgrid-scale velocity fluctuations must be parameterized, i.e., fluctuations with horizontal scales smaller than about 125 m and vertical scales less than about 50 m. This appendix formulates a parameterization scheme suitable for this purpose and implements and tests it with the simulated Wangara data described above.

The parameterization developed here is intended for use in generating the ensembles of particle trajectories required to determine the one- and two-particle displacement probability density functions $p(\underline{r},t|\underline{r}',t')$, which is the probability density that a particle released at $\underline{r}'$ at time t' will be found at $\underline{r}$ at time t; and $p_2(\underline{r}_1,t_1;\underline{r}_2,t_2|\underline{r}_1',t';\underline{r}_2',t')$, the probability density that a pair of particles released at the same time t' at points $\underline{r}_1'$ and $\underline{r}_2'$ will be found at $(\underline{r}_1,t_1)$ and $(\underline{r}_2,t_2)$, respectively. For simplicity, we also restrict our attention to the case in which the subgrid-scale velocities are isotropic, a condition that is satisfied in Deardorff's model.

The function p yields the mean particle concentration $\overline{c}$ through the general expression

$$\overline{c}(\underline{r},t) = \int\int_0^t p(\underline{r},t|\underline{r}',t')\, S(\underline{r}',t')\, dt'\, d\underline{r}' \quad , \qquad \text{(B-1)}$$

where S is the source strength function and p_2 gives the mean square concentration $\overline{c^2}$ through

$$\overline{c^2}(\underline{r},t) = \int\int\int_0^t\int_0^t p_2(\underline{r},t;\underline{r},t|\underline{r}',t';\underline{r}'',t'')\, S(\underline{r}',t')\, S(\underline{r}'',t'')\, dt'\, dt''\, d\underline{r}'\, d\underline{r}'' \quad .$$

(B-2)

Equation (B-1) has been used by Lamb, Chen, and Seinfeld (1975) in conjunction with numerical turbulence data to study diffusion in the planetary boundary layer. Lamb and Shu (1977) and Shu, Lamb, and Seinfeld (1977) have used Eq. (B-2), implemented with the aid of Deardorff's Wangara data, in a model of nonlinear chemical reaction among the constituents of a point source plume and species in the ambient air.

Each realization of the ensemble of trajectories needed to compute p and p_2 is given by

$$\underset{\sim}{x}(t;\underset{\sim}{x}_0) = \int_0^t \left\{ \hat{\underset{\sim}{u}}[\underset{\sim}{x}(t';\underset{\sim}{x}_0),t'] + \underset{\sim}{u}(t') \right\} dt' \quad , \qquad \text{(B-3)}$$

where $\underset{\sim}{x}_0$ denotes the particle release point (at t = 0), $\hat{\underset{\sim}{u}}(\underset{\sim}{r},t)$ is the resolvable Eulerian velocity at $(\underset{\sim}{r},t)$ given by Deardorff's model, and $\underset{\sim}{u}(t)$ is the subgrid-scale component of the particle velocity at time t. This appendix develops an approximation of $\underset{\sim}{u}$.

1. CONSTRAINTS ON THE SUBGRID-SCALE PARTICLE DISPLACEMENTS

Since p is a marginal density of p_2, i.e., p can be obtained by integrating p_2 with respect to the coordinates of one of the particles over all space, it is sufficient to develop a scheme for the joint subgrid-scale velocities of a pair of particles. To develop an overall framework for the scheme, we assume that from a knowledge of the characteristics of the subgrid-scale velocity field we can specify the statistical properties of the particle displacements these velocities produce. For example, the mean subgrid-scale velocity is always zero; so we assume, for example, that

$$\overline{x_1}(t) = x_{10} \quad , \qquad \text{(B-4a)}$$

$$\overline{x_2}(t) = x_{20} \quad , \qquad \text{(B-4b)}$$

where x_{10} and x_{20} denote the release points of particles 1 and 2, respectively. Under the assumption that the subgrid-scale velocities are isotropic, the x, y, and z displacement components are statistically equal; so expressions similar to Eq. (B-4) apply to the y and z displacement component. Similarly, we assume that

$$\overline{x_1^2}(t) = \sigma_1^2(t) + x_{10}^2 \qquad \text{(B-5a)}$$

$$\overline{x_2^2}(t) = \sigma_2^2(t) + x_{20}^2 \qquad \text{(B-5b)}$$

$$\overline{[x_1(t) - x_2(t)]^2} = \ell^2(t) + (x_{10} - x_{20})^2 \quad , \qquad \text{(B-6)}$$

where σ_1, σ_2, and $\overline{\ell^2}$ are assumed, for the moment, to be given functions. The mean values of Eqs. (B-4) through (B-6) uniquely determine the single-time joint statistics of x_1 and x_2.

Suppose we have found a random function $x_1(t)$ that satisfies Eqs. (B-4a) and (B-5a). What form must $x_2(t)$ have to fulfill Eqs. (B-4b), (B-5b), and (B-6)? Consider the function

$$x_2 - x_{20} = (x_1 - x_{10})a + b\chi \quad , \qquad \text{(B-7)}$$

where χ is a random variable that is statistically independent of x_1, and a and b are deterministic functions. To satisfy Eq. (B-4b), we must have

$$\overline{\chi} = 0 \quad . \qquad \text{(B-8)}$$

Consequently, owing to the independence of χ and x_2,

$$\overline{x_2\chi} = \overline{x}_2\overline{\chi} = 0 \quad . \qquad \text{(B-9)}$$

In view of this, Eq. (B-5b) will be satisfied if

$$b^2\overline{\chi^2} = \sigma_2^2 - a^2\sigma_1^2 \quad , \tag{B-10}$$

and Eq. (B-6) will be fulfilled if

$$a = \frac{\sigma_1^2 + \sigma_2^2 - \overline{\ell^2}}{2\sigma_1^2} \quad . \tag{B-11}$$

From Eq. (B-6), we see that in the limit as the two particles begin to wander independently, $\overline{\ell^2} \to \sigma_1^2, + \sigma_2^2$, or from Eq. (B-11) $a \to 0$. This fact and the deterministic character of b suggest that we make [cf. Eq. (B-10)]

$$\overline{\chi^2} = \sigma_2^2 \quad . \tag{B-12}$$

It follows then from Eqs. (B-10) and (B-11) that

$$b^2 = 1 - \frac{a^2\sigma_1^2}{\sigma_2^2} \quad . \tag{B-13}$$

Thus, given a random function x_1 that satisfies Eqs. (B-4a) and (B-5a), we have determined that Eq. (B-7) is the general form x_2 must have to satisfy the remainder of the constraints in Eqs. (B-4) through (B-6) on the joint displacement statistics of the particle pair.

We are interested in the velocity form of Eq. (B-7), which we can obtain by differentiating Eq. (B-7) with respect to t:

$$u_2 = au_1 + \dot{a}(x_1 - x_{10}) + b\dot{\chi} + \dot{b}\chi \quad . \tag{B-14}$$

Here

$$u_1 = \frac{dx_1}{dt} \quad , \quad u_2 = \frac{dx_2}{dt} \tag{B-15}$$

and the over-dot ($\dot{}$) denotes a time derivative. With a and b given by Eqs. (B-11) and (B-13), respectively, and with χ satisfying Eqs. (B-8), (B-9), and (B-12), Eq. (B-14) becomes one of the basic parts of our parameterization scheme.

2. SPECIFICATION OF x_1 AND χ

Our choice of a form for x_1 is guided by our knowledge of σ_1, which until now, we have regarded as a given function. In actuality, we have very little information about the form of σ_1. We know only that for small times

$$\sigma_1^2 = \overline{v'^2} t^2 \quad , \tag{B-16}$$

where $\overline{v'^2}$ is the mean square subgrid-scale velocity fluctuation and t is travel time. The behavior of σ_1 at large times is not known. Lamb (1971) showed that if the turbulence is stationary and the Lagrangian velocity spectrum is a band-pass spectrum, similar to that which the Eulerian spectrum of the subgrid-scale velocity is known to be, then in the limit of large travel times the mean square particle displacement σ^2 approaches a constant value. This is in marked contrast to the effect that a white noise velocity spectrum would produce, namely, $\sigma^2 \propto t$ in the limit of large travel times. Whether the subgrid-scale velocities in a given turbulence model produce a constant, a linearly increasing, or an altogether different dispersion σ^2 in the limit of large travel times is not known, but we expect that the details of the σ variations in this regime are not crucial. Our reason for this expectation is that even if particles are released near a boundary where the subgrid-scale velocities constitute a significant fraction of the total turbulence field, by the time the dispersion enters the long term regime, the particles will have moved into a region of the fluid where the resolvable-scale, rather than the subgrid-scale, motions dominate the particle displacements. Proceeding under this assumption, we adopt an expression for the velocity u_1 that is consistent with Eqs. (B-16), (B-4a), and other available information, and we let the long term behavior of x_1 fall where it will.

A suitable expression for u_1 is the Markov-1 form

$$u_1(t_n) = \alpha[u_1(t_{n-1}) + \rho_1(t_n)] \quad , \tag{B-17}$$

where $t_n = n\Delta t$, Δt is the time step used in the turbulence model, α is a constant, and $\rho_1(t_n)$ is a random variable with the following properties:

$$\overline{\rho_1}(t) = 0 \quad , \tag{B-18a}$$

$$\overline{\rho_1(t_n)u_1(t_m)} = 0 \quad , \quad n \neq m \quad . \tag{B-18b}$$

The first of these properties is necessary to satisfy Eq. (B-4a).

Through straightforward analyses, we find that with u_1 given by Eq. (B-17), its autocorrelation is

$$\overline{u_1(t_n)u_1(t_{n-m})} = \alpha^m \, \overline{u_1^2}(t_{n-m}) \quad , \tag{B-19}$$

and its mean square varies temporally as

$$\overline{u_1^2}(t_n) = \alpha^2\left[\overline{u_1^2}(t_{n-1}) + \overline{\rho_1^2}(t_n)\right] \quad . \tag{B-20}$$

In stationary, homogeneous turbulence,

$$\overline{u_1^2}(t) = \overline{v'^2} = \text{Constant} \quad , \tag{B-21}$$

where $\overline{v'^2}$ is the mean square subgrid-scale velocity fluctuation. To ensure that Eq. (B-21) is satisfied when Eq. (B-17) is used to describe particle velocities in stationary, homogeneous turbulence, we must set [see Eq. (B-20)]

$$\alpha = \frac{1}{\sqrt{2}} \quad , \qquad \text{(B-22)}$$

$$\overline{\rho_1^2}(t) = \overline{v'^2} \quad , \qquad \text{(B-23)}$$

and the initial values of u_1 must be selected such that

$$\overline{u_1^2}(0) = \overline{v'^2} \quad . \qquad \text{(B-24)}$$

With α given by Eq. (B-22), the Lagrangian integral time scale of u_1 is found from Eq. (B-19) to be

$$T_L = \frac{1}{\overline{u_1^2}} \int_0^\infty \overline{u_1(t)u_1(t - \tau)}\, d\tau \simeq 8\Delta t \quad . \qquad \text{(B-25)}$$

This value is not inconsistent with the likely time scale of the subgrid-scale velocities.

When the parameterization scheme is implemented, a computer-generated random variable can be used for ρ_1. A Gaussian random number generator would be an obvious choice for this purpose, considering that small-scale turbulence fluctuations tend to be normally distributed. However, generating numbers with a Gaussian density requires more computer time than producing numbers that have a uniform distribution. Furthermore, we believe that errors introduced by an improper choice of the porbability density of ρ_1 are of the same order of magnitude as those incurred through assumptions made earlier. Therefore, we chose to use a uniform density for ρ_1.

If a random variable ξ has a uniform distribution in the range $-A \leq \xi \leq A$, then its mean and mean square values are $\overline{\xi} = 0$ and $\overline{\xi^2} = (1/3)A^2$, respectively. Combining these results with the assumed isotropy of the subgrid-scale velocities, i.e.,

$$\overline{v'^2} = \frac{2}{3} E \quad , \tag{B-26}$$

where E is the kinetic energy of the subgrid-scale field, we conclude that ρ_1 will satisfy both Eqs. (B-18) and (B-23) if it is uniformly distributed in the range

$$-\sqrt{2}\, E_1^{1/2}(t) \leq \rho_1(t) \leq \sqrt{2}\, E_1^{1/2}(t) \quad , \tag{B-27}$$

where $E_1(t)$ denotes the subgrid-scale kinetic energy at time t at the location of Particle 1. (We should add that E is given by Deardorff's model at each grid point and time step.) In conclusion, the subgrid-scale velocity at time t_n of one particle of the pair is given by

$$u_1(t_n) = \frac{1}{\sqrt{2}} [u_1(t_{n-1}) + \rho_1(t_n)] \quad , \tag{B-28}$$

where ρ_1 is a computer-generated random number uniformly distributed in the range given by Eq. (B-27). In accordance with Eq. (B-27), u_1 must be initialized by

$$u_1(0) = \rho_1(0) \quad .$$

On noting the similarities in the statistical properties that x_1 and x must possess, we conclude that an expression similar to Eq. (B-28) should be suitable for $\dot{x}$. In particular, if

$$\dot{\chi}(t_n) = \frac{1}{\sqrt{2}} [\dot{\chi}(t_{n-1}) + \rho_2(t_n)] \quad , \qquad \text{(B-29)}$$

where ρ_2 is a random number uniformly distributed in the range

$$-\sqrt{2}\, E_2^{1/2} \leq \rho_2 \leq \sqrt{2}\, E_2^{1/2} \quad , \qquad \text{(B-30)}$$

then all of the conditions imposed upon χ, namely, Eqs. (B-8), (B-9), and (B-12), are satisfied. In Eq. (B-30), E_2 represents the subgrid-scale energy at time t_n at the location of Particle 2. The expressions for x_1 and χ follow immediately from those of u_1 and $\dot{\chi}$:

$$x_1(t) = x_1(0) + \sum_{m=1}^{n} u_1(t_m)\Delta t \quad , \qquad \text{(B-31)}$$

$$\chi(t_n) = \chi(0) + \sum_{m=1}^{n} \dot{\chi}(t_m)\Delta t \quad . \qquad \text{(B-32)}$$

These equations, together with Eqs. (B-14), (B-28), and (B-29), constitute the basis of our parameterization scheme. All that remains to render these equations operational is to express the functions a and b in terms of available quantities (like E).

3. SPECIFICATION OF a AND b

When two particles are separated by a distance that is larger than the largest turbulent eddies, the random motions of those particles are uncorrelated. In this case, it is easy to show that $\overline{\ell^2} = \sigma_1^2 + \sigma_2^2$. At the other extreme, where the particles are released at virtually the same time and location, they never separate (under the action of turbulence alone); thus, $\overline{\ell^2}$ remains zero for all time. These two limiting cases indicate that a, as given by Eq. (B-11), ranges in value from unity for particles whose motions are totally correlated to zero for those whose velocities are statistically independent. These observations indicate that in the limit of large travel times, as the mean particle separation becomes large compared with the grid size, the function a approaches zero. To determine the initial value of a and the manner in which a approaches its final value, we need explicit expressions for σ_1, σ_2, and $\overline{\ell^2}$.

Regarding the first two, it is reasonable to assume that if the initial separation of two particles is smaller than the grid size, the dispersions σ_1 and σ_2 should be approximately the same for all t. Under this assumption, we have

$$a = 1 - \frac{\overline{\ell^2}}{2\sigma^2} \quad , \quad |\ell_0| << \Delta \quad ; \tag{B-33}$$

$$b^2 = 1 - a^2 \quad , \quad |\ell_0| << \Delta \quad ; \tag{B-34}$$

where $\ell_0 = x_{01} - x_{02}$ is the initial particle separation and Δ denotes the grid size, for example,

$$\Delta = (\Delta x \Delta y \Delta z)^{1/3} \quad , \tag{B-35}$$

where Δx, Δy, and Δz are the grid cell dimensions.

Like σ, $\overline{\ell^2}$ is a parameter about which we have little information. Using Kolmogorov's similarity hypothesis, Batchelor (1949) showed that if the initial separation ℓ_0 of two particles lies in the inertial subrange, then for small times,

$$\overline{\ell^2} = \frac{10}{3} c_1 \, \ell_0^{2/3} \varepsilon^{2/3} t^2 \quad , \quad t << \ell_0^{2/3} \varepsilon^{-1/3} \quad , \tag{B-36}$$

where c_1 is a constant on the order of one, ε is the energy dissipation rate of the turbulence, and t is travel time. In Deardorff's model, Δ itself lies in the inertial subrange, and so Eq. (B-36) should apply for all ℓ_0 less than Δ but large enough that viscous effects are unimportant.

Deardorff and Drake (1974) suggest the semi-empirical formula

$$\varepsilon = E^{3/2}\left(\frac{0.7G}{\Delta}\right) \quad , \qquad \text{(B-37)}$$

where

$$G = 1 + \frac{2}{\left(\frac{z}{\Delta z} + \frac{3}{2}\right)^2 - 3.3} \quad , \quad z \geq \frac{1}{2}\Delta z \quad , \qquad \text{(B-38)}$$

and where z is elevation above ground and E is the subgrid-scale kinetic energy. Combining Eqs. (B-16), (B-26), (B-33), (B-36), (B-37), and assuming for convenience that $c_1 = 2/5$, we obtain

$$a_0 = a(t_0) = 1 - (0.7G)^{2/3}\left(\frac{\ell_0}{\Delta}\right)^{2/3} \quad . \qquad \text{(B-39)}$$

It is interesting that the initial value of a, as given by Eq. (B-39), is independent of E. The indicated dependence of a_0 on ℓ_0 is consistent with the fact that $a_0 \to 1$ as $\ell_0 \to 0$, but Eq. (B-39) cannot be valid for $\ell_0 >> \Delta$ because it results in large negative values for a. Although it is possible that a could achieve a value of -1, in our applications of the parameterization scheme we hold a to the interval $0 \leq a \leq 1$.

In addition to deriving Eq. (B-36), Batchelor (1949) also obtained an expression for the temporal variation of $\overline{\ell^2}$ during the intermediate time period $t >> \ell_0^{2/3}\varepsilon^{-1/3}$, but with t small enough that the particle separation is small compared with the scale of the energy-containing eddies of the turbulence. Although we could utilize this information to help describe the behavior of a(t) between its initial and final values, the results would be of very limited use: since it applies only in the range $\ell_0 << \left(\overline{\ell^2}\right)^{1/2} << \Delta$, this additional information would be of value only when ℓ_0 is several orders of magnitude smaller than Δ. Rather than piece together an expression for a(t), we adopt a single ad hoc formulation that is consistent with available information.

Specifically, we note from Eq. (B-39) that the slope of a(t) is zero at t = 0. Also, we expect that $\Delta^{2/3}\varepsilon^{-1/3}$ must be the characteristic time scale of a(t). This information and the known initial and final values of a(t) can all be taken into account by the simple formula

$$a(t) = a_0 \exp(-A) \quad , \qquad \text{(B-40a)}$$

$$A = \int_0^t \frac{t'\,dt'}{T^2(t')} \quad , \qquad \text{(B-40b)}$$

$$T(t') = \frac{\beta\Delta}{E^{1/2}(t')} \quad , \qquad \text{(B-40c)}$$

where E(t') is the subgrid-scale energy at the centroid of the particle pair at time t' and β is a constant.

4. RECAPITULATION

For convenience, we summarize the complete two-particle velocity parameterization scheme below:

$$u_2(t_n) = a(t_n)u_1(t_n) + \dot{a}(t_n)\left[x_1(t_n) - x_{10}\right] + b(t_n)\dot{x}(t_n) + \dot{b}(t_n)x(t_n)$$

(B-41)

$$u_1(t_n) = \frac{1}{\sqrt{2}}\,[u_1(t_{n-1}) + \rho_1(t_n)] \quad , \qquad \text{(B-42a)}$$

$$u_1(0) = \rho_1(0) \quad , \qquad \text{(B-42b)}$$

$$\dot{x}(t_n) = \frac{1}{\sqrt{2}}\,[\dot{x}(t_{n-1}) + \rho_2(t_n)] \quad , \qquad \text{(B-43a)}$$

$$\dot{x}(0) = \rho_2(0) \quad , \qquad \text{(B-43b)}$$

where ρ_1 and ρ_2 are random numbers uniformly distributed in the ranges

$$-\sqrt{2}\,E_1^{1/2}(t_n) \leq \rho_1(t_n) \leq \sqrt{2}\,E_1^{1/2}(t_n) \quad , \qquad \text{(B-44)}$$

$$-\sqrt{2}\,E_2^{1/2}(t_n) \leq \rho_2(t_n) \leq \sqrt{2}\,E_2^{1/2}(t_n) \quad ; \qquad \text{(B-45)}$$

$E_1(t)$ and $E_2(t)$ are the subgrid-scale kinetic energy at the locations of Particles 1 and 2, respectively, at time t; and the functions $a(t)$ and $\dot{a}(t)$ are obtained from Eq. (B-40) and $b(t)$ and $\dot{b}(t)$ are calculated from Eq. (B-34).

APPENDIX C

LAGRANGIAN ANALYSIS OF A PASSIVE SCALAR IN TURBULENT FLUID--PART 2

R. G. LAMB

APPENDIX C

LAGRANGIAN ANALYSIS OF A PASSIVE SCALAR IN TURBULENT FLUID--PART 2

Abstract

A model is proposed for the joint probability density (p_2) of the displacements of two marked particles in stationary, homogeneous turbulence. The model is based on the assumption of jointly normal displacement statistics and it utilizes, among other theoretical expressions, the formulas derived by Batchelor (1950) for the mean square separation of two particles in stationary, homogeneous turbulence. The model equation for p_2 is then used in formulas derived in Part 1 of this paper to construct models of the mean $\langle c(\underline{r},t)\rangle$, the mean square $\langle c^2(\underline{r},t)\rangle$, and the spectrum $D(\underline{k},t)$ of a passive scalar quantity c in turbulent fluid. In an application of the spectrum model, it is shown analytically that for wave numbers k in the viscous-convective subrange, the model predicts $D(k) \propto k^{-1}$ as was first proposed by Batchelor (1958). In applications of the model equations for $\langle c\rangle$ and $\langle c^2\rangle$, the mean and mean square scalar fluctuations (msf) are computed in three situations for which empirical data are available for comparison.

1. INTRODUCTION

Part 1 of this paper was devoted to the derivation of the mathematical relationships between the statistics of marked particle concentrations in turbulent fluid and the joint statistics (call them p for the moment) of the displacements of the particles in the flow. The resulting formulas were said to be of the Lagrangian type because they express the scalar statistics in terms of the Lagrangian quantity p. The distinction was made between formulas of this type and those of another group known as the Eulerian formulas. The latter are so-called because being derived from the scalar conservation equation, they express the scalar statistics in terms of the Eulerian fluid velocities.

As we stated in Part 1, the basic aim of this two part paper is to explore the Lagrangian method in more detail. Our approach consists of two complementary aspects. The first relates the statistics of the scalar field to the statistics of the displacements of the "scalar particles" in the turbulent fluid. This was the topic of Part I of this paper. The second aspect seeks quantitative descriptions of the particle displacement statistics in specific flow situations. This aspect will be treated here and the results will be used in the formulas derived in Part I to predict several of the statistical properties of passive scalar quantities in situations where empirical data or other theoretical expressions are available for comparison.

There are a number of ways in which descriptions of Lagrangian statistics, specifically the particle displacement probability density function (pdpd), can be obtained. The most straightforward of these is direct measurements.

This is not the most practical method, however, because tracking individual particles in a turbulent fluid is a very difficult task. An alternative to this approach which overcomes the tracking difficulties is to compute the pdpd from numerically simulated turbulence fields. This technique has been demonstrated by Lamb, Chen, and Seinfeld (1974) who used the planetary boundary layer model of Deardorff (1972). Another method of obtaining Lagrangian statistics is to relate the desired quantities analytically to the more easily measureable Eulerian statistics. This approach has not been very successful because the mathematical problems involved in relating the Eulerian and Lagrangian statistics (the so-called Euler-Lagrange problem) have not been solved. Interesting attempts along these lines have been made by Roberts (1961), Kraichnan (1961), and Saffman (1969), each of whom derived approximate expressions for the Green's function of the scalar conservation equation. This function is equivalent to the single particle pdpd and is expressed in terms of Eulerian velocity statistics. Unfortunately, due to the nature of the closure schemes that were used in these studies, the resulting pdpd's either exhibit unphysical behavior in certain situations, some of which are of interest to us here, or they are too complicated to be of practical value. Still another, apparently unexplored, source of information on Lagrangian statistics is the scalar conservation equation expressed in Lagrangian form.

Since for one reason or another each of the techniques outlined above is limited in its applicability, we propose in this paper to obtain pdpd's simply by postulating expressions that are consistent with theory and available data and subsequently to refine the postulated expressions as is deemed necessary by comparisons of the resulting scalar statistics with empirical data. This same technique is utilized in developing closure approximations except in that case one postulates relationships among certain of the joint stochastic moments of the scalar and the Eulerian velocity fields. We emphasize, however, that the two approaches differ in one fundamental aspect: closure hypotheses place a constraint on both the scalar and velocity fields whereas the postulated Lagrangian statistics constrain the velocity field alone. It is not surprising, therefore, that many closure schemes lead to unphysical results when applied to certain scalar fields.

In the next section we develop a model of the joint probability density of the displacements of two particles in a turbulent fluid. This model serves as the basis for subsequent analytical and numerical analyses of the mean, mean square, and spectrum of scalar quantities in turbulent flow. For future reference we rewrite here the formulas derived in Part 1 for these three quantities.

The mean concentration $\langle c(\underline{r},t)\rangle$ of marked particles at the point $\underline{r}$ at time t is given by

$$\langle c(\underline{r},t)\rangle = \int p(\underline{r},t|\underline{r}',t_o)Q(\underline{r}')d\underline{r}', \tag{C-1}$$

where the particles are released instantaneously at time t_o in the form of a cloud of concentration distribution $Q(\underline{r})$, and $p(\underline{r},t|\underline{r}',t_o)$ is the conditional probability density that a particle released at $(\underline{r}',t_o)$ is found at $\underline{r}$ at time t. The mean square concentration of the particles is given by

$$\langle c^2(\underline{r},t)\rangle = \int\int p(\underline{r},\underline{r},t|\underline{r}',\underline{r}'',t_o)Q(\underline{r}')Q(\underline{r}'')d\underline{r}'d\underline{r}'', \tag{C-2}$$

where $p(\underline{r}_1,\underline{r}_2,t|\underline{r}',\underline{r}'',t_o)$ is the joint conditional probability density that a pair of particles released from $(\underline{r}',t_o)$ and $(\underline{r}'',t_o)$ will be found at $(\underline{r}_1,t)$ and $(\underline{r}_2,t)$, respectively. Finally, the generalized spectrum $D_{12}(\underline{k}_1,\underline{k}_2,t)$ of the concentration fluctuations at wave numbers $\underline{k}_1$ and $\underline{k}_2$ is given by

$$D_{12}(\underline{k}_1,\underline{k}_2,t) = \left(\frac{1}{8\pi^3}\right)^2 \int\int \Phi(\underline{k}_1,-\underline{k}_2;\underline{r}'\underline{r}'',t_o)Q(\underline{r}')Q(\underline{r}'')d\underline{r}'d\underline{r}'', \tag{C-3}$$

where Φ is the characteristic function of the joint probability density $p(\underline{r}_1,\underline{r}_2,t|\underline{r}',\underline{r}'',t_o)$ which enters in (C-2).

2. MODEL OF THE SINGLE TIME TWO PARTICLE PROBABILITY DENSITY $p(\underline{r}_1,\underline{r}_2,t|\underline{r}_1',\underline{r}_2',t_o)$.

a. General form of the Density Function

The relationship between this probability density and that entering in equation (C-1) is

$$p(\underline{r},t|\underline{r}',t_o) = \int p(\underline{r},\underline{r}_2,t|\underline{r}',\underline{r}_2',t_o)d\underline{r}_2; \qquad \text{(C-4)}$$

and its relationship to the characteristic function entering in (C-3) is by definition

$$\Phi(\underline{k}_1,\underline{k}_2,t) = \int\int p(\underline{r}_1,\underline{r}_2,t|\underline{r}_1',\underline{r}_2',t_o)e^{i(\underline{r}_1\cdot\underline{k}_1+\underline{r}_2\cdot\underline{k}_2)}d\underline{r}_1 d\underline{r}_2 \quad . \qquad \text{(C-5)}$$

For brevity let us call the single particle density on the left side of (C-4) p_1 and the two particle density in the integrands of both (C-4) and (C-5), p_2. Thus, all three of the formulas (C-1)-(C-3) can be evaluated once the functional form of p_2 has been established.

Since neither theoretical nor empirical descriptions of p_2 are available, we shall postulate a form for this function which is consistent with the few facts which are known. One established fact is that in homogeneous, stationary turbulence p_1 has a Gaussian form. This was first pointed out by Batchelor (1949). The only other significant information pertinent to p_2 are some theoretical expressions (to be described shortly) which permit the second moments of p_2 to be determined under special conditions of homogeneous turbulence. No information about the higher moments of p_2 is available. Thus, a logical postulate is that in homogeneous turbulence, p_2 is jointly normal because this assumption gives rise, through (C-4), to the required Gaussian form for p_1; and moreover, since the jointly normal density is completely determined by its first and second moments, the available information cited above is sufficient to determine completely the functional form of p_2.

The joint normal form of the probability density of n variables x_i with zero mean values is

$$p(x_1,x_2,\ldots x_n) = [(2\pi)^n|\underline{\mu}|]^{-1} \exp(-\tfrac{1}{2}\,\underline{x}\underline{\mu}^{-1}\underline{x}^t) \tag{C-6}$$

where $\underline{x}$ represents the row vector $(x_1,x_2,\ldots x_n)$ and $\underline{x}^t$ is its transpose; $\underline{\mu}$ is the covariance matrix with elements $\mu_{ij} = \langle x_i x_j\rangle$; and $\underline{\mu}^{-1}$ and $|\underline{\mu}|$ denote the inverse and determinant, respectively, of $\underline{\mu}$. The corresponding density function of n variables with nonzero mean values is obtained from (C-6) by simply replacing each x_i, including those in the covariance matrix, by $x_i - \langle x_i\rangle$.

Starting with (C-6) and assuming isotropic turbulence, we obtain after considerable algebra the following general form for p_2:

$$p_2 = p(\underline{r}_1,\underline{r}_2,t|\underline{r}_1',\underline{r}_2',t_o) = [2\pi\sigma^2(1-\rho^2)^{1/2}]^{-3} \exp\left(-\frac{\Delta\underline{r}_1\cdot\Delta\underline{r}_1-2\rho\Delta\underline{r}_1\cdot\Delta\underline{r}_2+\Delta\underline{r}_2\cdot\Delta\underline{r}_2}{2\sigma^2(1-\rho^2)}\right) \tag{C-7}$$

where $\underline{r}_i = (x_i, y_i, z_i)$;

$$\Delta\underline{r}_i = \underline{r}_i - \langle\underline{r}_i\rangle \; ; \tag{C-8}$$

$$\begin{aligned}\sigma^2 &= \langle(x_1-\langle x_1\rangle)^2\rangle = \langle(y_1-\langle y_1\rangle)^2\rangle = \ldots \\ &= \langle(z_2-\langle z_2\rangle)^2\rangle \; ;\end{aligned} \tag{C-9}$$

and

$$\begin{aligned}\rho &= [<(x_1-<x_1>)(x_2-<x_2>)>]/\sigma^2 \\ &= [<(y_1-<y_1>)(y_2-<y_2>)>]/\sigma^2 \qquad \text{(C-10)} \\ &= [<(z_1-<z_1>)(z_2-<z_2>)>]/\sigma^2\end{aligned}$$

Each of the variables $<\underline{r}_i>$, σ, and ρ is generally a function of both t and t_o. However, under the assumption of stationary turbulence, which we have already adopted, each of these variables depends only on the travel time $t - t_o$. The next step, therefore, is to determine the explicit functional form of the travel time dependence of each variable. Before proceeding to this task, we first introduce the system of nondimensional variables which will be used frequently.

b. Nondimensional Coordinates and Parameters

In the analyses which are to come later it is found convenient to work with nondimensional space and time coordinates. The length and time scales which were found to produce the most desirable nondimensional system are the Kolmogoroff microscale

$$\eta \equiv (\nu^3/\varepsilon)^{1/4} , \qquad \text{(C-11)}$$

where ν is the kinematic viscosity of the turbulent fluid and ε is the turbulent energy dissipation per mass of fluid; and the time scale

$$\tau \equiv (\nu/\varepsilon)^{1/2} . \qquad \text{(C-12)}$$

The scales η and τ represent the smallest length and time scales associated with the turbulence.

When the theoretical formulas which we develop are applied later to specific problems, it will be necessary to transform the nondimensional coordinate system into the laboratory frame. To accomplish this we shall make use of the following approximate relationships:

$$\varepsilon = \frac{u'^3}{\ell_e} , \tag{C-13}$$

$$\ell_e = u'T , \tag{C-14a}$$

where u' is the root-mean-square turbulent kinetic energy per mass of fluid, and T is the Lagrangian integral time scale defined by

$$T \equiv \frac{1}{<v_p^2>} \int_0^\infty < v_p(t)v_p(t + t') > dt' \tag{C-14b}$$

and v_p is the "fluid particle" velocity. The parameter ℓ_e is a length scale characteristic of the energy containing eddies of the turbulence. Both (C-4) and (C-14a) are discussed and used extensively in the book by Tennekes and Lumley.

A concise relationship is found to exist among the nondimensionalized parameters T, u', and ℓ_e. We have

$$T^* = T/\tau = R_\ell^{1/2} , \tag{C-15a}$$

$$u'^* = u'\tau/\eta = R_\ell^{1/4} , \tag{C-15b}$$

$$\ell_e^* = \ell_e/\eta = R_\ell^{3/4} \tag{C-15c}$$

where R_ℓ is the turbulence Reynolds number

$$R_\ell \equiv \frac{u'\ell_e}{\nu} \tag{C-16}$$

Each of the above relationships will be used in the ensuing work.

c. The mean particle position, $\langle \underline{r}_i \rangle$.

We shall assume from here on that the turbulent fluid has a constant mean velocity $\underline{U}$ with respect to a fixed coordinate system. We shall also assume, without loss of generality, that the initial instant $t_o = 0$. Under these conditions it follows that the mean position at time t of the ith particle is

$$\langle \underline{r}_i \rangle = \underline{r}_i' + \underline{U}t \quad , \tag{C-17}$$

where $\underline{r}_i'$ denotes the release point of the ith particle.

d. The Root Mean Square Particle Dispersion, σ.

In order to maintain generality, it will be assumed that both molecular and turbulent scale processes affect the particle velocities. However, no allowance will be made for gravitational forces, thereby precluding the application of this analysis to large aerosol particles.

The derivation of the dispersion σ proceeds in the manner first outlined by Taylor (1921). Let $v_s(t)$ denote the instantaneous scalar particle velocity at time t. (Only one of the velocity components need be considered because all three are statistically equal under the isotropy assumption.) Then according to Taylor

$$\sigma^2(t) = 2 \int_o^t \int_o^{t'} \langle v_s(t')v_s(t'')\rangle dt''dt' \ . \tag{C-18}$$

We shall assume that the particle velocity $v_s(t)$ is composed of two distinct parts: a component v(t) representing the effects of the turbulence and a component $v_M(t)$ arising from the molecular agitation. Due to the fact that the characteristic frequencies of turbulent motion are less than about $10^4 \sec^{-1}$ while those of molecular scale agitations are of the order of 10^9 $\sec^{-1}$, a time average of the particle velocity v_s, say $\bar{v}_s$, over a period of about 10^{-6}sec should be independent of molecular scale effects, i.e.

$$\bar{v}_s(t) = \bar{v}(t) + \bar{v}_m(t) = v(t) \qquad \text{(C-19)}$$

Moreover, in view of the great disparity in the characteristic frequencies of the turbulent and molecular velocities, we have

$$< v(t)v_m(t') > = 0 \quad , \text{ all } t \text{ and } t'. \qquad \text{(C-20)}$$

With the aid of these relationships, (C-18) can be reduced to

$$\sigma^2(t) = 2\int_0^t\int_0^{t'} < v(t')v(t'')> dt'dt'' + 2\int_0^t\int_0^{t'} <v_m(t')v_m(t'')> dt''dt' \qquad \text{(C-21)}$$

In the derivation of the classical diffusion equation (see, for example, Chandrasekhar (1943)) the particle velocities are decomposed into drifting and molecular agitation components like those that we have defined above. From that analysis one finds that in the limit as the drift velocity (v in our case) vanishes, $\sigma^2 = 2\kappa t$ where κ is the molecular diffusivity of the scalar. Thus, the last term on the right side of (C-21) is equivalent to $2\kappa t$. The first term on the right side of (C-21) may also be evaluated when t is either very small or very large. Again following Taylor we obtain

$$\sigma^2(t) \begin{cases} = v'^2t^2 + 2\kappa t, & t << T_s; \\ = 2v'^2T_st + 2\kappa t, & t >> T_s; \end{cases} \qquad \text{(C-22)}$$

whever v' is the root-mean-square particle velocity and T_s is the Lagrangian scalar integral time scale defined for the scalar velocity v_s in exactly the same way that the integral time scale T was defined earlier for the fluid particle velocity v_p (see (C-14b)). According to Lumley (1962), the root-mean-square scalar and fluid particle velocities v' and u' are equal. However, according to Saffman (1960), the time scale T_s of the scalar particle is smaller than that, i.e. T, of a fluid particle, and as a result a scalar particle will disperse at a slower rate than a fluid particle released from the same point. According to Saffman's analysis, the differences between T and T_s are small if the Péclet number of the system is large. This condition is satisfied in the problems that we shall consider later, so we shall assume that $T_s = T$. Using this assumption and extrapolating the limiting expressions given by (C-22) into the domain of intermediate times, we arrive finally at the nondimensional dispersion formula

$$\sigma^{*2}(t^*) \begin{cases} = u'^{*2}t^{*2} + 2N_s^{-1}t^*, & t^* < T^*; \\ = 2u'^{*2}T^*t^* + 2N_s^{-1}t^* - u'^{*2}T^{*2}, & t \geq T^*; \end{cases} \qquad \text{(C-23)}$$

where N_s is the Schmidt number defined by

$$N_s \equiv \nu/\kappa \ . \qquad \text{(C-24)}$$

Equation (C-23) is the expression for σ which will be used in all of the analyses which follow.

e. The Two Particle Correlation Function, ρ.

Let $\underline{r}_1$ and $\underline{r}_2$ denote the positions at time t of two given marked particles, and let ℓ represent the distance between these particles at time t, i.e.

$$\ell^2 = (x_1-x_2)^2 + (y_1-y_2)^2 + (z_1-z_2)^2 \quad . \tag{C-25}$$

Taking the mean value of (C-25) we obtain

$$<\ell^2> = <x_1^2> -2 <x_1x_2> + <x_2^2> \quad + \; . \; . \; . \quad <z_2^2> \tag{C-26}$$

From (C-9) we have

$$<x_1^2> \; = \sigma^2 \; + <x_1>^2 \tag{C-27}$$

and similarly for x_2, y_1, etc. From (C-10) we have

$$<x_1x_2> = \sigma^2\rho + <x_1><x_2> \; , \tag{C-28}$$

with similar expressions for the other coordinates. Substituting the relationships represented by (C-27) and (C-28) into (C-26) and making use of (C-17) we obtain a general expression for the correlation function ρ:

$$\rho(\ell_o,t) = 1 - \frac{<\ell^2>-\ell_o^2}{6\sigma^2} \tag{C-29}$$

where ℓ_o is the initial particle separation, i.e.

$$\ell_o^2 = (x_1' - x_2')^2 + (y_1' - y_2')^2 + (z_1' - z_2')^2 \; . \tag{C-30}$$

Batchelor (1950) has derived expressions for the mean square separation $<\ell^2>$ of particles lying within the universal equilibrium range of homogeneous turbulence. If we modify these formulas to account for molecular diffusion, and if we develop approximate expressions for $<\ell^2>$ applicable to particles lying outside the equilibrium range, we will have a complete description of $<\ell^2>$ which we can use in conjunction with (C-23) to evaluate (C-29)

To begin this task, consider two particles located at the points $\underset{-}{r}$ and $\underset{-}{r} + \underset{-}{\ell}$ at time t. (In this section only, subscripts will refer to vector components and the summation convention will be adopted for Greek subscripts.) The quantity of immediate interest to us is the time rate of change of $<\ell^2>$, where $\ell = |\underset{-}{\ell}|$. First, we note that

$$\frac{d}{dt} \ell^2 = 2\ell_\alpha \frac{d\ell_\alpha}{dt} \quad (\text{sum on } \alpha). \tag{C-31}$$

Let

$$v_i = \frac{d\ell_i}{dt} \tag{C-32}$$

denote the separation speed of the particles at time t. In analogy with the analysis of the previous section, we decompose v_i into two components: one, v_i', representing the effects of the turbulence; and another, v_i'', representing the effects of molecular agitation. The turbulent component can be expressed in terms of the Eulerian velocity components $u_i(\underset{-}{r},t)$ at the particle's locations:

$$v_i'(t) = u_i(\underset{-}{r} + \underset{-}{\ell},t) - u_i(\underset{-}{r},t). \tag{C-33}$$

The molecular velocity component v_i'' is given simply by

$$v_i''(t) = v_M(\underline{r} + \underline{\ell}, t) - v_M(\underline{r}, t) , \qquad \text{(C-34)}$$

(v_M was introduced in section 2d).

By expanding the Eulerian velocities in a Taylor series about the point $(\underline{r}, t)$ we can write (C-33)

$$v_i'(t) = u_{i,\alpha}\ell_\alpha + \frac{1}{2} u_{i,\alpha\beta}\ell_\alpha\ell_\beta + \ . \ . \ . \qquad \text{(C-35)}$$

With this and the above expressions we obtain from (C-31)

$$\frac{d\ell^2}{dt} = 2\ell_\alpha \ [v_\alpha'' + u_{\alpha,\beta}\ell_\beta + \frac{1}{2} u_{\alpha,\beta\gamma}\ell_\beta\ell_\gamma + \ . \ . \ .] \qquad \text{(C-36)}$$

and on taking the mean value we get

$$\frac{d}{dt} \ \langle\ell^2\rangle = 2[\langle\ell_\alpha v_\alpha''\rangle + \langle u_{\alpha,\beta}\ell_\alpha\ell_\beta\rangle + \frac{1}{2} \langle \ u_{\alpha,\beta\gamma}\ell_\alpha\ell_\beta\ell_\gamma\rangle \ + \ . \ . \ . \qquad \text{(C-37)}$$

Consider the term $\langle\ell_\alpha v_\alpha''\rangle$ in this expression. With the aid of (C-32) written in the form

$$\frac{d\ell_i}{dt} = v_i' + v_i'' , \qquad \text{(C-38)}$$

we obtain

$$\langle\ell_\alpha v_\alpha''\rangle = \int_0^t \langle v_\alpha''(t)[v_\alpha'(t') + v_\alpha''(t')]\rangle \ \ dt' . \qquad \text{(C-39)}$$

Now v_i'' and v_i' are uncorrelated as previously assumed. Furthermore, the molecular velocity components v_M of any two scalar particles separated by a distance $\underline{\ell} \neq 0$ are uncorrelated.

i.e. $\langle v_M(\underline{r}+\underline{\ell},t)v_M(\underline{r},t)\rangle = 0$ for all i, j, t and $\underset{\sim}{\ell} \neq 0$. These facts together with (C-34) and earlier discussions (following (C-21)) permit a reduction of (C-39) to

$$\langle \ell_\alpha v''_\alpha \rangle = 6\kappa \quad . \tag{C-40}$$

Combining this with (C-37) we arrive at the final general form of the rate equation for $\langle \ell^2 \rangle$:

$$\frac{d}{dt}\langle \ell^2 \rangle = 2[6\kappa + \langle u_{\alpha,\beta}\ell_\alpha \ell_\beta \rangle + \frac{1}{2}\langle u_{\alpha,\beta\gamma}\ell_\alpha \ell_\beta \ell_\gamma \rangle + \ldots] \ . \tag{C-41}$$

It is known from experimental data that on scales small compared to the microscale η, i.e. $\ell^* \leq 1$, the strain rate $u_{i,i}$ is of the order of $(\varepsilon/\nu)^{1/2}$ and is nearly constant on time scales comparable to $(\nu/\varepsilon)^{1/2}$. Thus, it is apparent from (C-41) that molecular diffusion dominates the separation rate of particles whose separation is of the order

$$\ell \ll \left(\frac{\kappa^2\nu}{\varepsilon}\right)^{1/4} \quad \text{or} \quad \ell^* \ll N_2^{-1/2} \ .$$

By contrast, (C-23) reveals that if the effective turbulent diffusivity $u'^{*2}T^*$ is much larger than the reciprocal of the Schmidt number, i.e.

$$u'^{*2}T^* \gg N_s^{-1} \ ,$$

molecular diffusion has negligible effect on σ. Consequently, since σ enters into the formulas for both $\langle c \rangle$ and $\langle c^2 \rangle$ while $\langle \ell^2 \rangle$ enters only in the latter (this will be seen later), we conclude that for all practical purposes, molecular diffusion may be neglected in calculations of the mean concentration but not in calculations of the mean square concentration.

For particles whose separation is in the range $\ell^{*2} << 1$, the turbulence appears as a pure straining motion characterized by (in an incompressible fluid and in the principal axes frame of the rate of strain tensor)

$$\begin{aligned} &u_{\alpha,\alpha} = 0 \;; \\ &u_{i,j} = 0 \,, \quad i \neq j \quad ; \qquad \text{(C-42)} \\ &u_{i,jk} = u_{i,jk\ell} = \ldots = 0 \,. \end{aligned}$$

Under these conditions (C-41) gives

$$\frac{d}{dt} \langle \ell_i^2 \rangle = 4\kappa + \langle u_{i,i} \ell_i^2 \rangle \;. \qquad \text{(C-43)}$$

In its unaveraged form, (C-43) describes the time rate of change of ℓ_i during a single realization of the turbulent flow. Here ℓ_i denotes a time average of the separation over a period that is long compared to molecular fluctuations but yet short compared to the time scale of the smallest turbulent eddies. The equation governing ℓ_i^2 is found to have the solution

$$\ell_i^2 = \ell_{io} e^{s_i t} + \frac{\kappa}{s_i} (e^{s_i t} - 1) \qquad \text{(C-44)}$$

where ℓ_{io} is the initial value of ℓ_i and where s_i denotes the strain rate $u_{i,i}$, assumed constant, on any given realization of the fluid flow. In actuality s_i is a random variable which varies from one realization to another. Assuming that $\ell_{io}^2 = \frac{1}{3} \ell_o^2$ and that the strain rate fluctuations s_i have a normal distribution with zero mean and variance s, we find after expanding (C-44) in a Taylor series, averaging the resulting equation, and collecting terms that for times $t^* \leq 1$, $<\ell^2>$ is given to good approximation by

$$<\ell^2> - \ell_o^2 = \frac{2}{3} \ \ell_o^2(\cosh 2st - 1) + 4\kappa(t + \frac{1}{s} \sinh 2st). \qquad \text{(C-45)}$$

It was remarked earlier that in the region of pure straining motion the strain rate is of the order of $(\epsilon/\nu)^{1/2}$. Upon using this as the value of s in (C-45) and nondimensionalizing the resulting equation, we obtain

$$<\ell^{*2}> - \ell_o^{*2} = \frac{2}{3} \ell_o^* \ (\cosh 2t^* - 1) + 4N_s^{-1}(t^* + \sinh 2t^*), <\ell^{*2}>^{1/2} << 1. \qquad \text{(C-46)}$$

This is the first of the set of equations for $<\ell^{*2}>$ which we will use to determine ρ.

For particle separations $<\ell^{*2}>$ comparable to or larger than unity, the high order velocity derivations entering in (C-41) cannot be neglected and as a result the equation is unclosed and unsolvable. However, it can be seen from the analysis leading up to this equation that (C-41) is equivalent to

$$\frac{d}{dt^*} <\ell_i^{*2}> = 4N_s^{-1} + 2V_i^*, \qquad \text{(C-47)}$$

where

$$V_i^* = <v_i'\ell_i>\tau/\eta^2 = <v_i'\ell_i>/\nu \ .$$

The term V* represents the instantaneous time rate of change of $<\ell^{*2}>$ due to the action of the turbulence alone. It is generally assumed (see for example, Corrsin (1962)) that the turbulent eddies which are primarily responsible for the instantaneous relative velocity of two particles a distance ℓ apart are those with length scales comparable to ℓ.

Based on this assumption and the fact that V^* involves the turbulence velocities only, we postulate that V^* can be expressed as a function of $\langle \ell^{*2} \rangle$ independent of the molecular diffusivity. For reasons discussed earlier in section 2d, this assumption should be valid if the Peclet number is sufficiently large. The functional form of the proposed relationship may be determined from the set of formulas for $d/dt \langle \ell^2 \rangle$ which Batchelor (1950) derived for the case of infinite Schmidt number (zero molecular diffusivity) in homogeneous, stationary turbulence. We now turn to this task, considering first the case:

(i) $\langle \ell^{*2} \rangle^{1/2} \sim 1$, the viscous subrange.

Based in part on dimensional analysis and in part on the assumption that the turbulence structure in the universal equilibrium range is isotropic, Batchelor showed that for small travel times

$$\langle \ell_i^2 \rangle - \ell_{oi}^2 = t^2(\varepsilon\nu)^{1/2}\left[F + \frac{\ell_{oi}^2}{2\ell_o}\,\frac{dF}{d\ell_o}\right], \text{ small } t \;; \qquad \text{(C-48)}$$

where $F \equiv F\left(\frac{\ell_o \varepsilon^{1/4}}{\nu^{3/4}}\right) = F(\ell_o^*)$ is a universal function. The exact form of F is not known so we shall assume it to be of the power law form

$$F = d_1 \ell_o^{*\beta} \;, \qquad \text{(C-49)}$$

where β and d_1 are constants to be determined later. By construction we make $\ell_{oi}^2 = 1/3\ell_o^2$, $i = 1,2,3$. Thus, (C-48) and (C-49) yield

$$\langle \ell^{*2} \rangle - \ell_o^{*2} = 3t^{*2} d_1 \ell_o^{*\beta}\,(1 + \beta/6), \quad N_s = \infty \;; \qquad \text{(C-50)}$$

and from this equation it follows that

$$\frac{d}{dt^*}\langle \ell^{*2} \rangle = 6t^* d_1 \ell_o^{*\beta}\,(1 + \beta/6), \quad N_s = \infty \,. \qquad \text{(C-51)}$$

On comparing this expression with (C-47) we find that in the case where $N_s = \infty$, the right side of (C-51) is equivalent to $2V_i^*$. Now under the postulate made earlier, V^* is independent of N_s when it is expressed in terms of $\langle \ell^{*2} \rangle$. Thus, the general expression for V^* which we seek (for the viscous subrange and small travel times) may be obtained by writing the right side of (C-51) in terms of $\langle \ell^{*2} \rangle$. This may be done with the aid of (C-50), the process being simply that of solving (C-50) for t^* and substituting the result into (C-51). The proper way to handle this operation is first to make a transformation of the dependent variable in both (C-50) and (C-51), namely

$$\omega^2 \equiv \langle \ell^{*2} \rangle - \ell_o^{*2} \quad , \qquad \text{(C-52)}$$

which implies

$$2\omega\,{}^{d\omega}/{}_{dt^*} = \frac{d}{dt^*} \langle \ell^{*2} \rangle \quad . \qquad \text{(C-53)}$$

Then from (C-53) and (C-51) we get

$$\omega\,{}^{d\omega}/dt^* = 3t^* d_1 \ell_o^{*\beta} (1 + \beta/6) \quad , \qquad \text{(C-54)}$$

and from (C-52) and (C-50) we obtain

$$t^* = \omega [3d_1 \ell_o^{*\beta} (1 + \beta/6)]^{-1/2} \quad . \qquad \text{(C-55)}$$

Substituting this result into (C-54) we arrive at

$$d\omega/dt^* = [3d_1 \ell_o^{*\beta} (1 + \beta/6)]^{1/2}, \; N_s = \infty \quad . \qquad \text{(C-56)}$$

Note that the solution of this equation is, correctly, (C-50). Now we write (C-47) in terms of ω:

$$\frac{d\omega}{dt^*} = \frac{6}{\omega N_s} + \frac{3V^*}{\omega} \quad . \tag{C-57}$$

Setting $N_s = \infty$ in this equation and comparing the result with (C-56) we conclude that

$$V^* = \omega/\sqrt{3}\ [d_1 \ell_o^{*\beta}(1 + \beta/6)]^{1/2} \quad . \tag{C-58}$$

The desired equation for $\langle \ell^{*2} \rangle$ in the viscous subrange thus becomes

$$\frac{d}{dt^*}\,\omega = \frac{6}{N_s}\,\omega^{-1} + \sqrt{3}\ [d_1 \ell_o^{*\beta}(1 + \beta/6)]^{1/2} \ , \ \langle \ell\ ^2 \rangle \leq 10\ell_o^{*2}. \tag{C-59}$$

where

$$\langle \ell^{*2} \rangle = \omega^2 + \ell_o^{*2} \quad .$$

It will be noted in this equation that we have replaced the condition "t* small," used earlier, by $\langle \ell^{*2} \rangle \leq 10\ \ell_o^{*2}$. In theory the condition stems from the fact that the initial growth rate of $\langle \ell^{*2} \rangle$ is dependent on the initial separation ℓ_o^{*2}, but that once $\langle \ell^{*2} \rangle$ becomes large compared to ℓ_o^{*2}, the dependence on the initial separation is lost. Batchelor showed that in the latter period, i.e. when $\langle \ell^2 \rangle \gg \ell_o^2$, that

$$\frac{d}{dt}\langle \ell_i^2 \rangle = \nu G_2 \left(\frac{t\varepsilon^{1/2}}{\nu^{1/2}} \right)$$

or

$$\frac{d}{dt^*} \langle \ell_i^{*2} \rangle = G_2(t^*) \ . \tag{C-60}$$

Here again G_2 is a universal function of unknown form; as in the case of F, we adopt the power law form

$$G_2(t^*) = d_2 t^{*\gamma} \tag{C-61}$$

where d_2 and γ are constants to be determined. Substituting (C-61) into (C-60) and making use, as before, of the isotropy assumption and the initial condition $\ell_{oi}^{*2} = 1/3\ell_o^{*2}$, we obtain

$$\frac{d}{dt^*} \langle \ell^{*2} \rangle = 3d_2 t^{*\gamma} \quad , \ N_s = \infty \quad ; \tag{C-62}$$

and integrating this we get

$$\langle \ell^{*2} \rangle - \ell_o^{*2} = 3d_2(\gamma + 1)^{-1} t^{*\gamma+1} \ . \tag{C-63}$$

From this point on the derivation of the desired equation for $d/dt^* \langle \ell^{*2} \rangle$ follows a course similar to that which led up to (C-59). Without going through the details, we state simply that the result is

$$\frac{d}{dt^*} \omega = (\gamma + 1)^{-1} \left[\frac{12}{N_s} \omega^{-\gamma} + 3d_2 \left(\frac{\gamma+1}{3d_2} \right)^{\gamma/\gamma+1} \right] , \ 10 \ \ell_o^{*2} < \langle \ell^{*2} \rangle \sim 1 \tag{C-64}$$

where

$$\langle \ell^{*2} \rangle = \omega^{\gamma+1} + \ell_o^{*2} \ .$$

Having already derived the required equations for $\langle \ell^{*2} \rangle$ in the range $\langle \ell^{*2} \rangle << 1$, we now move on to a consideration of the remaining region $\langle \ell^{*2} \rangle^{1/2} >> 1$. We consider first the portion

(ii) $\ell_e^{*2} >> \langle \ell^{*2} \rangle >> 1$, the inertial subrange.

The turbulence structure within the inertial subrange is determined by the turbulent energy dissipation rate ε. Using this fact Batchelor was able to show that when ℓ_o^* is within this subrange and when t^* is within the period such that $\langle \ell^{*2} \rangle \leq 10\, \ell_o^{*2}$ (and $\langle \ell^{*2} \rangle^{1/2}$ still within the inertial subrange),

$$\langle \ell_i^2 \rangle - \ell_{oi}^2 = \frac{10}{9} c_1 \, (t\varepsilon^{1/3} \ell_o{}^{1/3})^2 \ ,$$

or

$$\langle \ell_i^{*2} \rangle - \ell_{oi}^* = \frac{10}{9} c_1 t^{*2} \ell_o^{*2/3} \ , \quad \langle \ell_i^{*2} \rangle \leq 10\, \ell_{oi}^{*2} \ , \qquad \text{(C-65)}$$

where c_1 is another constant to be determined. The corresponding equation which is applicable to the range $\langle \ell^{*2} \rangle > 10 \ell_o^{*2}$ is found to be

$$\langle \ell^{*2} \rangle - \ell_o^{*2} = c_2 t^{*3} \ , \qquad \text{(C-66)}$$

where c_2 is yet another constant. Following a procedure similar to that used in the analysis of the viscous subrange, we obtain

$$\frac{d}{dt^*}\omega \begin{cases} = \frac{6}{N_s}\omega^{-1} + \left(\frac{10c_1}{3}\right)^{1/2}\ell^{*\,1/3}_o & \langle\ell^{*2}\rangle \le 10\,\ell^{*2}_o \; , \\ \langle\ell^{*2}\rangle = \omega^2 + \ell^{*2}_o \; ; & \\ = \frac{4}{N_s}\omega^{-2} + c_2^{1/3} \; , & \langle\ell^{*2}\rangle > 10\,\ell^{*2}_o \; , \\ \langle\ell^{*2}\rangle = \omega^3 + \ell^{*2}_o \; . & \end{cases} \tag{C-67}$$

Only one final region remains to be considered --

(iii) $\langle\ell^{*2}\rangle \gtrsim \ell_e^{*2}$, the energy eddy range.

Because of the paucity of information regarding the influence of the energy containing eddies on the rate of separation of a pair of particles with $\langle\ell^2\rangle \sim \ell_e^2$, it will be necessary to hypothesize a rate equation for this range. To this end we note first that since the two point Eulerian velocity correlation vanishes as the separation of the points approaches and exceeds ℓ_e, a pair of particles with initial separation $\ell_o \gtrsim \ell_e$ should wander independently, i.e.

$$\rho(\ell_o) = 0 \quad , \text{ if } \; \ell_o \gtrsim \ell_e \tag{C-68}$$

This is not necessarily true, however, for particle pairs with $\langle\ell^2\rangle \gtrsim \ell_e^2$ whose initial separations ℓ_o were much smaller than ℓ_e. Indeed, empirical data to be presented later indicate that the separation rates of such pairs are such that ρ = constant $\neq 0$ for a considerable period of time. Specifically, the data show that sufficiently far from the source of the scalar quantity, the mean square scalar fluctuation $\langle c^2(x,r)\rangle$ is self-preserving when the radial distance r from the plume axis is scaled by $\sigma(x)$ and $\langle c^2\rangle$ is scaled by $\langle c(x,0)\rangle^2$. Now it can be shown using the model equations for $\langle c\rangle$ and $\langle c^2\rangle$ (see (C-100) and (C-101)) that self-preservation is possible only if $d\rho/dx = 0$, and it can in turn be shown using (C-29) that $d\rho/dx = 0$ only when

$$\frac{d}{dt}\,\ln\,[\langle \ell^2\rangle - \ell_o^2] = \frac{d}{dt}\,\ln\,[\sigma^2] \qquad \text{(C-69)}$$

The data also reveal that in the regions of self-preservation, $\sigma^2 \sim t$ and that $\langle \ell^2\rangle \sim \ell_e^2$ for the majority of particle pairs. From these facts and (C-69) we surmise that

$$\frac{d\langle \ell^{*2}\rangle}{dt^*} = \frac{\langle \ell^{*2}\rangle - \ell_o^{*2}}{L^{*2}(t^*)}[2u'^{*2}T^* + 2/N_s], \quad \langle \ell^{*2}\rangle \geq \ell_e^{*2} \text{ and } \ell_o^* < \ell_e^*. \qquad \text{(C-70a)}$$

where L(t) is a length scale which approaches σ as $t \to T$. For lack of better information, it will be assumed that

$$L^2 \begin{cases} = \exp\left(-\dfrac{10\ell_o^2}{\ell_e^2}\right)[\ell_e^2 - \sigma^2] + \sigma^2\,, & t < T; \\ = \sigma^2 & t \geq T. \end{cases} \qquad \text{(C-70b)}$$

It is of interest to note that the integral scale Λ of the Eulerian two point velocity correlation satisfies an equation like (C-70) with $L^2 = \sigma^2$ during the latter part of the initial period of decay of isotropic turbulence (see, for example, Batchelor and Townsend (1948)). This similarity between the growth rates of $\langle \ell^2\rangle$ and Λ^2 (which is roughly equivalent to ℓ_e^2) is not altogether surprising because the empirical data mentioned above which guided the formulation of (C-70) were gathered in the core region of fully developed pipe flows where the turbulence is predominately in a state of decay.

Formulas (C-70) and (C-68) complete the list of rate equations for $<\ell^2>$. Before these can be implemented, the constants entering into the equations must be specified and the boundaries between the various subranges must be more precisely defined. These two tasks become related when the constraint is imposed that $d<\ell^2>/dt$ be continuous across all subrange boundaries. For example, it is found that when the boundary between the viscous and inertial subranges is chosen as $\ell^* = 1$, the continuity constraint requires that

$$d_1 = 2(1 + \beta/6)^{-1}.$$

By the same technique a range of values is found for the constant c_1(we chose $c_1 = 1$); but each of the other constants must be established by other means (to be discussed later).

3. THE SPECTRUM OF CONCENTRATION FLUCTUATIONS

A brief review of some of the results of Part I is required here to make clear the meaning of the spectrum D_{12} given in the introduction.

The scalar fluctuation c' is defined in the usual manner

$$c'(\underline{x},t) \equiv c(\underline{x},t) - \langle c(\underline{x},t)\rangle \; . \qquad \text{(C-71)}$$

Two-point scalar correlation functions can also be defined:

$$S(\underline{x},\underline{r},t) \equiv \langle c(\underline{x},t)c(\underline{x} + \underline{r},t)\rangle \quad , \qquad \text{(C-72)}$$

$$S'(\underline{x},\underline{r},t) \equiv \langle c'(\underline{x},t)c'(\underline{x} + \underline{r},t)\rangle \quad . \qquad \text{(C-73)}$$

Using these functions we define the generalized spectrum

$$D_{12}(\underline{k}_1,\underline{k}_2,t) \equiv \left(\frac{1}{8\pi^3} \right)^2 \int\!\!\int S(\underline{x},\underline{r};t)e^{i(\underline{k}_1\cdot\underline{x}-\underline{k}_2\cdot(\underline{x}+\underline{r}))}d\underline{r}d\underline{x} \qquad \text{(C-74)}$$

and a similar spectrum D'_{12} for the scalar fluctuations. It is the relationship between D_{12} and the two particle characteristic function ϕ that is given in the introduction, equation (C-3). Our interest in this section will be not with D_{12} but with its "marginal spectrum" D_2 defined by

$$D_2(\underline{k}_2,t) \equiv \int D_{12}(\underline{k}_1,\underline{k}_2,t)d\underline{k}_1 \quad , \qquad \text{(C-75)}$$

which is related to S by

$$D_2(\underline{k}_2,t) = \left(\frac{1}{8\pi^3} \right) \int S(0,\underline{r},t)e^{i\underline{k}_2\cdot\underline{r}}d\underline{r} \quad . \qquad \text{(C-76)}$$

To obtain an expression for D_2 we begin by substituting the density function (C-7) into (C-5) and performing the integrations. We obtain

$$\Phi(\underline{k}_1,\underline{k}_2;\underline{x}',\underline{x}'',t) = \exp[i(\underline{k}_1\cdot\underline{x}' + \underline{k}_2\cdot\underline{x}'') - \frac{1}{2}\sigma^2(\underline{k}_1\cdot\underline{k}_1 + \underline{k}_2\cdot\underline{k}_2 + 2\rho\underline{k}_1\cdot\underline{k}_2)]. \tag{C-77}$$

where $\sigma^2 = \sigma^2(t)$ and $\rho = \rho(|\underline{x}' - \underline{x}''|,t)$ as given in Figure 1. To keep the analysis as simple as possible we have assumed in deriving (C-77) that the mean fluid velocity $\underline{U} = 0$. This condition can generally be realized by a transformation of the coordinate system. Substituting (C-77) into (C-3) and making use of (C-75), we obtain after some integration

$$D_2(\underline{k}_2,t) = \frac{Q^2}{(2\pi)^{9/2}\sigma^3}\int_V\int_V \exp\left[-\frac{\sigma^2}{2}(1-\rho^2)\underline{k}_2\cdot\underline{k}_2 - i\underline{k}_2\cdot(\underline{x}'' - \rho\underline{x}') - \frac{\underline{x}'\cdot\underline{x}'}{2\sigma^2}\right]d\underline{x}'d\underline{x}'' \tag{C-78}$$

where V denotes the initial volume of the marked fluid cloud and $Q(r) = Q$ denotes the initial marked fluid concentration.

It has already been assumed that the turbulence is isotropic. Suppose, in addition, that the particle cloud is initially a sphere of volume V centered at $\underline{x} = 0$. In this case $D_2(\underline{k}_2,t)$ should be invariant with respect to the direction of the vector $\underline{k}_2$. A more useful spectrum, therefore, is

$$D_2(k_2,t) \equiv \int D_2(\underline{k}_2,t)dA(k_2) \tag{C-79}$$

where $k_2 = |\underline{k}_2|$ and $A(k_2)$ denotes the surface of a sphere in $\underline{k}_2$ space of radius k_2. From (C-78) and (C-79) we get

$$D_2(k_2,t) = B_3 \int_V \int_V \exp\left[-\frac{\sigma^2}{2}(1-\rho^2)\underline{k}_2\cdot\underline{k}_2 - \frac{\underline{x}'\cdot\underline{x}'}{2\sigma^2}\right] \int \exp\left[-i\underline{k}_2\cdot\underline{\mu}\right]$$

$$dA(k_2)d\underline{x}'d\underline{x}'' \qquad \text{(C-80a)}$$

where

$$B_3 = \frac{Q^2}{(2\pi)^{9/2}\,\sigma^3} \qquad \text{(C-80b)}$$

and

$$\underline{\mu} = \underline{x}'' - \rho\underline{x}' . \qquad \text{(C-80c)}$$

The integration over $A(k_2)$ in (C-80a) is easily performed in a spherical coordinate system in which the vector $\underline{\mu}$ coincides with one of the $\underline{k}_2$ coordinate axes, and we arrive finally at the expression for the spectrum of a three dimensional scalar distribution —

$$D_2(k_2,t) = 4\pi k_2^2 B_3 \int_V \int_V \exp\left[-\frac{\sigma^2 k_2^2}{2}(1-\rho^2) - \frac{x'^2}{2\sigma^2}\right] \frac{\sin k_2\mu}{k_2\mu}\, d\underline{x}'d\underline{x}'' . \qquad \text{(C-81)}$$

With the variance σ and correlation function ρ given by the expressions in Figure 1, equation (C-81) can be evaluated numerically for any problem in which the turbulence is homogeneous and isotropic and the source distribution is spherically symmetric. We note in passing that in a two-dimensional scalar field the corresponding spectrum is defined by

$$D_2(k_2,t) \equiv \int D_2(\underline{k}_2,t)\,ds(k_2) \quad , \text{ 2-D}; \qquad \text{(C-82)}$$

where $s(k_2)$ denotes the perimeter of a circle in k_2 space of radius k_2; and that it has the form

$$D_2(k_2,t) = \frac{k_2 Q^2}{(2\pi\sigma)^2} \int_V \int_V \exp\left[-\frac{\sigma^2 k_2^2}{2}(1-\rho^2) - \frac{x'^2}{2\sigma^2} \right] J_o(k_2\mu)\,d\underline{x}'\,d\underline{x}'', \qquad \text{(C-83)}$$

where k_2, x', and μ are the amplitudes of the two dimensional counterparts of the vectors in (C-81) and J_o is the Bessel function of order zero. This spectrum can also be evaluated in specific problems using the expressions for σ and ρ given in Figure C-1.

a. The Scalar Spectrum in the Viscous-Convective Subrange.

The boundaries of this subrange are defined roughly by

$$(\varepsilon/\nu^3)^{1/4} << k << (\varepsilon/\nu\kappa^2)^{1/4} \ ,$$

or in terms of the nondimensional coordinates that we are using

$$1 << k^* << N_s^{1/2} \quad , \text{ viscous-convective subrange boundaries} \ . \qquad \text{(C-84)}$$

This latter expression shows clearly that only those systems possessing extremely large Schmidt numbers are likely to exhibit a viscous-convective subrange. If the subrange exist, then according to Batchelor (1958) it will be characterized by a spectrum of the form

$$D(k) = \frac{1}{k} \exp\left(\frac{\kappa}{s} k^2 \right), \qquad \text{(C-85)}$$

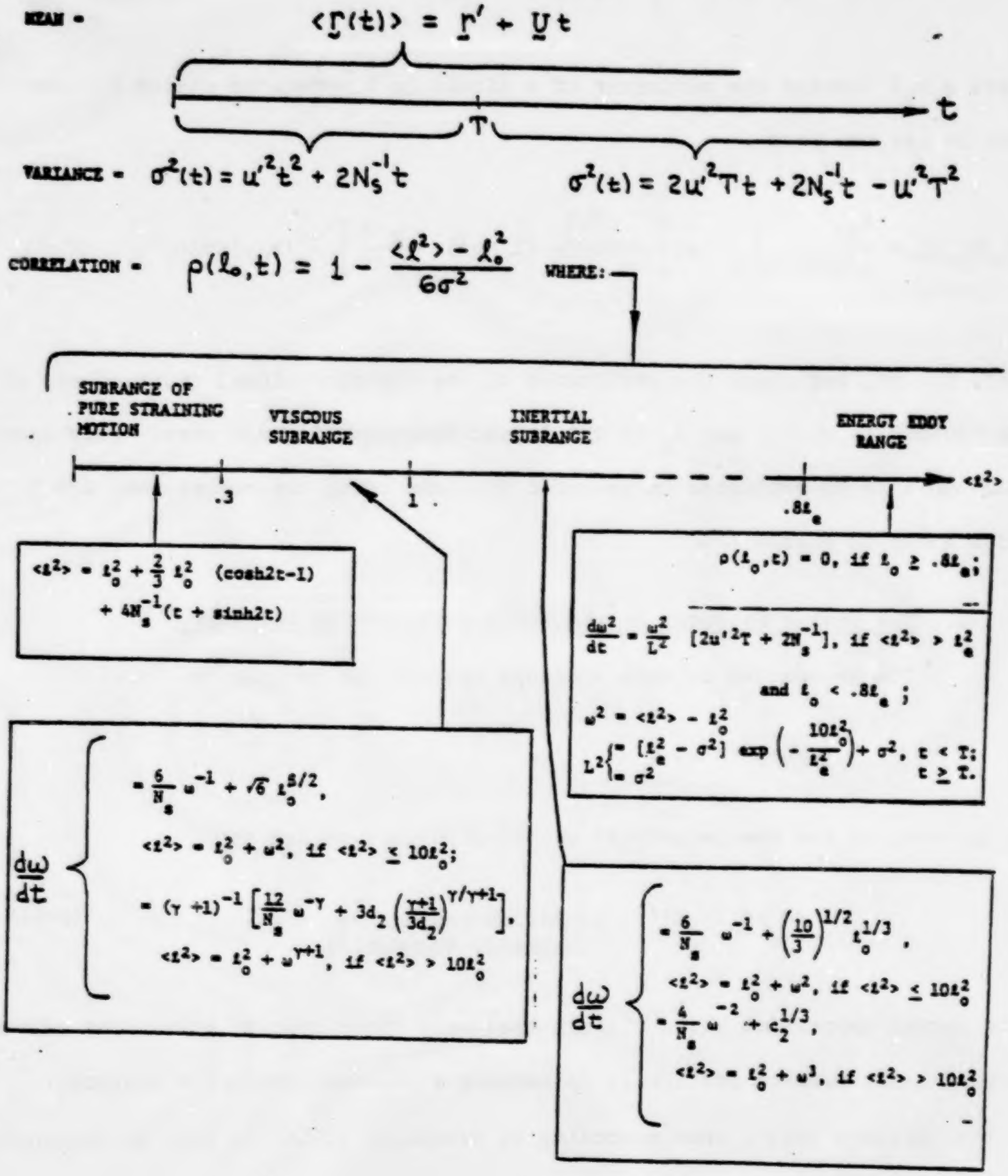

MEAN =

$$\langle \underset{\sim}{r}(t)\rangle = \underset{\sim}{r}' + \underset{\sim}{U}t$$

VARIANCE =

$$\sigma^2(t) = u'^2t^2 + 2N_s^{-1}t \qquad \sigma^2(t) = 2u'^2Tt + 2N_s^{-1}t - u'^2T^2$$

CORRELATION =

$$\rho(\ell_o,t) = 1 - \frac{\langle \ell^2\rangle - \ell_o^2}{6\sigma^2}$$

WHERE:

$$\langle \ell^2\rangle = \ell_o^2 + \frac{2}{3}\ell_o^2\,(\cosh 2t-1) + 4N_s^{-1}(t + \sinh 2t)$$

$$\frac{d\omega}{dt}\begin{cases} = \dfrac{6}{N_s}\omega^{-1} + \sqrt{6}\,\ell_o^{5/2}, \\ \langle \ell^2\rangle = \ell_o^2 + \omega^2, \text{ if } \langle \ell^2\rangle \leq 10\ell_o^2; \\ = (\gamma+1)^{-1}\left[\dfrac{12}{N_s}\omega^{-\gamma} + 3d_2\left(\dfrac{\gamma+1}{3d_2}\right)^{\gamma/\gamma+1}\right], \\ \langle \ell^2\rangle = \ell_o^2 + \omega^{\gamma+1}, \text{ if } \langle \ell^2\rangle > 10\ell_o^2 \end{cases}$$

$$\rho(\ell_o,t) = 0, \text{ if } \ell_o \geq .8\ell_e;$$

$$\frac{d\omega^2}{dt} = \frac{\omega^2}{L^2}\,[2u'^2T + 2N_s^{-1}], \text{ if } \langle \ell^2\rangle > \ell_e^2 \text{ and } \ell_o < .8\ell_e;$$

$$\omega^2 = \langle \ell^2\rangle - \ell_o^2$$

$$L^2\begin{cases} = [\ell_e^2 - \sigma^2]\exp\left(-\dfrac{10\ell_o^2}{\ell_e^2}\right) + \sigma^2, & t < T; \\ = \sigma^2 & t \geq T. \end{cases}$$

$$\frac{d\omega}{dt}\begin{cases} = \dfrac{6}{N_s}\omega^{-1} + \left(\dfrac{10}{3}\right)^{1/2}\ell_o^{1/3}, \\ \langle \ell^2\rangle = \ell_o^2 + \omega^2, \text{ if } \langle \ell^2\rangle \leq 10\ell_o^2 \\ = \dfrac{4}{N_s}\omega^{-2} + c_2^{1/3}, \\ \langle \ell^2\rangle = \ell_o^2 + \omega^3, \text{ if } \langle \ell^2\rangle > 10\ell_o^2 \end{cases}$$

FIGURE C-1. SCHEMATIC SUMMARY OF THE MODEL EQUATIONS FOR THE MEAN, VARIANCE, AND CORRELATION OF THE DISPLACEMENTS OF A PAIR OF PARTICLES IN STATIONARY, HOMOGENEOUS TURBULENCE. (All variables are in units of η and τ.)

where s is the mean strain rate of the turbulence. Assuming as before that s is of the order $(\varepsilon/\nu)^{1/2}$, (C-85) has the nondimensional form

$$D^*(k^*) = \frac{1}{k^*} \exp\left(-\, k^{*2}/N_s\right) , \tag{C-86}$$

where $D^* = D/\eta$, and where the strain rate s is assumed to be negative. Let us see whether (C-81) yields a spectrum of this form in the viscous-convective subrange.

Suppose that the scalar quantity is released at $t = 0$ in the form of a spherical cloud of radius L_r and uniform concentration Q into homogeneous turbulence with no mean velocity. After a sufficiently long travel time the cloud will have grown to a size much larger than its initial dimensions (i.e. $\sigma \gg L_r$) and the mean scalar distribution near the center of the cloud will be approximately homogeneous. Under these conditions (C-81) reduces to

$$D(k,t) = 4\pi k^2 B_3 \int_V \int_V \exp\left[-\,\frac{\sigma^2 k^2}{2}\,(1-\rho^2)\right] \frac{\sin k\mu}{k\mu}\, d\underline{x}'\, d\underline{x}'' . \tag{C-87}$$

where we have replaced D_2 by D to signify that the scalar distribution is approximately homogeneous.

Since the viscous-convective subrange comprises wave numbers $k^* \gg 1$, it is apparent from (C-87) that only particle pairs with correlations ρ near unity will contribute significantly to the spectrum in this region. The assumption of a large Schmidt number, which we have already recognized as necessary for the existence of this spectral subrange, is compatible with this requirement on ρ; because when N_s is very large, particle pairs whose initial separation ℓ_o is in the pure strain rate region will experience very low separation velocities. This is in contrast to those pairs with ℓ_o^* of order unity or larger which are driven apart by the turbulence much more rapidly than those with $\ell_o^* << 1$, regardless of the value of N_s. Based on these observations, we surmise that after a sufficient travel time, a high Schmidt number system is characterized by

$$\rho(\ell_o^*) \begin{cases} \sim 1, & \ell_o^* << 1; \\ \sim 0 & \text{otherwise} \end{cases} . \tag{C-88}$$

In this case the variable μ entering in (C-87) becomes (cf. (C-80c))

$$\mu = |\underline{x}'' - \rho\underline{x}'| = |\underline{x}'' - \underline{x}'| = \ell_o . \tag{C-89}$$

From (C-29) we find that in the case where $\rho \sim 1$,

$$1 - \rho^2 = \frac{<\ell^2> - \ell_o^2}{3\sigma^2} . \tag{C-90}$$

With $\rho(\ell_o^*)$ given by (C-88), only particle pairs with $\ell_o^* << 1$ need to be considered. The functional form of $<\ell^2> - \ell_o^2$ for these pairs given in Figure C-1 combined with (C-90), (C-89), and (C-87) yields

$$D(k,t) = 4\pi k^2 B_3 \int_V \int_V \exp\left[- a k^{*2} \ell_o^{*2} - b N_s^{-1} k^{*2}\right] \left[\frac{\sin k^* \ell_o^*}{k^* \ell_o^*}\right] d\underline{x}' d\underline{x}'' , \tag{C-91}$$

where

$$a = 1/9\ (\cosh 2t^* - 1)$$
$$b = 2/3(t^* + \sin 2t^*) \tag{C-92}$$

and $\ell_o = |\underset{-}{x}'' - \underset{-}{x}'|$.

It turns out that if the radius L_r of the initial cloud of marked fluid satisfies certain conditions (to be specified later), the integrals in (C-91) can be evaluated analytically. To accomplish this we employ a special approach which avoids the difficulties which one would encounter in attempting to evaluate (C-91) by straightforward methods. In the first step of this technique we notice that the double integral in (C-91) is essentially a summation of the integrand over all possible pairs of particles in the volume V. (In the present instance V is a sphere of radius L_r.) Next we notice that the integrand depends only on the distance between the two particles in each pair and not on the location of either particle. Combined, these facts allow us to write (C-91) in the form*

$$\int_V \int_V f(\ell_o) d\underset{-}{x}' d\underset{-}{x}'' = V^2 \int_o^{2L_r} f(\ell_o) g(\ell_o) d\ell_o, \tag{C-93}$$

where $V = \frac{4}{3}\pi(L_r)^3$ denotes the initial volume of the cloud, $f(\ell_o)$ is any function of $|\underset{-}{x}'' - \underset{-}{x}'|$, and $g(\ell_o)$ is the fraction of all possible particle pairs in V with separations in the range ℓ_o to $\ell_o + d\ell_o$. That is, $g(\ell_o)$ is the probability density that two points picked at random in the sphere V will have a separation in the range ℓ_o to $\ell_o + d\ell_o$. This fact makes it possible to evaluate $g(\ell_o)$ by random number techniques on a digital computer. (It is found in the case of the sphere considered here that $g(\ell_o)$ has a maximum near $\ell_o = .8\ L_r$ and that it drops to zero at $\ell_o = 0$ and $\ell_o = 2L_r$.) In the range $\ell_o << 2L_r$ the functional form of $g(\ell_o)$ can be determined analytically for use in the evaluation of (C-91). Thus, consider any point A in the sphere. The number of points within a distance ℓ_o to $\ell_o + d\ell_o$ of this point is $4\pi\ell_o^2 d\ell_o p$, where p is the density of points in the sphere. (The concept of a point density p as used here is an artificial device to facilitate the derivation of $g(\ell_o)$. It has no effect on the final result.) Now there are pV "A" points in the sphere (assuming $\ell_o << 2L_r$), so the total number of particle pairs with separations in the range ℓ_o to $\ell_o + d\ell_o$ is

---

*The proof of (C-93) can be derived from probability theory and the concepts of Lebesgue integration

$$n(\ell_o) = (4\pi)\ p^2 \ell_o^2 V d\ell_o\ ; \tag{C-94}$$

but there are a grand total of

$$T = p^2 V^2 \tag{C-95}$$

particle pairs in the sphere. Consequently, since by definition

$$g(\ell_o) = \frac{n(\ell_o)}{T d\ell_o}\quad ,$$

we have

$$g(\ell_o) = \frac{4\pi}{V}\ \ell_o^2 \qquad , \ \ell_o << 2L_r\ . \tag{C-96}$$

Suppose that

$$L_r/\eta = L_r^* >> 1\ . \tag{C-97}$$

Since we are concerned only with wave numbers $k^* \gg 1$, the integrand in (C-91) will differ significantly from zero only for distances $\ell_o^* \lesssim 1$. Consequently, under the assumption (C-97), the expression (C-96) for $g(\ell_o)$ may be used to evaluate (C-91). These operations yield

$$D^*(k^*,t^*) = (4\pi)^2 B_3 V k^* e^{-\frac{bk^{*2}}{N_s}} \int_0^{2L_r^*} \ell_o^* \, e^{-ak^{*2}\ell_o^{*2}} \sin k^*\ell_o^* \, d\ell_o^* \qquad \text{(C-98)}$$

In view of (C-97) and the fact that the integrand of (C-98) vanishes for $\ell_o^* \gg 1$, we may replace the upper limit on the integral in (C-98) by infinity. In this case the integral can be evaluated analytically (see, for example, Gradshteyn and Ryzhik). We get finally

$$D^*(k^*,t^*) = \left(\frac{4\pi^{5/2} B_3 V}{a^{3/2}} \right) \frac{1}{k^*} \exp\,(-\,bk^{*2}/N_s) \;, \qquad \text{(C-99)}$$

in agreement with Batchelor's result (C-86). The time dependence of the parameters a and b entering in (C-99) (see (C-92)) results in a decrease with time not only of the amplitude of D^* but also of the cut-off wave number of the spectrum. Part of the decrease in the amplitude of D^* is due to the decay of $\langle c \rangle$; but even after this effect is removed by nondimensionalizing D^* by $\langle c(t^*) \rangle^2$, a decay remains. The precise rate of this decay cannot be deduced from (C-92) because this expression was obtained under the assumption that the mean strain rate s of the turbulence is constant, and of course this assumption is not valid for indefinite periods of time, particularly times $t^* \gg 10$.

4. THE MEAN AND MEAN SQUARE CONCENTRATION

Relatively few theoretical studies of the mean square of a scalar quantity in turbulent fluid can be found in the literature. Those with which the author is most familiar are studies by Gifford (1959), Hinze (1959), Corrsin (1964), and Csanady (1967). Apparently Gifford's is the only Lagrangian type study of scalar fluctuations heretofore reported. His model is based on the heuristic concept of the so-called fluctuating plume. There are some interesting similarities between that model and the present one but there is not space to elaborate on them here.

Hinze's analysis begins with the equation for the two point scalar correlation which is analogous to the Karman-Howarth equation for the two point turbulent velocity correlation. Hinze closes the equation by neglecting the transfer term in the equation. This assumption implies that the dimensionless group $\frac{u'\lambda_c}{\kappa}$ is very small, i.e. that diffusion by the small eddies is small compared to molecular diffusion. Here u' denotes the root mean square turbulent velocity fluctuation, λ_c is the microscale of the scalar correlation function, and κ is the molecular diffusivity of the scalar. A result of Hinze's analysis is that the mean square fluctuation $\langle c'^2 \rangle$ decays with time according to

$$\langle c'^2 \rangle \propto t^{-3/2} .$$

Corrsin starts his analysis with the equation for $\langle c'^2 \rangle$ itself. He achieves closure by writing the dissipation term in the equation as a function of $\langle c'^2 \rangle$ and the microscale λ_c and then assuming the latter parameter to be a constant. By this method he arrives at

$$\langle c'^2 \rangle \propto e^{-at}$$

where a is a constant. Both Hinze's and Corrsin's studies assume, in addition to the other assumptions embodied in their analyses, that the mean value of the scalar <c> is uniform in space. This is a very strong assumption in so far as applied studies are concerned because it restricts the applicability of the results to regions far from the sources of the scalar quantity.

The analysis by Csanady is more general in that it allows spatial inhomogeneity in <c>. However, like the other two Eulerian studies it contains a (different) closure approximation whose validity is difficult to assess. In addition, it assumes self-similar profiles of <c> and $\langle c'^2 \rangle$. For reasons which will become clear later, the self-similarity assumption precludes the use of Csanady's results near the admixture source. In fact, it appears that the closure assumption he makes is also invalid near sources.

In the present study the model equations for the mean and mean square scalar distribution are obtained from (C-1), (C-2), (C-4) and (C-7)--

$$\langle c(\underline{x},t)\rangle = \frac{Q}{(2\pi\sigma^2)^{3/2}} \int_V \exp\left(-\frac{|\underline{x}-\underline{x}'|^2}{2\sigma^2}\right) d\underline{x}', \qquad \text{(C-100)}$$

$$\langle c^2(\underline{x},t)\rangle = \frac{Q^2}{(2\pi\sigma^2)^3} \int_V \int_V (1-\rho^2)^{-3/2} \exp\left[-\frac{|\underline{x}-\underline{x}'|^2+|\underline{x}-\underline{x}''|^2}{2\sigma^2(1-\rho^2)}\right.$$

$$\left. + \frac{\rho(\underline{x}-\underline{x}')\cdot(\underline{x}-\underline{x}'')}{\sigma^2(1-\rho^2)}\right] d\underline{x}'\, d\underline{x}'' , \qquad \text{(C-101)}$$

where σ and ρ are given in Figure C-1 and the mean fluid velocity $\underline{U} = 0$. (In these formulas it is assumed that the sample volume Δv has dimensions that are small compared to σ.)

In contrast to the models cited above, (C-100) and (C-101) contain no closure approximations, no assumptions regarding the relative magnitudes of molecular and turbulent diffusion, no homogeneity assumptions, and no self-similarity hypotheses. The only approximations embodied in the present models are those contained in the model of the two particle statistics developed in section two, and these impose a constraint only on the turbulence whereas the Eulerian models impose conditions on both the turbulence and the scalar fields.

Consequently, (C-100) and (C-101) are not restricted, in principle, to any particular region of space-time and therefore they may be used to analyze the entire evolution of the distribution of mean square fluctuation (msf), $\langle c'^2 \rangle$. Let us examine how well the predictions of these models agree with observational data.

5. COMPARISON OF COMPUTED AND OBSERVED SCALAR STATISTICS

Only three empirical studies of $<c>$ and $<c'^2>$ have been found which are extensive enough to meet the needs of our comparison. These are by Lee and Brodkey (1964), Crum and Hanratty (1965), and Becker, Rosensweig, and Gwozdz (1966). A fourth study by Baldwin and Walsh (1961) provides information about the mean but not the mean square scalar distribution. The study by Lee and Brodkey treats the dispersion of a dye in a stream of water; Becker, et al. examined the diffusion of an oil fog in air; and the other two teams of investigators measured the diffusion of heat in an airstream. In each case the scalar was released from a steady, continuous source into a fully developed turbulent pipe flow. Therefore, in order to simulate these experiments using (C-100) and (C-101) which pertain to instantaneous sources in a fluid with no mean velocity, we will have to assume that diffusion in the direction of the mean flow is negligible compared to the transport and that the coordinate system is advected downstream at the speed of the mean flow.

Before the experimental results can be compared with the model predictions, it is necessary to determine the Reynolds and Schmidt numbers for each system and to determine the transformations between the laboratory and nondimensional coordinate systems.

a. Determination of the Reynolds Number R_ℓ and the Coordinate Transformations.

Let D denote the diameter of the pipe in any given experiment and let the length scale ℓ_e of the turbulent energy containing eddies be related to D by

$$\ell_e = \lambda D . \qquad \text{(C-102)}$$

Also, let the root mean square turbulent (isotropic) velocity fluctuation u' be related to the mean pipe flow rate $\bar{u}$ by

$$u' = \alpha\bar{u} \quad . \qquad \text{(C-103)}$$

The parameter α is often called the turbulence intensity. Thus, the Reynolds number defined by (C-15) is related to the pipe Reynolds number R_p by

$$R_\ell \equiv \frac{u'\ell_e}{\nu} = \alpha\lambda\frac{\bar{u}D}{\nu} = \alpha\lambda R_p \quad . \qquad \text{(C-104)}$$

The values of λ and α were determined from the experimental data in the following way. First, the expressions given in Figure C-1 for the width σ of the plume were converted to expressions in ℓ_e and the downstream distance x using the transformation

$$x = \bar{u}t \quad . \qquad \text{(C-105)}$$

and the relationship (C-14a) between T and ℓ_e. The resulting expressions for $\sigma(x;u',\ell_e,N_s)$ were then "fitted" to the measured $\sigma(x)$ profiles by adjusting the values of u' and ℓ_e(N_s is given). In this way it was found that when λ was assigned the constant value

$$\lambda = .041 \quad , \qquad \text{(C-106)}$$

the values of α that were required in each experiment to obtain the best agreement between the observed and computed profiles of $\sigma(x)$ clustered in the narrow range α = .025 - .030. That the values of α should fall so close together is quite remarkable because as we shall see shortly, the Reynolds number in these four experiments range over nearly two orders of magnitude. From these values and (C-104) we find that the pipe Reynolds number R_p is approximately 1000 times larger than the turbulence Reynolds number R_ℓ.

The conversions between the nondimensional travel time t* used in the model equations and x*, x, or t are found from (C-105) and (C-15b,c) to be

$$x^* = \alpha^{-1} R_\ell^{1/4} t^* \ , \tag{C-107a}$$

$$x = (\alpha^{-1} \lambda D R_\ell^{-1/2}) t^* \ , \tag{C-107b}$$

and

$$t = (\nu^{-1} \lambda^2 D^2 R_\ell^{-3/2}) t^* \ . \tag{C-107c}$$

b. Experimental Conditions of the Observations.

A concise description and comparison of the experimental conditions behind each of the four data sets is given in Table C-1. The value of λ given by (C-106) was used to determine the relevant parameters in the table in all four cases. The source diameter in each experiment is indicated by L_D and the approximate sample volume by δv. Also shown are the ranges of distances x* and the corresponding travel times t* over which data were collected.

c. Comparison of the Observed and Computed Mean Value, <c>.

Without exception the profiles of <c> measured normal to the plume axis were very closely Gaussian in all four empirical studies. The largest departure from a Gaussian form occurs at the edges of the plumes far downstream from the source. This is primarily a result of the effect of the increasing velocity shear experienced by the plume edge as it approaches the pipe wall. Thus, for the most part the model equation (C-100) predicts the correct shape of the profiles of <c>.

At points sufficiently far from the source that the plume width σ is much larger than the source diameter L_D, (C-100) reduces to

$$\langle c(r,x) \rangle / (q/\bar{u}) = \frac{1}{2\pi\sigma^2(x)} \exp\left(- \frac{r^2}{2\sigma^2(x)} \right) \tag{C-108}$$

Table C-1. Experimental Conditions of Four Data Sets. (cgs units)

Experimenter	Fluid	Tracer	D	ν	N_s	$\bar{u}$	L_e	α	R_λ	η	τ	L_D^*	δv	x^*	t^*
Becker, Rosensweig and Gwozdz	Air	Oil fog	20.0	.15	6.10^5	$41-61\cdot10^2$	.84	.026	597-888	$6.9-5.2\cdot10^{-3}$	$.32-.18\cdot10^{-3}$	36[†]	10^{-3}	2900-16000[†]	13-75[†]
Lee and Brodkey	Water	dye	7.7	.009	7760	55.6	.31	.028	49	$16.6\cdot10^{-3}$	$31\cdot10^{-3}$	36	10^{-3}	1800-4600	19-48
Crum and Hanratty	Air	Heat	7.7	.15	.7	250	.34	.030	17	$41\cdot10^{-3}$	$11\cdot10^{-3}$	.8	10^{-7}	6-375	0.1-5.5
Baldwin and Walsh	Air	Heat	20.3	.15	.7	$22\cdot10^2$	.82	.025	300	$11\cdot10^{-3}$	$.85\cdot10^{-3}$	9	10^{-6}	800-8500	4.5-49.

[†] Based on lowest Reynolds number

where $\langle c(r,x)\rangle$ is the mean scalar in unit cross-section of the plume a distance x downstream from the source; r denotes radial distance from the plume axis; and q is the time rate of release of the admixture by the source. Thus, both the width of the plume and the value of the scalar at its centerline are functions of the single variable σ. Figure C-2 presents a graphical comparison of the measured and computed profiles of σ. These are presented in the nondimensional form σ* vs. x* because in these terms the equations for σ assume the particularly useful forms

$$\sigma^{*2} \begin{cases} = \alpha^2 x^{*2} + 2\alpha R_\ell^{-1/4} N_s^{-1} x^*, & x^* \leq R_\ell^{3/4}\alpha^{-1}; \\ = 2\alpha R_\ell^{3/4} x^* + 2\alpha R_\ell^{-1/4} N_s^{-1} x^* - R_\ell^{3/2}, & \text{otherwise} . \end{cases} \qquad \text{(C-109)}$$

The theoretical curves of σ* shown in the figure were derived from this expression using a constant value of .028 for the turbulence intensity α. This value is roughly the median of those given in Table 1 which were found to yield the best fit of (C-109) to each of the data sets. These "best fit" values reveal that α is inversely proportional to the Reynolds number. However, the variation is so slight that over the range of Reynolds numbers depicted in Figure C-2, a constant value of .028 is sufficient to obtain a quite accurate estimate of σ*. We conclude from this and the observed Gaussian form of $\langle c\rangle$ that the model equations (C-100) and (C-109)with $\alpha = 0.28$, provide a reasonably accurate, universal description of the mean value of a passive scalar in homogeneous turbulence.

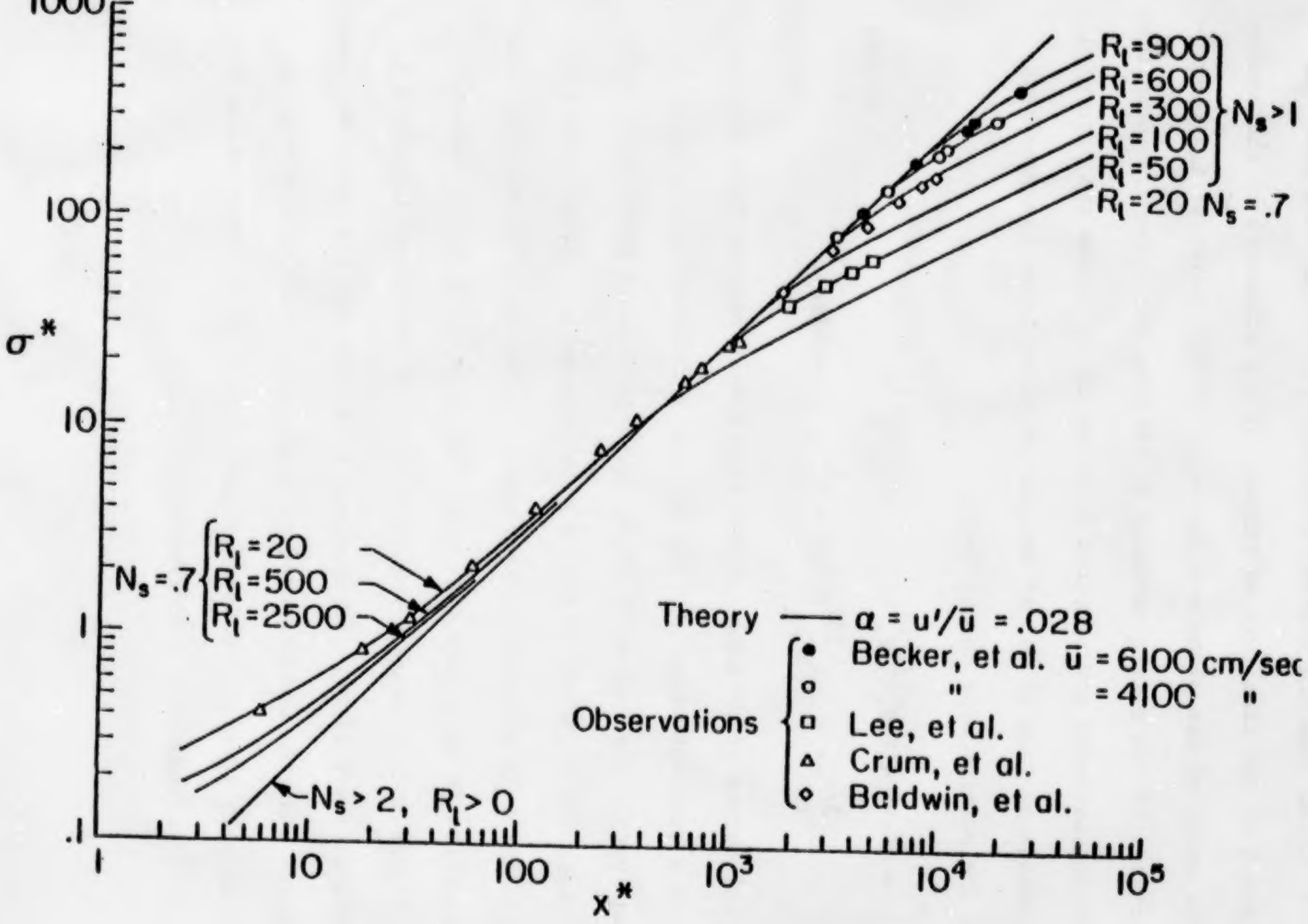

FIGURE C-2. COMPARISON OF THE NONDIMENSIONALIZED ROOT-MEAN-SQUARE PARTICLE DISPLACEMENT σ^* GIVEN BY THE MODEL EQUATION (C-109) WITH EMPIRICAL DATA AS A FUNCTION OF NONDIMENSIONAL DISTANCE x^* FROM THE POINT OF RELEASE

d. Comparison of the Observed and Computed Mean Square Scalar Fluctuations, $<c'^2>$.

Since the model of the single particle statistics has now been found to be reasonably accurate, any discrepancies between the observed and computed values of $<c'^2>$ will reflect inadequacies in the model of the two particle statistics. Rather than treat the msf $<c'^2>$ itself, it is found convenient to work with the normalized quantity

$$\Gamma_o(r,x) = \frac{<c'^2(r,x)>^{1/2}}{<c(0,x)>} . \qquad \text{(C-110)}$$

where r is a vector normal to the plume axis a distance x from the source.

In the model of ρ which enters into the expression for $<c'^2>$, there are as yet four unspecified constants: c_2, d_2 β, and γ. The last three of these are pertinent to the viscous subrange only. Because the viscous subrange is rather narrow in the present model, it was found that the values assigned to d_2 β, and γ had very little effect on the function ρ except in high Schmidt number—low Reynolds number situations. The values which were ultimately chosen for use in all of the ensuing calculations are $d_2 = .1$, $\gamma = 2.0$, $\beta = 5.5$. The value of the constant c_2 is generally more critical. In the preliminary calculations of $<c'^2>$ to be discussed presently, we assigned c_2 the nominal value of unity.

Using the above values for the model constants and those given in Table C-1 for the parameters R_ℓ, N_s, L_D, etc., we evaluated (C-110) numerically and thereby arrived at theoretical predictions of Γ_o for each of the four experimental systems. The predicted and observed profiles of Γ_o are compared graphically in Figure C-3a-c (Baldwin and Walsh did not measure msf). Looking first at Figure C-3a, we see that the amplitude, growth rate, and shape of the Γ_o profiles observed by Crum and Hanratty are all reproduced quite faithfully by the model. However, the comparisons are not as favorable in the other two experiments, shown by the solid curves in Figures C-3b and C-3c. In both of these cases there is considerable amplitude and shape distortion in the simulated profiles of Γ_o and in the case of the Becker system, there is also a slight error in the predicted degree of self-preservation.

A possible source of these errors is the neglect in the model of the influence of turbulence which might be generated by the device used to inject the scalar into the pipe stream. (Both Lee and Becker observed large disturbances in the flow immediately downstream of the scalar source.) Considering the fact that the injector wake is composed initially of eddies with length scales comparable to the injector width and that it is just such eddies which are most efficient in separating the majority of the scalar particle pairs, one might expect significant wake effects in Γ_o. In an attempt to parameterize these effects to first order accuracy, we assumed that the dispersive action of the wake is describable in terms of an eddy diffusivity

$$\kappa_w \sim u_w \ell_w$$

where u_w and ℓ_w are the characteristic velocity and length scales, respectively, of the wake turbulence. The effective or total diffusivity κ' is thus assumed to be

$$\kappa' = \kappa + \kappa_w$$

where κ is the molecular diffusivity. Assuming that u_w and ℓ_w are constant fractions of the mean velocity $\bar{u}$ and the source width L_D, respectively, the effective Schmidt number $N_s' = \nu/\kappa'$ becomes

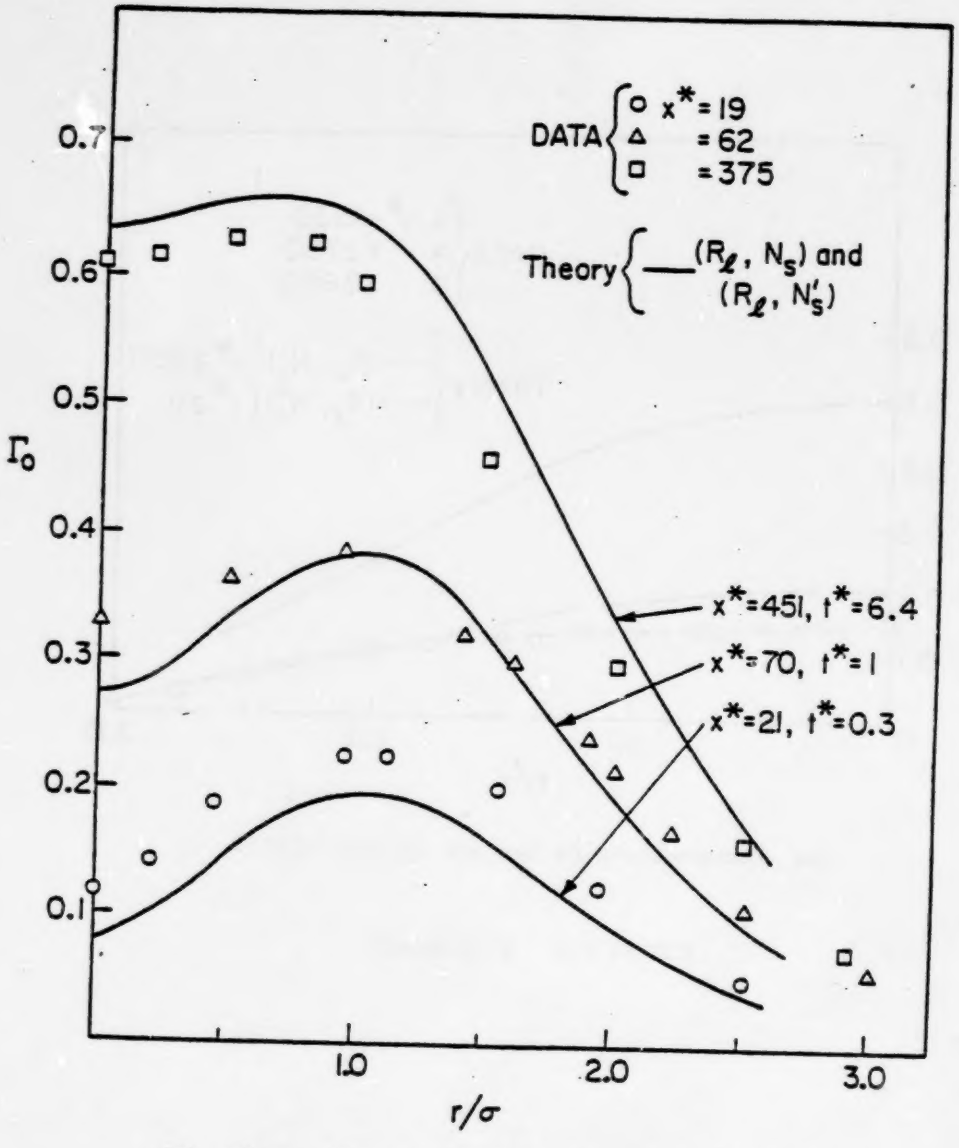

(a) Observations by Crum and Hanratty (1965)

FIGURE C-3. COMPARISON OF THE PREDICTED NORMALIZED ROOT-MEAN-SQUARE CONCENTRATION FLUCTUATION Γ_o WITH OBSERVATIONS. See Table C-1 for the experimental conditions of each case.

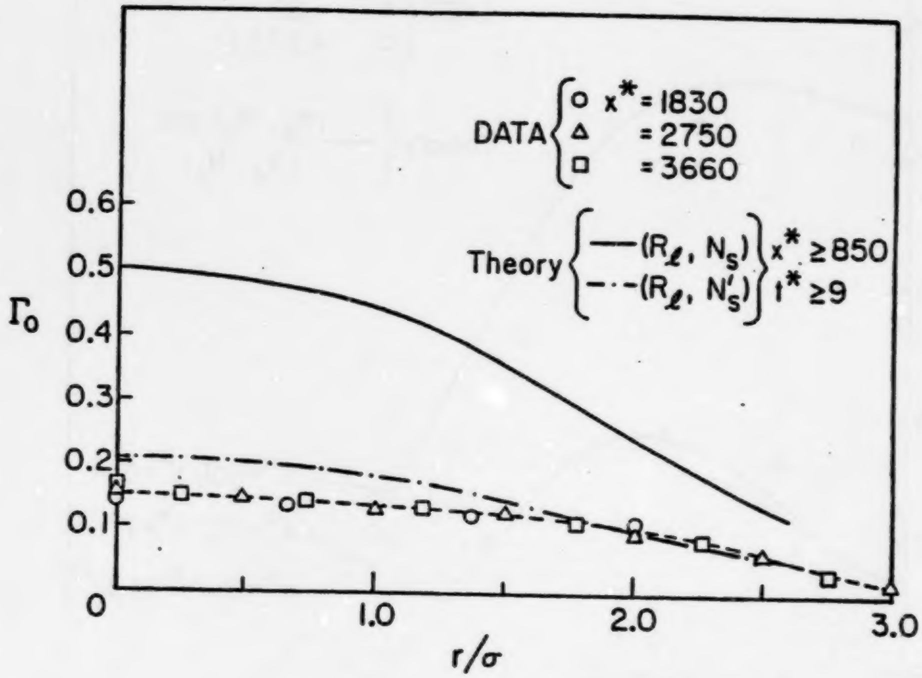

(b) Observations by Lee and Brodkey (1974)

FIGURE C-3 (Continued)

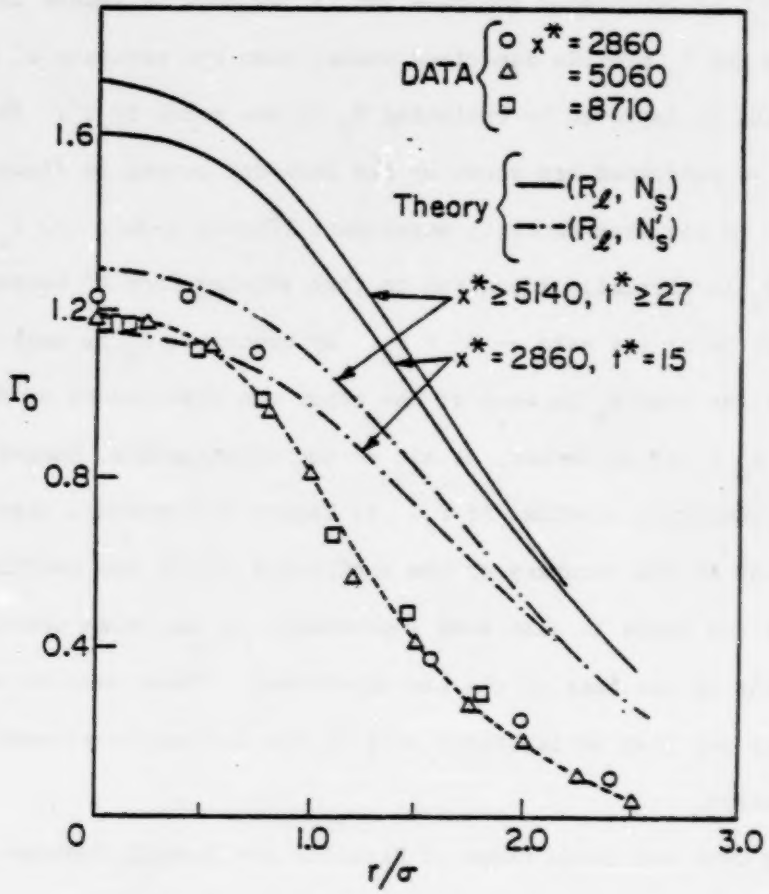

(c) Observations by Becker, Rosensweig, and Gwozdz (1966)

FIGURE C-3 (Concluded)

$$N_s' = \frac{N_s}{1+\gamma' R_\ell N_s L_D/D} \qquad \text{(C-111)}$$

where D is the pipe diameter and γ' is a constant. If this parameterization of the wake effect is reasonably accurate and if the wake is indeed the source of the errors in the Γ_o profile described above, then the accuracy of the simulations should be improved by replacing N_s in the model by N_s'. The results of calculations so performed are shown by the dash-dot curves in Figure C-3a-c.

In the case of the Crum-Hanratty experiment (Figure C-3a), the Γ_o profile obtained using N_s is virtually identical to that arising from N_s' because there is apparently little if any wake — $N_s' \approx N_s$. By contrast, N_s' is many orders of magnitude smaller than N_s in each of the other two experiments — $N_s' = .28$ in Lee-Brodkey; $N_s' = .18$ in Becker, et al. — and considerable changes are manifest in the resulting profiles of Γ_o. As Figure C-3 reveals, there is a marked improvement in the accuracy of the amplitudes of the new profiles in both experiments and there is also some improvement in the shape characteristics, particularly in the case of the Lee experiment. These results suggest that wake effects may play an important role in the initial development of the msf distribution.

Considering both the large range of Reynolds and Schmidt numbers represented by the three data sets described above and the fact that the model constants c_2, d_2, etc. were not changed throughout all of the calculations, the results indicate that the model embodies a reasonably accurate description of the processes which govern the development of msf. Moreover, due to the structuring of the model in terms of physical concepts rather than mathematical approximations, the model provides valuable insights into the mechanisms which affect msf.

The analyses that we have presented here represent but a first step in the application of Lagrangian theory to problems of turbulent diffusion. Refinements to this approach must await the coming of new data and theoretical techniques.

ACKNOWLEDGEMENT

The author is indebted to a reviewer for many valuable comments and suggestions and to Professor P. G. Saffman for a helpful discussion. This work was supported in part by National Science Foundation Grant GK-35476.

APPENDIX D

LAGRANGIAN ANALYSIS OF NONLINEAR CHEMICAL REACTIONS IN TURBULENT FLUID

R. G. LAMB

PARTIAL INDEX OF SYMBOLS USED

Vectors

$\underline{r} = (x,y,z)$

$\underline{r}_{oi}$	point of release of the i-th particle.
$\underline{r}_{mi}$	see (D-14)
$\underline{Y}_{m,ij\ldots\phi}$	see (D-15)
$\underline{Y}_{o}$	see (D-16)
$\underline{\Psi}_{m}$	see (D-17a)

Operators

I_{λ}	integration operator defined by (D-30).
$D_{\lambda,\gamma\delta\ldots,ij\ldots}$	Operates on I_{λ} as defined by (D-32)
$a_{\alpha}D^{\alpha}_{n}$	see (D-42) and (D-43)

Integration domains

$\Omega^{n}_{ij\ldots\omega}$	see (D-21)
$\chi^{n}_{ij\ldots\omega}$	see paragraph following (D-25)
ΔV_{nj}	the volume δv centered at the point $\underline{r}_{nj}$

Functions and other parameters

$\langle c(\underline{r},t)\rangle$	mean particle concentration at $(\underline{r},t)$.
$p_{i}(\underline{r},t\,|\,\underline{r}_{oi},t_{o})$, $p_{ij}(\underline{r},t;\underline{r}',t'\,|\,\underline{r}_{oi},t_{o};\underline{r}_{oj},t_{o})$	displacement probability density function (see paragraph following (D-4)).
$p_{i}(\underline{r},t), p_{ij}(\underline{r},t;\underline{r}',t')$	same as above.
$\hat{p}(\underline{\Psi}_{m}|\underline{Y}_{o},t_{o})$ or $\hat{p}(\underline{\Psi}_{m})$	the m-time joint probability density of the positions at times $t-t_{o} = n\Delta t$, $n = 1,2,\ldots m$ of N inert particles released at $t = t_{o}$ in the configuration $\underline{Y}_{o}$.

ϕ_n	see (D-39)
$\hat{P}_{mi}$	see (D-36)
δv	"reaction volume" swept out by a particle in time Δt (see (D-12).
$k = \delta v/\Delta t$	
T_C	reaction time scale defined by (D-55)
s_i	see (D-46) and (D-47)
$\mathcal{T}$	Lagrangian time scale of the turbulence, (D-84).
$\overline{w'^2}^{1/2}$	root-mean-square turbulent velocity fluctuation
R_o λ	see (D-83) and (D-85).
γ	radius of a particle's "collision cross-section."

APPENDIX D

LAGRANGIAN ANALYSIS OF NONLINEAR CHEMICAL REACTIONS IN TURBULENT FLUID

Abstract

A model of chemical reactions in turbulent fluid is proposed which permits the concentration statistics of chemically reactive particles to be expressed in terms of the Lagrangian velocity statistics of the turbulence and a parameter which represents the reactivity of the particles. The model is used to derive the general expression for the mean concentration of both first and second order reactants. In the case of the second order reactant, only the reaction A + A → B is considered. The resulting expression for the mean concentration of species A is then applied to two specific problems. The first of these is the case of a reaction in a well stirred vessel. Here the resulting expression for the mean concentration is found to agree exactly with the classical theory. In the second example, the problem of an infinite, finite width line source of the substance A in a homogeneous turbulent flow is considered. Suitable empirical data are apparently not available for a rigorous test of the theory in this case, but qualitative accuracy is demonstrated through an application of the expression for the mean concentration to several flow situations.

1. INTRODUCTION

Many of the turbulent diffusion problems of interest in applied studies concern the dispersion of marked fluids, or particles, which interact chemically with one another. As an example, consider the situation where only two reactive particle species, say A and B, are present. If α molecules of A combine with β molecules of B to form δ molecules of a third species D, i.e.

$$\alpha A + \beta B \rightarrow \delta D, \tag{D-1}$$

and if the resulting rates of change of the concentrations of A, B, and D are expressible in the form

$$\frac{1}{\alpha}\frac{dc_A}{dt} = \frac{1}{\beta}\frac{dc_B}{dt} = -k[c_A]^{\alpha}[c_B]^{\beta} = -\frac{1}{\delta}\frac{dc_D}{dt} \tag{D-2}$$

where c_A, c_B, and c_D denote the concentrations of species A, B, and D, and where k is the rate coefficient for the reaction, then (D-1) is said to be of α-th order with respect to reactant A, of β-th order with respect to B, and to be of overall order $n = \alpha + \beta$.

The theoretical problem of describing the concentrations of reactive substances in turbulent flow has received attention from Corrsin (1958), Toor (1962), Lee (1966), Vassilatos and Toor (1965), O'Brien (1968, 1971), and others. The starting point is usually the set of equations formed by incorporating the rate formulas (D-2) into the set of mass continuity equations which govern the transport and diffusion of each of the chemical species. The main drawback of this approach is the well-known closure problem which is made even more acute when the overall order n of the reactions is greater than unity.

In another paper, Lamb (1974), hereafter referred to as L1, it is shown that the closure problem can be circumvented by formulating the particle concentration statistics in terms of the statistics, call them p for the moment, of the particle displacements. Moreover, this is demonstrated without the aid of any assumptions regarding the chemical behavior of the particles. Thus, provided that the statistics p can be determined for each marked particle species present, the formulas derived in L1 can be used to compute the particle concentration statistics regardless of their chemical characteristics. The immediate problem with this approach, however, is the determination of p, because only a few of the p statistics are feasible to determine even for chemically inert substances. In cases where chemical reactions of orders $n > 1$ occur, the problem of determining p is further compounded. This is because the rates of second and higher order reactions are intimately connected with the particle motions. For example, the reaction (D-1) with $\alpha = \beta = \delta = 1$ can occur only when a particle of A and a particle of B collide; and during each such collision, there is a finite probability that the A and B particles will combine to form a single particle of D. Therefore, the probability density $p_{Bi}(\underline{r},t|\underline{r}_{A1},t_{A1},\dots \underline{r}_{AN}, t_{AN},\dots t_{BN'})$ of finding the i-th particle of B at $(\underline{r},t)$ given that N particles of A were released at the points $(\underline{r}_{Ai},t_{Ai})$, $i = 1,\dots, N$, and that N' particles of B were released from $(\underline{r}_{Bj},t_{Bj})$, $j=1, 2,\dots, N'$, is dependent on the nature of the substances A and B as well as on each of the independent variables $\underline{r}_{Ai},t_{Ai},\underline{r}_{Bi}$, and t_{Bi}. By contrast, if the B particles are chemically inert and noninteracting,

$$p_{Bi}(\underline{r},t|\underline{r}_{A1},\dots t_{BN}) = p_{Bi}(\underline{r},t|\underline{r}_{Bi},t_{Bi}).$$

Due to the large number of variables on which the position statistics p depend when the particles react nonlinearly ($n > 1$), a direct determination of p is beyond the realm of feasibility in nearly all problems of applied interest. It would be highly desirable, therefore, to be able to express the statistics p of chemically reactive particles in terms of the corresponding statistics, say $\hat{p}$, of chemically inert particles; because if the marked particles do not interact dynamically, then $\hat{p}$ is a function only of the turbulence and the molecular diffusivity of the particles. The purpose of this paper is to develop a mathematical relationship between p and $\hat{p}$.

This task proves to be relatively straighforward for particles which undergo first order reactions ($n = 1$) because one of the characteristics of this type of reaction is that its rate is independent of the particle interactions. This is not the case, however, for second and higher order reactions and herein lies the source of considerable difficulty in developing a generalized mathematical relationship between $\hat{p}$ and p. Nevertheless, we arrive in section 3 at a theory for treating second order reations. Although we consider only a single reaction, namely

$$A + A \rightarrow B$$

and derive only the formula for the mean concentration of A, the technique is applicable to other types of reactions, including those of higher order, and to the determination of the concentrations of the reaction products. After deriving the formula for the concentration of A, we apply it to the problem of a well-stirred reaction cell, and to the problem of a slender plume of A in a homogeneous turbulent stream.

For future reference we rewrite here the formulas derived in L1 for the mean and mean square particle concentrations $c(\underline{r},t)$ in a sample volume Δv of arbitrary size centered at the point $\underline{r}$ at time t:

$$< c(\underline{r},t) > = \frac{1}{\Delta v} \sum_{i=1}^{N} \int_{\Delta V} p_i(\underline{r}',t|\underline{r}_{oi},t_o)\, d\underline{r}' \qquad \text{(D-3)}$$

$$< c^2(\underline{r},t) > = \frac{<c(\underline{r},t)>}{\Delta v} + \frac{2}{\Delta v^2} \sum_{i=1}^{N-1} \sum_{j=i+1}^{N} \iint_{\Delta V} p_{ij}(\underline{r}',t;\underline{r}'',t|\underline{r}_{oi},t_o; \qquad \text{(D-4)}$$

$$\underline{r}_{oj},t_o)\, d\underline{r}'\, d\underline{r}''$$

where $p_i(\underline{r}',t'|\underline{r}_{oi},t_o)$ is the probability density of finding the i-th marked particle at $(\underline{r}',t')$ given that it was released from $(\underline{r}_{oi},t_o)$; $p_{ij}(\underline{r}',t';\underline{r}'',t''|\underline{r}_{oi},t_o;\underline{r}_{oj},t_o)$ is the joint probability density of finding the i-th particle at $(\underline{r}',t')$ and the j-th particle at $(\underline{r}'',t'')$ given that the respective release points of these particles are $(\underline{r}_{oi},t_o)$ and $(\underline{r}_{oj},t_o)$; and $d\underline{r} = dxdydz$.

Before proceeding we should point out that since the statistics of the particle displacements are assumed known, the nature of the mechanism which produces the random particle motions is immaterial to the calculation of the particle concentrations. However, to facilitate a conceptual understanding of the problem, we shall assume in the discussions which follow that it is turbulent fluid motions alone which are responsible for the particle motions.

2. FIRST ORDER REACTIONS

Consider marked particles A which undergo chemical transformation at a rate given by the first order law

$$\frac{dc_A}{dt} = -k(t)\, c_A, \quad k(t) \neq f(c_A) \qquad \text{(D-5)}$$

where $k(t)$ is the rate constant, possibly time dependent, and c_A is the concentration of A. Radioactive decay and the photolysis of sulfur dioxide in the atmosphere are examples of chemical processes which can be described by (D-5). The important feature of reactions of this type is that the rate is independent of the collision interactions of the particles. Therefore, the probability $p_i(\underline{r},t|\underline{r}_{oi},t_o)\, d\underline{r}$ of finding the i-th marked particle of A at $(\underline{r},t)$ given that it was at $\underline{r}_{oi}$ at time t_o is just the probability that two events occur, namely (1) that the particle suffers a displacement $\underline{r} - \underline{r}_{oi}$ during the period $t - t_o$ and (2) that no chemical transformation of the particle occurs during that time. The latter event, as we have already mentioned, is statistically independent of the particle motions; but for the motions to be independent of the reaction, we must require that the reactions do not perturb the fluid motion through either the release of large quantities of heat or the production of particles of radically different density than that of the fluid. If these requirements are satisfied, then $p_i(\underline{r},t|\underline{r}_{oi},t_o)\,d\underline{r}$ is equal to the product of the probabilities of the two events defined above.

The probability of the displacement $\underline{r} - \underline{r}_{oi}$ during $t - t_o$ is just $\hat{p}_i(\underline{r},t|\underline{r}_{oi},t_o)\,d\underline{r}$, i.e. the probability that an inert particle released from $(\underline{r}_{oi},t_o)$ would move to $(\underline{r},t)$.

The probability, call it ρ, that the particle does not undergo chemical change during $t - t_o$ could be determined directly by solving (D-5) . However, the essence of the problem is more fully illustrated by the following approach.

First, we notice from (D-5) that $k(t)$ is the probability density that any single particle will change chemically during the time t to $t + dt$. Now let $t - t_o$ be transformed into a new time frame

$$\xi(t) = \int_{t_o}^{t} k(t')\,dt', \qquad \text{(D-6)}$$

which we divide into M equal subintervals $d\xi$, i.e.

$$d\xi = \frac{\xi(t)-\xi(t_o)}{M} .$$

Since according to (D-6) $d\xi = k(t)\,dt$, the probability of a chemical change during any interval ξ to $\xi + d\xi$ is simply equal to $d\xi$. Therefore, the probability of no change during $t - t_o$ is clearly

$$\rho = (1 - d\xi)^M = 1 - Md\xi + \frac{1}{2!}M(M-1)\,d\xi^2 - \ldots \qquad \text{(D-7)}$$

On taking the limit $d\xi \to 0$ for fixed $\xi(t)$ we obtain

$$\rho = \lim_{d\xi\to 0} (1-d\xi)^M = e^{-\xi(t)} . \qquad \text{(D-8)}$$

We conclude finally that

$$p_i(\underline{r},t|\underline{r}_{oi},t_o) = \hat{p}_i(\underline{r},t|\underline{r}_{oi},t_o) \exp \left(- \int_{t_o}^{t} k(t')\, dt'\right). \qquad (D\text{-}9)$$

This expression can be used in (D-3) to compute the concentration of any first order chemical reactant in a turbulent fluid for which $\hat{p}$ is known.

By a similar process we obtain

$$p_{ij}(\underline{r}',t';\underline{r}'',t''|\underline{r}_{oi},t_o;\underline{r}_{oj},t_o) = \hat{p}_{ij}(\underline{r}',t';\underline{r}'',t''|\underline{r}_{oi},t_o;\underline{r}_{oj},t_o)$$

$$\left[\exp\left(- \int_{t_o}^{t'} k(t)\, dt - \int_{t_o}^{t''} k(t)\, dt\right)\right] \qquad (D\text{-}10)$$

which may be used in (D-4) to compute the mean square concentration, and in like manner we could obtain expressions for the probability density functions needed to compute higher stochastic moments of the concentration.

3. SECOND ORDER REACTIONS — Derivation of the general formula for $p_i(\underline{r},t|\underline{r}_{oi},t_o)$.

In this section we shall deal exclusively with the second order reaction

$$A + A \rightarrow B. \qquad (D\text{-}11)$$

This reaction is typical of that used to describe the coagulation of aerosols, with A denoting a particle of some given size and B denoting the larger particle formed by the union of two A particles.

Our aim is to determine the statistics $p_i(\underline{r},t|\underline{r}_{oi},t_o)$, which yield the mean concentration through (D-3), of the particle A, in the case where N particles of A are released at the same instant t_o from known points $\underline{r}_{oi}$, $i = 1, 2, \ldots, N$. (The same techniques can be applied to B or to either A, B, or D in the more general reaction (D-1).) This type of chemical process is more difficult to treat than the previous case because in a second order reaction the chemical behavior of each particle is intimately connected to its motion. Thus, the first task is to describe the reaction mechanism in terms of the particle motion.

For this purpose we adopt a model based on the one commonly used in chemical kinetics. That is, we envisage that each particle of A has a "collision cross-section" of radius γ such that during a time Δt each particle sweeps out a volume δv of average size

$$\delta v \equiv \pi \gamma^2 \, \overline{u'^2}^{1/2} \, \Delta t \tag{D-12}$$

where $\overline{u'^2}$ denotes the mean square particle velocity, assumed constant. If during the interval $t - \Delta t/2 \leq t' < t + \Delta t/2$ any particle passes through the spherical volume δv centered at the position of any other particle at time t, the two particles "collide" with probability approaching one as $\Delta t \to 0$.

In kinetic theory it is assumed that during each such collision the particles involved may react chemically provided that the relative velocities and orientations of the particles satisfy certain conditions established by the nature of both the particles and the reaction mechanism. To include these additional assumptions in our model of turbulent flow reactions requires much more labor in the theoretical analysis than seems warranted at this time. Consequently, we shall assume simply that every particle collision, as defined above, between two particles of A produces a particle of B. In this case we have

$$P_i(\underline{r},t|\underline{r}_{oi},t_o) = \rho_i(\underline{r},t|\underline{r}_{o1},\underline{r}_{o2},\ldots,\underline{r}_{oN},t_o) \tag{D-13}$$

where $\rho_i(..)$ is the joint probability density that the i-th particle of A suffers no collisions with any other particle of A while undergoing a displacement $\underline{r} - \underline{r}_{oi}$ in the time interval $t - t_o$, given the release points $(\underline{r}_{oj}, t_o)$ of all N particles of A. Thus, we have reduced the problem of determining the density $p_i(\underline{r},t|\underline{r}_{oi},t_o)$ of chemically reactive particles to that of deriving the probability density $\rho_i(..)$ which is a function only of the particle motions and the parameter δv which characterizes the chemical reaction. From here on we shall often omit reference to the particle release points when writing p_i and ρ_i —

$$p_i(\underline{r},t) = p_i(\underline{r},t|\underline{r}_{oi},t_o),$$

$$\rho_i(\underline{r},t) = \rho_i(\underline{r},t|\underline{r}_{o1},\ldots \underline{r}_{oN},t_o).$$

To derive $\rho_i(\underline{r},t)$ we begin by defining three general vectors. The first is

$$\underline{r}_{mi} = (x_{mi}, y_{mi}, z_{mi}) \equiv \text{position at time } t-t_o = m\Delta t \text{ of the } i\text{-th particle.} \tag{D-14}$$

The second vector that will be needed is the $3(N-\ell)$ dimensional vector

$$\underline{Y}_{m,ij\ldots\phi} = (\underline{r}_{m1},\ldots, \underline{r}_{m(i-1)}, \underline{r}_{m(i+1)},\ldots \underline{r}_{m(j-1)}, \underline{r}_{m(j+1)}\ldots \underline{r}_{mN}) \equiv \text{the vector configuration of the positions at time } t-t_o = m\Delta t \text{ of all N particles } \underline{\text{except}} \text{ the } \ell \text{ particles indicated by the subscripts } i, j,\ldots\phi\,. \tag{D-15}$$

A special example of a $\underline{Y}$ vector, and one that will be used frequently, is

$$\underline{Y}_o \equiv (\underline{r}_{o1}, \underline{r}_{o2},\ldots, \underline{r}_{oN}), \tag{D-16}$$

i.e. the vector configuration of the release points r_{oi} of all N particles of A. Finally, we define the third vector

$$\underline{\Psi}_m \equiv (\underline{Y}_1, \underline{Y}_2, \ldots, \underline{Y}_m) = \text{the space-time configuration of the positions of all N particles at each of the times } t - t_o = n\Delta t,\ n = 1,2,\ldots, m. \qquad \text{(D-17a)}$$

Note that

$$\underline{\Psi}_m = (\underline{Y}_m, \underline{\Psi}_{m-1}) = (\underline{Y}_m, \underline{Y}_{m-1}, \underline{\Psi}_{m-2}) \ldots \qquad \text{(D-17b)}$$

The main purpose in defining each of the above vectors is to keep the notation as concise as possible.

We now introduce the many-time joint probability density

$$\hat{p}(\underline{\Psi}_m | \underline{Y}_o, t_o) \qquad \text{(D-18)}$$

that N *inert* particles released at time t_o in the configuration $\underline{Y}_o$, (D-16), assume the configurations described by $\underline{\Psi}_m$ at each of the times $t - t_o = n\Delta t$, $n = 1,2,\ldots,$ m. In principle, the density (D-18) is a property solely of the turbulence.

If Δt is sufficiently small the trajectories traced out by each of the N particles during $t - t_o$ are completely described by the single vector $\underline{\Psi}_m$, where

$$t = m\Delta t + t_o. \qquad \text{(D-19)}$$

For each realization of the turbulent flow, $\underline{\Psi}_m$ is a random vector. By performing the flow experiment many, many times each time releasing the N (inert) particles in the same configuration $\underline{Y}_o$, an ensemble of vectors $\underline{\Psi}_m$ could be constructed from which $\hat{p}(\underline{\Psi}_m | \underline{Y}_o, t_o)$ could, in principle, be determined.

Now in view of the definition given earlier of a particle collision, the probability density $\rho_i(\underline{r},t)$ that the $\underline{i}$-th particle suffers no collisions while undergoing a displacement $\underline{r}-\underline{r}_{oi}$ during $t - t_o = m\Delta t$ is just the probability density of observing a vector $\underline{\Psi}_m$ with coordinate $\underline{r}_{mi} = \underline{r}$ and with coordinates $\underline{Y}_n$, $n = 1,2,\ldots m-1$, such that $\underline{r}_{ni}$ lies outside the volumes δv centered on every other coordinate $\underline{r}_{nj}$, $j = 1,2,\ldots N$ (except $j = i$) which represents a particle of A at time $t = n\Delta t$. In short, provided that Δt is sufficiently small (see section 5)

$$\rho_i(\underline{r},t) = \int d\underline{Y}_{m,i} \int_{\Omega_i^{m-1}} d\underline{\Psi}_{m-1} \left[\hat{p}(\underline{\Psi}_m | \underline{Y}_o, t_o) \right]_{\underline{r}_{mi}=\underline{r}} \qquad \text{(D-20)}$$

where t and m are related by (D-19), and where

$\Omega^n_{ij\ldots\omega} \equiv$ the region of the vector space of $\underline{\Psi}_n$ in which for each $\ell = 1,2,\ldots, n$ the $\underline{i}$-th, $\underline{j}$-th,..., and $\underline{\omega}$-th coordinates of $\underline{Y}_\ell$ lie outside the volume δv centered on each other and on every other coordinate of $\underline{Y}_\ell$ which represents a particle of A; (D-21)

$$d\underline{\Psi}_n = d\underline{r}_{11} d\underline{r}_{12} \cdots d\underline{r}_{1N} d\underline{r}_{21} \cdots d\underline{r}_{nN} \;; \qquad \text{(D-22)}$$

and

$$d\underline{Y}_{n,ij..\phi} \equiv d\underline{r}_{n1} \cdots d\underline{r}_{n(i-1)} d\underline{r}_{n(i+1)} \cdots d\underline{r}_{n(j-1)} d\underline{r}_{n(j+1)} \cdots d\underline{r}_{nN} . \qquad \text{(D-23a)}$$

Note that

$$d\underline{Y}_{n,ij..\phi}\, d\underline{r}_{ni} d\underline{r}_{nj} \cdots d\underline{r}_{n\phi} = d\underline{Y}_n \; . \qquad \text{(D-23b)}$$

Combining (D-20) and (D-13) we obtain an expression for $p_i(\underline{r},t)$ which may be used in (D-3) to compute the mean concentration of the reactive particles A in terms of the parameter δv and the Lagrangian statistics $\hat{p}(\underline{\Psi}_m|\underline{Y}_o,t_o)$ of the turbulence.

In a similar fashion we can derive expressions for the higher order position probability densities. For example, we find that

$$p_{ij}(\underline{r}',t;\underline{r}'',t) = \int d\underline{Y}_{m,ij} \int_{\Omega_{ij}^{m-1}} d\underline{\Psi}_{m-1} \left[\hat{p}(\underline{\Psi}_m|\underline{Y}_o,t_o) \right]_{\substack{\underline{r}_{mi}=\underline{r}' \\ \underline{r}_{mj}=\underline{r}''}} \tag{D-24}$$

where t is given by (D-19), and where Ω_{ij}^{m-1} and $d\underline{Y}_{m,ij}$ are defined by (D-21) (D-23) , respectively. Expression (D-24) may be used in (D-4) to compute the mean square concentration of the particles A.

Returning to equation (D-20), we evaluate the outer integrals using the definition of the marginal densities of a probability density function, namely

$$\hat{p}(\underline{r}_{mi},\underline{\Psi}_{m-1}) = \int d\underline{Y}_{m,i} \;\; \hat{p}(\underline{\Psi}_m) \; .$$

Then, with the aid of (D-17b), we write the result in the form

$$p_i(\underline{r},t) = \int_{\Omega_i^{m-2}} d\underline{\Psi}_{m-2} \int_{X_i^{m-1}} d\underline{Y}_{m-1} \left[\hat{p}(\underline{r}_{mi},\underline{\Psi}_{m-1}|\underline{Y}_o,t_o) \right]_{\underline{r}_{mi}=\underline{r}} \tag{D-25}$$

where X_i^{m-1} is the space of the vector $\underline{Y}_{m-1}$ in which the $\underline{i}$-th coordinate of $\underline{Y}_{m-1}$ lies outside the volumes δv centered on all the other coordinates $\underline{r}_{(m-1)j}$, $j = 1, 2, \ldots, N$ except $j = i$.

According to the definition of the space X_i^m, if Δt is suitably small (see section 5) the inner integral in (D-25) can be represented to good approximation by

$$\int_{X_i^{m-1}} d\underline{Y}_{m-1}\, \hat{p}(\underline{r}_{mi},\underline{\Psi}_{m-1}|\underline{Y}_o,t_o) = \int d\underline{Y}_{m-1}\, \hat{p}(\underline{r}_{mi},\underline{\Psi}_{m-1}|\underline{Y}_o,t_o)$$

$$-\sum_{j\neq i} \int d\underline{Y}_{m-1,i}\, U_j(\underline{\Psi}_{m-2}) \int_{\Delta V_{(m-1)j}} d\underline{r}_{(m-1)i}\, \hat{p}(\underline{r}_{mi},\underline{\Psi}_{m-1}|\underline{Y}_o,t_o) \qquad \text{(D-26)}$$

where we have used (D-23b) and where

$$U_j(\underline{\Psi}_n) = \begin{cases} 0, \text{ if } \underline{\Psi}_n \text{ is such that the } \underline{j}\text{-th particle has experienced at least one collision up to time } t = n\Delta t + t_o; \\ 1, \text{ otherwise;} \end{cases} \qquad \text{(D-27)}$$

ΔV_{nj} is the volume δv centered at the position $\underline{r}_{nj}$ of the $\underline{j}$-th particle at time $t_n = n\Delta t + t_o$; and $\sum_{j\neq i}$ denotes a summation on all N values of the index j except $j = i$. Substituting (D-26) into (D-25), comparing the definition (D-27) of $U_j(\underline{\Psi}_n)$ with that of Ω_i^n, (D-21), and making use of (D-13), we conclude that

$$p_i(\underline{r},t) = \int d\underline{Y}_{m-1} \int_{\Omega_i^{m-2}} d\underline{\Psi}_{m-2} \left[\hat{p}(\underline{r}_{mi},\underline{\Psi}_{m-1}|\underline{Y}_o,t_o)\right]_{\underline{r}_{mi}=\underline{r}}$$

$$-\sum_{j\neq i} \int d\underline{Y}_{m-1,i} \int_{\Delta V_{(m-1)j}} d\underline{r}_{(m-1)i} \int_{\Omega_{ij}^{m-2}} d\underline{\Psi}_{m-2} \left[\hat{p}(\underline{r}_{mi},\underline{\Psi}_{m-1}|\underline{Y}_o,t_o)\right]_{\underline{r}_{mi}=\underline{r}} \; . \qquad \text{(D-28)}$$

In order for (D-28) to be a consistant representation of the probability density $p_i(\underline{r},t)$ of the position of a reactive particle, it must reduce to the inert particle density function $\hat{p}_i(\underline{r},t)$ in the limit as the chemical reactivity vanishes. That (D-28) meets this requirement is readily seen because for inert particles the collision radius r and hence δv are zero and because when $\delta v = 0$, the space Ω_i^{m-1} (see (D-21)) becomes the entire space of $\underline{\Psi}_{m-1}$. Thus,

$$\lim_{r\to 0} p_i(\underline{r},t) = \int d\underline{Y}_{m-1} \int d\underline{\Psi}_{m-2} \left[\hat{p}(\underline{r}_{mi},\underline{\Psi}_{m-1}|\underline{Y}_o,t_o) \right]_{\underline{r}_{mi}=\underline{r}}$$

$$= \int d\underline{\Psi}_{m-1} \left[\hat{p}(\underline{r}_{mi},\underline{\Psi}_{m-1}|\underline{Y}_o,t_o) \right]_{\underline{r}_{mi}=\underline{r}}$$

$$= \hat{p}_i(\underline{r},t).$$

(Recall that we have been suppressing the reference to the particle release points in the density functions $\hat{p}_i$, p_i, ρ_i, etc.)

Equation (D-28) is the general expression for the density function $p_i(\underline{r},t)$ which we set out to derive. It describes the position probability density p_i of the particles A (which react chemically in the manner of (D-11)) in terms of the parameter δv and the Lagrangian statistics $\hat{p}(\underline{r}_{mi},\underline{\Psi}_{m-1}|\underline{Y}_o, t_o)$ of the turbulence. In a future report it will be shown that when the random, turbulence induced particle displacements can be represented by Markoff sequences in time, (D-28) combined with (D-3) yield both finite difference and differential equations for the mean particle concentrations. For the present we shall attempt to evaluate the integrals in (D-28) explicitly and thereby obtain expressions for the mean concentration which are of a more general nature.

4. EVALUATION OF THE INTEGRALS IN (D-28) — THE RELATIONSHIP BETWEEN $p_i(\underline{r},t)$ AND THE MARGINAL DENSITIES OF $\hat{p}(\underline{r}_{mi},\underline{\Psi}_{m-1})$.

In the general case where m is of arbitrary size, the evaluation of the integrals entering in (D-28) requires a series of complicated mathematical manipulations which is most easily demonstrated through the use of special operators and notations. Without these artifices the analysis is hopelessly unwieldy. The formulas derived here will be applied to two specific problems in Section 6.

Only two basic operators will be needed, I_λ and $D_{\lambda,\gamma\delta\ldots,ij\ldots}$. The first of these is a simple integration operator defined such that if

$$f(\underline{Y}_1,\underline{Y}_2,\ldots,\underline{Y}_n) = f(\underline{\Psi}_n) = f(\underline{Y}_n,\underline{\Psi}_{n-1}) = \ldots, \tag{D-29}$$

(cf. (D-17b)) is a function of the configuration vectors $\underline{Y}_i$, then

$$I_\lambda f(\underline{\Psi}_n) = \int d\underline{Y}_\lambda\ f(\underline{\Psi}_n), \qquad \lambda \leq n\ ; \tag{D-30}$$

where λ and n are integers and $d\underset{\sim}{Y}_n$ is defined by (D-23a). Multiple operations are clearly possible:

$$I_\lambda I_\mu\ f(\underline{\Psi}_n) = \int d\underline{Y}_\mu \int d\underline{Y}_\lambda f(\underline{\Psi}_n), \qquad \lambda \neq \mu, \quad \lambda,\mu \leq n\ ; \tag{D-31}$$

etc.; provided that no two of the operators involved are identical. It follows that the operator I is commutative, e.g. $I_\lambda I_\mu = I_\mu I_\lambda$, etc.

The second operator $D_{\lambda,\gamma\delta\ldots,ij\ldots}$, is designed to operate only on I_λ. We define it such that

$$D_{\lambda,\gamma\delta..b,ij..\beta} I_\lambda f(\underline{\gamma}_m) = \sum_{\gamma\neq i,j..\beta} \sum_{\delta\neq i,j..\beta} \cdots \sum_{b\neq i,j..,\beta} \int d\underline{\Upsilon}_{\lambda,ij..\beta} \int_{\Delta V_{\lambda\gamma}} d\underline{r}_{\lambda i} \cdots \int_{\Delta V_{\lambda b}} d\underline{r}_{\lambda\beta}\, f(\underline{\gamma}_m) \tag{D-32}$$

where $\Delta V_{\lambda j}$ denotes the volume δv (D-12) centered at the point $\underline{r}_{\lambda j}$. As examples of the operation of D on I we cite the following:

$$D_{\lambda,j,i}\, I_\lambda\, f(\underline{\gamma}_n) = \sum_{j\neq i} \int d\underline{\Upsilon}_{\lambda,i} \int_{\Delta V_{\lambda j}} d\underline{r}_{\lambda i}\, f(\underline{\gamma}_n), \tag{D-33}$$

$$D_{\lambda,k\ell,ij}\, I_\lambda\, f(\underline{\gamma}_n) = \sum_{k\neq i,j} \sum_{\ell\neq i,j} \int d\underline{\Upsilon}_{\lambda,ij} \int_{\Delta V_{\lambda k}} d\underline{r}_{\lambda j} \int_{\Delta V_{\lambda \ell}} d\underline{r}_{\lambda i}\, f(\underline{\gamma}_n). \tag{D-34}$$

Note that operations such as

$D_{\lambda,j,i}\, f(\underline{\gamma}_n)$; $D_{\lambda,j,i}\, I_\mu$, $\lambda \neq \mu$; etc. are undefined.

Using these newly defined operators, we can write (D-28) in the form

$$P_i(\underline{r},t) = I_{m-1} \int_{\Omega_i^{m-2}} d\underline{\gamma}_{m-2}\, \hat{P}_{mi} - D_{m-1,j,i}\, I_{m-1} \int_{\Omega_{ij}^{m-2}} d\underline{\gamma}_{m-2}\, \hat{P}_{mi}, \tag{D-35}$$

where for brevity we have written

$$\hat{P}_{mi} = [\hat{p}(\underline{r}_{mi}, \underline{\gamma}_{m-1} | \underline{\Upsilon}_o, t_o)]_{\underline{r}_{mi}=\underline{r}} \tag{D-36}$$

and where $t = m\Delta t + t_o$ as before. The integral over the space Ω_i^n was discussed in the previous section. The result obtained there (compare (D-25) and (D-11)) may be used to evaluate the first integral in (D-35). We obtain

$$\int_{\Omega_i^{m-2}} d\underline{\Psi}_{m-2}\, \hat{P}_{mi} = \int_{\Omega_i^{m-3}} d\underline{\Psi}_{m-3} \int_{X_i^{m-2}} d\underline{\Psi}_{m-2}\, \hat{P}_{mi} \,. \qquad \text{(D-37)}$$

The integral over X_i^{m-2} entering here is evaluated in turn by analogy with (D-26). Without going through the details, which are rather straightforward, we state simply that

$$\int_{X_i^{m-2}} d\underline{\Psi}_{m-2}\, \hat{P}_{mi} = (I_{m-2} - D_{m-2,j,i}\, I_{m-2}\, \Phi_{m-3})\, \hat{P}_{mi}, \qquad \text{(D-38)}$$

where Φ_{n-1} is a function such that

$$\int_{\Omega_{\lambda\mu..r}^{n-1}} \Phi_{n-1} D_{n,\gamma\delta..b,ij..} I_n \hat{P}_{mi}\, d\underline{\Psi}_{n-1} = \int_{\Omega_{\lambda\mu..r\gamma\delta..b}^{n-1}} D_{n,\gamma\delta..b,ij..} I_n \hat{P}_{mi}\, d\underline{\Psi}_{n-1} \qquad \text{(D-39)}$$

Combining (D-37) and (D-38) yields

$$\int_{\Omega_i^{m-2}} d\underline{\Psi}_{m-2}\, \hat{P}_{mi} = I_{m-2} \int_{\Omega_i^{m-3}} d\underline{\Psi}_{m-3}\, \hat{P}_{mi} - D_{m-2,j,i}\, I_{m-2} \int_{\Omega_{ij}^{m-3}} d\underline{\Psi}_{m-3}\, \hat{P}_{mi}. \qquad \text{(D-40)}$$

Next, we consider the last integral on the right-hand side of (D-35). In analogy with (D-37) we write

$$\int_{\Omega_{ij}^{m-2}} d\underline{\Psi}_{m-2}\, \hat{P}_{mi} = \int_{\Omega_{ij}^{m-3}} d\underline{\Psi}_{m-3} \int_{X_{ij}^{m-2}} d\underline{\Psi}_{m-2}\, \hat{P}_{mi} \qquad \text{(D-41)}$$

where χ_{ij}^{m-2} is the region of the vector space of $\underline{Y}_{m-2}$ in which neither of the coordinates $\underline{r}_{(m-2)i}$ and $\underline{r}_{(m-2)j}$ lies within the volumes δv centered on each other and on the coordinates of every other particle of A. The evaluation of the integral over χ_{ij}^{m-2} proceeds in a manner similar to that which led to (D-26) but the analysis is more complicated and it gets worse with each successive higher order space χ_{ijk}^{n}, $\chi_{ijk\ell}^{n}$, etc. However, it is found that if the total number N of particles released is very large, N >> 1, integrations over χ space may be expressed in the form

$$\int_{\chi_{ij..\beta}^{n}} d\underline{\Psi}_n \, \hat{P}_{mi} = \left[I_n + \sum_{\alpha=1}^{\nu} (-1)^{\alpha} a_{\alpha} D_n^{\alpha} \phi_{n-1} I_n \right] \hat{P}_{mi} \tag{D-42}$$

where ν is the total number of subscripts on $\chi_{ij..r}^{n}$; and

$$\left.\begin{aligned} a_1 D_n^1 &= D_{n,\gamma,i} + D_{n,\gamma,j} + \cdots D_{n,\gamma,\beta} \\ a_2 D_n^2 &= D_{n,\gamma\delta,ij} + D_{n,\gamma\delta,ik} + \cdots D_{n,\gamma\delta,i\beta} + D_{n,\gamma\delta,jk} + \\ &\qquad D_{n,\gamma\delta,j\ell} + \cdots D_{n,\gamma\delta,\alpha\beta} \\ &\text{etc.,} \end{aligned}\right\} \tag{D-43}$$

i.e. $a_\alpha D_n^\alpha$ is the sum of the $a_\alpha = \frac{\nu!}{\alpha!(\nu-\alpha)!}$ operators $D_{n,\gamma\delta..,\lambda\mu...}$ which can be formed by taking the α subscripts $\lambda,\mu,\ldots$ on D from the set $i,j,\ldots\beta$ in combinations α at a time.

Upon using (D-42) in (D-43) we get

$$\int_{\Omega_{ij}^{m-2}} d\underline{\Psi}_{m-2}\,\hat{P}_{mi} = I_{m-2}\int_{\Omega_{ij}^{m-3}} d\underline{\Psi}_{m-3}\,\hat{P}_{mi} - D_{m-2,\gamma,i}\,I_{m-2}\int_{\Omega_{ij\gamma}^{m-3}} d\underline{\Psi}_{m-3}\,\hat{P}_{mi}$$

$$-D_{m-2,\gamma,j}\,I_{m-2}\int_{\Omega_{ij\gamma}^{m-3}} d\underline{\Psi}_{m-3}\,\hat{P}_{mi} + D_{m-2,\gamma\delta,ij}\,I_{m-2}\int_{\Omega_{ij\gamma\delta}^{m-3}} d\underline{\Psi}_{m-3}\,\hat{P}_{mi}\;; \qquad \text{(D-44)}$$

and on substituting (D-44) and (D-40) into (D-35), we obtain an expression for $p_i(\underline{r},t)$ in terms of integrals over $\Omega_{ij..}^{m-3}$ — we started, (D-35) with $p_i(\underline{r},t)$ as a function of integrals over $\Omega_{ij..}^{m-2}$. By repeating the above process of reducing Ω integrals to multiple integrals over Ω are χ and applying (D-42) to the resulting χ integrals, we can eventually (after m iterations) eliminate all of the Ω integrals and thereby obtain the desired expression relating $p_i(\underline{r},t)$ to the marginal densities of p_{mi}. However, upon undertaking this task one soon finds that the number of terms in the final expression for $p_i(\underline{r},t)$ is enormous even when m is relatively small. To illustrate this point, if $m = 2$ the required expression for $p_i(\underline{r},t)$ is found immediately from (D-35):

$$p_i(\underline{r},t) = I_1\hat{p}_{2i} - D_{1,j,i}\,I_1\hat{p}_{2i}, \quad m = 2. \qquad \text{(D-45)}$$

This equation contains only two basic terms. For the case $m = 3$, it is found from (D-35), (D-40), and (D-44) that $p_i(\underline{r},t)$ is the sum of six basic terms; and in like manner, 42 terms are found in the formula for $p_i(\underline{r},t)$ when $m = 4$; the case $m = 5$ requires 1806 terms to describe $p_i(\underline{r},t)$; $m = 6$ requires over 3.3 million terms; etc. Fortunately, the full expression can be handled rather easily by grouping the terms in ascending orders of the operator D. The meaning of the term "order" of the operator as used here is best explained by examples; $D_{n,\gamma,i}$ is of order one, $(D_{n,\gamma,i} D_{n-1,\gamma,i})$ is order two, $D_{n,\gamma\delta,ij}$ is order two, etc. The expression for $p_i(\underline{r},t)$ to fourth order in D is as follows:

$$p_i(\underline{r},t) = \sum_{q=0}^{m-1} s_q \, \hat{p}_i(\underline{r},t) \ , \quad t = m\Delta t; \qquad \text{(D-46)}$$

where

$$\left.\begin{aligned}
s_o &= 1 \\
s_1 &= - \sum_{a=1}^{m-1} D_a \\
s_2 &= \sum_{a=1}^{m-2} (2D_a) \sum_{b=a+1}^{m-1} D_b \\
s_3 &= - \sum_{a=1}^{m-3} (3D_a) \sum_{b=a+1}^{m-2} (2D_b) \sum_{c=b+1}^{m-1} D_c - \sum_{a=1}^{m-2} D_a^2 \sum_{b=a+1}^{m-1} D_b \\
s_4 &= \sum_{a=1}^{m-4} (4D_a) \sum_{b=a+1}^{m-3} (3D_b) \sum_{c=b+1}^{m-2} (2D_c) \sum_{d=c+1}^{m-1} D_d \\
&\quad + \sum_{a=1}^{m-3} (4D_a) \sum_{b=a+1}^{m-2} D_b^2 \sum_{c=b+1}^{m-1} D_c + \sum_{a=1}^{m-3} (3D_a^2) \sum_{b=a+1}^{m-2} (2D_b) \sum_{c=b+1}^{m-1} D_c
\end{aligned}\right\} \text{(D-47)}$$

Keep in mind that $\hat{p}_i(\underline{r},t) = I_{m-1} I_{m-2} \cdots I_1 \hat{P}_{mi}$. The meaning of the term $b_\alpha D_d^\alpha$ entering in (D-47) is different than that of (D-43). For example, in (D-47)

$$\sum_{d=e}^{m-1} D_d = \sum_{d=e}^{m-1} D_{d,\gamma,i} \qquad ; \qquad \text{(D-48)}$$

$$(2D_d) \sum_{e=d+1}^{m-1} D_e = \left[D_{d,\lambda,\gamma} + D_{d,\lambda,i} \right] \sum_{e=d+1}^{m-1} D_{e,\gamma,i}; \qquad \text{(D-49)}$$

$$(3D_c) \sum_{d=c+1}^{m-2} (2D_d) \sum_{e=d+1}^{m-1} D_e = \left[D_{c,\nu,\lambda} + D_{c,\nu,\gamma} + D_{c,\nu,i} \right] \sum_{d=c+1}^{m-2} (2D_d) \sum_{e=d+1}^{m-1} D_c ; \qquad \text{(D-50)}$$

$$D_d^2 \sum_{e=d+1}^{m-1} D_d = D_{d,\lambda\mu,\gamma i} \sum_{e=d+1}^{m-1} D_{e,\gamma,i} ; \qquad \text{(D-51)}$$

etc.

where the subscript i refers to the same particle as the subscript i in (D-46) and where the number N of particles is assumed to be very large. Referring to the general form $D_{n,\dagger,*}$ of the operator D, we note from the above examples that $(b_\alpha D_d^\alpha)$ in (D-47) denotes the sum of the b_α α-th order operators $D_{d \cdot\cdot,\cdot\cdot}$ whose * subscripts are unique combinations, taken α at a time, of the distinct indices in both the † and * subscripts of all operators to the right of $(b_\alpha D_d^\alpha)$. A further example of the application of (D-47) may be found in Section 6.1.

Equations (D-46) and (D-47) together with the definition (D-32) of the operator D provide the desired general relationships between the position probability density $p_i(\underset{-}{r},t)$ of the chemically reactive A particles (see (D-11)) and the position probability densities of inert particles in the fluid, i.e. the Lagrangian statistics of the turbulence. One of the obvious points revealed by these formulas is the great complexity of the relationship between the mean concentration of a nonlinearly reactive substance, obtained from $p_i(\underset{-}{r},t)$ through (D-3), and the Lagrangian statistics of the turbulence. Because of the magnitude of this complexity, only a limited class of problems can be treated with the Lagrangian theory that we have developed here. In Section 6 we shall apply (D-46) and (D-47) to two problems in which the analysis is relatively simple but first it is necessary to establish the conditions which the interval Δt must meet in order for the formulas to be accurate.

5. CONDITION ON THE DISCRETIZATION INTERVAL Δt.

In deriving the theory in Section 3, only two basic restrictions were placed on Δt. The first of these is embodied in the fundamental premise that two particles collide during the period $t - \Delta t/2 \le t' \le t + \Delta t/2$ if the position of one of them at time t' falls within the volume δv, of size (D-12) and of spherical shape, centered on the other's position at time t. Intuitively, this premise seems plausable if the radius r_s of the sphere of volume δv satisfies $r_s \ge \overline{u'^2}^{1/2}\,\Delta t$, i.e. if

$$\Delta t \le \frac{\gamma}{\overline{u'^2}^{1/2}} \quad ; \qquad \text{(D-52)}$$

because otherwise, the actual position of the one particle during $t - \Delta t/2$ to $t + \frac{\Delta t}{2}$ may lie outside the spherical volume δv centered at its position at the midpoint t of the interval.

The second restriction on Δt is implicit in the approximation (D-26) of the integral over the space χ. By definition χ_i^{m-1}, for example, denotes the space of the configuration vector $\underline{Y}_{m-1}$ in which (1) the coordinate $\underline{r}_{(m-1)i}$ of the *i*-th particle lies outside the (spherical) volumes δv centered at the position $\underline{r}_{(m-1)j}$ of all reactant particles, e.g. particles of A; and (2) the coordinates of all particles other than the *i*-th lie anywhere. Now (D-26) approximates the integral with respect to $\underline{r}_{(m-1)i}$ over χ_i^{m-1} by the integral of $\underline{r}_{(m-1)i}$ over its entire space, i.e. $-\infty$ to $+\infty$, minus the integral with respect to $\underline{r}_{(m-1)i}$ over the volume δv centered on each particle of A. Clearly, this approximation is valid as long as none of the volumes δv overlap. To insure that this is the case, we must require that δv be much smaller than the average volume occupied by the particles in the region of maximum particle concentration. That is, if $< c_{max} >$ denotes the maximum concentration that is likely to be observed in the fluid, say

$$< c_{max} > = \max_{\underline{r},t} \; [< c^2(\underline{r},t) > ^{1/2}] \,, \qquad \text{(D-53)}$$

then we require that

$$\Delta t << T_c, \qquad \text{(D-54)}$$

where

$$T_c = [k < c_{max} >]^{-1} \qquad \text{(D-55)}$$

and

$$k \equiv \pi\gamma^2 \overline{u'^2}^{1/2} . \qquad \text{(D-56)}$$

Note that in terms of k, which incidentally has the dimensions of a reaction rate coefficient, we have

$$\delta v = k\Delta t. \qquad \text{(D-57)}$$

In light of this fact, it is clear that T_c is essentially a characteristic time scale of the particle reaction, and that (D-54) is a requirement that Δt be sufficiently small to resolve the smallest temporal variations in the concentration produced by the chemical reaction.

Due to the heuristic nature of the model of chemical reactions proposed in section 3, satisfying condition (D-52) and (D-54) will not of itself guarantee the accuracy of results derived from this model. Thus, these conditions should be viewed more as necessary, rather than sufficient, conditions for achieving accuracy. In this regard, (D-54) is probably the more important of the two conditions since it stems from a mathematical approximation.

6. APPLICATION OF EQUATION (D-46) to SPECIFIC PROBLEMS.

6.1 Slow second-order reaction in a well-stirred vessel.

As a first example of an application of (D-46) we consider the situation where a dilute mixture of the substance A which reacts chemically according to (D-11) is present in a reaction cell. It is assumed that the cell is continually stirred so that if any foreign substance is introduced into the cell at any time, it becomes thoroughly mixed throughout the cell within a time T_m. Suppose that the time scale T_c, (D-55), of the reaction is sufficiently large that an interval Δt exists such that

$$T_c \gg \Delta t \gg T_m . \qquad \text{(D-58)}$$

This value of Δt satisfies (D-54); so if we assume that it also meets condition (D-52), it can be used in (D-46).

Since Δt is much larger than the mixing time scale T_m, it is to be expected that the position of any particle at time $n\Delta t$ is statistically independent of its position at any other time $m\Delta t$, $m \neq n$; and that the positions of the particles at any given time are statistically independent of one another. These two results give rise to the relationships

$$\hat{p}_{mi} \equiv \hat{p}(\underline{r}_{mi}, Y_{m-1} | \underline{Y}_o, t_o)$$

$$= \hat{p}(\underline{r}_{mi})\, \hat{p}(\underline{Y}_{m-1})\, \hat{p}(\underline{Y}_{m-2}) \cdots \hat{p}(\underline{Y}_1) \quad ; \qquad \text{(D-59)}$$

and

$$\hat{p}(\underline{Y}_n) \equiv \hat{p}(\underline{r}_{n1}, \underline{r}_{n2}, \ldots, \underline{r}_{nN})$$

$$= \hat{p}(\underline{r}_{n1})\hat{p}(\underline{r}_{n2}) \ldots \hat{p}(\underline{r}_{nN}); \qquad \text{(D-60)}$$

respectively. Furthermore, when the above conditions are satisfied it is logical that the marginal densities $\hat{p}(\underline{r}_{ni})$ of each particle will be equal and will be constant in space and time, i.e.

$$\hat{p}(\underline{r}_{ni}) = \rho = \text{constant}, \qquad i = 1,2,\ldots N. \qquad \text{(D-61)}$$

Turning now to the evaluation of (D-46)-(D-47), we have from (D-47), (D-48), and (D-33)

$$s_1\hat{p}_i(\underline{r},t) = -\sum_{a=1}^{m-1} \sum_{\gamma \neq i} \int d\underline{Y}_{a,i} \int_{\Delta V_{a\gamma}} d\underline{r}_{ai} \left[\hat{p}(\underline{r}_{mi}, \underline{Y}_a)\right]_{\underline{r}_{mi}=\underline{r}} \qquad \text{(D-62)}$$

where the integration range of the outer integral is the entire volume of the reaction vessel. Due to (D-59)-(D-61), (D-62) reduces to

$$s_1\hat{p}_i(\underline{r},t) = (m-1)(N-1)\ \delta v \rho^2 \ . \qquad \text{(D-63)}$$

The second order term in (D-46)-(D-47) is found from (D-49) and (D-33):

$$s_2\hat{p}_i(\underline{r},t) = \sum_{a=1}^{m-2} \left\{ \sum_{\lambda \neq \gamma} \int d\underline{Y}_{a,\gamma} \int_{\Delta V_{a\lambda}} d\underline{r}_{a\gamma} \left[\sum_{b=a+1}^{m-1} \sum_{\gamma \neq i} \int d\underline{Y}_{b,i} \int_{\Delta V_{b\gamma}} d\underline{r}_{bi} \right.\right.$$

$$\left. \hat{p}(\underline{r}_{mi}, \underline{Y}_b, \underline{Y}_a) \right]_{\underline{r}_{mi}=\underline{r}} + \sum_{\lambda \neq i} \int d\underline{Y}_{a,i} \int_{\Delta V_{a\lambda}} d\underline{r}_{ai}$$

$$\left[\sum_{b=a+1}^{m-1} \sum_{\gamma \neq i} \int d\underline{Y}_{b,i} \int_{\Delta V_{b\gamma}} d\underline{r}_{bi} \, \hat{p}(\underline{r}_{mi}, \underline{Y}_b, \underline{Y}_a) \right]_{\underline{r}_{mi}=\underline{r}} \Bigg\} . \tag{D-64}$$

This expression reduces by virtue of (D-59)-(D-61) to the form

$$s_2 P_i(\underline{r},t) = (m-1)(m-2)(N-1)^2 \, \delta v^2 \rho^3 . \tag{D-65}$$

Similarly we find

$$s_3 \, \hat{P}_i(\underline{r},t) = -(m-1)(m-2)(m-3)(N-1)^3 \delta v^3 \rho^4$$

$$- 1/2 \, (m-1)(m-2)(N-1)^3 \delta v^3 \rho^4 , \tag{D-66}$$

etc. Substituting (D-63), (D-64), (D-65), etc. into (D-46) and making use of (D-57) we obtain for the case of large N,

$$P_i(\underline{r},t) = \rho[1 - (N\rho)(m-1)k\Delta t + (N\rho)^2(m-1)(m-2) \, k^2\Delta t^2$$

$$- (N\rho)^3(m-1)(m-2)(m-3)k^3\Delta t^3 - \frac{1}{2}(N\rho)^3(m-1)(m-2)k^3\Delta t^3$$

$$+ (N\rho)^4(m-1)(m-2)(m-3)(m-4)k^4\Delta t^4 + \ldots]$$

$$= p(m\Delta t). \tag{D-67}$$

The mean particle concentration is found from (D-3) and (D-67), to be

$$< c(m\Delta t) > = Np(m\Delta t). \tag{D-68}$$

It is evident from (D-68) and (D-67) that

$$< c(0) > = N\rho . \tag{D-69}$$

Since this is the maximum concentration which will be observed in the vessel, $N\rho$ is a suitable measure of $< c_{max} >$, which enters in the definition (D-55) of T_c. Thus, we write

$$T_c = (N\rho k)^{-1}. \tag{D-70}$$

At this point it is convenient to nondimensionalize the time and concentration variables as follows:

$$\Delta t^* = \Delta t/T_c \ , \ t^* = m\Delta t^* \ ; \tag{D-71}$$

$$< c^* (t^*) > = \frac{<c(t^*)>}{<c(0)>} = \frac{<c(t^*)>}{N\rho} \ ; \tag{D-72}$$

because with these variables, the passage of equation (D-67) to the limit $\Delta t^* \to 0$ for fixed $t^* = m\Delta t^*$ yields the simple result

$$< c^*(t^*) > = 1 - t^* + t^{*2} - t^{*3} + \dots \ . \tag{D-73}$$

It should be pointed out that the limit $\Delta t^* \to 0$ is achieved by taking $\Delta t \to 0$ because T_c is fixed; but since T_m is also fixed, condition (D-58) places a lower bound on the permissible values of Δt. As a result, the validity of (D-73) requires that the mixing time T_m be several orders of magnitude smaller than T_c.

The important aspect of (D-73) which we wish to stress here is that the right hand side of this equation is the series expansion of the binomial

$$(1 + t^*)^{-1}$$

which in turn is the solution of the differential equation

$$\frac{d<c^*>}{dt^*} = - < c^* >^2 \tag{D-74}$$

with initial condition $<c^*(0)> = 1$.

This is the classical equation for describing the rate of second order reactions such as $A + A \rightarrow B$ in well-stirred reaction cells (cf. (D-2)). The fact that the assumptions which were employed to derive (D-73) are consistant with those under which (D-74) have been found correct serves to corroborate, to some extent, the theory developed here.

6.2 A slender plume of a second order reactant in homogeneous, stationary turbulence.

To illustrate the application of (D-46) to a more general problem, we consider the problem of an infinite continuous line source of particles A, which undergo the second order reaction $A + A \rightarrow B$, in a field of stationary, homogeneous, turbulence. It is assumed that the line source lies on the y axis and has finite width, L: and that the fluid has a mean speed $\bar{u}$ directed along the x axis. Furthermore, the variation of mean particle concentration in the x direction is assumed to be so small that diffusion in this direction is negligible compared to the transport (the slender plume approximation). Under these conditions the concentration distribution in the plume can be represented by a one-dimensional, time dependent model with space variable z, and time coordinate t related to x through the transformation

$$x = \bar{u}t \, . \tag{D-75}$$

The initial condition is taken to be

$$c(z,0) = \begin{cases} Q/\bar{u}L & , \; |\, z \,| < L/2; \\ 0 & , \; \text{otherwise.} \end{cases}$$

Here Q denotes the number of particles emitted per unit length of the source per unit time.

Several measures will be taken to keep the ensuing analysis as simple as possible. These are as follows:

First, only the simplest nontrivial case of (D-46) will be considered. In particular, we set $m = 2$ in this equation and thereby obtain

$$p_i(z,t_2) = \hat{p}_i(z,t_2) - \sum_{j \neq i} \int dz_j(t_1) \int_{z_j(t_1)-\delta z}^{z_j(t_1)+\delta z} dz_i(t_1) \left[\hat{p}(z_i(t_2), z_i(t_1), z_j(t_1)) \right]_{z_i(t_2)=z} \tag{D-76}$$

where $z_i(t_n)$ denotes the position of the $\underline{i}$-th particle at time $t_n = n\Delta t$, and where $2\delta z$ is the characteristic dimension of δv. Due to restriction (D-54), (D-76) will be valid only in the time range $0 \leq t_2 \lesssim T_c/5$, where the time scale T_c is based on $c(z,o)$.

Secondly, for the sake of brevity we adopt the following notation throughout the remainder of this section

$$\left. \begin{array}{l} z_i(\Delta t) = z_i' \\ z_i(2\Delta t) = z_i'' \end{array} \right\} . \tag{D-77}$$

Finally, we shall assume that the root-mean-square particle displacement $< z_i'^2 >^{1/2}$ at time $t = \Delta t$ is large compared to the distance L over which the particles are initially distributed. This assumption is not essential but it leads to a considerable simplification of the mathematics. This is because when $L << <z'^2>^{1/2}$, the displacement statistics entering in (D-76) are nearly equal for all particles, i.e.

$$\hat{p}(z_i') = \hat{p}(z_j') = \hat{p}(z,t_1), \text{ if } z_i' = z_j' = z. \tag{D-78a}$$

For convenience we shall further assume that the statistics of all particle pairs are effectively the same, viz.

$$\hat{p}(z_i'',z_i',z_j') = \hat{p}(z_k'',z_k',z_\ell'), \text{ if } z_i'' = z_k'', \text{ etc.} \tag{D-78b}$$

Under these conditions the expression for the mean concentration distribution at a point $x = 2\bar{u}\Delta t$ from the source is easily found from (D-76) and (D-3) to be

$$< c(z,t_2) > = N\hat{p}(z,t_2) - N^2 \int dz_2' \int_{z_2'-\delta z}^{z_2'+\delta z} dz_1' \hat{p}(z_1'',z_1',z_2')_{z_1''=z} . \qquad \text{(D-79)}$$

where $N = Q/\bar{u}$, i.e. the number of particles released in a square cylinder with x and y dimensions of unity. Note that $N\hat{p}(z,t_2) = < c_I(z,t_2) >$ is the mean concentration which would be observed if the species A were chemically inert.

Neither empirical data nor theoretical methods are currently available which can specify the forms of the joint probability density $p(z_1'',z_1',z_2')$ entering in (D-79). Therefore, it will be necessary to hypothesize a form consistent with the limited information which is available.

First, we know that if the turbulence is homogeneous, as assumed here, the marginal densities $p(z_1'')$, $p(z_1')$, and $p(z_2')$ are all Gaussian. This fact was first pointed out by Batchelor (1949) based on empirical data and theoretical arguments.

Secondly, due to the absence of a mean velocity component in the z direction we must have

$$< z_i(t_n) > = 0. \qquad \text{(D-80)}$$

By formulating the second moments of $\hat{p}(z_1'',z_1',z_2')$ in terms of the Lagrangian velocity correlation functions, we can use data on those statistics to obtain additional information. Following the lead of Taylor (1921) we obtain an expression for the second moments of the general density $\hat{p}(z_j(t+\Delta t),z_j(t),z_i(t))$, namely

$$< z_i(t) z_j(t+\Delta t) > = \int_{0}^{t} \int_{-\Delta t}^{t''} R_{ij}(t'',\xi) d\xi dt'' + \int_{\Delta t}^{t+\Delta t} \int_{\Delta t}^{t''} R_{ji}(t'',\xi) \, d\xi dt'' \qquad \text{(D-81)}$$

where

$$R_{ij}(t,\xi) \equiv < w_i(t) \; w_j(t - \xi) > \qquad \text{(D-82)}$$

is the covariance of the radial component of the Lagrangian turbulent velocities of the *i*-th and *j*-th particles.

Deardorff (1970) has found in an empirical-theoretical study of plane Poiseuille flow that the Lagrangian covariance $R_{ij}(t,\xi)$ is described to good approximation by

$$R_{ij}(t,\xi) = \overline{w'^2} \, R_o \exp \left[- \left(\frac{|\xi|}{T} + \frac{\mu |t|}{T} \right) \right] \qquad \text{(D-83)}$$

in the case where the turbulent intensity $\overline{w'^2}$ is stationary. In (D-83) T is the Lagrangian time scale

$$T \equiv \frac{1}{\overline{w'^2}} \int_{0}^{\infty} R_{ii}(t,\xi) \, d\xi \qquad \text{(D-84)}$$

which is independent of t by virtue of the assumption of homogeneous, stationary turbulence; R_o is a constant in the range $0 \leq R_o \leq 1$ depending on the initial separation of the particles; and

$$\mu = \frac{1-R_o}{\lambda} \qquad \text{(D-85)}$$

where $\lambda > 1$ is a constant whose value is established by the nature of the turbulence. In lieu of a detailed analysis of the two particle statistics, as would be possible, for example, using the work of Batchelor (1950), we shall adopt the rather simple statistics (D-83) leaving a more detailed analysis to a future study.

Non-dimensionalizing time with the time scale T and length with $\overline{w'^2}^{1/2}\,T$ and then substituting (D-83) into (D-81), we obtain

$$< z_1(\Delta t^*)z_2(\Delta t^*) >^* = <z_1'z_2' >^* = \frac{2R_o}{1+\mu}\left(e^{-(1+\mu)\Delta t^*}-1\right) - \frac{2R_o}{\mu}\left(e^{-\mu\Delta t^*}-1\right) \qquad \text{(D-86)}$$

$$< z_1(2\Delta t^*)z_2(\Delta t^*) >^* = <z_1''z_2' >^* = \frac{R_o}{1+\mu}\left(e^{-2(1+\mu)\Delta t^*}-1\right)$$

$$- \frac{R_o}{\mu}\left(e^{-\mu\Delta t^*}-1\right)\left(2 + e^{-(1+\mu)\Delta t^*}-e^{-\Delta t^*}\right) \qquad \text{(D-87)}$$

where a star (*) denotes a non-dimensional variable, e.g.

$$\Delta t^* = \Delta t/T \ ,$$

$$< z_i(t)z_j(t') >^* = \frac{<z_i(t)z_j(t')>}{\overline{w'^2}\,T^2} \ , \text{etc.}$$

The mean square particle displacements and the two-time auto-covariances of the particle positions are also obtainable from (D-81) and (D-83). We set $R_o = 1$ ($\mu=0$) in (D-83), to simulate the release of two particles from the same point, and thereby obtain an expression for the auto correlation function $R_{ii}(\xi)$. The resulting expression is then used in (D-81) to obtain

$$< z_1'z_1'' >^* = e^{-2\Delta t^*} + 2\Delta t^* - 1 \quad , \qquad \text{(D-88)}$$

$$< z_1'^2 >^* = <z_2'^2>^* = 2(e^{-\Delta t^*} +\Delta t^* - 1), \qquad \text{(D-89)}$$

$$< z_1''^2 >^* = 2(e^{-2\Delta t^*} + 2\Delta t^* - 1). \qquad \text{(D-90)}$$

We now have expressions for all of the second moments of $\hat{p}(z_1'',z_1',z_2')$. Since information about the third and higher moments is unavailable, a logical step at this point is to assume that $\hat{p}$ is a jointly normal density function because this density is completely determined by its first and second moments. (While this assumption is compatible with the normality of the marginal densities of $\hat{p}$, it is inconsistent with the fact that for small particle separations the joint particle displacements are dominated by small scale features of the turbulent velocity field which are known not to have Gaussian properties.) Accordingly we have

$$\hat{p}(z_1'',z_1',z_2') = [2\pi^3|\mu|]^{-1/2} \exp\left(-\frac{1}{2}\,\underset{-}{Z}\,\mu^{-1}\,\underset{-}{Z}^t\right) \qquad \text{(D-91)}$$

where $\underset{-}{Z}^t$ is the transpose of the vector $\underset{-}{Z} = (z_1'',z_1',z_2')$, and $|\mu|$ and μ^{-1} are the determinant and inverse, respectively, of the covariance matrix

$$\mu = \begin{bmatrix} < z_1'^2 > & < z_1' z_2' > & < z_1' z_1'' > \\ < z_1' z_2' > & < z_2'^2 > & < z_2' z_1'' > \\ < z_1' z_1'' > & < z_2' z_1'' > & < z_1''^2 > \end{bmatrix}. \qquad \text{(D-92)}$$

The elements μ_{ij} of the matrix μ are given by equations (D-86)-(D-88). The first moments $<z_1'> = <z_2'> = <z_1''> = 0$ have already been incorporated in (D-91).

If it is assumed that the interval δz is small compared to the length scale of variations in $\hat{p}(z_1'',z_1',z_2')$ for fixed z_1'' and z_2', then (D-79) reduces to

$$< c(z,t_2) > = < c_I(z,t_2) > - 2\delta z N^2 \int_{-\infty}^{\infty} dz_2' \left[\hat{p}(z_1'', z_1', z_2') \right]_{\substack{z_1''=z \\ z_1'=z_2'}} \quad . \tag{D-93}$$

Upon inserting (D-91) into (D-93) and performing the integration, we obtain after some heavy algebra

$$< c(z,t_2) > = [1 - \beta(z,t_1,t_2)] < c_I(z,t_2) > , \tag{D-94}$$

where

$$< c_I(z,t_2) > = N[2\pi < z_1''^2 >]^{-1/2} \exp\left(- \frac{1}{2} \frac{z^2}{<z_1''^2>}\right) , \tag{D-95}$$

and

$$\beta(z,t_1,t_2) = \frac{(Nk\Delta t) \exp\left[- \frac{z^2}{2\sigma''^2} \left(\frac{\frac{1}{2}(\rho_2''-\rho_1'')^2}{1-\rho' - \frac{1}{2}(\rho_2''-\rho_1'')^2} \right) \right]}{2\pi^{1/2}\sigma' [1-\rho' - \frac{1}{2}(\rho_2'' - \rho_1'')^2]^{1/2}} \quad . \tag{D-96}$$

Here $k\Delta t = 2\delta z$ and

$$\left.\begin{aligned} \sigma'^2 &= < z_1'^2 > = < z_2'^2 > , \\ \sigma''^2 &= < z_1''^2 > , \end{aligned}\right\} \tag{D-97a}$$

$$\rho_j'' = \frac{<z_1'' z_j'>}{\sigma''\sigma'} \quad , \tag{D-97b}$$

and

$$\rho' = \frac{<z_1' z_2'>}{\sigma'^2} \quad . \tag{D-97c}$$

The significance of the factor β becomes clearer when we note from (D-9) that if the chemical reaction which consumes the species A were a first order reaction, the expression analogous to (D-94) would be

$$< c_f(z,t_2) > = (1 - \beta_f(t_2)) < c_I(z,t_2) > , \tag{D-98}$$

where

$$\beta_f(t_2) = k_f t_2 \tag{D-99}$$

and k_f is the first order rate constant. An important difference between β and β_f, which we shall explore shortly, is that β varies in z while β_f does not.

Equation (D-94) is the basic result of this section. It gives the mean concentration within a distance $x \leq \frac{\bar{u}T_c}{5}$ of a continuous, thin, infinitely long line source of the reactant A. We emphasize that this solution was obtained without recourse to any closure approximation. The only assumptions implicit in (D-94) are the jointly normal form (D-91) of the probability density $p(z_1'', z_1', z_2')$ and the assumptions embodied in the model of chemical reactions proposed in section 3. Since empirical data are not available for testing (D-94), we shall examine the qualitative accuracy of this equation by testing whether its behavior as the parameters R_o and λ are varied is consistent with our knowledge of the physical processes involved.

Recall that R_o is a dimensionless measure of the correlation of the particle's initial motion. In particular, if the initial separation of the two particles is ℓ, then $\lim_{\ell \to \infty} R_o = 0$ and $\lim_{\ell \to 0} R_o = 1$. The parameter λ is also dimensionless and has a value directly proportional to the period, measured in units of the Lagrangian time scale $\mathcal{T}$, (D-84), during which the motions of a pair of particles are correlated after their simultaneous release. Thus, the effective values R_o and λ which are required in (D-94) depend on the number N and initial spread L of the particles and also on the turbulence structure and the molecular diffusivity of the particles. It should be mentioned at this point that the expression (D-83) for the particle velocity correlation function from which the moments (D-97) are obtained is based on a single set of values of R_o and λ. Therefore, we are taking considerable liberty in using this expression with arbitrary values of these parameters. Our justification for this is that we do not intend the results of these calculations to be quantitatively definitive. Rather we are using (D-83) as a convenient, but representative, description of the particle velocity statistics from which we may derive, via the basic equation (D-94), a qualitative picture of how the concentration of a second order reactant varies as the nature of the particle motions changes.

With the above points in mind, consider Figure D-1 where we have plotted β^*, i.e. the function β normalized by the factor $\frac{50Nk\Delta t}{\overline{w'^2}^{1/2}\mathcal{T}}$, for three different combinations of values of R_o and λ. The abscissa in this graph represents the nondimensional distance $z^* = z/<z''^2>^{1/2}$. All three curves are based on a value of .2 for Δt^*. Hence, in order to satisfy condition (D-54) it is necessary that $T_c >> .2\mathcal{T}$; and in order for (D-78) to be valid, it is required that $L << <z_1'^2>^{1/2}$. The latter would require $L << .2\ \overline{w'^2}^{1/2}\mathcal{T}$ if the initial particle dispersion increased as $< z^2> = \overline{w'^2}^{1/2} t^2$ and the resulting magnitude of the parameter β would have to be no larger than one tenth the values of β^* shown in Figures D-1a-c. That is, β would be of order .01 or smaller. It is clear from this that condition (D-78) restricts the applicability of (D-94) to very weak reactions.

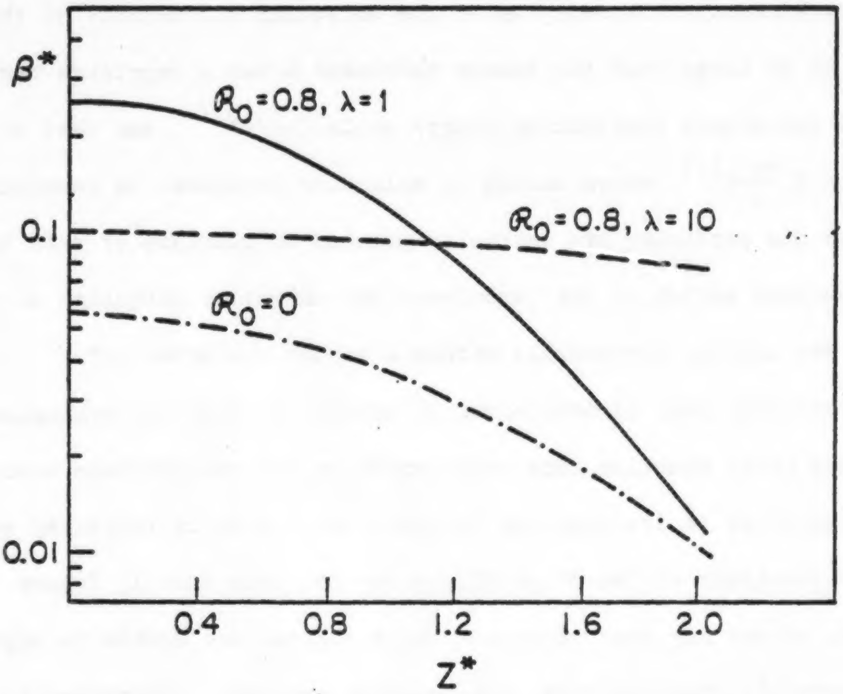

FIGURE D-1. PROFILES OF THE NONDIMENSIONALIZED FUNCTION β FOR THREE DIFFERENT TURBULENCE REGIMES

Look first at the β^* profile for the case $R_o = .8$, $\lambda = 10$. This represents a condition in which the particle motions are initially strongly correlated and where they remain correlated for a relatively long time (of order λT). Physically, this corresponds to a situation in which the energy dissipation rate ϵ of the turbulence is so small and the particle's Schmidt number (ν/κ) (ν being the kinematic viscosity and κ the molecular diffusivity of the A particles) is so large that the source thickness L has a magnitude between that of the turbulence dissipation length scale $(\nu^3/\epsilon)^{1/4}$, and that of the length scale $(\frac{\nu\kappa^2}{\epsilon})^{1/4}$ where mixing by molecular processes is important; because when the particles are initially grouped in clusters of this size (L), the combined action of the turbulence and molecular diffusion is unable to distort the cluster appreciably within a period the order Δt^*. Thus, the particles tend to move about in patches so that the collision frequency and hence reaction rate experienced by any one particle remains nearly constant regardless of its position in the plume. This is reflected quite well in the near constancy of the β^* profile shown for this case in Figure D-1. Viewed another way, we may say that since the fluid motions are unable to significantly alter the particle reaction rate, the reaction proceeds independently of the turbulence as in the case of a first order chemical reaction, where the parameter β_f corresponding to β is constant with respect to z(see (D-98) and (D-99)).

Now consider the case $R_o = .8$, $\lambda = 1$. Here again the particle motions are initially strongly correlated but they become uncorrelated much faster (ten times faster) than in the previous case. This corresponds to a situation in which the Schmidt number is smaller and/or the turbulent energy dissipation is larger than in the previous example so that a mixing of the particles by turbulent and molecular processes occurs before appreciable numbers of the particles have had time to react. This leads to the rapid decline in the magnitude of β with increasing z as shown in Figure D-1. The reason for the larger value of β at the origin in this case is that the correlation (ρ') between the particle positions at time $t^* = \Delta t^*$ happens to be larger in the present instance.

Finally, regarding the case $R_0 = 0$, we have here a situation in which the motions of all of the particles are uncorrelated. However, the position of any one particle at time Δt^* is highly correlated with its position at time $2\Delta t^*$ (this is true in all three examples because the single particle statistics are independent of R_0 and λ). Because of this last feature it is hard to imagine a physical analogue of this system. The one feature which stands out most clearly in Figure D-1 is the low amplitude of the β profile. This is due to the fact that when the motions of the particles are uncorrelated, they come into contact less often than when their motions are positively correlated, as in the other two examples. For this reason we anticipate that the β profile in this example is probably characteristic of that of a system in which for given source thickness L, the Schmidt number is sufficiently low and the turbulent energy dissipation sufficiently large that the particle motions become uncorrelated within a time of order Δt^*.

The foregoing analysis has attempted to find physical systems with properties compatible with the conditions under which each of the theoretical β profiles presented in Figure D-1 is applicable. In each case the profiles are consistent with our intuitive knowledge of the behavior of the physical analogues. Based on this finding, we conclude that the theory developed in this paper provides at least a qualitatively accurate description of the combined phenomena of turbulent diffusion and chemical reaction. A more rigorous test of the theory will be possible once suitable empirical data become available.

7. CONCLUSION

In this paper we have developed expressions which relate the concentration statistics of chemically reactive particles in turbulent fluid to the Lagrangian statistics of the turbulence. The expression for the mean concentration consist of equation (D-3) coupled with (D-9), for the case of a first order or linear reaction; and (D-3) coupled with (D-28), where second order reactions of the type (D-11) are concerned. Higher order concentration statistics could be found using the techniques presented here but this would require an unwarranted amount of labor.

The general equation (D-28) was reduced to the alternate form (D-46) and this was subsequently combined with (D-3) to compute the mean concentration of a nonlinearly reactive substance in two particular situations. In one of these (see section 6.1) the results were found to be identical to those of the classical theory. In the second example (section 6.2), several interesting aspects of the combined phenomenon of turbulent diffusion and chemical reaction were examined.

It is clear from the complex nature of the formulas and the general lack of information regarding the Lagrangian properties of turbulence that the techniques developed here will be of limited value in applied work. However, two important general uses of this method are foreseen. First, with this approach the problem is viewed from a different perspective than in the Eulerian methods so that new insights into the combined phenomenon of turbulent diffusion and chemical reaction may be gained. Second, this method may provide an invaluable testing ground for closure approximations and thereby permit more general applications of Eulerian techniques to turbulent diffusion problems.

ACKNOWLEDGEMENT

I am grateful to Professor John Seinfeld for reading the manuscript and for suggesting several improvements. I also appreciate the assistance of Mr. Winston Shu with the numerical calculations reported here. This work was supported in part by a gift from the John A. McCarthy Foundation.

REFERENCES

Baldwin, L. V., and T. J. Walsh (1961), "Turbulent Diffusion in the Core of Fully Developed Pipe Flow," *A.I.Ch.E. Journal*, Vol. 7, pp. 53-61.

Batchelor, G. K. (1959), "Small-Scale Variation of Convected Quantities Like Temperature in Turbulent Fluid--Part 1: General Discussion and the Case of Small Conductivity," *J. Fluid Mech.*, Vol. 5, pp. 113-133.

——— (1952), "Diffusion in a Field of Homogeneous Turbulence--Part 2: The Relative Motion of Particles," *Proc. of the Cambridge Philosophical Society*, Vol. 48, pp. 345-362.

——— (1950), "Application of the Similarity Theory of Turbulence to a Atmospheric Diffusion," *Quart. J. Roy. Meteor. Soc.*, Vol. 76, pp. 133-146.

——— (1949), "Diffusion in a Field of Homogeneous Turbulence--Part 1: Eulerian Analyses," *Australian J. Scientific Res.*, Vol. 2, pp. 437-450.

Batchelor, G. K., and A. A. Townsend (1948), "Decay of Isotropic Turbulence in the Initial Period," *Proc. of the Roy. Soc.*, Vol. 193, pp. 539-558.

Becker, H. A., R. E. Rosensweig, and J. R. Gwozdz (1966), "Turbulent Dispersion in a Pipe Flow," *A.I.Ch.E. Journal*, Vol. 12, pp. 964-972.

Brodkey, R. S., ed. (1975), *Turbulence in Mixing Operations - Theory and Application to Mixing and Reaction* (Academic Press, New York, New York).

Chandrasekhar, S. (1943), "Stochastic Problems in Physics and Astronomy," *Reviews of Mod. Physics*, Vol. 15, pp. 1-89.

Chock, D. P. (1976), "The General Motors Sulfate Dispersion Experiment: Assessment of the EPA HIWAY Model," General Motors Research Publication GMR-2126.

Clarke, R. H., et al. (1971), "Boundary Layer Data," Technical Paper No. 19, CSIRO Division of Meteorological Physics, Australia.

Corrsin, S. (1964), "The Isotropic Turbulent Mixer--Part II: Arbitrary Schmidt Number," *A.I.Ch.E. Journal*, Vol. 10, pp. 870-877.

__________ (1962), "Theories of Turbulent Dispersion," *Mechanique de la Turbulence*, pp. 27-52.

__________ (1958), "Statistical Behavior of a Reacting Mixture in Isotropic Turbulence," *Physics of Fluids*, Vol. 1, No. 1, pp. 42-47.

Csanady, G. T. (1967), "Concentration Fluctuation in Turbulent Diffusion," *J. Atmos. Sci.*, Vol. 24, pp. 21-28.

Crum, G. F., and T. J. Hanratty (1965), "Dissipation of a Sheet of Heated Air in a Turbulent Flow," *Appl. Scientific Res.*, Vol. A15, pp. 177-195.

Davis, D. D., and G. Klauber (1975), "Atmospheric Gas Phase Oxidation Mechanisms for the Molecule SO$_2$," *Proc. of the Symposium on Chemical Kinetics Data for the Lower and Upper Atmosphere*, September 1974, Warrenton, Virginia.

Davis, D. D., G. Smith, and G. Klauber (1974), "Trace Gas Analysis of Power Plant Plumes via Aircraft Measurement: O$_3$, NO$_x$, and SO$_2$ Chemistry," *Science*, Vol. 186, pp. 733-736.

Deardorff, J. W. (1974a), Three-Dimensional Numerical Study of the Height and Mean Structure of a Heated Planetary Boundary Layer," *Bound. Layer Meteor.*, Vol. 7, pp. 81-106.

__________ (1974b), "Three-Dimensional Numerical Study of Turbulence in an Entraining Mixed Layer," *Bound. Layer Meteor.*, Vol. 7, pp. 199-226.

__________ (1973), "The Use of Subgrid Transport Equations in a Three-Dimensional Model of Atmospheric Turbulence," *J. Fluids Eng.*, Vol. 95, pp. 429-438.

__________ (1972), "Numerical Investigation of Neutral and Unstable Planetary Boundary Layers," *J. Atmos. Sci.*, Vol. 29, pp. 91-115.

__________ (1970a), "Preliminary Results from Numerical Integration of the Unstable Planetary Boundary Layer," *J. Atmos. Sci.*, Vol. 27, pp. 1209-1211.

__________ (1970b), "Lagrangian Statistics from Numerically Integrated Turbulent Shear Flow," *Physics of Fluids*, Vol. 13, No. 3, pp. 584-595.

Deardorff, J. W., and M. A. Drake (1974), "Boundary Layer Data from a Numerical Integration in Three Dimensions," National Center for Atmospheric Research, Boulder, Colorado.

Deardorff, J. W., and R. L. Peskin (1970), "Lagrangian Statistics from Numerically Integrated Turbulent Shear Flow," *Physics of Fluids*, Vol. 13, pp. 584-595.

Deardorff, J. W., and G. E. Willis (1975), "A Parameterization of Diffusion into the Mixed Layer," J. Appl. Meteor., Vol. 14, p. 1451.

__________ (1974), "Computer and Laboratory Modeling of the Vertical Diffusion of Nonbuoyant Particles in the Mixed Layer," Advances in Geophysics, Vol. 18B, pp. 187-200.

Dryden, H. L. (1943), "A Review of the Statistical Theory of Turbulence," Quart. of Applied Math., Vol. 1, pp. 7-42.

Gifford, F. A. (1959), "Statistical Properties of a Fluctuating Plume Dispersion Model," Advances in Geophysics, F. N. Frenkiel and P. A. Sheppard, eds., Vol. 6, pp. 117-138 (Academic Press, New York, New York).

Gradshteyn, I. S., and I. W. Ryzhik (1965), Tables of Integrals Series and Products (Academic Press, New York, New York).

Hill, J. C. (1976), "Homogeneous Turbulent Mixing with Chemical Reaction," Ann. Rev. of Fluid Mech., Vol. 8.

Hinze, J. O. (1959), Turbulence (McGraw-Hill Book Company, New York, New York).

Hotchkiss, P. S., and F. H. Harlow (1973), "Air Pollution Transport in Street Canyons," EPA-R4-73-029, Los Alamos Scientific Laboratory, Los Alamos, New Mexico.

Jerskey, T. N., et al. (1976), "Analysis of the Data from the Three-Dimensional Gradient Study," ARB 4-250, California Air Resources Board, Sacramento, California.

Kattan, A., and R. J. Adler (1967), "A Stochastic Mixing Model for Homogeneous, Turbulent, Tubular Reactors," A.I.Ch.E. Journal, Vol. 13, No. 3, pp. 580-585.

Keeler, R. N., E. E. Peterson, and J. M. Prausnitz (1965), "Mixing and Chemical Reaction in Turbulent Flow Reactors," A.I.Ch.E. Journal, Vol. 11, pp. 221-227.

Lamb, R. G. (1977), "Effect of Source Height on Material Dispersion in the Unstable Planetary Boundary Layer," in preparation.

__________ (1976), "Continued Research in Mesoscale Air Pollution Simulation Modeling--Volume III: Modeling of Microscale Phenomena," EPA 600/4-76-016a, Systems Applications, Incorporated, San Rafael, California.

__________ (1975), "The Calculation of Long-Term Air Pollutant Concentration Statistics Using the Concept of a Macro-Turbulence," Proc. of the Conference on Air Pollution Modeling, Venice, Italy.

__________ (1974), "Lagrangian Analysis of a Passive Scalar in Turbulent Fluid-- Part 1: General Theory," submitted for publication to the J. Fluid Mech.

__________ (1973), "Lagrangian Analysis of a Passive Scalar in Turbulent Fluid--Part 1: Theory," unpublished manuscript.

__________ (1971), "Numerical Modeling of Urban Air Pollution," Ph.D. Dissertation, University of California at Los Angeles, Department of Meteorology, Los Angeles, California (available from University Microfilms, Ann Arbor, Michigan).

Lamb, R. G., and W. R. Shu (1977), "A Model of Second-Order Chemical Reactions in Turbulent Fluid--Part I: Formulation and Validation," submitted for publication to Atmos. Environ.

Lamb, R. G., W. H. Chen, and J. H. Seinfeld (1975), "Numerico-Empirical Analyses of Atmospheric Diffusion Theories," J. Atmos. Sci., Vol. 32, pp. 1794-1807.

__________ (1974), "Numerico-Empirical Analysis of Atmospheric Diffusion Theories," Proc. of the AMS Conference on Atmospheric Diffusion, Santa Barbara, California.

Lee, J. (1966), "Isotropic Turbulent Mixing Under Second-Order Chemical Reaction," Physics of Fluids, Vol. 9, pp. 1753-1763.

Lee, J., and R. S. Brodkey (1964), "Turbulent Motion and Mixing in a Pipe," A.I.Ch.E. Journal, Vol. 10, pp. 187-193.

Lenchow, D. H. (1970), "Airplane Measurements of Planetary Boundary Layer Structure," J. Appl. Meteor., Vol. 9, pp. 874-884.

Lin, C. H., and E. E. O'Brien (1972), "Two Species Isothermal Reactions in Homogeneous Turbulence," Astronautica Acta, Vol. 17, pp. 771-781.

Lumley, J. L. (1962), "The Mathematical Nature of the Problem of Relating Lagrangian and Eulerian Statistical Functions in Turbulence," Mecanique de la Turbulence, pp. 17-26.

Mao, K. W. (1969), "Chemical Reactions with Turbulent Mixing," Ph.D. Thesis, Carnegie-Mellon University, Pittsburgh, Pennsylvania.

Mao, K. W., and H. L. Toor (1971), "Second Order Chemical Reaction with Turbulent Mixing," Indus. Eng. and Chem. Fundamentals, Vol. 10, pp. 192-197.

__________ (1970), "A Diffusion Model for Reactions with Turbulent Mixing," A.I.Ch.E. Journal, Vol. 16, No. 1, pp. 49-52.

McKelvey, K. H. (1968), "Turbulent Mixing with Chemical Reaction," Ph.D. Thesis, Ohio State University, Columbus, Ohio.

O'Brien, E. E. (1971), "Turbulent Mixing of Two Rapidly Reacting Chemical Species," Physics of Fluids, Vol. 14, pp. 1326-1331.

__________ (1968), "Closure for Stochastically Distributed Second-Order Reactions," Physics of Fluids, Vol. 11, pp. 1883-1888.

Riley, J. J., and G. S. Patterson, Jr. (1974), "Diffusion Experiments with Numerically Integrated Isotropic Turbulence," Physics of Fluids, Vol. 17, pp. 292-297.

Rounds, W. (1955)," Solutions of the Two-Dimensional Diffusion Equation," Trans. Amer. Geophys. Union., Vol. 36, pp. 395-405.

Saffman, P. G. (1960), "On the Effect of Molecular Diffusivity in Turbulent Diffusion," J. Fluid Mech., Vol. 8, pp. 273-283.

Shu, W. R. (1976), "Turbulent Chemical Reactions: Application to Atmospheric Chemistry," Ph.D. Thesis, California Institute of Technology, Pasadena, California.

Shu, W. R., R. G. Lamb, and J. H. Seinfeld (1977), "A Model of Second-Order Chemical Reactions in Turbulent Fluid--Part II: Application to Atmospheric Plumes," submitted for publication to Atmos. Environ.

Taylor, G. I. (1921), "Diffusion by Continuous Movements," Proc. of the London Math Society, Vol. 2, No. 20, pp. 196-202.

Toor, H. L. (1975), in Turbulence in Mixing Operations--Theory and Application to Mixing and Reaction, R. S. Brodkey, ed. (Academic Press, New York, New York).

__________ (1969), "Turbulent Mixing of Two Species with and Without Chemical Reactions," Indus. Eng. and Chem. Fundamentals, Vol. 8, pp. 655-659.

__________ (1962), "Mass Transfer in Dilute Turbulent and nonturbulent Systems with Rapid Irreversible Reactions and Equal Diffusivities," A.I.Ch.E. Journal, Vol. 8, pp. 70-78.

Torrest, R. S., and W. E. Ranz (1970), "Concentration Fluctuations and Chemical Conversion Associated with Mixing in Some Turbulent Flows," A.I.Ch.E. Journal, Vol. 16, pp. 930-942.

Turner, D. B. (1969), "Workbook of Atmospheric Dispersion Estimates," AP-26, Environmental Protection Agency, Research Triangle Park, North Carolina.

Vassilatos, G., and H. L. Toor (1965), "Second-Order Chemical Reaction in a Nonhomogeneous Turbulent Fluid," A.I.Ch.E. Journal, Vol. 11, pp. 666-673.